Doctoral Thesis | 2024

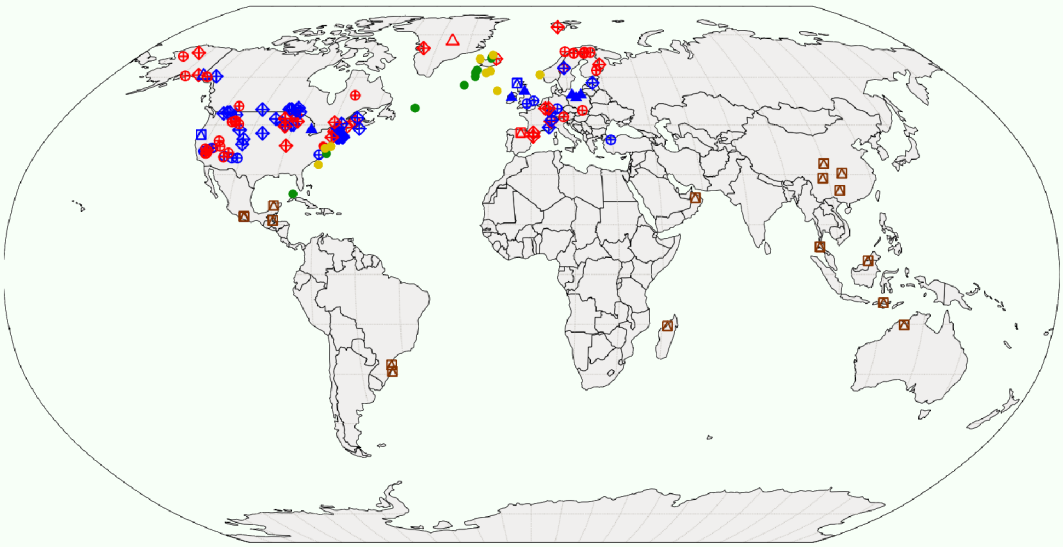

Investigation of paleoclimatic hydroclimatic variability with emphasis on the role of oceanic circulation

Shailendra Pratap

Department of Water Resources and Environmental Modeling
Faculty of Environmental Sciences
Czech University of Life Sciences Prague
Czech Republic

Supervised by
doc. Ing. Mgr. Ioannis Markonis, Ph.D.

Department of Water Resources and Environmental Modeling
Faculty of Environmental Sciences
Czech University of Life Sciences Prague, Czech Republic

Investigation of paleoclimatic hydroclimatic variability with emphasis on the role of oceanic circulation

Submitted by SHAILENDRA PRATAP

PhD thesis in LANDSCAPE ENGINEERING (ENVIRONMENTAL MODELLING)

April, 2024

SUPERVISED BY
DOC. ING. MGR. IOANNIS MARKONIS, PH.D.

Declaration

I hereby affirm that, unless explicitly referenced to external sources, this dissertation represents an original work, not submitted in full or in part for evaluation in pursuit of any other academic degree or credential, whether within this institution or any other. The contents of this thesis are the product of my independent effort and do not incorporate any results arising from collaborative endeavors, except for instances explicitly delineated within the manuscript and the Acknowledgments section. All sources and information used in this thesis are properly credited in accordance with academic standards and guidelines.

Shailendra Pratap

February, 2024

Author's statement

I hereby declare that I have independently elaborated the diploma/final thesis with the topic of: "Investigation of paleoclimatic hydroclimatic variability with emphasis on the role of oceanic circulation" and that I have cited all the information sources that I used in the thesis and that are also listed at the end of the thesis in the list of used information sources.

I am aware that my diploma/final thesis is subject to Act No. 121/2000 Coll., on copyright, on rights related to copyright and on amendment of some acts, as amended by later regulations, particularly the provisions of Section 35(3) of the act on the use of the thesis.

I am aware that by submitting the diploma/final thesis I agree with its publication under Act No. 111/1998 Coll., on universities and on the change and amendments of some acts, as amended, regardless of the result of its defence.

Shailendra Pratap

February, 2024

Acknowledgements

I am deeply indebted to Dr. Ioannis Markonis for his invaluable guidance, motivation, and constructive suggestions, which significantly contributed to the success of this thesis. I would also like to extend my thanks to Prof. Martin Hanel, Petr Máca, and other individuals who provided unwavering support and encouragement throughout this endeavor.

I would like to express my gratitude to Helena Michálková, Jana Stýblová, Slavěna Zajícová, and Petr Bašta for their invaluable assistance with administrative tasks and all matters related to the doctoral program. I am also thankful to my colleagues Mijael Rodrigo Vargas Godoy, Rajani Kumar Pradhan, and Ujjwal Singh for their support in overcoming various challenges encountered during the research process.

I express gratitude to the Czech University of Life Sciences Prague for furnishing the necessary research facilities and offering a scholarship to successfully accomplish this doctoral thesis. Furthermore, I would like to acknowledge the support received from the Internal Grant Agency of the Faculty of Environmental Sciences at the Czech University of Life Sciences Prague, under Grants 2020B0039, 2021B0006, 2022B0039, and 2023B0009, which provided additional financial backing for this research.

I reserve special appreciation for the unwavering support of my parents, brother, and sister, whose continuous motivation has played a pivotal role in this undertaking. Their encouragement has been instrumental in my PhD journey.

Abstract

The growing concern regarding global warming emphasizes the critical need for an in-depth understanding of its impact on the water cycle, both locally and globally, given its significant impact on society. A prevailing hypothesis suggests that global warming will intensify the water cycle. However, uncertainties persist as some studies project drier climatic conditions. Hence, accurately predicting regional-level changes in the water cycle remains a challenge, hindering precise anticipation of future alterations. To overcome these limitations and uncertainties and to capture long-term climate patterns, this study employs a multi-proxy data approach to investigate hydroclimate changes within warm climates. Furthermore, the study explores the influence of oceanic circulation on hydroclimatic variability. By examining past hydroclimate data sourced from natural archives, this research aims to establish valuable reference points aimed at enhancing the accuracy of climate models.

Our study suggests that the hypothesis that a warmer climate is a wetter climate could be an oversimplification. This is because the water cycle exhibits considerable variability across different temporal and geographical contexts. Our observations highlighted dry conditions primarily associated with climates that are warmer than their centennial average, whereas slightly warmer climates, which are closer to their centennial average, tend to be correlated to wetter conditions on continents. Our findings provide new insights into the complex relationship between ocean circulation and shifts in the hydroclimate patterns, particularly emphasizing the Atlantic Meridional Overturning Circulation (AMOC). Our investigation reveals that the AMOC plays a critical role in shaping both global and regional changes in the hydroclimate/water cycle. Its fluctuations are intricately linked to instabilities in the state of the North Atlantic Ocean. For instance, a weakened AMOC may induce low sea surface temperatures and a southward shift in the Intertropical Convergence Zone. These changes limit the dispersion of atmospheric heat and moisture, thereby exerting a significant impact on the global hydroclimate. Furthermore, our study indicates that long-term changes in oceanic circulation patterns over the North Atlantic influence latitudinal temperature distributions, consequently affecting shifts in the hydroclimate/water cycle patterns at various latitudes.

Contents

List of Figures

List of Tables

Chapter 1

Thesis chapters and objectives

1.1 Chapters division

Each chapter of this thesis serves a specific purpose in addressing our research objectives and exploring the complex relationships within the field of paleo-hydroclimatology. The chapters included in this thesis are as follows:

Chapter 1. Thesis chapters details and objectives.

Chapter 2. Motivation, thesis structure, and thesis introduction.

Chapter 3. Literature Research: Identifying research gaps.

Chapter 4. Data & methods

Chapter 5. The response of the hydrological cycle to temperature changes in recent and distant climatic history.

Chapter 6. Investigation of changes in hydroclimate (precipitation and temperature) patterns related to the North Atlantic Ocean circulation during the Medieval Climate Anomaly.

Chapter 7. Conclusions

1.2 Thesis objectives

The primary objective of this study was to identify and tackle major research gaps, as outlined in Chapter 3, through a comprehensive literature review. Several studies have highlighted that despite the availability of instrumental data spanning centuries, it is inadequate to fully capture the responses of hydroclimate variability and understand the role of human and natural influences. Hence, there is a necessity for climate investigations utilizing paleo-evidence, such as proxy records that preserve signals of past hydroclimate variation. Consequently, there is a notable scarcity of paleo records available to comprehensively cover the variability in the state of the Atlantic Ocean, particularly regarding the Atlantic Meridional Overturning Circulation (AMOC). To address this gap in hydroclimate and ocean state data, this thesis created paleo-hydroclimatic data, including both empirical and proxy-based records, spanning various geological periods. A significant feature of

this database is its inclusion of paleo-oceanic data, specifically emphasizing the AMOC, sea surface temperature (SST), and intertropical convergence zone (ITCZ) shifts, which are not widely available in other databases. This comprehensive database is elaborated in Chapter 4.

Furthermore, Chapter 4 also provides detailed insights into the scaling behavior and slope of each hydroclimate record, accomplished using the cross-scale analyses algorithm. The scaling behavior was used to explore how the statistical patterns of the data change across different scales, to understand how the variability of hydroclimate variables changes across different scales, providing insights into the variability of hydroclimate variables and their potential impacts.

The relationship between the hydrological cycle and temperature is highly intricate. Therefore, in Chapter 5, the thesis focus delved deeper into understanding how the hydrological cycle responds to temperature variations across both recent and distant climatic histories. The factors contributing to hydroclimate changes remain subjects of ongoing investigation and lively debate. Through our literature review, we uncovered that oceanic circulation, notably the AMOC, emerges as a plausible driver of global hydroclimate changes. Given the projected decline in AMOC by the end of the 21st century, significant shifts in global hydroclimate patterns, particularly in Europe and North America, are anticipated.

Therefore, in Chapter 6, the focus shifted to estimating AMOC changes and investigating their role in temperature and precipitation distribution during a warm period. For this, the Medieval Climate Anomaly warm period was selected as an analogue to the present warm period. The analysis and results pertaining to AMOC and its impact on hydroclimate changes are detailed in this chapter. Alongside global-scale changes, hydrological cycle alterations associated with a warmer climate will also have regional implications. However, estimating hydrological changes at regional scales remains challenging and uncertain. In the final chapter, Chapter 7 of this thesis, the focus is on the conclusion, which encompasses a summary of the thesis, key research findings, limitations of the study, future research directions, and the benefits to the scientific community and society/humanity.

Chapter 2

Introduction

2.1 Motivation

Climate change has become a central focus of research due to its anticipated impact on the global water cycle, leading to increased frequency of extreme events such as heavy rainfall, floods, and droughts on a global scale [399]. Specifically, global warming is expected to intensify the water cycle and influence hydroclimate (temperature and precipitation) variability [538]. Undoubtedly, global warming has also affected the extent, duration, timing, and intensity of extreme events [168, 478]. Nevertheless, uncertainty remains regarding whether a warmer climate will lead to wetter or drier hydrological conditions [246].

Moreover, a warmer climate is projected to impact the state of the ocean, particularly in the North Atlantic regions. Subsequently, changes in the Atlantic Ocean circulation and sea surface temperature, key drivers of terrestrial hydroclimate patterns, necessitate further investigation to better understand the causes of this change. The alterations in the water cycle, hydroclimate patterns, and the state of the ocean due to climate change and global warming have significant socioeconomic and ecological consequences worldwide. Rising global temperatures and the uncertainty surrounding hydroclimate and oceanic circulation changes have motivated the objectives of this study. We explore variations in hydroclimate and investigate their potential link with changes in the state of the North Atlantic Ocean in warm climates to advance our understanding of current changes and establish connections between these changes and both natural and human-induced climate factors.

2.2 Thesis importance

This thesis holds significant importance as it aims to address critical uncertainties related to hydroclimatic changes in warm climates and their link with changes in ocean circulation state. The objective is to enhance our understanding of present and future hydroclimate changes by examining past hydroclimate variability. The significance of understanding these shifts in hydroclimate lies in their direct and severe impacts on human lives and infrastructure. By acquiring knowledge and a deeper understanding of changing hydroclimate conditions, policymakers and resource managers can effectively prepare for the future. More details on the importance of the thesis are elaborated in Chapter 8.

2.3 Thesis introduction

Presently, climate change stands as a widespread global concern, particularly in the context of a hydrologically variable and warm climate system. Frequent extremes associated with the hydrological cycle, such as flood, drought, heavy precipitation, and their uneven spatio-temporal distribution highlight the growing impact of global warming on the hydrological resources, specifically at continental and regional scales [599, 349]. Additionally, numerous observations suggest that the Earth's climate system has undergone significant changes in recent centuries due to global warming [205], and is anticipated to undergo substantial alterations as a result of this warming. The global water cycle (GWC) and the hydroclimate system are intricately connected to global warming. Increased global temperatures have been identified to alter the hydrological cycle patterns, given that its processes strongly depend on temperature variations. Particularly, a warmer atmosphere has the capacity to retain larger amounts of water, potentially leading to more intense precipitation [523]. Conversely, rising temperatures may also result in increased aridity or more frequent occurrences of drought in certain regions [389]. Moreover, climatologists have observed both wet and dry scenarios in a warmer climate. Consequently, the influence of global surface temperature changes on the GWC remains an unresolved question [274]. Thus, this question needs considerable attention because intensification in the water cycle and related hydroclimate events may influence the availability of water resources, increase the frequency and intensity of extreme events, droughts, and floods. In any case, in a warmer climate, hydroclimate shifts may exert significant impacts on both natural ecosystems and human societies. Therefore, assessment of the GWC and hydroclimate variability is a great matter of political and public concern worldwide to develop policies and mitigation strategies for socio-economic security.

Currently, a majority of climate studies and projections rely on climate models. Climate simulations using different climate models show that the residence period of water in the atmosphere has increased, representing a reduction of the global cycle rate [70]. On the other hand, Greenhouse gas experiments using coupled ocean-atmosphere models indicate that an increase in surface temperature will increase precipitation rate in response to increased surface evaporation, and total precipitable water will increase with the water-holding ca-

pacity of the atmosphere [452, 233]. These coupled Ocean-land-atmosphere model simulations infer that precipitation, runoff, and evaporation are expected to increase globally by 5.2%, 7.3%, and 5.2%, respectively, in response to an increase in mean surface air temperature of 2.3°C by 2050 [586, 452, 233]. Model simulations and theory suggest an intensification of the wet-dry contrast across low latitudes and widespread expansion of dry areas overland [218, 319]. Specifically, available records suggest drying over the subtropics and a general intensification in monsoons, while regional complexity persists across the low to mid-latitudes regions [474]. Studies have analyzed the unequal distribution of precipitation across the high, mid, and low latitudes. Specifically, landmasses in the high and low latitudes are likely to receive large amounts of precipitation due to the warmer troposphere with additional water-carrying capacity [356]. However, a lower precipitation rate is projected over the mid-latitude, subtropical arid, and semi-arid regions [436]. The most extensive precipitation changes are projected over North America and northern Eurasia during the winter [513]. As a consequence of enhanced evapotranspiration, it is expected that in the future drought frequency might be higher over the mid-latitude regions [156]. One of the main hypotheses of GWC intensification is that the drier region will be drier and the wetter region will be wetter as a consequence of climate warming [159, 218].

Despite the availability of various advanced global and regional climate models, their outputs are not precise enough to understand atmospheric perturbations [272, 269]. Specifically, for precipitation, most climate model simulations tend to show overestimation [541]. On the other hand, in the hydrological cycle, uncertainties remain at regional scales, as regional processes introduce feedback that may amplify or reduce the global response, concerning both the mean climate state and the frequency and intensity of extremes. Additionally, the climate simulations obtained using the climate model outputs require verification by the observations. Because, the availability of instrumental data for climate variables, i.e., precipitation and temperature typically spans a century or less. To address data limitations, the quantification of the rate and magnitude of climate variability using paleoclimate reconstructions offers a much wider time window. Therefore, ongoing climate concerns have highlighted the demands of interpreting observational records, i.e., proxy archives to understand climate changes during the past and their connection with modern and future climates.

Natural resources such as ice cores, tree rings, corals, stalagmites, ocean sediments, speleothems, and lake sediments are the proxy archives of past climates. These proxy records preserve chronological information on weather and climate variability extending from decadal to millennium-long scale. Additionally, past hydroclimate observations can be useful for understanding and identifying possible mechanisms of climate variability and verifying the modern climate model in warming climate scenarios. The spatio-temporal proxy records will help to assess the variability in the hydrological process and also in the investigations of present and future hydroclimate patterns [319]. Furthermore, this proxy-based climate information could probably act as an essential source not only in model-observation integration but also for probabilistic inference, such as evaluation of the reoccurrence cycle of extreme events [350]. In this regard, the assessment of millennium-long paleoclimate data could be useful to constrain climate projections better and improve climate models.

Back to Earth's history, most of the paleoclimate evidence shows a positive relationship between the warmer climate and higher precipitation activities. For instance, during the Eemian interglacial phase (about 122 thousand years ago (ka) before the present (BP) the global climate conditions were warmer nearly the same as we are facing today [4]. Meanwhile, paleoclimate evidence suggests intensification in a hydrological cycle over most of the regions of the Northern Hemisphere [4]. Over the past few million years, the planet has witnessed numerous rapid climate transitions occurring on timescales ranging from decades to centuries. Analyzing precipitation time series, a study reveals a negative shift starting around 30 ka and extending to the Last Glacial Maximum, with estimated precipitation values approximately 15-20% lower than present [185]. Over the past 18-20 ka, water budget assessments show significant variability in both the seasonal and spatial distribution of precipitation with hydrologic regime [505]. For instance, during the 18 ka BP, total precipitation was 14% lower than today [186]. However, increased warming and monsoon circulation, during 13 to 12 ka BP, in low-latitude causes a rise in lake levels, and over the desert zone, this increase causes an increase in precipitation by about 200-300 mm [271].

These long-term changes are attributed to natural variability. In contrast, over the last 50 years, anthropogenic factors have influenced the precipitation pattern, and atmospheric

warming causes the intensification in precipitation minus evaporation (P-E) [425]. Significant rapid climate changes have also been monitored during the present interglacial (Holocene) with cold and dry phases with the time cycle of the 1500 year and climate transitions of on decade to century timescale [62]. Over the past few centuries, there were several time intervals when climate conditions were warmer than today, such as mid-to-late Holocene [345, 427, 573, 320, 619]. However, climate forcings during these warm intervals differed from current anthropogenic change [171]. Investigations on such intervals can provide insights into future climate impacts, especially over centennial to millennial timescales usually not covered by modern climate model simulations.

All the above evidence suggests that long-term climate change occurs in sudden jumps rather than incremental changes. The extreme conditions that arose in different geological time scales and their transition periods still leave unanswered questions on the linkage between climate variables and the water budget on the planet. Therefore, a comprehensive understanding of year-long as well as seasonal variability in climate, over the past millennium, structured a principal basis for the investigation of the observational, i.e., proxy records to measure the response of the hydroclimate system to various climate forcing [183]. The warmer climate has been observed not only to affect regional and continental hydroclimate systems but has also been noted to have significant consequences on land-ocean-atmospheric circulation, subsequently impacting global hydroclimate [8]. Additionally, changes in the state of ocean circulation are observed to be correlated with regional and global weather patterns. The Atlantic Meridional Overturning Circulation (AMOC) is a thermohaline circulation and a critical tipping element in the global climate system as it maintains the global climate system by circulating water from the tropics to the polewards and back in a long cycle within the Atlantic Ocean. While uncertainties persist, there is currently increased attention on the AMOC as its weakening due to warm climate conditions may lead to significant changes in the global hydroclimate system. While some models project the collapse of the AMOC by the end of the 21^{st} century, many argue that such a collapse is highly unlikely [191, 154]. The majority of the abrupt events during the distant past were probably the response to the Atlantic long-term variability, the AMOC in particular.

Notably, paleoclimate investigations reveal that the hydrological cycle variations were correlated with variations in the AMOC. For instance, during the last glacial period, Dansgaard-Oeschger (D-O) events had a significant global impact, causing abrupt warm conditions. The signs of these events were evident not only in terrestrial proxy records but also in global deep-sea evidence, suggesting a connection with the AMOC and Ocean circulation changes [483]. Deep-ocean proxy records further unveil the relationship between AMOC intensity, D-O events, and the Eemian Interglacial phase [331, 222, 465]. Additionally, Heinrich events, the Younger Dryas, the 8.2 ka event, and specifically cold phases were likely consequences of a weakened AMOC [11, 160]. The weakening of the AMOC has been associated with freshwater pulses resulting from the melting of Arctic ice and high-latitude glaciers [309]. Changes in AMOC intensity can impact the strength of Westerlies, consequently influencing the distribution of atmospheric moisture across North Atlantic terrestrial regions [132]. Consequently, the weak AMOC affects areas from western Europe to Asia, leading to reduced precipitation [401] and weak monsoon activity [204].

Additionally, the consequences of AMOC variation have been observed to correlate with changes in the temperature gradient between tropical and North Atlantic regions. The weakening of AMOC has been noted to induce lower sea surface temperatures (SST) over the North Atlantic and influence the shift of the Intertropical Convergence Zone (ITCZ) [384]. Notably, the southward displacement of the ITCZ influences the northern tropical regions with the cold phases and dry conditions, the evidences are the Heinrich events [297], Younger Dryas [420], and the weak monsoon during the Eemian Interglacial phase [367]. Mostly, the effect of the ITCZ latitudinal shift has been experienced over tropical and Asian regions which caused the reduced summer-monsoon, for instance, during the D-O and Heinrich events [248]. However, the northward shifting of the ITCZ has been recorded to have a warmer climate and an increased summer monsoon over the Asian regions [469]. For instance, during the mid-Miocene (16 to 14.8 Million years ago), the increased precipitation over northern Colombia regions was the response to the northward shift of the ITCZ [472]. The monsoon process shares a large portion of global precipitation and has positive feedback with the ITCZ variations.

Given all these influences, further investigations are necessary to comprehend the cor-

relation between oceanic state, particularly AMOC, SST, and ITCZ variations, and changes in hydroclimate patterns during distant past climates. Understanding these relationships is crucial for interpreting the present and anticipating future changes, enabling the development of mitigation strategies to address potential socio-economic losses. Accordingly, our research aims to estimate the variation in the hydrological cycle in response to temperature, considering ocean state changes. We anticipate that this study could yield meaningful conclusions on water cycle variability, and the outcomes could be promising for developing mitigation strategies, informing policy-making, and safeguarding against socio-economic losses. Additionally, the outcomes of the study may serve as a benchmark for future research related to climate change. Moreover, detailed information regarding the research objectives is provided in Chapter 2.

Chapter 3

Literature Review: Identifying research gaps

3.1 Summary

The chaotic behavior of the climate system, mainly, the undeniable impact of global warming on altering the global distribution of the water cycle, presents challenges in accurately assessing and predicting hydroclimate variability at various scales. Despite the relatively limited duration of the instrumental period, which fails to capture the complete range of natural hydroclimate variability, a retrospective examination of past climate could provide valuable insights into present and future changes. The utilization of millennium-long proxy archives, such as tree rings, stalagmites, lake levels, and ice cores, offers a foundation for understanding past hydroclimate dynamics and the discernment of anthropogenic influences on the hydrological cycle. Therefore, this chapter understands the dynamics of the Earth's hydroclimate, particularly how precipitation responds to temperature changes, as well as temperature and precipitation patterns across different time periods using proxy records.

The study found that past climate systems have experienced numerous unforeseen temperature oscillations, transitioning between cold and warm phases and vice versa. Most abrupt hydroclimate changes tend to occur prominently during shifts from one climatic state to another. Evidence supports the notion that spatial and temporal variations in the hydrological cycle are influenced by temperature-dependent factors. The anthropogenic-induced global warming has become widespread since the mid-19^{th} century, with the warming trend observed in the 20^{th} century strongly linked to human activities. Furthermore, recent decades have seen considerable hydroclimate changes and model projects worldwide increase in precipitation and alterations in ocean circulation under global warming scenarios. The investigation of hydroclimatic fluctuations during various geological epochs holds significant value in quantifying global responses to diverse climate forcings and greenhouse gas-induced warming. This understanding is also vital for validating climate projections and estimating potential consequences, providing valuable insights for policymakers in formulating effective strategies for mitigation, adaptation, and response.

Keywords: Global hydrological cycle, water cycle intensification, paleohydroclimate, proxy reconstructions

3.2 Introduction

The hydrological cycle is a fundamental component of life on Earth, connecting the atmosphere, land, and ocean into an integrated system. This intricate journey involves water transitioning between solid, liquid, and gaseous states. These phase changes, along with the exchange of energy among the land, atmosphere, and ocean, directly influence the properties of the climate system itself [104]. Given the biosphere's strong reliance on climatic conditions, ecosystem functionality is intricately tied to the inherent variability within the hydrological cycle. Additionally, human societies depend on water resources, inherently linked to the state of the hydrological cycle, to meet their consumption needs. Consequently, changes in the hydrological cycle have significant impacts on both environmental systems and human societies. Throughout Earth's history, substantial transformations in the hydrological cycle have been observed, particularly in precipitation patterns and global temperature distributions.

Paleoclimate observations spanning the past 18-20 thousand years (ka) reveal significant fluctuations in both spatial and temporal (seasonal) precipitation distribution [505]. Specifically, during the 18 ka period, when sea surface temperature (SST) in the North Pacific and North Atlantic were approximately 10°C lower than present conditions [373]. Moreover, paleoclimatic evidence suggests that total precipitation during this period was 14% lower than current levels [186]. However, from 13 to 12 ka, a period of amplified warming and monsoon circulation contributed to a notable increase in precipitation by approximately 200-300 mm in lower latitudes [271]. Furthermore, within the temporal range of 12 to 6 ka, the intensification of solar radiation likely resulted in increased thermal disparity between land and sea surfaces, subsequently leading to intensified monsoonal activity during that period [373]. Similarly, a significant warming event occurred during the Holocene, spanning from 8 to 3 ka [486].

Over the past several million years, numerous rapid shifts in climatic conditions have occurred on timescales ranging from decades to centuries [422]. Additionally, the frequency of sudden climate changes, observed during both the current interglacial period (Holocene) and the last glacial period, remains consistent, spanning approximately 1500 years [62].

Investigations conducted during the Last Glacial Maximum (approximately 23-18 ka) reveal prevailing arid conditions in both the Northern and Southern hemispheres, accompanied by increased temperatures on land and sea surfaces in lower tropical regions [185].

Throughout the present interglacial period, the climate has exhibited significant variations that still need to be determined on a continental scale, where climate variability has stronger connections to society and ecosystems compared to globally averaged situations [7]. Indeed, understanding the magnitude of these variances is essential for characterizing anthropogenic impacts against the backdrop of various natural variabilities.

Due to the multi-scale fluctuations inherent in the climate system, accurately assessing and quantifying the variability of the hydrological cycle at global, continental, and regional scales presents significant challenges. The analysis of paleoclimate data obtained from ice cores extracted from Greenland and Antarctica suggests that Earth's climate is responsive to fluctuations in greenhouse gases (GHGs) concentrations [293, 72]. Furthermore, paleoclimate evidence indicates that the current rate of climate warming is ten times higher than the mean rate observed during ice age warming [133]. Additionally, there is compelling evidence linking the increased concentration of GHGs to global warming [498]. Presently, the influence of global warming is notably affecting global water cycle patterns, thereby impacting the quality of human life [532].

In addition to the ongoing global warming, recent research has illuminated the role of GHGs concentrations in modifying Earth's energy balance, thereby influencing the hydrological cycle [538]. Comprehensive energy budget analyses have revealed an augmentation in downwelling infrared radiation, attributed to the increasing levels of GHGs in the atmosphere. Furthermore, it is suggested that this increased radiation has led to not only increased atmospheric and SST but also increased levels of hydrological cycle components such as evapotranspiration, evaporation, atmospheric moisture content, and precipitation [574]. Further investigations have indicated that atmospheric warming and increased values of hydrological cycle components will expedite and amplify the global hydrologic cycle. This, in turn, is projected to contribute to an increased frequency of extreme climatic events, encompassing heavy rainfall, floods, and drought conditions [241]. Moreover, studies also suggest global warming as a potential driver for abrupt changes and the intensification of

the hydrological cycle [539, 220, 577, 511, 9].

The intensification of the hydrological cycle is characterized by accelerated rates of atmospheric water vapor content, precipitation, evaporation, and evapotranspiration [241]. Conversely, disparities in Earth's energy budget at varying scales [593, 23] and anthropogenic influences (e.g., GHG emissions, water resource exploitation, and land-use changes) have been identified as factors driving hydrological variability and the enhancement of precipitation minus evaporation patterns [425]. Given the increasing frequency of hydrological extremes, it becomes imperative to examine hydroclimate variability across regional, continental, and global scales [592, 213].

Currently, general circulation models (GCMs) are used as fundamental tools to understand the behavior of land-ocean-atmospheric circulation processes. Understanding these circulation processes might also provide a framework for assessing hydrological cycle variability. However, GCMs still face significant challenges that can impact the reliability of their results and projections. One of the issues is that GCMs heavily rely on observational data for validation, and often, the record length is insufficient to capture the complete range of variations in the hydrological cycle [269]. Moreover, the GCM outputs offer considerable potential for comprehending the underlying mechanisms of climate variability. Additionally, GCM simulations, including paleoclimate reconstruction, could hold promise in minimizing the uncertainties linked with model physics, internal climate variability, and external forcings [476]. Consequently, this kind of coupled approach will allow us to identify the chronological paleoclimatic variations, thereby enhancing our understanding of both past and future hydroclimate regimes. To address this shortcoming, millennium-long proxy records could be valuable in model validation and in improving the ability to simulate the hydrological cycle [73].

This study aims to identify variability in the hydrological cycle, specifically pertaining to precipitation and temperature, during various geological periods. The geological times to be included are as follows: the Mid-Miocene Climate Optimum, Ice Age, Eemian (Last Interglacial), Last Glacial Maximum, Heinrich and Dansgaard–Oeschger Events, Holocene, Bølling-Allerød, Younger Dryas, the 8.2 ka event, Medieval Climate Anomaly, and Little Ice Age. This understanding will contribute to achieving more precise monitoring of the

hydroclimate system, ranging from the regional to the continental scale, and its impacts on ecosystems, crop production, and water resources.

3.3 Intensification of hydrological cycle

3.3.1 Basic theory

There exists a robust theoretical foundation linking atmospheric warming to the intensification of the hydrological cycle. Furthermore, a positive correlation has been observed between atmospheric temperature, evaporation, and precipitation [151]. This relationship finds its basis in the Clausius–Clapeyron (C-C) relation, which posits an exponential association between specific humidity and temperature elevation [242]. Additionally, the C-C relation proposes that the slope of this connection should remain below 6.5% per Kelvin degree, owing to the energy-limited nature of evaporation [13]. While both evaporation and precipitation are energy-limited processes, the atmosphere must be capable of radiating away the latent heat generated during precipitation events [407]. This intricacy renders the estimation of precipitation response under energy-constrained conditions a challenging endeavor.

3.3.2 Model experiments

Given the intricacy, climate models are extensively utilized for estimating the intensification of the hydrological cycle [338, 466, 578]. Nevertheless, there persists considerable variability in the outcomes of GCMs, although a consensus exists that there is an observable anthropogenic impact on the rise of global mean precipitation [539, 409, 382]. For instance, Allen and Ingram [13] reported an approximate 3.4% increase in precipitation per Kelvin degree, while [585] suggests a more gradual rate of around 1 to 3% per kelvin. Notably, a study employing 20 coupled ocean-land-atmosphere models projects a global increase of 5.2% in precipitation, 7.3% in runoff, and 5.2% in evaporation in response to a mean surface air temperature increase of 2.3°C by 2050 [586].

Furthermore, congruent findings emerge from simulations of the hydrological cycle

over the past half-century [159]. In this context, a 4% rise in precipitation was documented in response to a 0.5°C warming. Additionally, following the Clausius-Clapeyron equation, tropospheric warming is predicted to increase the atmospheric water holding capacity by approximately 7% per Kelvin [540, 497, 396]. Nonetheless, the precise quantification of the relationship between temperature and the hydrological cycle remains unresolved.

Model experiments also reveal that the intensification effect extends beyond global precipitation, significantly impacting regional amplification of the hydrological cycle [298]. Moreover, regional model analyses over the United States indicate increased variability in daily precipitation, with some areas displaying reduced precipitation frequency but higher daily mean precipitation amounts [369]. Further investigations into regional daily precipitation variability suggest a rise in convective precipitation across low and mid-latitudes, alongside a decrease in non-convective precipitation over mid-latitudes and an increase in high-latitudes [220]. The primary conjecture concerning regional changes (as a consequence of hydrological cycle intensification) is that wet regions become wetter and dry regions become drier [218]. However, in contrast to the global scale, hydroclimate variability at the regional scale holds great significance, as evidenced by a zonal average precipitation increase of about 7 to 12% between 30°-85°N and a 2% increase over 0°-55°S [233].

3.3.3 Observational evidence

Ground-based observations are widely acknowledged as more reliable sources for tracking and estimating climate perturbations. Additionally, for discerning the chronological patterns of global hydrological cycle variations, consistent, long-term spatio-temporal data records hold considerable significance. Observational paleoclimate (proxy) records reveal that the environment and climate conditions were distinct from today's state centuries to millennia ago [212]. Pertaining to the hydrological cycle, a comparative examination of long-term precipitation reconstructions over western Central Asia during the late 19^{th} and 20^{th} centuries suggests a substantial intensification since the onset of industrialization and global warming [543].

Moreover, spatial reconstructions of hydroclimate variability over the past twelve cen-

turies across the Northern Hemisphere indicate a larger percentage of land area experiencing relatively wetter conditions in the 9^{th} to 11^{th} centuries, and again in the 20^{th} century, while drier conditions prevailed from the 12^{th} to 19^{th} centuries [319]. Notably, the Earth's climate encountered a significant abrupt cold event during the Eemian interglacial period (approximately 122 ka). Intriguingly, the anticipated global climate conditions during this period resembled the current interglacial (Holocene) [4]. Conversely, climate changes throughout the deglaciation period brought about alterations in inland water sources, exerting a profound influence on regional hydrological cycles [328]. For instance, studies spanning from 1900 to 1979 indicate a global average precipitation increase of about 2% over land [146, 240].

Additionally, proxy evidence suggests that warming due to variations in Earth's orbital parameters (eccentricity, obliquity, and precession), increasing greenhouse gas concentrations and feedback processes intensified deglaciation during the Last Glacial Maximum [18]. Similarly, proxy analyses demonstrate that around 21 ka, the area and volume of water stored in the form of ice were more than twice as large as today's values [114]. Conversely, deglacial records indicate a mean sea-level rise of about 10 mm/year, punctuated by two extreme episodes at 19 ka and 14.5 ka, causing sea levels to surge by approximately 50 mm/year [598, 116]. Moreover, during the last interglacial (approximately 125 ka), sea levels rose by 4 to 6 meters compared to today [56]. These shifts in ice status and rising sea levels underscore the significant role of these major water distribution resources across the globe, which exhibit sensitivity to climate change.

Rain gauge analyses have indicated a global annual land precipitation increase of 9mm during the twentieth century [393]. Moreover, evaporation, a key component of the hydrological cycle, has displayed increased rates across all continents, with significant changes observed in eastern South America, various parts of Africa, and southern Asia [381]. Substantial evaporation changes have also been documented over North America, western Asia, and Europe [273]. Climatologists anticipate that a warmer future climate will heighten drought frequency by decreasing regional precipitation and increasing evaporation [485]. Furthermore, it is expected that increased global temperatures will not only intensify global ET and precipitation (P) but also lead to an increase in ET over mid-latitude regions, poten-

tially resulting in an increased drought frequency [156].

Moreover, hydroclimate evaluations across the tropics and subtropics under warming scenarios suggest a trend: 'dry regions becoming drier and wet regions becoming wetter' [218, 425], accompanied by a widespread expansion of dry land areas [218, 319]. However, assessments of hydroclimate during the Pliocene suggest the opposite trend, with subtropics becoming wetter and certain tropical regions experiencing drying, encapsulated by the phrase 'Dry is getting wetter, wet is getting drier' [95]. Furthermore, an analysis based on observed SST proposes that the residence time of water vapor has extended, linked to a decline in the global water vapor cycling rate [70]. Notably, tropical precipitation over land areas has exhibited a decrease concomitant with increased SST [283].

Moreover, precipitation trend analyses using both model simulations and observations over the twentieth century reveal increased precipitation over the tropics and subtropics of the Southern Hemisphere, as well as over areas poleward of 50°N in the Northern Hemisphere. Conversely, decreased precipitation has been noted over the tropics and subtropics of the Northern Hemisphere [612]. The El Niño-Southern Oscillation, a recurring climate pattern characterized by El Niño (warming) and La Niña (cooling) phases over the eastern and central tropical Pacific Ocean, plays a substantial role in directing the total volume of atmospheric water vapor originating from continental land surfaces [294, 382]. Furthermore, it is anticipated that future El Niño conditions may intensify [122], potentially leading to a progressive reduction in the total water flux into the atmosphere [382].

Considering the increasing Earth's temperature, the Intergovernmental Panel on Climate Change has proposed that the global average surface temperature has risen by approximately 0.6°C, surpassing observations from the past 1000 years, and is projected to surge by 1.48 to 5.88°C by 2100 [233, 365]. Furthermore, rising temperatures are anticipated to be a driving force behind the augmentation of atmospheric moisture and water vapor transport rates. As a result, evaporation and precipitation rates have increased, causing alterations in the global spatio-temporal distribution [542, 169, 425].

In addition, climatologists are currently concentrating on estimating and quantifying the intensification trend in the global hydrological cycle under the influence of increasing

temperature scenarios. Moreover, studies examining natural variations in the hydrological cycle and spatial coverage across six continents (Africa, Asia, Europe, North America, Oceania, and South America) indicate that time spans of 35 to 70 years are necessary to discern warming-induced intensification in the global hydrological cycle [622]. Additionally, to detect potential trends in hydrological cycle changes under climate change, primarily global warming, sustained climate observations spanning several decades to over a century will be of significant importance [363].

3.4 Hydrological cycle shifts and past climatic variability

3.4.1 Deep past: Mid-Miocene Climate Optimum

It is anticipated that past warming-related climate events, driven by the effects of GHGs, could serve as analogs for projected climates under existing GHG emission scenarios [370]. Such assessments of past warming events can provide insights into the biogeochemical and physical interactions that occur during rapid climate shifts. Paleoclimate investigations suggest that Earth has undergone numerous warm and cold abrupt events with relatively high-amplitude temperature fluctuations over the last approximately 65 million years and beyond [604]. Among these events, one of the most recent warming-related occurrences, relative to future projections based on current warming scenarios, is noted during the middle Miocene period (17 to 14.50 million years ago) [600]. Enhancing our comprehension of climate records, global hydrological cycle trends, and the factors driving them is crucial for monitoring their impacts on both society and ecosystem evolution.

During the middle Miocene, both deep-ocean waters and middle to high-latitude regions experienced significantly warmer conditions, a phase referred to as the Mid-Miocene Climatic Optimum (MMCO) [61]. The MMCO is characterized by high-amplitude climate variations attributed to intense perturbations in the carbon cycle [229]. The driving hypothesis behind the MMCO event revolves around fluctuations in the partial pressure of carbon dioxide (pCO_2) [559]. Proxy reconstructions utilizing alkenones [613], paleosols [81], stomata [199], and marine boron isotopes [198] indicate that during the MMCO, at-

mospheric pCO_2 was around 450 ppm or lower, a value in close proximity to current levels and expected pCO_2 predictions [510]. Additionally, it has been observed that during the MMCO, CO_2 concentrations were similar to present levels [190]. However, the role of CO_2 in driving the warming of the Miocene period remains a subject of controversy. This is because alkenone [613] and boron [176] based proxy records suggest CO_2 concentrations equal to or less than today's levels [417]. In contrast, stomatal analysis proposes significantly higher concentrations (approximately 400 to 500 ppm) [284].

Conversely, the hydrogen isotope record from the middle Miocene, obtained from central North America, indicates an increased global temperature around 14 million years ago (Mya) that led to a climatic optimum and increased regional-scale variability in the hydrological cycle [265]. Similar conditions are evident in macrofossils and continental paleosols sampled from North America, suggesting increased precipitation [448] and temperature [177]. Modeling approaches for the Miocene also imply widespread increases in mean annual precipitation across northern and central Africa, North America (above 50°N), northern Eurasia, and Greenland [224]. Temperature reconstruction and modeling further reveal that the annual global mean temperature during this period was approximately 3 to 8°C higher than pre-industrial levels [428]. Isotope analysis of a network of deep-sea cores also indicates perturbations in global climate, with peaks of warmth around 16 Mya [604].

Investigations into nannoplankton also support the idea of a warmer climate and sea-level fluctuations during the middle Miocene [207]. Additionally, the global volume of ice was low, and slightly warmer sea bottom water conditions are suggested around 15 Mya [380], although there were some brief episodes of glaciation (such as Mi-events) [379]. Moreover, during the MMCO event, deep-ocean water temperatures are estimated to have been approximately 5 to 6°C warmer than present conditions [605]. The increased value of δ^{18}O indicates a significant change in the ocean-atmosphere system, likely linked to deep-water circulation and a significant step towards a colder polar climate [590].

Between about 16 to 14.8 Mya, the competition between warm low latitude (eastern Tethyan-northern Indian Ocean) and cold high-latitude (Southern Component Water) sources is believed to have influenced variability in the Antarctic climate and cryosphere [174]. During this time, short-term changes in the volume of the East Antarctic Ice Sheet have also

been observed [174]. Furthermore, the middle Miocene record indicates significant changes in continental climates, including increased aridity across mid-latitude continents such as Africa [449], Australia [508], South America [411], and North America [588].

3.4.2 Ice age

3.4.2.1 The Eemian: Last Interglacial

The Last Interglacial, also known as the Eemian Interglacial Stage and Marine Isotope Stage (MIS) 5e, was a period characterized by a globally warmer climate, considered as an analogue to the present interglacial. However, there are different proposed temporal scales for the Last Interglacial, ranging from about 130 to 115 thousand years ago (ka) [484, 144] to about 129 to 116 ka [313]. Oxygen isotope estimations suggest relatively stable climate conditions during this period, with temperatures around 5°C higher than present [20]. However, various proxy reconstructions indicate global surface temperatures up to approximately 1.3°C higher than today [170], with global average land surface temperatures about 1.7°C higher and ocean temperatures about 0.8°C warmer than pre-industrial levels [405].

Furthermore, middle and high northern latitude land masses experienced significantly warmer temperatures, around 2°C to 5°C higher [546], which aligns with future projections based on global warming scenarios [106]. Ice core analyses from the Last Interglacial age suggest higher concentrations of GHGs compared to preindustrial values, with about 10% higher summer insolation observed over high-latitudes [422]. Variations in Earth's orbital parameters are believed to have influenced the patterns of seasonal insolation over the Northern Hemisphere, resulting in greater variability than observed today [51].

Additionally, it is hypothesized that Earth's orbital changes may have led to fluctuations in temperature at seasonal scales [385]. Water isotope estimations from Greenland ice cores suggest a warmer Arctic atmosphere, which implies a reduction in the area of average annual sea ice [337]. During the Last Interglacial (MIS-5e), the warmer climate caused the retreat of ice sheets, resulting in higher sea levels compared to the present [275]. The SST during this period is estimated to have been nearly the same, but global sea levels were higher by about 6 to 9 meters compared to today [275].

Paleoclimate reconstructions indicate that SSTs were around 0.5°C warmer (up to 1°C over high-latitudes) on average globally during the Last Interglacial, with the peak warmth occurring during its early stages [228]. On the other hand, reconstructions of global mean surface temperatures, using annually-averaged and seasonal temperature evidence, suggest a warming of up to 2°C (maximum) during the middle of the Last Interglacial period [496].

Additionally, there has been considerable variability in climate on a large scale. Climate conditions during the Eemian period are expected to be similar to the ongoing interglacial period [354]. Moreover, evidence from proxies indicates a probable increase in summer monsoons across the Northern Hemisphere during the Last Interglacial period [572]. Proxy evidence also suggests enhanced precipitation over the Northern Hemisphere, primarily in the equatorial region, with most proxy sites indicating wetter conditions [587]. In contrast to the Holocene period, both proxy evidence and modeling approaches suggest wetter conditions in most regions of the Arctic [268] and the boreal mid-latitude regions [372] during the Last Interglacial period.

Furthermore, both proxy data and modeling approaches explicitly suggest greater monsoon activity over North Africa and Asia, while the Australian monsoon appears to be weaker during this time [473]. Conversely, an analysis of oxygen isotopes and elemental ratios in fossilized coral samples from North Sulawesi, Indonesia, suggests interannual fluctuations in precipitation and SST as consequences of the El Niño-Southern Oscillation (ENSO) [236].

Additionally, assumptions derived from global ocean model simulations propose that the hydrological cycle was stronger during the Eemian Interglacial compared to the Holocene [579]. Proxy estimates indicate that the Last Interglacial Asian monsoon lasted for approximately 9.7 thousand years, marking its onset with an abrupt decrease in O^{18}/O^{16} values at 129.3 ka and its conclusion with a sudden increase in O^{18}/O^{16} values at 119.6 ka [600]. Furthermore, the conclusion of the Last Interglacial period was characterized by colder conditions, whereas the onset saw abrupt climate variations [20].

Moreover, GCMs propose a stronger Southeast Asian monsoon during the Last Interglacial period. This phenomenon is attributed to the maximum insolation forcing over the

northern hemisphere resulting from Earth's orbital precession [431]. It is suggested that if climate warming led to sudden and substantial climate variability during the Eemian period, similar warming events could occur in the future during the ongoing interglacial period [4]. Therefore, investigations into this interglacial period will enable us to examine the behavior of the hydroclimate system under varying radiative forcing and the associated conditions of higher surface temperatures.

3.4.2.2 Last Glacial Maximum

The Last Glacial Maximum (LGM) corresponds to the peak of the last ice age, ranging from 26.5 to 19 ka, when ice sheets reached their maximum extent and total mass over much of the continent. This period is commonly referred to as the LGM [117]. However, radiocarbon dating of sediment samples taken from Lake Ioannina in Greece suggests an alternate timeframe for this period, spanning from 30 to 15 ka [432]. During the LGM, climate conditions in the high-latitudes of the Northern Hemisphere are generally believed to have been colder and drier compared to the present [53, 406]. Additionally, global temperatures during the LGM were noticeably lower than present temperatures [598].

Moreover, temperature estimates for the Greenland Summit during the LGM indicate temperatures approximately 20°C cooler than present [251, 252]. Furthermore, the tropics experienced lower temperatures [580], with cooling of up to about 26°C over the Laurentide ice sheet region [96]. Coral, ice core, and ocean core analyses collectively suggest significantly cooler tropical temperatures during the LGM compared to modern values [42, 528, 141]. Different reconstructions based on Mg/Ca ratios also indicate that the tropical region was 2 to 3.5°C cooler than present during the LGM [41], a range consistent with model results that suggest a cooling of approximately 2.5°C across equatorial regions [137].

Furthermore, simulations involving annual average insolation at 21 ka indicate that areas equatorward of 45°N and 45°S experienced slightly higher insolation, while areas poleward of these latitudes received less insolation [96]. Additionally, model simulations using the Community Climate System Model 3.0 (CCSM3) slab ocean model suggest that roughly half of the global cooling during the LGM can be attributed to the reduced atmospheric concentration of CO_2 (about 50% of today's levels) [406]. While the expansion of continental

ice and the decrease in atmospheric CO_2 concentrations both contributed to global cooling, the impact of the ice sheets was primarily limited to the Northern Hemisphere, whereas the reduction in CO_2 affected cooling in both hemispheres [83]. Furthermore, most proxy records indicate prevailing dry conditions in both hemispheres, likely associated with lower tropical land and SST. Additionally, the global hydrological cycle during the LGM is inferred to have been weaker compared to the present [185].

Furthermore, simulations of the LGM reveal a considerable temperature decrease associated with a drop in atmospheric water vapor concentration, resulting in a weakening of the global hydrological cycle due to around a 10% reduction in both evaporation and precipitation [97]. Alongside LGM simulations, it has been hypothesized that excess precipitation relative to evaporation led to a decrease in the net amount of water vapor in the atmosphere [96]. Over the African region, a negative shift in precipitation time series has been identified, with a rising trend since 30 ka and a decline during the LGM. Calculated precipitation values during the LGM are approximately 15 to 20% lower than present levels [413]. Furthermore, analyses of ice cores and marine sediments suggest increased eolian (dust) deposition compared to modern levels [134, 506], likely due to the reduced intensity of the hydrological cycle [603] and drier conditions. Interestingly, the extra-tropical regions during the LGM indicate wetter conditions [114].

Estimates of global LGM climate also indicate drier atmospheric conditions, with a decrease of about 18% in precipitable water and annual average precipitation of approximately 2.49 mm per day [406]. Additionally, evaluations of lake sediments from Lake Baikal for climate simulations over southern East Siberia show an approximate 11% reduction in annual precipitation and an 80% decrease in summer precipitation around 21 ka compared to the present climate [403]. Furthermore, yearly precipitation over the Greenland Summit is predicted to be up to three times less than modern values [138, 252]. Conversely, both proxy records and model simulations (using CCSM3) suggest a weakened summer monsoon for both tropical and northern Africa [433].

In the contemporary climate, the precipitation pattern over central Europe is influenced by a westerly to northwesterly circulation system (across the northern and western slopes and the Mediterranean region). However, during the LGM, atmospheric moisture is ob-

served to be produced through south-westerly advection [44]. This is supported by oxygen isotope analysis of speleothems from the Sieben Hengste cave in the Bernese Alps, which indicates southwesterly moisture advection during the 26.5–23.5 thousand years period [322].

Regional climate modeling suggests an annual average air temperature about 6-9°C lower than present over central Europe, with increased winter precipitation rates over the southern region and decreased rates over the northern part of Europe [514]. Moreover, lake records from East and Southwest Amazonia also indicate lower precipitation levels than the present [3, 489]. Additionally, analysis of lake sediments from Pretoria Saltpan in South Africa suggests a negative shift in the onset and offset of monsoonal precipitation at around 30 ka and 20 ka, respectively, with assessed precipitation values approximately 15 to 20% lower than current levels [413].

Furthermore, diatom estimates from the same site also suggest drier conditions [374]. However, the climatic conditions of the LGM remain a topic of interest due to contradictory findings. For instance, assessments of lake levels in East Africa suggest wetter conditions for certain basins compared to the present, while analyses of paleovegetation indicate a dry climate [40]. Conversely, the expansion of mountain glaciers across the eastern and central Mediterranean regions implies a wetter LGM relative to the present [282].

3.4.2.3 Heinrich and Dansgaard–Oeschger Events

During the late stages of the last glacial period, Earth experienced significant fluctuations and abrupt changes in the climate system, particularly in the North Atlantic region [149]. Proxy evidence indicates a highly unstable climate marked by over 24 distinct cooling and warming events known as Dansgaard-Oeschger (D-O) events [442]. These events are characterized by abrupt warming across most of the Northern Hemisphere [353]. However, the underlying causes of D-O events remain a subject of intense debate, ranging from internal ocean-atmosphere system oscillations [86] to cyclic calving of the Greenland ice sheet [551] and external forcings [550].

Furthermore, it is hypothesized that the cooling and warming during D-O events might be linked to changes in the Atlantic thermohaline circulation [85]. Under warmer condi-

tions, the thermohaline circulation resembles the present pattern, with sinking occurring at shallower depths and lower latitudes during stadial states [15]. Isotope (δ^{18}O) analysis of the Greenland Ice Sheet Project 2 (GISP2) ice core reveals repetition periods between D-O events ranging from 1 to 12 thousand years over the past 90 thousand years [65].

In the context of D-O events, pollen proxy records from the western Mediterranean [390] and Italy [15] exhibit lower δ^{13}C values, suggesting an increased rate of precipitation over the western Mediterranean region [94]. Additionally, δ^{18}O records from GISP2 and GRIP ice cores show low δ^{13}C values and higher ice δ^{18}O values, indicating higher precipitation (at least in Greenland) and warmer climate conditions [187]. The increased δ^{18}O values correspond to higher temperatures [253]. Moreover, assessments of δ^{18}O values in Great Basin lakes reveal variations in lake levels, with decreased δ^{18}O values suggesting increased lake levels likely due to enhanced precipitation [50]. On the contrary, ice core analyses from Greenland suggest rapid increases in atmospheric temperature, ranging from around 10°C [94] to 16°C [293], occurring within a few decades. These analyses also indicate an abrupt temperature shift between the interstadial (warm) and stadial (cold) states during D-O events [149]. Furthermore, polar ice core analyses highlight a positive association between methane (CH_4) levels and the widespread effects of D-O events, which act as warming events [91].

Furthermore, these large-scale climate oscillations are evident in oxygen isotope estimates from the Soreq cave in Israel [37] and deep-sea records [483]. Additionally, analyses of lake sediment from Lago Grande di Monticchio in southern Italy and sediment cores from the Mediterranean Sea, incorporating tephrochronology, indicate that the ocean-atmosphere system in the Northern Hemisphere not only influenced the North Atlantic and Greenland regions but also had impacts on the central Mediterranean area [15]. Similarities are found between a multitude of high-resolution climate records from South America [421] and Asia [571] and the records from Greenland ice cores.

Marine core data from the Indian Ocean also exhibit strong correlations with the D-O cycles [19]. Analysis of Bahamian stalagmites reveals the occurrence of D-O events around 44 ka, with the onset of events 7 and 8 occurring around 34 - 41 ka [43]. Comparisons of isotope analyses between the Greenland ice core and stalagmites from Socotra Island in

the Indian Ocean suggest an age of D-O event 12 around 45 ka, consistent with estimates from the GISP2 ice core [187], as well as the GISP1 ice core [149]. Moreover, D-O event 19 (approximately 70 ka) has been proposed as one of the larger events during the glacial period [293].

The climate system during the last glacial period was far from stable, as both Heinrich events and D-O events occurred recurrently throughout this period. Paleo-climatologist Hartmut Heinrich investigated six distinctive intervals of extreme cold events (ranging from about 14 to 70 ka) between D-O events. These events, however, occurred less frequently than D-O events [63, 215]. Analysis of North Atlantic sediments, detailing the last glacial cycle, suggested a higher occurrence of iceberg discharges and ice-rafted debris at intervals of approximately 7 to 10 thousand years, which are known as Heinrich events [408]. Furthermore, examinations of sediment cores from the Andaman Sea and northeastern Indian Ocean (Bay of Bengal) indicate that fluctuations akin to D-O events during interstadials led to increased variability in the Indian summer monsoon, while drier conditions prevailed during North Atlantic Heinrich events [121].

Radiocarbon assessments conducted using accelerator mass spectrometry at the Deep-Sea Drilling Project (DSDP) site 609 provided ages for the first three Heinrich events at around 14.3 ka, 21 ka, and 28 ka, and ages for the subsequent three events at approximately 41 ka, 52 ka, and 69 ka [88]. Globally, Heinrich events are widely recognized, impacting vast regions of Eurasia and North America, resulting in colder and drier conditions [26, 563].

During Heinrich Events, a cooling of about 5 to 8°C in Mediterranean surface waters has been observed, evident from the abundance of plankton N. Pachyderma (sin.) in sediment records [457]. Pollen analysis from crater lake sediments during Heinrich event 1 indicates a dominance of grasses, suggesting increased continental aridity over the tropics [304]. Lower ocean surface productivity and alterations in circulation processes over the North Atlantic mid-latitude regions [528] are believed to have caused cold and arid climates not only in Greenland but also in Antarctica and central China [529]. The impact of Heinrich events on the Laurentide ice sheet, leading to a decrease in its height, resulted in the development of a low-strength glacial anticyclone causing cold and wet conditions over the Pacific Northwest [312, 201]. During the last glacial period, the North Atlantic was

bordered by extensive ice sheets, which periodically released large amounts of fresh water into the region [306].

Furthermore, it has been noted that increased trade winds heightened moisture supply and heat transport from the equator to the North, potentially contributing to the buildup of ice sheets across the Northern Hemisphere [462]. This process is believed to have led to enhanced calving and the formation of Heinrich layers in the North Atlantic. Paleoclimate records indicate significantly reduced precipitation during stadials, while interstadials experienced increased precipitation [340]. A study conducted on Lake Tulane in Florida reveals that Pine phases coincided with long stadials across the North Atlantic. During these Pine phases, lake levels were higher and the climate was significantly wetter [202]. However, the factors driving Heinrich events remain unknown and continue to be a subject of debate.

3.4.3 Holocene

3.4.3.1 Bølling-Allerød

The upturn in abrupt temperatures across the Northern Hemisphere and the reinvigoration of the Atlantic Meridional Overturning (AMO) circulation at the onset of the Bølling-Allerød interstadial, around 14.7 ka, are among the most remarkable deglacial events [115]. However, the underlying physical mechanisms behind these events remain unknown. It is speculated that the influx of warm waters into the deep North Atlantic Ocean played a role in triggering the Bølling-Allerød interstadial and the revival of the AMO circulation [526]. Paleotemperature reconstructions based on δ^{18}O analysis of the GRIP ice core suggest that the Bølling climate was about 1°C colder than present, the Allerød was 5-12°C colder, and the Bølling-Allerød interstadial marked a warmer climate period [251].

Similarly, analyses of lake records also indicate that the Bølling-Allerød interstadial was a warmer and wetter period, spanning from around 14.8 to 12.85 ka [400]. Dust concentration-based estimations suggest the duration of the Bølling to be approximately 1432 years, and the Allerød around 736 years [477]. Sediments from Lago di Origlio in the Southern Swiss Alps indicate that the onset of the Bølling-Allerød interstadial saw an abrupt warming of

about 2.5 to 3.2°C around 14.55 ka [463]. Additionally, quantitative temperature estimates based on sediment analysis from the Aegean Sea and Lake Maliq reveal an increase in average annual temperature of around 10°C during the onset of the Bølling, which remained relatively stable thereafter [67, 276]. This abrupt warming event is also considered one of the D-O warm events [517]. On the other hand, δ^{18}O analysis of Crawford Lake in southern Canada indicates the occurrence of three colder events of century-scale duration within the Bølling-Allerød interstadial, accompanied by negative carbon isotope excursions of 0.5-0.8 ‰. These events are referred to as the intra-Bølling, intra-Allerød, and Older Dryas [263, 300, 149].

During the Older Dryas event, a dry and cold climate with high evaporation was observed. Europe and Greenland exhibited a similar cooling pattern during this time, but Greenland experienced significantly colder conditions during the intra-Bølling and intra-Allerød phases compared to Europe [602]. This suggests a shifting climate gradient over the Atlantic, possibly influenced by changes in atmospheric circulation patterns [194]. The oxygen isotopic composition (^{18}O/^{16}O) of precipitation is influenced by climate factors such as precipitation amount and temperature [148]. Oxygen isotope analysis from the Timta Cave stalagmite in the western Himalayas indicates increased precipitation variability during the Bølling-Allerød interstadial over India [491].

Furthermore, the δ^{18}O record from Lake Panch Pokhari in Nepal reflects a strengthened (low δ^{18}O) Indian summer monsoon during the Bølling-Allerød interstadial and early Holocene, while it was weak (high δ^{18}O) throughout the Younger Dryas stadial [608]. Sediment analysis using radiocarbon dating from Lake Laguna de Los Anteojos in Venezuela suggests wetter and warmer conditions at the onset of the Bølling event across the northern tropics [502]. A significant increase in tropical precipitation across the Atlantic region of Africa has also been observed around 14.6 ka [435]. Moreover, the isotopic concentration of deuterium in leaf waxes in a marine core from the Gulf of Aden indicates abrupt rewetting over equatorial Africa [533].

Sediment analysis from Lake Prespa in Greece suggests increased humid conditions during the Bølling-Allerød interstadial due to enhanced atmospheric moisture availability [27]. This increased humidity is consistent with a higher number of annual rainfall re-

constructions at Lake Maliq [67], in the Eastern Mediterranean [38], and at Lago Grande di Monticchio in Italy [11]. Analysis of lake sediment cores from Lake Petén Itzá in Guatemala indicates prevailing humid conditions during the Bølling-Allerød interstadial, with a short dry phase around 13.8 ka [227].

At the onset of the Bølling-Allerød interstadial, a decrease in gypsum precipitation and an increase in clay sediment content in the Cariaco Basin suggest wetter conditions, consistent with growing lake levels in La Yeguada and El Valle, Panama [98]. Similarly, element and sediment analyses imply increased rainfall over the Caribbean region during the Bølling-Allerød interstadial, associated with the northward movement of the Intertropical Convergence Zone (ITCZ) [237]. The higher proportion of *Artemisia* and *Chenopodiaceae*, negative δ^{13}C, and lower values of magnetic susceptibility in peat suggest the Bølling-Allerød interstadial was characterized by higher precipitation and increased monsoon activity over the northwest margin of China [618]. The variable timescales and amplitudes of cold and warm phases are well-documented in terrestrial records across widespread regions, leading to the fundamental assumption that these phases are hemispheric in response throughout the late-glacial interstadial [552].

3.4.3.2 Younger Dryas

The last deglaciation period experienced a general warming trend, which was disrupted by the Younger Dryas, an abrupt cooling phase characterized by widespread changes in environmental conditions [147]. The Younger Dryas is identified as the last glacial cold event in the North Atlantic region, spanning from 13,000 to 11,700 years ago [164]. This period is marked by alternating severe and less arid climate states [419]. The onset of the Younger Dryas is associated with dry conditions [227], while its end is marked by a short-term severe cold period, including dry winter monsoons [618].

The dry conditions during the Younger Dryas are evident in the GISP2 ice core records, with distinct episodes of increased dustiness occurring at approximately 12.64 ka, 12.22 ka, and 11.81 ka [359]. The cooling event of the Younger Dryas is also characterized by a reduction in pine vegetation and negative δ^{13}C values as analyzed from the Sofular Cave [487, 173]. Hydrogen isotope composition in lake sediments from Lake Meerfelder Maar in

western Europe indicates decreased values for both terrestrial and aquatic lipids (around 12.8 ka), suggesting a cooler climate in the region, which is synchronized with the abrupt cooling event recorded in Greenland [438].

The transition from the Allerød to the Younger Dryas climate, as seen in the lake geochemistry and microfacies analysis from Meerfelder Maar in western Germany, is marked by a sudden increase in storminess during the autumn and spring seasons. This pattern is thought to be linked with changes in the North Atlantic Oscillation (NAO) overturning circulation and reduced heat transport to western Europe due to advancing sea ice southward [77]. Proxies and modeling approaches suggest a significant decline in the NAO overturning circulation, which could be a contributing factor to the Younger Dryas cold event [368]. However, the Younger Dryas event does not show consistent patterns globally. It exhibits cool conditions across high-latitudes and relatively warmer conditions over low-latitudes [181]. In mid-latitudes, such as China, records suggest alternating cool-wet and cold-dry conditions on a century-scale [618].

During deglaciation in the Northern Hemisphere, the release of meltwater into the North Atlantic region is believed to have had a significant impact. This influx of freshwater likely decreased temperatures in western Europe by 4 to 6°C on centennial timescales and might have led to widespread environmental changes [193]. However, due to the scarcity of high-resolution and well-dated terrestrial paleo-hydrological records, the precise role of hydrological changes during the Younger Dryas is still not fully understood [438]. The sequence of events during the onset of the Younger Dryas in Europe and the records from Greenland ice cores remain a topic of debate [441].

Reconstructions of temperatures during the Younger Dryas period reveal significant cooling in various regions. For example, temperature records show a cooling of about 15°C over central Greenland [251], 6 to 7°C over Poland [193], and a reduction of 6 to 9°C in the Norwegian Sea based on diatom analysis [263]. In contrast, temperature reconstructions using pollen records from east Beringia suggest a milder drop in temperature of about 1.5°C, accompanied by reduced net precipitation during the Younger Dryas [179].

The variation in precipitation and temperature during the Younger Dryas is linked to the

presence of a persistent high-pressure cell over the re-extended North European ice sheet. This led to the southward flow of cold northern air masses towards the Mediterranean region, resulting in drier and colder conditions over the Mediterranean area and the Aegean Sea [67]. The reduction in precipitation during the Younger Dryas and other cold stadials corresponds with cooler North Atlantic SST and is associated with the strengthened Trade Winds and the southerly mean location of the ITCZ [420]. The southward shift of the ITCZ during the Younger Dryas onset explains the cooler phases across the northern tropics and the expansion of precipitation-sensitive glaciers in the southern tropical mountains [469, 502]. However, a northward shift of the ITCZ after about 12.65 ka corresponds to a warming trend and increased moisture balance over the northern tropics [469, 502].

In the southern hemisphere, enhanced precipitation is observed during the Younger Dryas and the Heinrich Events [25]. Pollen records from Lake Hulun in China indicate the dominance of the plant *Betula*, which thrives in cool and wet conditions, suggesting increased monsoon precipitation [569]. Most records from South America indicate more arid conditions across the northern tropical Andes and wetter conditions over the southern tropical Andes during the onset of the Younger Dryas [502]. The hydrology and land temperatures in tropical South America are strongly influenced by low latitude SST, suggesting that climatic variability during the Younger Dryas may have been influenced by tropical oceans' atmospheric dynamics [119].

Sediment analysis from Lake Meerfelder Maar in western Germany reveals positive values of hydrogen isotopes for precipitation and reduced evapotranspiration at around 12.2 ka and 12.04 ka, indicating wetter and warmer conditions during those periods [438]. These conditions are likely related to increased climatic instability, including fluctuating westerly storm tracks, driven by changing sea ice cover in the North Atlantic region [32, 462].

Greenland ice core analyses suggest radical and abrupt changes in the North Atlantic region during the transition from the Younger Dryas to the Pre-Boreal event, including a decrease in storminess, a 50% increase in precipitation rate, and a 7°C warming [147]. Radiocarbon analysis of lake sediments from Laguna de Los Anteojos in Venezuela also points to abrupt cold and drier phases during the Younger Dryas [502]. Lake sediments

from Lake Titicaca, near Bolivia and Peru, suggest an overflow of the lake and increased precipitation between 13 ka and 11.5 ka, coinciding with the Younger Dryas period in the North Atlantic region [31]. Concentration variations of trapped CH^4 gases in the GRIP ice core indicate that tropical and subtropical climates were cooler and drier during the Younger Dryas [107]. However, it's important to note that CH^4 concentrations might be influenced by the areal coverage of wetlands, which are significant sources of this gas in low latitude regions [107].

3.4.3.3 The 8.2 ka event

The '8.2 ka cold event' is a significant climate anomaly in Earth's history that had a global impact, although its most pronounced effects were observed over the North Atlantic region [14]. This event lasted for approximately 160.5 ± 5.5 years, with the coldest conditions lasting for about 69 ± 2 years [527]. Other estimates suggest that the event lasted around 150 years [495] or 200 years [561]. Proxy evidence indicates that this cold event affected the entire Baltic Sea basin, except for regions north of 70°N [68]. Western Europe also experienced cooling during this event, with the coldest temperatures occurring in areas near the NAO [481]. Greenland's proxy records show abrupt cooling of up to about 6°C, accompanied by enhanced windiness and dry conditions over much of the Northern Hemisphere [536], which is similar to present climatic conditions [17]. Atmospheric-sea-ice-ocean models suggest that a weakened thermohaline circulation might explain the occurrence of the 8.2 ka event, and this is consistent with proxy records [446].

Throughout the Holocene and Late Pleistocene, abrupt climate changes and variations in ocean circulation have been closely associated, though the exact driving factors remain uncertain [516, 17]. In the case of the 8.2 ka event, one hypothesized mechanism is perturbations in the Atlantic Meridional Overturning Circulation (AMOC), which could have been triggered by the influx of freshwater into the North Atlantic region. This freshwater input could have led to abrupt climate fluctuations like the 8.2 ka event [39], the Younger Dryas [87], and Heinrich events [215]. It's believed that these freshwater pulses originated from the melting of the Laurentide Ice Sheet and the discharge of meltwater from proglacial Agassiz and Ojibway Lakes around 8.4 ka, potentially causing the 8.2 ka event [39].

The '8.2 ka cold event' is believed to have multiple contributing factors, and its exact cause is still a subject of debate within the scientific community [234]. One proposed factor is the rerouting of runoff from the western Canadian plains due to the collapse of an ice dam across Hudson Bay, which could have contributed to the event's cooling effects [102]. Solar forcing has also been suggested as a potential driver for this event [388]. However, many climatologists support the hypothesis that the 8.2 ka event was linked to perturbations in the North Atlantic thermohaline circulation, weakened by the catastrophic influx of meltwater, particularly during the final phases of deglaciation in North America [185].

Proxy records, including alterations in the oxygen isotope ratios found in Greenland ice cores, indicate that the 8.2 ka event was indeed a cold period, with temperatures decreasing by approximately 6 ± 2°C [10, 17, 149]. The cooling was relatively stable, and the warm climate was interrupted by the cooling conditions, with temperatures decreasing by about 0.9 to 1.8°C between 8.35 ka and 8.15 ka [214]. The most pronounced abrupt changes occurred between 8.4 and 8 ka, resulting in temperature decreases of about 4 to 8°C over central Greenland [17], 1.5-3°C over terrestrial [270, 561] and marine [270, 62] sites in the northeastern NAO region. Model simulations for the 8.2 ka event suggest a cooling of about 2 to 5°C and a reduction of about 30% in precipitation over Greenland [185], consistent with ice core records showing average annual cooling of 3 to 8°C and significant decreases in accumulation [561]. Model simulations also predict a temperature decrease of about 1 to 2°C over northwestern Europe, which agrees with proxy records indicating cooling of approximately 2°C over Germany and the North Sea [270].

During this cold period, increased snowfall is observed globally [68]. Dry and cold conditions prevailed over much of the northern hemisphere, particularly during wintertime, possibly due to a massive outburst flood [14]. Sediment analysis from Lake Annecy in France shows an annual cooling of about 2.5°C and an increase in annual precipitation minus evaporation (P-E) of about 130 mm between 8.3 and 8.2 ka (linked with the 8.2 event), which aligns with various marine and European paleoclimate records [335]. Rising lake levels corresponded with increased yearly precipitation, available moisture, and runoff [332]. The rise in lake levels was particularly strong in central Alpine regions such as Switzerland, France, and northern Italy, while drier conditions prevailed north of approximately

50°N and south of approximately 43°N, including regions like Spain, northern Africa, and southern Italy [334]. Analysis of ice cores from the GISP and GRIP projects also indicated a drop in average temperatures of about 5°C and reduced precipitation during the event [118, 17]. Pollen reconstruction from sediment cores in northern Finland showed an increase in average July temperatures to a maximum of about 12.5 to 13°C, which was 1.4 to 1.7°C higher than today, along with reduced annual precipitation between 8.2 and 6.7 ka [480]. Similarly, a significant decrease in precipitation was observed in records of African lake levels [185].

3.4.3.4 Medieval Climate Anomaly or Medieval Warm Period

The Medieval Climate Anomaly (MCA) is characterized by multi-centennial-scale warm climate events with global implications, spanning roughly from 800 to 1300 CE [239]. During this period, Europe and the North Atlantic region experienced relatively warmer conditions, comparable to or even exceeding temperatures in the later 20^{th} century [239]. Temperature reconstructions from China and surrounding areas also suggest higher-than-average temperatures during the MCA [595]. The warmer conditions in the central North Pacific during the MCA align with the expected extratropical response of a strong La Niña-like pattern over the tropical Pacific, involving cooling in the eastern part and warming in the western part [342]. However, some regions, such as northwestern North America, central Eurasia, and the South Atlantic, experienced anomalous cooling during this period [256].

Most continental temperature records indicate that the initial four centuries from 1000 to 1400 CE were warmer (with an average temperature variation of about 0.1°C) than the subsequent four centuries from 1400 to 1800 AD, despite a cooling trend that began between 1200 and 1300 CE across the Arctic, Asia, and Europe [7]. Climate reconstructions over the Iberian Peninsula reveal warmer and more humid conditions in the northwest, while other parts experienced warm and dry (or arid) conditions [387].

The MCA is also associated with hydroclimatic anomalies at both regional and global levels [394]. While the exact influencing mechanisms for the MCA remain uncertain, some findings using global proxy data suggest a positive NAO associated with La Niña-like processes, amplified by an enhanced Atlantic Multidecadal Oscillation (AMO) circulation [545].

Other factors that may have played a role in the cooling between the 10^{th} and 16^{th} centuries include volcanic activity, solar irradiance variations, orbital-limited insolation changes, and alterations in land cover [135, 162].

The NAO is thought to drive oscillations in the position of storm tracks and the jet stream across Eurasia and the North Atlantic region. A negative state of the NAO can lead to a southward shift in the axis of cyclonic storm tracks and enhanced moisture transport over the North Atlantic, including moist winds from the Mediterranean Sea, resulting in increased precipitation over westerly-influenced areas of Asia [243, 314].

In addition, pollen estimates from Maili Pond in northeast China reveal wet conditions (from 950 to 1290 AD), suggesting an increase in the East Asian summer monsoon during this period [444]. However, proxy analysis over southern China indicates comparatively weak monsoonal precipitation over most regions [111]. Furthermore, the positive state of the NAO results in a northeastward shifting of the axis of cyclonic storm tracks and the highest moisture transport. Synoptic climate conditions and moisture sources lead to drier weather [498]. Additionally, the NAO index (based on tree-ring reconstruction) shows positive NAO indices for the MCA and negative for the Little Ice Age (LIA) [545]. Consequently, this pattern suggests relatively dry climatic conditions across westerly prevailed Asia during the MCA and wet conditions in the LIA [111]. Moreover, most proxy records suggest a decrease in precipitation over the East Asian summer monsoon region during the transition period between the MCA and LIA, around 1300 CE [292].

Furthermore, the assessment of lake sediment oxygen isotopes (δ^{18}O) in the Central Peruvian Andes shows higher values from 900 to 1100 AD, indicating a weakened South American summer monsoon (SASM) and a prolonged period of aridity [55]. Although on millennial timescales, orbitally induced latitudinal variations in the ITCZ, continental convection (tropical), and North Atlantic SST are expected to be important factors for SASM fluctuations [2]. Additionally, evidence indicates high lake depth between 700 and 1350 CE over the Arizona-Monsoon affected region, and it is expected that monsoon intensification is consistent with high solar radiation, derived from minimum radiocarbon estimates [239]. Conversely, multi-decadal reconstruction over the Sierra Nevada shows drought conditions from 800 to 859, 1020 to 1070, 1197 to 1217, 1249 to 1365, 1443 to 1479, 1566 to 1602, 1764

to 1794, 1806 to 1861, and from 1910 to 1934 [197].

Furthermore, during the MCA, a highly variable climate across South America has been monitored, probably showing the humidity dipole between the southern and northern Amazon Basin [346]. Consequently, the wetter phase over the northeast tends to be synchronous with the drier phase over Southern Amazonia [530]. For instance, the El Niño flooding record using a marine core from Peru (at 12°S) shows intense aridity between 800 and 1250 CE [443], while the titanium record from the Cariaco Basin (Venezuela) indicates wetter conditions over the northeast Amazon Basin between 950 and 1450 CE [210].

3.4.3.5 Little Ice Age

The Little Ice Age (LIA) is identified as the most recent cooler period, spanning from around 1350 CE (or 1450) to approximately1900 CE [359]. Moreover, the LIA has been suggested to have undergone very recent interglacial abrupt changes in the climate system [65], which are akin to D-O events [89]. However, the factors that influenced the onset of the LIA remain a subject of debate. Alterations in thermohaline circulation [84], variability in insolation [397], and heightened volcanic activity [135, 453] are anticipated to have played major roles in shaping the LIA. Furthermore, estimates of lake levels and diatom records from Africa [515] and dust records from equatorial ice cores [531] suggest increased wind speed and aridity, linked with enhanced zonal circulation.

Additionally, the anticipated atmospheric circulation patterns during the LIA exhibit more meridional characteristics compared to present patterns [291]. Although increased strength and variability of meridional atmospheric circulation have been observed over the North Atlantic and polar South Pacific at the onset of the LIA, as evidenced by annually dated ice cores from central Greenland, Siple Dome, and West Antarctica [277]. Furthermore, the LIA, as depicted in numerous paleoclimatic records from the Northern Hemisphere and equatorial regions, suggests amplified atmospheric circulation, accompanied by colder and drier conditions [531, 397]. In essence, the rapid climate shifts during the LIA provide an opportunity to scrutinize the involvement of the climate system and its responses to swift changes.

Moreover, ice core analyses conducted near the Ross Sea in Antarctica reveal colder conditions, with surface temperatures approximately 2°C lower, encompassing cooler SST over the Southern Ocean (or expanded sea ice cover), reduced snow accumulation, and intensified katabatic winds [52]. Additionally, the lowest temperatures are estimated to have occurred during the summer, specifically from 1680 to 1730 AD, in both the Southern and Northern Hemispheres [516]. Furthermore, δ^{18}O estimations indicate colder conditions for East Antarctica, whereas West Antarctica experienced relatively warmer conditions [456]. Notably, instrumental records from Switzerland and England indicate warmer conditions during the early 1700s [76]. Furthermore, these records illustrate a correlation between spatially distributed temperatures and heightened atmospheric circulation [277].

Additionally, analysis of air bubbles in the GISP2 ice core suggests that atmospheric CO_2 levels remained relatively constant around 280 ppmv from 1530 to 1810 CE [564]. However, a decline in CO_2 concentrations of about 10 ppm has also been observed between 1550 and 1800 CE in Antarctica, as evident in both the Taylor Dome [245] and Law Dome [163] ice core records. Although modeling approaches using Law Dome records for the same period imply a CO_2 decrease of 6 ppb, which could potentially lead to global cooling of about 0.13°C to 0.21°C [522]. Nonetheless, there are no globally synchronous multi-decadal cold or warm periods that universally characterize the entire Little Ice Age. Instead, most proxy reconstructions generally depict cold phases from 1580 to 1880 AD, punctuated by warm decades in some regions during the 18^{th} century [7].

Furthermore, lower microparticle concentrations in ice core records from the Antarctic Peninsula indicate a likelihood of increased precipitation and intensified cyclonic activity during the LIA [456]. Additionally, the enhanced meridional circulation is also expected to have influenced mid and low latitude circulation, resulting in a shifted westerlies belt that increased precipitation (around 1400 AD) over regions such as Patagonia and California [512]. On the contrary, sediment core records from the northeastern Arabian Sea show a weakened Indian summer monsoon (from 1450 to 1750 AD) with dry conditions prevailing [5]. However, during the LIA, the arid central Asia region experienced relatively wetter conditions, while northern China faced moderately weak monsoons, and southern China experienced pluvial conditions [111]. Furthermore, the connection between the North At-

lantic climate and Asian monsoon patterns remains a consistent aspect of the global climate system [204].

Moreover, both the speleothem record from Scotland [434] and Lamb's reconstruction [290] from England-Wales exhibit notable similarities. They show a 10% decrease in precipitation (from September to June) during the later 13th to the middle of the 14th centuries, followed by a continuous decline from the mid-16^{th} to the late 18^{th} centuries, and a subsequent trend towards current conditions [545]. Correspondingly, a precipitation reconstruction in Banff, Alberta (Canada), indicates periods of increased precipitation from 1515 to 1550, 1585 to 1610, 1660 to 1680, and during the 1880s. However, the 1950s to 1970s demonstrate both enhanced precipitation and decreased summer temperatures [321].

Furthermore, oxygen isotope (δ^{18}O) analysis of speleothems in northeastern Peru reveals variations in monsoon precipitation across northern South America. From the 15th to the 18^{th} century, these records show an average of about 10% higher yearly precipitation compared to the 20^{th} century [450]. Additionally, glacier growth at high elevations in the Venezuelan Andes is interpreted as evidence of increased precipitation, potentially due to a steepened tropical lapse rate resulting from alterations in solar irradiance [424]. Moreover, oxygen isotopes (δ^{18}O) analysis of a lake sediment core in the Central Peruvian Andes shows lower δ^{18}O values during the LIA (from 1400 to 1820), indicating a regionally synchronous intensification of the SASM [55].

3.5 Conclusions

The conclusion drawn from this study suggests that the climate system has undergone numerous unforeseen temperature oscillations, transitioning between cold and warm phases and vice versa. Furthermore, paleoclimatic investigations indicate that abrupt climate changes tend to occur prominently during shifts from one climatic state (cold/warm) to another [58, 16]. Additionally, evidence supports the notion that spatial and temporal variations in the hydrological cycle are influenced by temperature-dependent factors. For example, proxy analyses of the Cariaco Basin (northern Venezuela) yield outcomes similar to those of Greenland ice cores during the last glaciation and deglaciation. This implies a robust

connection between tropical Atlantic temperatures and the hydrological cycle, particularly across the high-latitude North Atlantic [237, 296].

Moreover, since the mid-19^{th} century, the acknowledgment of anthropogenic-induced global warming has become widespread [261]. The gradual warming observed in the 20^{th} century is strongly linked to human activities [464]. Additionally, the 20^{th} century's warming trend clearly contrasts with the cooling observed during the LIA, suggesting that elements of the climate system may still be responding to the abrupt changes initiated during the LIA [289]. Furthermore, analysis indicates the possibility that conditions common to the LIA persisted into the 20^{th} century and may persist further [277].

In recent decades, abrupt climate changes have garnered considerable interest across a broader spectrum of climate studies, including their potential implications for the warming world of the future [16]. Substantial progress has been made in utilizing proxies from the past to construct centennial-scale trends and in employing climate models to discern the roles of anthropogenic and natural forcing in these trends [498]. Undoubtedly, gaining a deeper understanding of past hydroclimate conditions will aid in deciphering their underlying causes and enhancing predictions of hydroclimate changes. However, it's essential to recognize that climate forcings and atmospheric circulation also exert a significant influence on the distribution of the hydrological cycle. While paleoclimate forcings differ considerably from ongoing interglacial anthropogenic influences, many past abrupt events have demonstrated perturbations as a consequence of warm climates, much like the present, characterized by comparable ocean circulations and continental layouts [206].

Furthermore, climate forcings are expected to align with insolation variations on the order of orbital cycles, influencing long-term responses in atmospheric circulation patterns through changes in ice volume (including sea-level changes) [360]. Model projections under global warming scenarios suggest a worldwide increase in precipitation along with heightened precipitation variability [365]. In the context of warming scenarios, alterations in ocean circulation are anticipated to stem from high-latitudes due to surface ocean freshening in response to elevated P-E and ice melting [14]. This freshening effect is also projected for the NAO by nearly all global warming models [365]. This convergence of factors, including the anticipation of higher sea-level rise, the occurrence of abrupt events (such as

the 8.2 ka event) [455, 167], and climate events induced by warming, has prompted climatologists to closely monitor climate changes in the current context of warming and rising sea levels.

Additionally, the investigation of hydroclimatic fluctuations during various geological epochs holds significant value in quantifying global responses of the hydrological cycle to diverse climate forcings and greenhouse gas-induced warming, both at regional and global scales. A deeper understanding of historical climate change patterns and their repercussions becomes especially vital for validating climate projections and estimating the potential consequences of future climate changes. Presently, proxy records are gaining prominence due to their extended temporal coverage and their ability to capture the full spectrum of past climate conditions, thereby aiding in model validation. Furthermore, anticipating abrupt climate changes in the future underscores the importance of enhancing our comprehension of these processes, potentially providing more time for effective mitigation and adaptation strategies.

Moreover, achieving more realistic estimations of the consequences of abrupt changes in climate could enhance the efficacy of response measures. Overall, both instrumental observations and paleoclimatic data reveal instances of rapid, extensive, and widespread climate fluctuations that have occurred frequently in the past. While these fluctuations likely exert substantial influences on moisture and temperature patterns on land and in high-latitude regions, respectively, their climatic impacts are often global in scope. A better understanding of a wide array of abrupt climate phases through the amalgamation of instrumental observations, paleoclimatic data, advanced statistical methodologies, diverse model simulations, and impact assessments could provide valuable insights for policymakers in formulating effective strategies for mitigation, adaptation, and response.

Chapter 4

Data & Methods

4.1 Introduction

The instrumental climate record covers a relatively short period, mainly spanning the past century. This data scarcity poses a challenge for climatologists striving to understand the drivers of climate change, be they natural or anthropogenic, on a regional and global scale. Paleoclimatic reconstructions serve as invaluable resources, offering insights into past variations in the hydroclimate system. These reconstructions unveil significant fluctuations in precipitation and temperature patterns, as well as changes in hydrological regimes, corresponding to different states of ocean circulation. By examining paleoclimatic reconstructions of past hydroclimate conditions and ocean circulation states, researchers gain valuable insights into long-term trends and abrupt climate transitions. This understanding extends beyond the past, informing current climate conditions and future projections. Therefore, this objective aimed to establish a paleo-hydroclimatic database including paleo-ocean circulation-related data, with the goal of refining climate models and reducing uncertainties associated with present and future hydroclimate patterns.

4.2 Methodology

4.2.1 Data sources

For literature-based data, we used the empirical evidence on hydroclimate provided by the authors and compiled them into a table format. This approach facilitates the accessibility of data across different geological time scales. For data from different repositories, we utilize a variety of proxy reconstructions available in open-source databases, specifically the NOAA's National Centers for Environmental Information (https://www.ncei.noaa.gov/access/paleo-search/), PANGAEA (https://www.pangaea.de/), and the Past Global Changes (PAGES) (https://pastglobalchanges.org/science/data/databases).

4.2.2 Terrestrial hydroclimatic data

We chose precipitation and temperature-sensitive material, including stalagmites, lake sediments, tree rings, ice cores, and peatland sediments, which are distributed across North America and Europe. These materials serve as indirect indicators of changes in precipitation minus evaporation (P-E) patterns over the locations where the materials are collected. So when we refer to precipitation, it is actually denoting P-E. Additional information about the selected material, fraction, and proxies with their specific locations can be found in Figure 4.1. To ensure consistent and accurate representation of the relevant variables, such as temperature and precipitation (i.e., P-E), we maintained alignment with the specific variables as indicated by the original investigators in their respective data sources.

4.2.3 Ocean circulation related data

This study utilized marine sediment records for the estimation of the Oceanic circulation state. In characterizing the state of ocean circulation, we focused on parameters such as the AMOC, SST, and ITCZ parameters. For choosing AMOC and SST ITCZ-sensitive proxies, we selected a domain over the North Atlantic regions, defined by latitude -12.9 to 87°E and longitude 5 to -90°N. For ITCZ records, we targeted regions within the range of ITCZ movement across the equatorial region, encompassing both the northern and southern hemispheres.

Since direct measurements of AMOC started in 2004 [364], and instrumental data are not available for the period we investigated, we utilized well-established sensitive tracers, namely deep-sea (benthic foraminifera), δ^{13}C, cadmium/calcium (cd/ca) ratios, and sortable silts (mean size). The selection of these tracers was deliberate, driven by their utility as paleomicronutrient proxies critical for discerning patterns associated with the dynamics and movement of deep-water masses, as these nutrients are transported through oceanic circulation [344]. Variations in the concentration of these nutrients serve as reliable indicators of the state of oceanic circulation. Continuous monitoring of these tracer concentrations in deep and intermediate seawater is imperative for unraveling the intricacies of ocean circulation dynamics and evaluating the robustness of the global oceanic circulation system

across temporal scales. For detailed datasets and further elucidation, readers are directed to the corresponding sections, specifically Table 4.11, Table 4.12, and Table 4.13. Notably, the observed decline in δ^{13}C values and cd/ca ratios within deep/intermediate seawater serves as a significant indicator of the diminishing presence of North Atlantic Deep Water [45, 549]. Additionally, sortable silts (10-63μm), owing to their dynamic behavior (advection by ocean currents and temporal changes), offer valuable insights into the overarching dynamics of deep ocean currents as they are entrained within the flow of deep ocean water masses.

To track the ITCZ, we reconstructed the ITCZ shift index using the δ^{18}O values recorded from stalagmite by various investigators. For this reconstruction, we utilized 11 δ^{18}O records from different sites located in the Northern Hemisphere (NH) and 5 δ^{18}O records from various sites in the Southern Hemisphere (SH) due to data availability limitations. For SST variability Magnesium-calcium (Mg/Ca) ratios and $U^{k'}37$ proxies are widely recognized for their effectiveness in tracking SST conditions [48, 582]. Hence, we have incorporated these proxies into our study to assess variations in SST. Additionally, we have included model-based assimilation data on ITCZ and SST from Steiger et al. [507] to assess the reliability of model-based paleoclimate outputs.

This study utilized marine sediment records for the estimation of the Oceanic circulation state. In characterizing the state of ocean circulation, we focused on parameters such as the AMOC, SST, and ITCZ parameters. For choosing AMOC and SST ITCZ-sensitive proxies, we selected a domain over the North Atlantic regions, defined by latitude -12.9 to 87°E and longitude 5 to -90°N. For ITCZ records, we targeted regions within the range of ITCZ movement across the equatorial region, encompassing both the northern and southern hemispheres.

4.2.4 Model simulation data

For proxy and model comparative analysis, we obtained model assimilation data related to paleoclimate from two sources: the Paleo Hydrodynamics Data Assimilation product (PHYDA; for temperature, SST, ITCZ, and PDSI as an indicator of humid and arid condi-

tions) [507] and PaleoView (for temperature and precipitation) [175]. The Palmer Drought Severity Index (PDSI) is widely used to determine soil moisture availability, with higher values suggesting increased precipitation and wet conditions. Therefore, in this study, we utilized the PDSI as an indicator of humid and arid conditions. PHYDA is a global hydroclimate reconstruction generated by combining about 2978 proxy time series with the physical constraints of atmosphere-ocean climate models. The PHYDA provides data from 1 to 2000 CE with annual means (April to March), the boreal growing season of June, July, and August (JJA), and the austral growing season of December, January, and February (DJF). In contrast, PaleoView uses the TRaCE21ka experiment based on the daily simulated outcomes of the Community Climate System Model ver.3 (CCM3) [123]. It provides monthly and annual scale temperature and precipitation data from 22 ka BP to 1989 AD. We gained the climate model data at the annual scale, covering the time scale of 800-1399 CE, for the specified variables.

4.2.5 Data processing and database preparation

For the preparation of the database, we followed two steps. In the first step, we collected literature-based data through a comprehensive survey from peer-reviewed, novel, updated, and high-impacted publications. In the second step, we gathered proxy-based data from open-source data directories. The first step involved collecting data at a millennium scale, while the second step focused on gathering data primarily over the Holocene period. The database presentation focused on both terrestrial and oceanic data. After ensuring the correct transformation of values in all records, we standardized them by converting them into z-scores. Subsequently, these standardized values were aggregated into centennial time steps for each dataset individually. Locations of the data we collected can be found in Figure 4.1).

After collecting ITCZ-related records, we calculated the mean record for the NH and SH separately. Then, we subtracted the SH mean record from the NH mean record to obtain the ITCZ shift index. For comparison, we also utilized the ITCZ shift index reconstructions by Tan et al. [524] and Chawchai et al. [108].

Furthermore, we identified negative values in datasets, and to address this, we converted all values to positive using Equation 4.1 and subsequently performed a log transformation on them.

$$y(x) = X + |\min(x)| + 1 \tag{4.1}$$

In Equation 4.1, $y(x)$ denotes the transformation that is employed to ensure that the data possesses positive values suitable for a log transformation. $|\min(x)|$ represents the minimum value within the dataset, as an absolute value. Finally, X represents the values within the data that are being converted into positive values through this transformation.

The values of δ^{13}C and δ^{18}O allow us to assess past hydrological conditions, distinguishing between humid and arid periods and reflecting the prevailing precipitation conditions. Therefore, we ensured that δ^{13}C and δ^{18}O records were accurately represented in our analysis. Several studies have suggested a negative correlation between isotopic values (from δ^{13}C and δ^{18}O) and precipitation conditions [231, 524], indicating that low isotopic values correspond to increased precipitation conditions and vice versa. To align the values with this relationship, we applied a negative log transformation to reverse the δ^{13}C and δ^{18}O records, ensuring that low isotopic values correspond to low precipitation and high isotopic values correspond to high precipitation.

We performed a spatiotemporal investigation of precipitation-evaporation (P-E) and temperature, conducting time-series analysis (including model assimilated records, AMOC, and ITCZ) to assess overall continental-scale variability (Chapter 5). To this end, we employed maps of Europe and North America to visually illustrate the regional distribution of variables, facilitating our understanding of their relationships and interconnections. The spatiotemporal representation of data proved invaluable for examining latitudinal and spatial shifts in hydroclimate regimes. All analyses were conducted by the R statistical software [437].

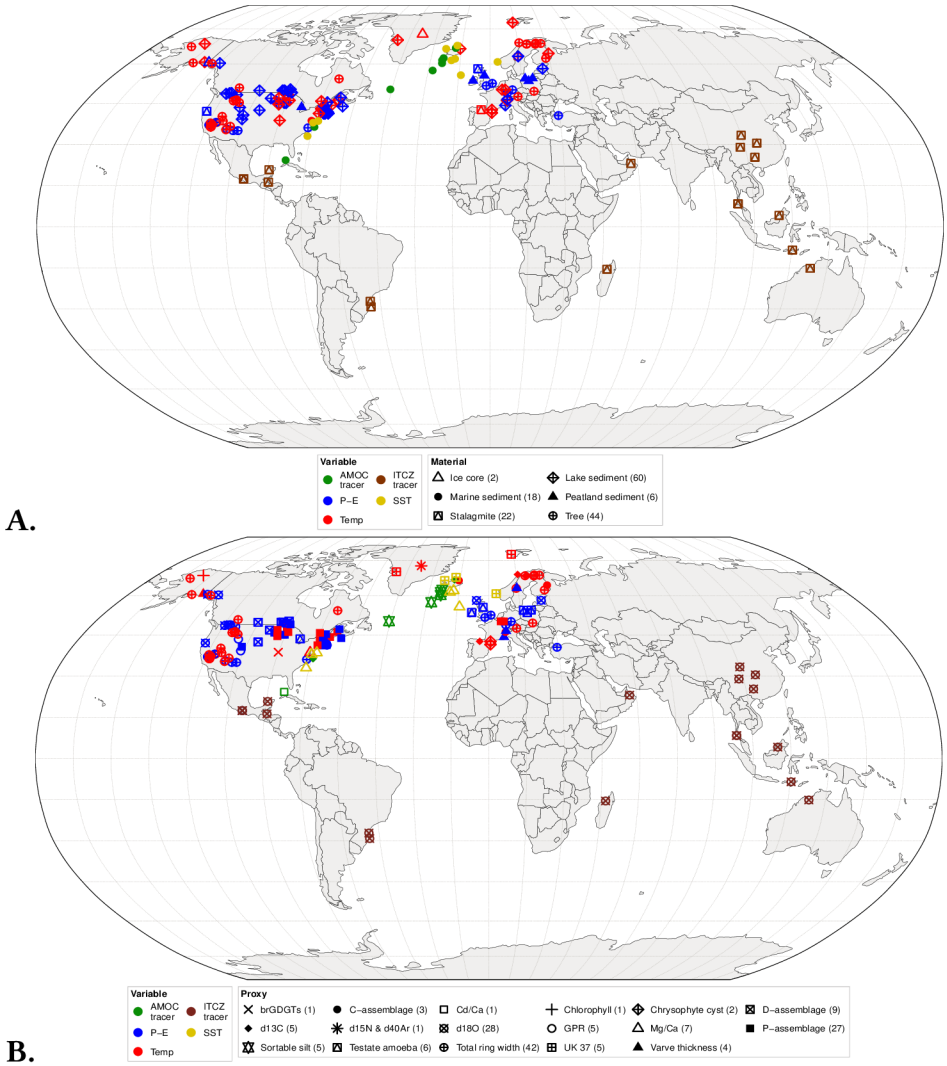

Figure 4.1: The map provided in this figure displays the spatial distribution of data sources categorized as material sources ('A') and proxy sources ('B'). These sources were utilized in our study to collect information related to precipitation minus evaporation (P-E), temperature (Temp), sea surface temperature (SST), Atlantic Meridional Overturning Circulation (AMOC), and the records of the Inter-Tropical Convergence Zone (ITCZ). In plot B, 'D-assemblage' denotes diatom assemblage data, 'P-assemblage' represents pollen data, and 'C-assemblage' corresponds to chironomid data. The numbers in the parentheses indicate the number of proxies.

4.2.6 Cross-scale analyses and estimation of slopes

The methodology for preparing the database involved assessing the scaling behavior of each hydroclimate record collected, particularly focusing on estimating cross-scale variability. To achieve this, we utilized cross-scale statistics, which explore how the structure of a process changes with alterations in its scale, employing the cross-scale analyses (CSA)

algorithm [339, 347]. Significantly, the estimation of cross-scale statistics is associated with a mathematically tractable stochastic modeling framework known as Fractional Gaussian Noise, enabling a quantitative interpretation and economical modeling of observed cross-scale variability patterns [349]. The scaling properties of all variables were meticulously examined and presented in Chapter 4, specifically under the sections "Spatio-temporal data information across Europe" and "Spatio-temporal data information across North America." Employing this approach offers a clear, visual overview of how hydroclimatic variables fluctuate across different scales.

Understanding the dynamics of paleo-hydroclimatic fluctuations is crucial for comparison with current or future changes. Therefore, alongside examining cross-scale variability, we have estimated the distribution of linear slopes for each variable. This approach provides insight into the long-term properties of the variables, which have not been previously presented. The estimation of slopes is conducted using the cross-scale statistical framework. Furthermore, we have included a plot displaying the locations of data, along with related basin and elevation profiles, in the section on spatio-temporal data information in Europe/North America.

Further, more details on these datasets are presented in the tables below.

4.3 Database

4.3.1 Empirical datasets

During this step, the main focus of this study was to collect all possible estimates on the hydroclimate/climatic regimes of the distant and recent past. Further information on the datasets is presented in the table below.

4.3.1.1 The number of studies per period and conditions

Table 4.1: The *Hydroclimate* column describes the most common condition. The average duration is estimated at a thousand years.

Period	Duration (ky)	Studies	Warm	Cold	Dry	Wet	Hydroclimate
MMCO	2500	40	49	0	22	39	Warm & wet
MIS-5e	14	32	12	2	7	21	Warm & wet
LGM	15	30	0	13	20	5	Cold & dry
D-O events	0.8	15	5	0	0	12	Warm & wet
H-events	1	18	1	13	17	10	Cold & dry
Bølling-Allerød	2	22	7	1	3	15	Warm & wet
Younger Dryas	1.3	35	3	12	14	17	Cold
The 8.2 ka event	0.16	13	0	16	6	6	Cold
MCA	0.4	28	11	0	24	10	Warm & dry
LIA	0.5	36	9	15	16	25	Cold & wet

4.3.1.2 Mid-Miocene Climate Optimum

Table 4.2: Temperature and precipitation conditions during the MMCO. NH: Northern Hemisphere, SH: Southern Hemisphere, H-L: High-latitudes, M-L: Mid-latitudes, L-L: Low-latitudes. Period units are in million years BP and average age uncertainty is $\pm$ 1 million years

Study site	Hemisphere	Zone	Period	T	P	Citation(s)
Global	NH/SH	0	17-14.5	Warm	0	[601, 428, 510]
N. Hemisphere	NH	M-L	17-14.5	Warm	Dry	[61, 93, 600, 604]
N. Hemisphere	NH	H-L	17-14.5	Warm	Dry	[61, 93, 600, 604]
Deep Ocean	NH	H-L	17-14.5	Warm	0	[207, 380, 605]
S. Hemisphere	SH	H-L	17-14.5	Warm	Wet	[600, 166]
Asia	NH	M-L	17-14.5	0	Dry	[250, 315]
Africa	NH	L-L	17-14.5	0	Dry	[449, 305, 161, 386]
Antarctica	SH	H-L	17-14.5	Warm	Wet	[600, 166]
S. America	SH	L-L	17-14.5	0	Dry	[411]
N. America	NH	M-L	20-14.5	Warm	Wet	[265, 448, 177, 221, 224]
N. America	NH	M-L	17-14.5	0	Dry	[588, 105]
Europe	NH	M-L	17-14.5	0	Wet	[61, 375, 281, 467]
Australia	SH	M-L	17-14.5	0	Dry	[508, 99, 594]
N. Eurasia	NH	H-L	21-14.5	Warm	Wet	[265, 448, 177, 221, 224]
Central Africa	NH	L-L	19-14.5	Warm	Wet	[265, 448, 177, 221, 224]
N. Africa	NH	M-L	18-14.5	Warm	Wet	[265, 448, 177, 221, 224]
Northern S. America	SH	L-L	17-14.5	0	Wet	[472]
China	NH	M-L	17-14.5	Warm	Wet	[519, 499, 509, 565, 120]
Greenland	NH	H-L	21-14.5	Warm	Wet	[265, 448, 177, 221, 224]
E. Idaho, USA	NH	M-L	17-14.5	0	Dry	[208]
N. Pakistan	NH	M-L	17-14.5	0	Dry	[12]
Alaska Range, Alaska	NH	H-L	18-14	Warm	0	[303]

4.3.1.3 Eemian Interglacial Stage or Marine Isotope Stage-5e

Table 4.3: Temperature and precipitation conditions during the Eemian Interglacial Stage. NH: Northern Hemisphere, SH: Southern Hemisphere, H-L: High-latitudes, M-L: Mid-latitudes, L-L: Low-latitudes. Period units are in ka BP and average age uncertainty is ± 5 ka.

Study site	Hemisphere	Zone	Period	T	P	Citation(s)
Global	NH/SH	0	130-116	Warm	0	[170, 496, 405]
Global	NH/SH	0	130-116	0	Wet	[579, 418, 254, 610]
N. Hemisphere	NH	0	130-116	Warm	0	[20]
N. Hemisphere	NH	0	130-116	0	Wet	[572, 587, 372, 268]
N. Hemisphere	NH	M-L	130-116	Warm	0	[546]
N. Hemisphere	NH	H-L	130-116	Warm	0	[546]
Asia	NH	M-L	130-116	0	Wet	[431, 473]
N. America	NH	M-L	130-116	Warm	Wet	[22]
Europe	NH	M-L	130-116	Cold	Dry	[82]
Australia	SH	M-L	130-116	0	Dry	[29]
N. Africa	NH	M-L	130-116	0	Wet	[431, 473]
S. Europe	NH	M-L	130-116	0	Wet	[78]
W. Australia	SH	M-L	130-116	0	Dry	[615]
Arabian desert	NH	M-L	130-116	Warm	Wet	[460, 423]
Greenland	NH	H-L	130-116	Warm	0	[547]
E. Mediterranean	NH	M-L	130-116	0	Wet	[35, 36]
Arabian Pen.	NH	M-L	130-116	0	Wet	[597]
Germany	NH	M-L	130-116	Cold	Dry	[492]
Bolivia	SH	L-L	130-116	Warm	Dry	[180]
Argentina	SH	M-L	130-116	0	Dry	[535]
Argentina	SH	M-L	130-116	0	Dry	[395]
S. Arabian Pen.	NH	M-L	130-116	0	Wet	[548]
Soreq Cave, Israel	NH	M-L	130-116	0	Wet	[402]

4.3.1.4 Last Glacial Maximum

Table 4.4: Temperature and precipitation conditions during the LGM. NH: Northern Hemisphere, SH: Southern Hemisphere, H-L: High-latitudes, M-L: Mid-latitudes, L-L: Low-latitudes. Period units are in ka BP and average age uncertainty is ±5 ka

Study site	Hemisphere	Zone	Period	T	P	Citation(s)
Global	NH/SH	0	30- 15	Cold	0	[96, 468]
Global	NH/SH	0	30- 15	0	Dry	[134, 603, 506, 310, 97, 185]
N. Hemisphere	NH	0	30- 15	Cold	Dry	[53, 406, 598]
Tropics	NH/SH	L-L	30- 15	Cold	0	[41, 24, 137, 34]
Tropics	NH/SH	L-L	30- 15	0	Dry	[433]
Europe	NH	M-L	30- 15	Cold	0	[514]
Extra-tropics	NH	L-L	30- 15	0	Wet	[114]
E. Africa	NH	L-L	30- 15	0	Wet	[40]
N. Africa	NH	M-L	30- 15	0	Dry	[433]
S. Africa	SH	L-L	30- 15	0	Dry	[413, 490]
N. Europe	NH	M-L	30- 15	0	Dry	[514]
S. Europe	NH	M-L	30- 15	0	Wet	[514, 282]
Mediterranean	NH	M-L	30- 15	0	Wet	[114]
SE. Siberia	NH	M-L	30- 15	0	Dry	[403]
E. & SW. Amazonia	SH	L-L	30- 15	0	Dry	[3, 489]
Greenland	NH	H-L	30- 15	Cold	0	[251, 139, 378]
Greenland	NH	H-L	30- 15	0	Dry	[138, 252]

4.3.1.5 Dansgaard–Oeschger and Heinrich Events

Table 4.5: Temperature and precipitation conditions during the Last Glacial. NH: Northern Hemisphere, SH: Southern Hemisphere, H-L: High-latitudes, M-L: Mid-latitudes, L-L: Low-latitudes. Period units are in ka BP and the average age uncertainty for this period is ± 10 ka.

Study site	Hemisphere	Zone	Event	Period	T	P	Citation(s)
Global	NH/SH	0	Heinrich	18-16.5	0	Dry	[186, 285, 520]
N. Hemisphere	NH	0	D-O	80-12	Warm	0	[353]
Tropics	NH/SH	0	Heinrich	70-14	0	Dry	[304]
Eurasia	NH	M-L	Heinrich	70-14	Cold	Dry	[187, 49, 26]
Asia	NH	M-L	D-O	80-12	0	Wet	[158, 112, 264]
Asia	NH	M-L	D-O	50-40	0	Wet	[571]
N. America	NH	M-L	Heinrich	70-14	Cold	Dry	[187, 49, 26]
S. America	SH	L-L	D-O	50-40	0	Wet	[421]
Antarctica	SH	H-L	Heinrich	70-14	Cold	Dry	[529]
Tropical S. America	SH	M-L	Heinrich	15 & 22	0	Wet	[570]
SW. Asia	NH	M-L	D-O	50-40	0	Wet	[21]
W. Europe	NH	M-L	D-O	80-12	Warm	Wet	[187]
N. Europe	NH	M-L	Heinrich	43-26	Cold	Dry	[340, 202]
Mediterranean	NH	M-L	Heinrich	70-14	Cold	0	[457]
India	NH	M-L	Heinrich	70-14	Cold	Dry	[121, 571]
Central China	NH	M-L	Heinrich	70-14	Cold	Dry	[529]
Iberian Peninsula	NH	M-L	D-O	80-12	0	Wet	[390, 94]
Greenland	NH	H-L	D-O	80-12	Warm	0	[253, 293, 94]
Italy	NH	M-L	D-O	80-12	0	Wet	[15]
Israel	NH	M-L	D-O	80-12	0	Wet	[37]
NE. Brazil	SH	L-L	Heinrich	40-15	0	Wet	[494]
SW. US	NH	M-L	Heinrich	70-14	0	Dry	[563]
W. US	NH	M-L	Heinrich	40-30	0	Wet	[49, 182, 404]
W. US	NH	M-L	Heinrich	28.5-26.5	0	Wet	[49, 182, 404]
Florida, US	NH	M-L	Heinrich	70-14	Warm	Wet	[202]
Great Basin (Nevada, US)	NH	M-L	D-O	80-12	0	Wet	[50]

4.3.1.6 Bølling-Allerød interstadial

Table 4.6: Temperature and precipitation conditions during the Bølling-Allerød interstadial. NH: Northern Hemisphere, SH: Southern Hemisphere, H-L: High-latitudes, M-L: Mid-latitudes, L-L: Low-latitudes. Period units are in ka BP and average age uncertainty is ±1 ka.

Study site	Hemisphere	Zone	Period	T	P	Citation(s)
N. Hemisphere	NH	L-L	13 - 12	0	Wet	[271, 336, 415]
S. & C. America	NH	M-L	14.8 - 12.85	Warm	Wet	[502, 227, 98, 237]
Equatorial Africa	NH	M-L	14.8 - 12.85	0	Wet	[435, 533]
Arctic	NH	H-L	14.5	Cold	0	[251]
E. Mediterranean	NH	M-L	14.8 - 12.85	0	Dry	[38]
Greece	NH	M-L	14.8 - 12.85	0	Dry	[27]
Italy	NH	M-L	14.8 - 12.85	0	Dry	[11]
W. USA	NH	M-L	13	0	Wet	[49, 182, 404]
Aegean Sea	NH	M-L	14.8 - 12.85	Warm	0	[67, 276]
S. Swiss Alps	NH	M-L	14.8 - 12.85	Warm	0	[463]
W. Himalayas (Nepal & India)	NH	M-L	14.8 - 12.85	0	Wet	[491, 608, 618]
Lake Maliq, Albania	NH	M-L	14.8 - 12.85	Warm	0	[67, 276]

4.3.1.7 Younger Dryas

Table 4.7: Temperature and precipitation conditions during the Younger Dryas. NH: Northern Hemisphere, SH: Southern Hemisphere, H-L: High-latitudes, M-L: Mid-latitudes, L-L: Low-latitudes. Period units are in ka BP and average age uncertainty is ± 0.5 ka.

Study site	Hemisphere	Zone	Period	T	P	Citation(s)
Global	NH/SH	0	13-11.7	Cold	Dry	[227, 361, 359, 164]
N. Hemisphere	NH	H-L	13-11.7	Cold	0	[181]
N. Hemisphere	NH	0	13-11.7	0	Dry	[143, 165, 238, 504, 554]
Tropics	NH/SH	L-L	13-11.7	Warm	0	[181]
Norwegian Sea	NH	H-L	13-11.7	Cold	0	[263]
N. America (Northern part)	NH	M-L	13-11.7	0	Dry	[101, 155]
N. America (Southern part)	NH	M-L	13-11.7	0	Wet	[202, 560, 446]
Central & Southern N. America	NH	M-L	13-11.7	0	Wet	[426, 563]
N. America (Central)	NH	M-L	13-11.7	Warm	Wet	[445]
W. Europe	NH	M-L	13-11.7	Cold	0	[193]
W. Europe	NH	M-L	12-12.2	Warm	Wet	[438]
Central Europe	NH	M-L	13-11.7	0	Wet	[333, 259, 581, 247]
S. Europe	NH	M-L	18-10	0	Wet	[412]
N. Tropical Andes	SH	M-L	13-11.7	0	Dry	[502]
S. Tropical Andes	SH	M-L	13-11.7	0	Wet	[502]
Tropical S. America	SH	L-L	13-11.7	0	Dry	[355]
Bolivia & Peru	SH	L-L	13-11.7	0	Wet	[31]
Poland	NH	M-L	13-11.7	Cold	0	[193]
Poland	NH	M-L	13-11.7	0	Wet	[461]
Netherlands	NH	M-L	13-11.7	0	Wet	[69]
Venezuela	NH	L-L	13-11.7	Cold	Dry	[502]
E. Beringia	NH	M-L	13-11.7	Cold	0	[179]
N. Scotland	NH	M-L	13-11.7	0	Wet	[323]
Aegean Sea	NH	M-L	13-11.7	Cold	0	[276]
Central Greenland	NH	H-L	13-11.7	Cold	0	[251]

4.3.1.8 The 8.2 ka event

Table 4.8: Temperature and precipitation conditions during the 8.2 event. NH: Northern Hemisphere, SH: Southern Hemisphere, H-L: High-latitudes, M-L: Mid-latitudes. Period units are in ka BP.

Study site	Hemisphere	Zone	Time	T	P	Citation(s)
Global	NH/SH	0	8.2	Cold	0	[14, 527, 214]
N. Hemisphere	NH	0	8.2	Cold	Dry	[536, 118, 17]
North Sea	NH	M-L	8.2	Cold	0	[270]
N. Africa	NH	M-L	8.2	Cold	Dry	[334]
NW. Europe	NH	M-L	8.2	Cold	0	[446]
Greenland	NH	H-L	8.2	Cold	0	[17, 561, 185]
Germany	NH	M-L	8.2	Cold	0	[270]
France	NH	M-L	8.2	Cold	0	[335]
Spain	NH	M-L	8.2	Cold	Dry	[334]
Italy	NH	M-L	8.2	Cold	Dry	[334]
Central Alps	NH	M-L	8.2	0	Wet	[332, 334]

4.3.1.9 Medieval Climate Anomaly

Table 4.9: Temperature and precipitation conditions during the MCA. NH: Northern Hemisphere, SH: Southern Hemisphere, H-L: High-latitudes, M-L: Mid-latitudes, L-L: Low-latitudes. Period units are in CE and the average age uncertainty for the MCA is ± 100 years.

Study site	Hemisphere	Zone	Time	T	P	Citation(s)
N. Hemisphere	NH	0	800-1400	Warm	Dry	[319]
Asia	NH	M-L	900-1300	0	Dry	[111]
N. America	NH	M-L	1197-1289 &1486-1581	0	Dry	[125, 410]
N. America	NH	M-L	1140-1162	0	Dry	[129]
N. America	NH	M-L	800-1400	Warm	0	[589]
N. America	NH	M-L	800-1400	Warm	0	[290]
Europe	NH	M-L	800-1400	Warm	0	[290]
N. Europe	NH	M-L	800-1400	0	Dry	[130]
S. Asia	NH	M-L	1230-1250 &1380-1410	0	Wet	[311]
E. Asia	NH	M-L	1300	0	Dry	[292]
NW. Europe	NH	M-L	1200-1300	Warm	0	[203]
S. America (NE area)	SH	L-L	800-1400	0	Wet	[530]
Western N. America	NH	M-L	900-1300	Warm	Dry	[589]
Western N. America	NH	M-L	1030-1100	0	Wet	[358]
Western N. America	NH	M-L	650-1050	0	Dry	[410]
Western N. America	NH	M-L	900-1300	0	Dry	[129]
E. Africa	NH	M-L	800-1400	0	Dry	[556]
S. Atlantic	SH	M-L	800-1400	Warm	0	[256]
N. Pacific	NH	M-L	800-1400	Warm	0	[342]
China	NH	M-L	800-1400	Warm	0	[595]
S. China	NH	M-L	800-1400	0	Dry	[111]
S. China	NH	M-L	1140-1220 & 1420-1490	0	Dry	[311]
NE. China	NH	M-L	950-1290	0	Wet	[444]
Southern Amazonia	SH	L-L	800-1400	0	Dry	[530]
Peru	SH	L-L	800-1250	0	Dry	[443]
Morocco	NH	M-L	1250-1300	0	Wet	[534]
Central America	NH	M-L	950-1250	0	Wet	[503]
Spain (Sierra Nevada)	NH	M-L	800-859, 1020-1070, 1197-1217, &1249-1365	0	Dry	[197]
Venezuela	NH	L-L	950-1450	0	Wet	[210]
Arizona, USA	NH	M-L	700-1350	0	Wet	[239]
California, USA	NH	M-L	1080-1129	0	Wet	[239]
Iberian Peninsula	NH	M-L	800-1400	Warm	Dry	[387]
Central Peruvian Andes	SH	L-L	900-1100	0	Dry	[55]
Alps	NH	M-L	12^{th} century	Warm	0	[537]

4.3.1.10 Little Ice Age

Table 4.10: Temperature and precipitation conditions during the LIA. NH: Northern Hemisphere, SH: Southern Hemisphere, H-L: High-latitudes, M-L: Mid-latitudes, L-L: Low-latitudes and average age uncertainty for the LIA is ± 50 years.

Study site	Hemisphere	Zone	Time	T	P	Citation(s)
Global	NH/SH	0	1350-1900 CE	Cold	0	[136, 197, 341, 113, 470]
Global	NH/SH	0	14th, Late 16^{th} & 17^{th} century	Cold	0	[537]
N. Hemisphere	NH	0	1570-1730 CE	Cold	0	[74]
S. Hemisphere	SH	0	1350-1900 CE	Cold	0	[451]
Africa	NH	L-L	1350-1900 CE	0	Dry	[515]
Antarctica	SH	H-L	1350-1900 CE	Cold	0	[52]
Europe	NH	M-L	1650-1750 CE	Warm	0	[64]
Europe	NH	M-L	Early 18^{th} century	0	Wet	[414]
Europe	NH	M-L	Early 18^{th} century	Warm	0	[392]
Europe	NH	M-L	1760-1800 CE	0	Wet	[57]
Europe	NH	M-L	1560-1580 CE	Warm	Wet	[189, 80]
Europe	NH	M-L	1840-1870 CE	Warm	Wet	[189, 80]
N. America	NH	M-L	Late 16^{th} & Early 17^{th} century	0	Dry	[126] [75, 357]
Central Asia	NH	M-L	1350-1900 CE	0	Wet	[111]
Central America	NH	M-L	1350-1900 CE	0	Dry	[503]
N. America (Central regions)	NH	M-L	1350-1900 CE	0	Wet	[286]
N. America (W & E Coast)	NH	M-L	1350-1900 CE	0	Dry	[286]
Southern S. America	SH	M-L	1280-1450 CE, 1550-1670 CE, & 1780-1830 CE	Cold	Dry	[558]
Southern S. America	SH	M-L	1220-1280 CE 1450-1550 CE, 1720-1780 CE, & 1830-1905 CE	Warm	Wet	[558]
Antarctic Pen.	SH	H-L	1350-1900 CE	0	Wet	[456]
Arabian Sea	NH	L-L	1450-1750 CE	0	Dry	[5]
Argentina	SH	M-L	1800 and 1930	0	Wet	[358]
Canada	NH	M-L	1515-1550 CE, 1585-1610 CE, 1660-1680 CE, & 1880s	0	Wet	[321]
Czech Republic	NH	M-L	1670-1710 CE	0	Wet	[79]
Venezuelan Andes	NH	L-L	1400-1700 CE	0	Wet	[424]
Scotland	NH	M-L	Late 13^{th} to mid 14^{th} century	0	Wet	[434]
Peru	SH	L-L	1400-1700 CE	0	Wet	[450, 55]
California, USA	NH	M-L	1400 CE	0	Wet	[512]
Wales, UK	NH	M-L	Late 13^{th} mid 14^{th} century	0	Wet	[290]
England	NH	M-L	Late 13^{th} mid 14^{th} century	0	Wet	[290]
Patagonia	NH	M-L	1400 CE	0	Wet	[512]
N. China	NH	M-L	1450-1750 CE	0	Dry	[111]
N. Taiwan	NH	M-L	1660, 1730, & 1820 CE	0	Wet	[568, 614]

4.3.2 Proxy datasets

4.3.2.1 Source and distribution information Precipitation and temperature data across Europe

Table 4.11: Source and distribution information for precipitation (Precip) and temperature (Temp) across the European region. In this table, 'P-assemblage' represents pollen data, 'C-assemblage' corresponds to chironomid data, 'TRW' represents Total ring width, and Lat and Long represent Latitude and Longitude, respectively. The time unit for 'Start' and 'End year' is in AD, while the 'Time step' is in years.

Location	Start year	End year	Time step	Material	Fractions	Proxy	Variable	Lat	Long	Investigators
North Aegean	1089	1989	1	Tree	Tree-rings	TRW	Precip	40.5	29.5	Griggs et al., 2007
Central and Eastern Pyrenees	578	1994	25	Lake sediment	Sediment	Chrysophyte cyst	Temp	41.5	0.75	Pla et al., 2004
Lake Redon	578	1994	25	Lake sediment	Sediment	Chrysophyte cyst	Temp	42.64	0.77	Pla et al., 2004
Northern inland Iberia	-1949	2000	varying	Stalagmite	Stalagmite	$\delta^{13}C$	Temp	42.69	-3.94	Martín-Chivelet et al., 2011
Lake Allos	650	2009	1	Lake sediment	Sediment	Varve thickness	Precip	44.25	6.72	Wilhelm et al., 2012
Seebergsee	1083	2001	1	Lake sediment	Chironomid	C-assemblage	Temp	46.12	7.47	Larocque et al., 2012
Lake Oeschinen	884	2008	1	Lake sediment	Sediment	Varve thickness	Precip	46.5	7.73	Amann et al., 2015
Alps	1	2003	1	Tree	Tree-rings	TRW	Temp	47.5	12.5	Büntgen et al., 2016
Upper Rhine Valley	265	2017	1	Tree	Tree-rings	TRW	Precip	48.75	7.75	Tegel et al., 2020
Tatra region	1040	2011	1	Tree	Tree-rings	TRW	Temp	49.5	20	Büntgen et al., 2013
Main River Region	1	2000	1	Tree	Tree-rings	TRW	Precip	50.05	10.2	Land et al., 2019
Meerfelder Maar	-9040	1787	varying	Lake sediment	Pollen	P-assemblage	Temp	50.1	5.5	Litt et al., 2009
Holzmaar	-8931	1973	varying	Lake sediment	Pollen	P-assemblage	Temp	50.12	6.88	Litt et al., 2009
Southern-Central England	950	2009	1	Tree	Tree-rings	TRW	Precip	51.6	-1.75	Wilson et al., 2012
East Anglia	900	2009	1	Tree	Tree-rings	TRW	Precip	52.5	1	Cooper et al., 2012
Stazki Bog	1000	2002	1	Peatland sediment	Sediment	Testate amoeba	Precip	53.42	18.08	Lamentowicz et al., 2010
Ireland	-3051	2008	varying	Peatland sediment	Sediment	Testate amoeba	Precip	53.5	-8	Swindles et al., 2013
Slowinskie Blota	1000	2002	1	Peatland sediment	Sediment	Testate amoeba	Precip	54.36	16.49	Lamentowicz et al., 2010
Northern Britain	-2493	2000	1	Peatland sediment	Sediment	Testate amoeba	Precip	55.5	-2.75	Charman et al., 2006
Uamh an Tartair	907	1993	1	Stalagmite	Stalagmite	$\delta^{18}O$	Precip	58.15	-5.98	Baker et al., 2010
Finnish Lakeland	760	2000	1	Tree	Tree-rings	TRW	Temp	62.33	28.33	Helama et al., 2014
Jämtland	850	2011	1	Tree	Tree-rings	TRW	Temp	63	14.05	Zhang et al., 2016
Stora Vidarvatn	107	2005	varying	Lake sediment	Chironomid	C-assemblage	Temp	66.24	-15.83	Axford et al., 2008
Northern Fennoscandia	-7	2010	1	Tree	Tree-rings	TRW	Temp	68.15	24.38	Matskovsky and Helama, 2014
Torneträsk	900	2008	1	Tree	Cellulose	$\delta^{13}C$	Temp	68.2	19.8	Loader et al., 2013
Torneträsk	401	2010	1	Tree	Tree-rings	TRW	Temp	68.26	19.63	Melvin et al., 2013
Laanila	886	2001	1	Tree	Tree-rings	TRW	Temp	68.5	27.5	Gagen et al., 2011
Northern Fennoscandia	-5500	2005	1	Tree	Tree-rings	TRW	Temp	68.63	24.69	Helama et al., 2012
Forfjorddalen	990	2001	1	Tree	Cellulose	$\delta^{13}C$	Temp	68.8	15.73	Young et al., 2012
Kongressvatnet	250	2008	varying	Lake sediment	Sediment	UK 37	Temp	78.02	13.93	Andrea et al., 2012
Lake Nuudsaku	-7497	2015	varying	Lake sediment	Sediment	$\delta^{18}O$	Precip	58.1969	25.6275	Nathan et al., 2017
Lake Storsjön	-9011	2006	varying	Lake sediment	Varve	Varve thickness	Precip	63.12	14.37	Labuhn et al., 2017
Kylmanlampi	-778	2000	varying	Lake sediment	Chironomid	C-assemblage	Temp	64.3	30.25	Luoto et al., 2003

4.3.2.2 Precipitation and temperature data across North America

Table 4.12: Source and distribution information for precipitation (Precip) and temperature (Temp) across the North American region. In this table, 'D-assemblage' denotes diatom assemblage data, 'P-assemblage' represents pollen data, 'TRW' represents Total ring width, GPR denotes Ground penetrating radar, and Lat and Long represent Latitude and Longitude, respectively. The time unit for 'Start' and 'End year' is in AD, while the 'Time step' is in years.

Location	Start year	End year	Time step	Material	Fractions	Proxy	Variable	Lat	Long	Investigators
Albemarle Sound Drainage Basin	780	1993	1	Tree	Tree-rings	TRW	Precip	36	-77	Stahle et al., 2011
Beaver Lake	-4500	1950	varying	Lake sediment	Diatom	D-assemblage	Precip	42.46	-100.67	Schmieder et al., 2011
Berry Pond	-9050	1950	50	Lake sediment	Pollen	P-assemblage	Precip	42.51	-73.32	Marsicek et al., 2013
Blood Pond	-9050	1950	50	Lake sediment	Pollen	P-assemblage	Precip	42.08	-71.96	Marsicek et al., 2013
Bufflehead Pond	550	1900	50	Lake sediment	Sediment	GPR	Precip	44.99	-93.54	Shuman et al., 2009
Castor Lake	500	2000	5	Lake sediment	Sediment	δ^{18}O	Precip	48.54	-119.56	Steinman et al., 2012
Chesapeake Bay	800	1394	varying	Marine sediment	Sediment	Mg/Ca	Temp	38.61	-76.4	Cronin et al., 2010
Clear pond	60	1940	40	Lake sediment	Pollen	P-assemblage	Temp, Precip	43	-74	Gajewski 1988
Conroy lake	10	1943	40	Lake sediment	Pollen	P-assemblage	Temp, Precip	46.17	-67.53	Gajewski 1988
Dark Lake	1045	1365	40	Lake sediment	Pollen	P-assemblage	Precip	45.16	-91.28	Gajewski 1988
Deep Lake	-9950	1900	50	Lake sediment	Pollen	P-assemblage	Precip	41.56	-70.64	Marsicek et al., 2013
Dixie Lake	2	2010	11	Lake sediment	Diatom	D-assemblage	Precip	49.83	-93.95	Laird et al., 2012
El Malpais	-136	2002	1	Tree	Tree-rings	TRW	Precip	34.97	-108.18	Stahle et al., 2009
El Malpais	-136	1992	1	Tree	Tree-rings	TRW	Precip	34.97	-106.18	Grissino and Henri 1995
ELA Lake 239	8	2004	19	Lake sediment	Diatom	D-assemblage	Precip	49.67	-93.73	Laird et al., 2012
ELA Lake 442	8	2004	16	Lake sediment	Diatom	D-assemblage	Precip	49.77	-93.82	Laird et al., 2012
Emerald Lake	-9950	1700	50	Lake sediment	Sediment	GPR	Precip	39.15	-106.41	Shuman et al., 2014
Étang_Fer-de-Lance	-35	2018	varying	Lake sediment	Pollen	P-assemblage	Precip	45.36	-72.23	Claire et al., 2021
Foy Lake	-201	2006	1	Lake sediment	Sediment	δ^{18}O	Precip	48.17	-114.35	Spruce et al., 2020
Fresh Pond	-9050	1950	50	Lake sediment	Pollen	P-assemblage	Precip	41.16	-71.58	Jeremiah et al., 2013
Gall Lake	17	2009	varying	Lake sediment	Diatom	D-assemblage	Precip	50.23	-91.45	Kathleen et al., 2011
Great Basin	-2574	2006	1	Tree	Tree-rings	TRW	Temp	38	-116.5	Salzer et al., 2013
Greenland-GISP2	1000	1993	1	Ice core	Ice	d15N & d40Ar	Temp	72.6	-38.5	Kobashi et al., 2010
Hell's Kitchen Lake	-90	1940	varying	Lake sediment	Pollen	P-assemblage	Temp, Precip	46.11	-89.42	Gajewski 1988
Horseshoe Lake (HORM12)	240	1989	varying	Lake sediment	Sediment	brGDGTs	Temp	38.7	-90.08	Munoz et al., 2020
Iceberg Lake	442	1998	1	Lake sediment	Sediment	Varve thickness	Temp	60.78	-142.95	Loso 2008
Jellybean Lake	-5606	2002	varying	Lake sediment	Sediment	δ^{18}O	Precip	60.35	-134.8	Anderson et al., 2005
Juxtlahuaca Cave	-241	2009	3	Stalagmite	Stalagmite	δ^{18}O	Precip	17.4	-99.2	Lachniet et al., 2017
Kurupa Lake	-3643	2003	3	Lake sediment	Sediment	Chlorophyll	Temp	68.35	-154.61	Boldt et al., 2015
L1_CANA458	910	2011	1	Tree	Tree-rings	TRW	Temp	54.21	-71.35	Bellen et al., 2019
Lake Braya Sø	-4999	2005	1	Lake sediment	Sediment	UK 37	Temp	69.99	-51.03	Gunten et al., 2012
Lake Mina	1120	1900	4	Lake sediment	Pollen	P-assemblage	Precip	45.89	-95.48	Jeannine et al., 2020
Lake of the Clouds	985	1965	varying	Lake sediment	Pollen	P-assemblage	Temp, Precip	48	-91.07	Gajewski 1988
Lake of the Woods	-15950	1900	50	Lake sediment	Sediment	GPR	Precip	43.48	-109.89	Pribyl and Shuman 2014
Lime lake	500	2000	5	Lake sediment	Sediment	δ^{18}O	Precip	48.87	-117.34	Steinman et al., 2012
Little Pond	-9050	1950	50	Lake sediment	Pollen	P-assemblage	Precip	42.68	-72.19	Marsicek et al., 2013
Little Raleigh	-2	2010	17	Lake sediment	Diatom	D-assemblage	Precip	49.45	-91.89	Kathleen et al., 2012
Meekin Lake	19	2010	16	Lake sediment	Diatom	D-assemblage	Precip	49.82	-94.77	Laird et al., 2012
Minden Bog	-1479	2000	varying	Peatland sediment	Sediment	Testate amoeba	Precip	43.61	-82.84	Booth and Jackson, 2003
Moon Lake	-354	1980	varying	Lake sediment	Diatom	D-assemblage	Precip	46.86	-98.16	Laird et al., 1998
Mt Logan	560	1995	25	Ice core	Ice	δ^{18}O	Precip	60.58	-140.5	Fisher et al., 2008
Nevada	-6000	1996	1	Tree	Tree-rings	TRW	Precip	38	-117	Huges and Graumlich, 2000
New Long Pond	-9950	1900	50	Lake sediment	Sediment	GPR	Precip	41.85	-70.68	Newby et al., 2009
No Bottom Lake	-9050	1950	50	Lake sediment	Sediment	GPR	Precip	41.29	-70.11	Marsicek et al., 2013
Oregon Caves	-6021	1715	varying	Stalagmite	Stalagmite	δ^{18}O	Precip	42.08	-123.42	Ersek et al., 2012
Oro Lake	-4946	1873	varying	Lake sediment	Diatom	D-assemblage	Precip	49.78	-105.33	Michels et al., 2007
Park Range	-540	1980	30	Lake sediment	Pollen	P-assemblage	Precip	40.7	-106.75	Parish et al., 2020
Path Lake	-7171	1943	varying	Lake sediment	Pollen	P-assemblage	Precip	43.87	-64.93	Neil et al., 2014
Renner lake	500	2000	5	Lake sediment	Sediment	δ^{18}O	Precip	48.78	-118.19	Steinman et al., 2012
Rogers Lake	-9050	1950	50	Lake sediment	Pollen	P-assemblage	Precip	41.21	-72.17	Marsicek et al., 2013
Sharkey Lake	-11088	1316	varying	Lake sediment	Pollen	P-assemblage	Temp	44.59	-93.41	Shuman et al., 2016
Southern Colorado Plateau	-250	1987	1	Tree	Tree-rings	TRW	Temp, Precip	36.56	-110.12	Salzer and Kipfmueller 2005
Southern Sierra Nevada	90	2012	1	Tree	Tree-rings	TRW	Precip	37.03	-119.43	Touchan et al., 2021
Spruce Pond	-27298	1850	60	Lake sediment	Pollen	P-assemblage	Temp	41.24	-74.2	Shuman et al., 2016
Steel Lake	-10350	2000	varying	Lake sediment	Pollen	P-assemblage	Temp	46.97	-94.68	Shuman et al., 2016
White Mountains	1085	2005	1	Tree	Tree-rings	TRW	Precip	37.45	-118.17	Bale et al., 2011
Baker lake	12	1997	1	Tree	Tree-rings	TRW	Temp	45.9	-114.3	Hughes et al., 2005
Boreal Plateau	831	1992	1	Tree	Tree-rings	TRW	Temp	36.3	-118.3	Graumlich et al., 2005
Cirque Peak	917	1987	1	Tree	Tree-rings	TRW	Temp	36.3	-118.2	Graybill 1995
Flint Creek Range	999	1998	1	Tree	Tree-rings	TRW	Temp	46.3	-113.2	Hughes et al., 2005
Flower Lake	898	1987	1	Tree	Tree-rings	TRW	Temp	36.5	-118.2	Graybill 1995
French Glacier	1069	1639	1	Tree	Tree-rings	TRW	Temp	50.8	-115.3	Colenutt et al., 1995
Kobuk_Noatak	978	1992	1	Tree	Tree-rings	TRW	Temp	67.1	-159.6	King and Graumlich, 2003
Landslide	913	2001	1	Tree	Tree-rings	TRW	Temp	60.2	-138.5	Luckman et al., 2006
Mount Washington	825	1983	1	Tree	Tree-rings	TRW	Temp	38.5	-114.2	Graybill, 1994
Pearl Peak	320	1985	1	Tree	Tree-rings	TRW	Temp	40.2	-115.5	Graybill, 1994
Pintlers	1026	2005	1	Tree	Tree-rings	TRW	Temp	46	-113.4	Gregory et al., 2011
Prince William Sound	873	1991	1	Tree	Tree-rings	TRW	Temp	60.5	-148.3	Barclay et al., 1999
San Franciso Peaks	1	2002	1	Tree	Tree-rings	TRW	Temp	35.3	-111.4	Salzer and Kipfmueller, 2005
Sheep Mountain	1	1990	1	Tree	Tree-rings	TRW	Temp	37.2	-118.1	Graybill 1995
Siberian Outpost View	494	2001	1	Tree	Tree-rings	TRW	Temp	36.5	-118.3	Kipfmueller et al., 2010
Spillway Lake	800	1996	1	Tree	Tree-rings	TRW	Temp	37.8	-119.2	King et al., 2000
Timber Gap Upper	699	1987	1	Tree	Tree-rings	TRW	Temp	36.3	-118.4	Graybill 1995
Upper Wright Lakes	-215	1992	1	Tree	Tree-rings	TRW	Temp	36.4	-118.2	Bunn et al., 2005
Yellow Mountain Ridge	470	1998	1	Tree	Tree-rings	TRW	Temp	45.3	-111.3	King et al., 2000
Lac Noir	1007	2006	10	Lake sediment	Pollen	P-assemblage	Temp	45.8	-75.1	Paquette and Gajewski, 2013
Basin pond	15	1605	varying	Lake sediment	Pollen	P-assemblage	Temp, Precip	44.28	-70.03	Gajewski 1988

Table 4.13: Source and distribution information for AMOC, SST, and ITCZ sensitive tracers. In this table, SS represents Sortable silt and Lat and Long represent Latitude and Longitude, respectively. The time unit for 'Start' and 'End year' is in AD, while the 'Time step' is in years.

Region	Location	Start year	End year	Time step	Material	Fractions	Proxy	Variable	Lat	Long	Investigators
Asia	Klang Cave	-695	2004	1	Stalagmite	Stalagmite	δ^{18}O	ITCZ	8.33	98.73	Tan et al., 2019
Africa	Anjohibe Cave	383	2014	varying	Stalagmite	Stalagmite	δ^{18}O	ITCZ	-15.53	46.88	Scroxton et al., 2017
Asia	Clearwater Cave	-13165	2005	40	Stalagmite	Stalagmite	δ^{18}O	ITCZ	4.1	114.83	Carolin et al. 2016
Asia	Dongge Cave	-6930	2000	varying	Stalagmite	Stalagmite	δ^{18}O	ITCZ	25.28	108.08	Wang et al., 2006
Asia	Heshang Cave	-7520	2002	2	Stalagmite	Stalagmite	δ^{18}O	ITCZ	30.45	110.42	Hu et al., 2008
Asia	Liang cave	-29555	2002	varying	Stalagmite	Stalagmite	δ^{18}O	ITCZ	-8.53	120.43	Scroxton et al., 2022
Asia	Shenqi Cave	-317	2010	varying	Stalagmite	Stalagmite	δ^{18}O	ITCZ	28.93	103.1	Tan et al., 2018
Asia	Tzabnah	487	2004	varying	Stalagmite	Stalagmite	δ^{18}O	ITCZ	20.73	-89.47	Elizalde et al., 2010
Asia	Wanxiang Cave	192	2003	varying	Stalagmite	Stalagmite	δ^{18}O	ITCZ	33.32	105	Zhang et al., 2009
Asia	Yok Balum Cave	-39	2004	1	Stalagmite	Stalagmite	δ^{18}O	ITCZ	16.21	-89.07	Kennett et al., 2012
Asia	Klang Cave	1	2004	1	Stalagmite	Stalagmite	δ^{18}O	ITCZ	8.33	98.73	Chawchai et al., 2021
Asia	Hoti Cave	-631	1996	varying	Stalagmite	Stalagmite	δ^{18}O	ITCZ	23.05	57.21	Fleitmann et al., 2022
Asia	Botuvera Cave	-7261	1754	varying	Stalagmite	Stalagmite	δ^{18}O	ITCZ	-27.22	-49.16	Bernal et al., 2016
Asia	Botuvera Cave	-114210	1950	varying	Stalagmite	Stalagmite	δ^{18}O	ITCZ	-29.22	-49.12	Cruz et al., 2005
Australia	Cave KNI-51	754	1416	3	Stalagmite	Stalagmite	δ^{18}O	ITCZ	-15.18	128.37	Denniston et al., 2016
North America	Juxtlahuaca Cave	-447	2010	varying	Stalagmite	Stalagmite	δ^{18}O	ITCZ	17.4	-99.2	Lachniet et al., 2012
North America	Juxtlahuaca Cave	457	2000	3	Stalagmite	Stalagmite	δ^{18}O	ITCZ	17.4	-99.2	Lachniet et al., 2013
North America	Juxtlahuaca Cave	-241	2009	2	Stalagmite	Stalagmite	δ^{18}O	ITCZ	17.44	-99.16	Lachniet et al., 2017
Ocean	KNR166-2 11MC-D	-32	1950	varying	Marine sediment	Sediment	Cd/Ca	AMOC	24.30	-83.30	Valley et al., 2022
Ocean	MD03-2661	-457	1881	5	Marine sediment	Foraminiferal	δ^{13}C	AMOC	38.89	-76.4	Cronin et al., 2010
Ocean	Island of Grimsey	953	2000	1	Marine sediment	Molusc	δ^{13}C	AMOC	66.53	-18.2	Wanamaker et al., 2012
Ocean	KN140-2-51	-9240	1860	varying	Marine sediment	Sediment	SS	AMOC	32.78	-76.28	Hoffmann et al., 2018
Ocean	NEAP-4K	-8112	1683	30	Marine sediment	Sediment	SS	AMOC	61.50	-24.17	Thornalley et al., 2013
Ocean	ODP983	-9850	1859	varying	Marine sediment	Sediment	SS	AMOC	62.40	-23.64	Thornalley et al., 2013
Ocean	Orphan Knoll	-8166	1934	32	Marine sediment	Sediment	SS	AMOC	50.21	-45.69	Hoogakker et al., 2011
Ocean	MD992251	-8057	1449	7	Marine sediment	Sediment	SS	AMOC	57.46	-27.91	Hoogakker et al., 2011
Ocean	GS06-144 08GC	-7942	1566	varying	Marine sediment	Sediment	SS	AMOC	60.32	-23.97	Mjell et al., 2014
Ocean	RAPiD-12-1K	-9919	1950	varying	Marine sediment	Foraminiferal	Mg/Ca	SST	62.09	-17.82	Thornalley et al., 2009
Ocean	RAPiD-17-5P	819	1794	varying	Marine sediment	Sediment	Mg/Ca	SST	61.48	-19.54	Sanchez et al., 2014
Ocean	RAPiD-35-25B	763	1914	varying	Marine sediment	Foraminiferal	Mg/Ca	SST	38.89	-76.39	Sanchez et al., 2014
Ocean	RD-2209	-184	1996	varying	Marine sediment	Foraminiferal	Mg/Ca	SST	38.89	-76.4	Cronin et al., 2010
Ocean	KNR140-2-59GGC	450	1850	50	Marine sediment	Foraminiferal	Mg/Ca	SST	32.98	-76.32	Arbuszewski et al., 2010
Ocean	ENAM9606	-368	1998	varying	Marine sediment	Foraminiferal	Mg/Ca	SST	55.65	-13.99	Richter et al., 2009
Ocean	Norwegian Sea	-111	2001	varying	Marine sediment	Alkenone	UK 37	SST	60.87	3.73	Eiriksson et al., 2006
Ocean	JR51-GC35	-8220	1888	varying	Marine sediment	Sediment	UK 37	SST	67.59	-17.56	Bendle & Rosell-Melé, 2007
Ocean	MD99-2266	-8794	1640	varying	Marine sediment	Foraminiferal	UK 37	SST	66.23	-24	Moossen et al., 2015

4.4 Spatio-temporal data information across the Europe

Cooper et al. (2012)

Region: East Anglia
Lon.: 0 – 2°E
Lat.: 51 – 53°N
Proxy: Tree rings
Start: 900 CE
End: 2009 CE
Length: 1110 years
Season: MAMJJ

Basin ID: 23303606
Level: 8
Order: 2
Area: 1082.6 km^2
Mean Elev.: 35 m
Slope: 9%
Mean P: 585 mm

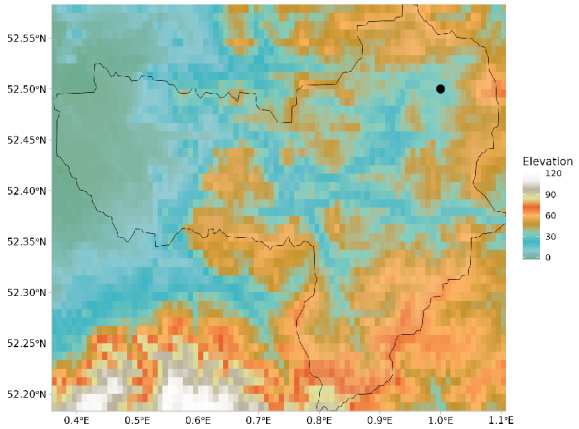

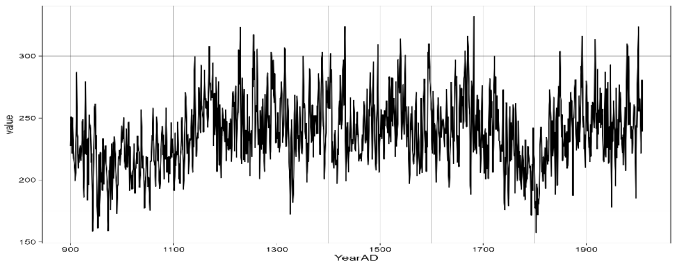

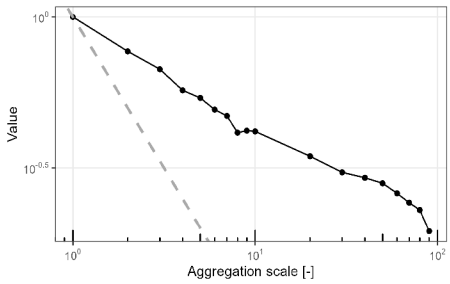

This dataset provides an annual precipitation (P) reconstruction derived from a network of 723 living (1590 – 2009 CE) and historical (781 – 1790 CE) oak (Quercus sp.). This time series exhibits near-decadal a periodic fluctuations during the last millennium with no links to NAO. Statistically significant anomalous dry conditions are reported throughout 900 – 1100 CE and around 1800 CE, while prolonged wetter conditions dominate the twelfth and thirteen centuries.

1-year scale	10-year scale	30-year scale	50-year scale
Mean: 237.99	Max slope: 4.44	Max slope: 3.18	Max slope: 2.38
St. Dev: 28.59	Min slope: -4.09	Min slope: -2.91	Min slope: -1.96
Min/Max: -0.33/0.33	Max diff: 2.69	Max diff: 2.20	Max diff: 1.6
H(ACF-1): 0.82 (0.55)	Min diff: -2.52	Min diff: -2.12	Min diff: -1.55

Box 4.4.1. Cooper et al. (2012) profile of tree ring precipitation reconstruction.

Amann et al. (2015)

Region: Lake Oeschinen
Lon.: 7.73°E
Lat.: 46.50°N
Proxy: Varve thickness
Start: 884 CE
End: 2008 CE
Length: 1125 years
Season: MJJA

Basin ID: 2326809
Level: 7
Order: 2
Area: 3213.4 km^2
Mean Elev.: 1530 m
Slope: 208%
Mean P: 1492 mm

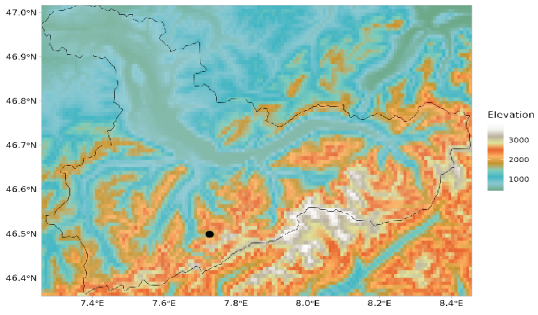

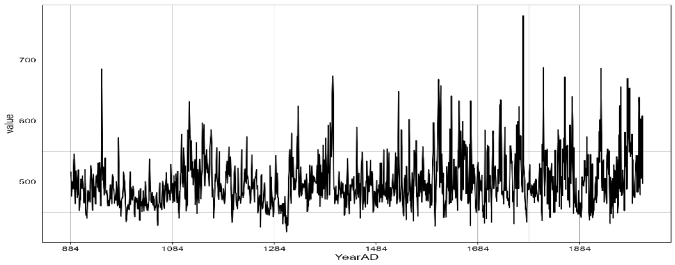

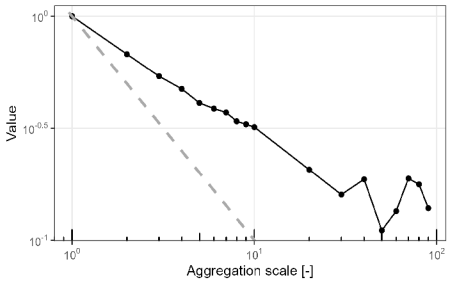

This dataset is an annually resolved record of warm-season P, from multiple varve counts within the sediments of Lake Oeschinen. Wet warm-season phases are evident between 920-950, 1100-1180, 1300-1400, 1590-1650, 1700-1790, 1820-1880, and 1960-2008 CE, while drier phases from 960-1080, 1250-1300, and 1880-1900 CE. This record shows no consistent link between warm-season P and temperature (T), revealing oscillations between negative (warmer-drier, cooler-wetter) and positive correlations (warmer-wetter, cooler-drier) with a multidecadal periodicity (60-70 years) over the last millennium.

1-year scale	10-year scale	30-year scale	50-year scale
Mean: 499.29	Max slope: 7.46	Max slope: 3.13	Max slope: 4.14
St. Dev: 42.93	Min slope: -7.5	Min slope: -3.98	Min slope: -2.67
Min/Max: 417.81/773.07	Max diff: 2.96	Max diff: 1.73	Max diff: 2.35
H(ACF-1): 0.72 (0.35)	Min diff: -3.02	Min diff: -2.32	Min diff: -1.72

Box 4.4.2. Amann et al. (2015) precipitation reconstruction using Varve thickness.

Land et al. (2019)

Region: Main River Region
Lon.: 8.2–12.2°E
Lat.: 49.3–50.8°N
Proxy: Tree rings
Start: 1 CE
End: 2000 CE
Length: 2000 years
Season: FMAMJJ

Basin ID: 23264
Level: 5
Order: 2
Area: 27404.6 km^2
Mean Elev.: 348 m
Slope: 46%
Mean P: 683 mm

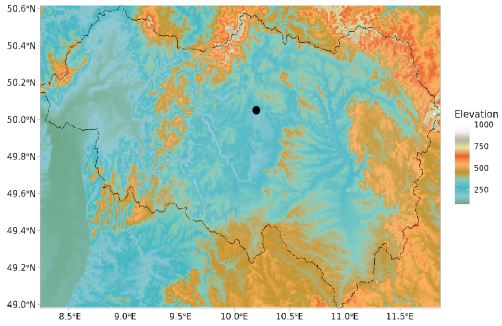

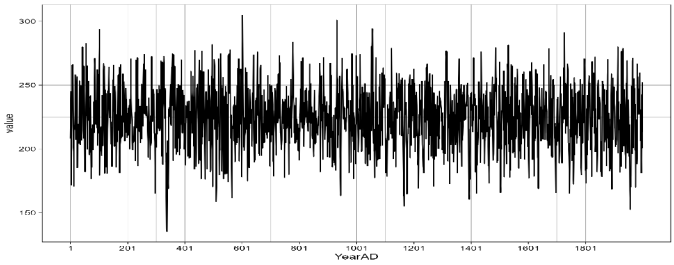

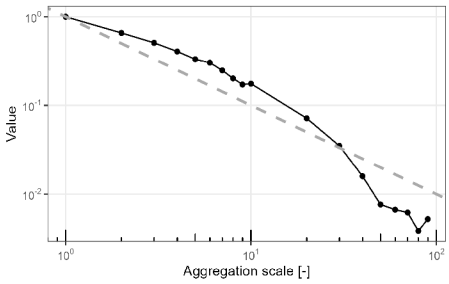

This annual P, based on the tree ring widths of living oak trees (Quercus robur, Quercus petraea), spans from spring to mid-summer. Over the past two millennia, this record shows significant variability on both high and mid-frequency scales. Instances of very dry spring to mid-summer seasons are observed in 500, 510, 940, 1170, 1390, and 1160 CE. Notably, a persistent multi-year drought with notably reduced rainfall occurred at the end of 330 CE, marking the driest decade in southern Germany over the past 2000 years. However, the 550, 1050, 1310, and 1480 CE experienced high rainfall. For instance, P during the spring to mid-summer of 338 CE was reduced by 38%, whereas it increased by 39% in 357 CE.

1-year scale	10-year scale	30-year scale	50-year scale
Mean: 224.51	Max slope: 3.75	Max slope: 1.64	Max slope: 1.19
St. Dev: 23.63	Min slope: -4.5	Min slope: -1.99	Min slope: -0.86
Min/Max: 135.3/304.8	Max diff: 2.42	Max diff: 2.13	Max diff: 3.17
H(ACF-1): 0.70 (0.31)	Min diff: -2.93	Min diff: -2.6	Min diff: -2.13

Box 4.4.3. Land et al. (2019) profile of tree ring precipitation reconstruction.

Griggs et al. (2007)

Region: North Aegean
Lon.: 22–37°E
Lat.: 39–42°N
Proxy: Tree rings
Start: 1089 CE
End: 1989 CE
Length: 901 years
Season: MJ

Basin ID: 2110590
Level: 7
Order: 0
Area: 4858.4 km^2
Mean Elev.: 316 m
Slope: 90%
Mean P: 729 mm

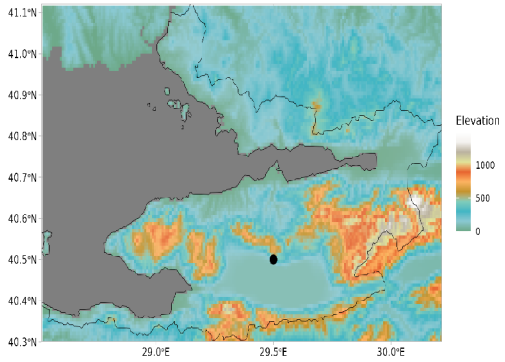

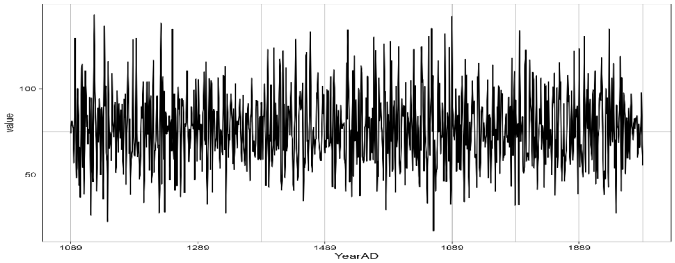

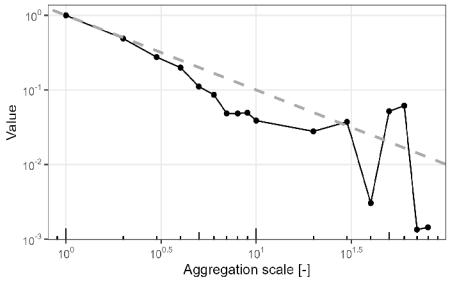

This summer P was created using oak tree-ring with 511 samples collected from 7 forests and 49 historic site tree-ring chronologies across the NE Greece and NW Turkey. It marks the challenges in accurately reconstructing P, mainly given the primary limitation imposed by T on annual tree-ring growth. After examining various methods, it is suggested that optimal techniques for regional climate reconstruction involve the removal of high-frequency variability and normalization of tree-ring data before merging them into a master chronology. Although this approach ensures a more reliable reconstruction of regional P, it may inadvertently remove the low-frequency signal and attenuate some evidence of local extremes.

1-year scale	10-year scale	30-year scale	50-year scale
Mean: 77.02	Max slope: 2.11	Max slope: 0.52	Max slope: 0.26
St. Dev: 21.79	Min slope: -2	Min slope: -0.62	Min slope: -0.28
Min/Max: 17.8/142.92	Max diff: 3.02	Max diff: 2.51	Max diff: 1.74
H(ACF-1): 0.33 (0.002)	Min diff: -2.87	Min diff: -2.83	Min diff: -1.91

Box 4.4.4. Griggs et al. (2007) profile of tree ring precipitation reconstruction.

Lamentowicz et al. (2010)

Region: Slowinskie Blota
Lon.: 16.49°E
Lat.: 54.36°N
Proxy: Testate amoebae
Start: 1000 CE
End: 2002 CE
Length: 1003 years
Season: Annual

Basin ID: 242300603
Level: 9
Order: 1
Area: 618.9 km^2
Mean Elev.: 34 m
Slope: 11%
Mean P: 661 mm

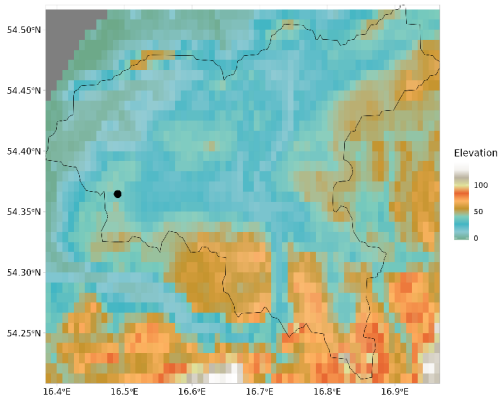

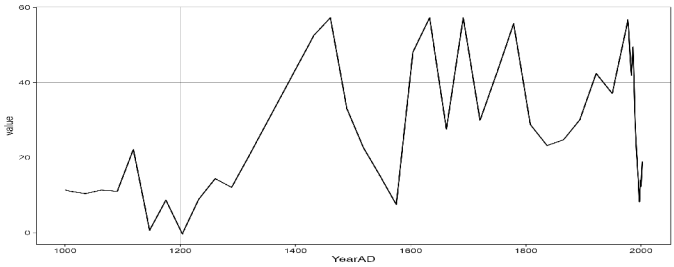

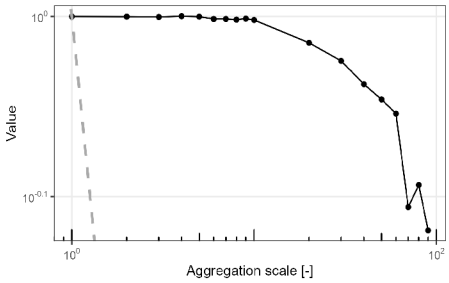

This record is based on the percentage of each species of Testate Amoeba in a sample from Slowinskie Bog (Poland), providing mixed signals of temperature and precipitation changes. The comparison of this macrofossil with local pollen indicates that changes on all spatial scales are linked, which is explained by a strong hydrologic connection between the bog and its local surroundings. The combination of proxies shows that groundwater levels were modified by both human impact and climate change.

1-year scale	10-year scale	30-year scale	50-year scale
Mean: 28.13	Max slope: 1.41	Max slope: 3.1	Max slope: 3.30
St. Dev: 16.08	Min slope: -2.69	Min slope: -2.01	Min slope: -2.49
Min/Max: -0.31/57.26	Max diff: 2.55	Max diff: 2.77	Max diff: 2.35
H(ACF-1): 1 (1)	Min diff: -4.9	Min diff: -1.87	Min diff: -1.8

Box 4.4.5. Lamentowicz et al. (2010) profile of Testae amoeba generated precipitation reconstruction.

Wilson et al. (2012)

Region: South central England
Lon.: -2.5– -1°E
Lat.: 51–52.2°N
Proxy: Tree rings
Start: 950 CE
End: 2009 CE
Length: 1060 years
Season: MJJ

Basin ID: 2330389
Level: 7
Order: 1
Area: 4608.4 km^2
Mean Elev.: 117 m
Slope: 18 %
Mean P: 655 mm

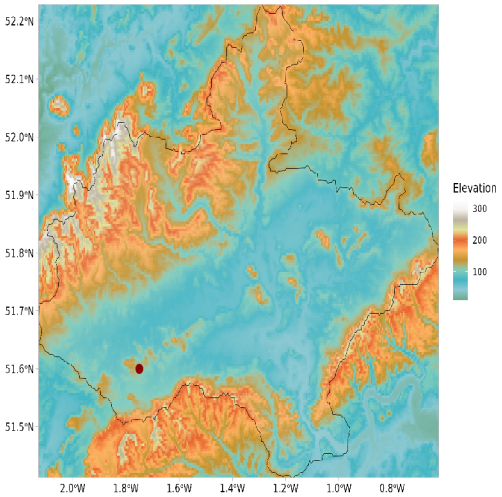

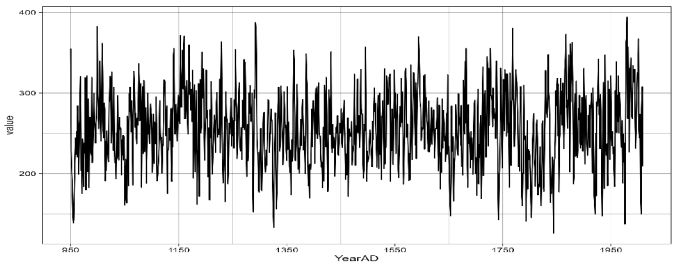

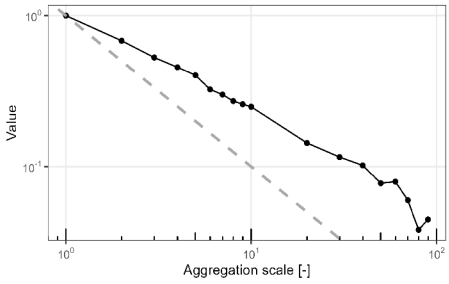

This millennial-long dendroclimatic reconstruction reveals a medieval period with multi-decade-long dry and wet periods. Notably, 1153-1172 CE appeared as the wettest period, while drier conditions prevailed from ~1300 to the early 16^{th} century, followed by a subsequent period of increasing precipitation. The centennial hydroclimatic trends broadly align with independent regional-scale hydroclimatic reconstructions from tree-ring data in East Anglia, historical records, speleothem, and peat water level proxy archives in the United Kingdom. These trends appear to be coupled with reconstructed sea surface temperature changes in the North Atlantic, which, in turn, influence the AMOC and westerly airflow across the UK.

1-year scale	10-year scale	30-year scale	50-year scale
Mean: 256.37	Max slope: 6.37	Max slope: 5.4	Max slope: 4.86
St. Dev: 46.64	Min slope: -6.12	Min slope: -2.97	Min slope: -3.27
Min/Max: 125.99/394.25	Max diff: 2.19	Max diff: 2.50	Max diff: 2.29
H(ACF-1): 0.74(0.37)	Min diff: -2.14	Min diff: -1.55	Min diff: -1.60

Box 4.4.6. Wilson et al. (2012) profile of tree rings precipitation reconstruction.

Lamentowicz et al. (2010)

Region: Stazki Bog
Lon.: 18.08°E
Lat.: 54.42°N
Proxy: Testae Amoeba
Start: 1000 CE
End: 2002 CE
Length: 1003 years
Season: Summer

Basin ID: 242300845
Level: 9
Order: 2
Area: 585.6 km^2
Mean Elev.: 147 m
Slope: 26%
Mean P: 650 mm

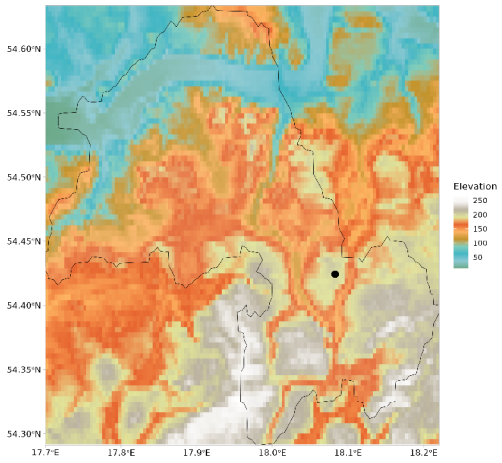

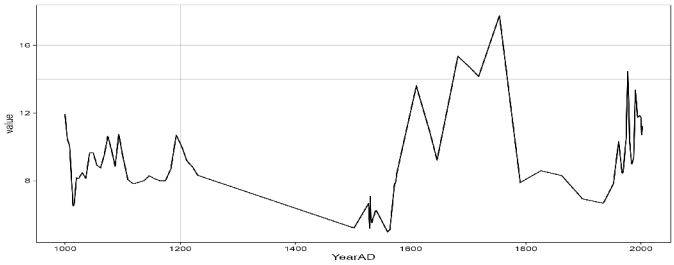

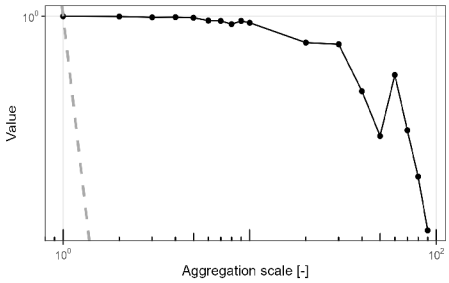

This precipitation reconstruction highlights significant wet-dry shifts and correlates this climate change with human impact on the Baltic bog ecosystem. The record indicates two dry periods, from 1100 to 1500 and from 1650 to 1900 CE, with wetter conditions observed from 1500 CE onwards. Further investigation suggests that the first shift to dry conditions is likely climate-driven, as pollen records show little evidence of human indicators. However, the second dry shift may be related to local peat exploitation of the mire.

1-year scale	10-year scale	30-year scale	50-year scale
Mean: 8.87	Max slope: 0.25	Max slope: 0.45	Max slope: 0.36
St. Dev: 2.8	Min slope: -0.33	Min slope: -0.65	Min slope: -0.39
Min/Max: 4.97/17.75	Max diff: 2.61	Max diff: 2.55	Max diff: 1.86
H(ACF-1): 0.99(0.99)	Min diff: -3.39	Min diff: -3.69	Min diff: -2.17

Box 4.4.7. Lamentowicz et al. (2010) profile of Testae Amoeba generated precipitation reconstruction.

Baker et al. (2010)

Region: Uamh an Tartair
Lon.: -4.98°E
Lat.: 58.15°N
Proxy: Stalagmite
Start: -991 CE
End: 2004 CE
Length: 2996 years
Season: Annual

Basin ID: 233023517
Level: 9
Order: 0
Area: 2800.4 km^2
Mean Elev.: 222 m
Slope: 89%
Mean P: 1219 mm

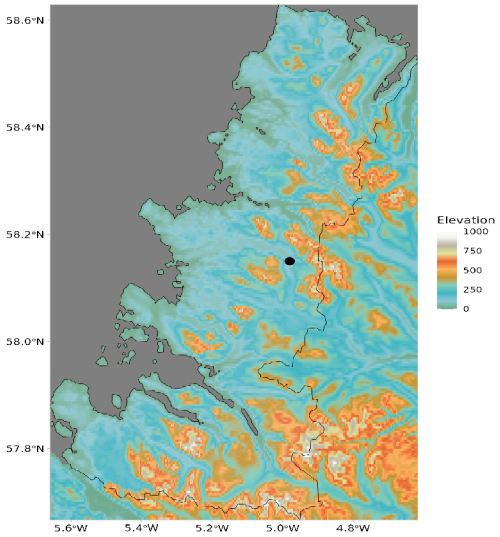

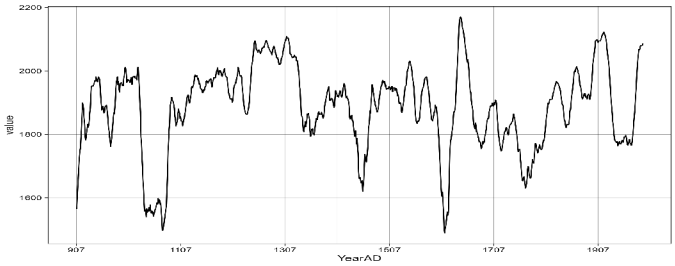

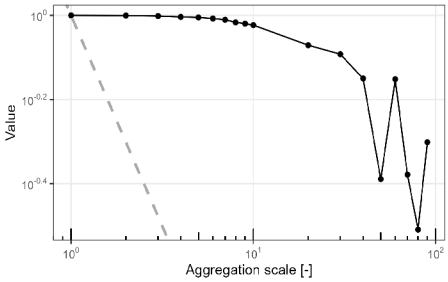

This precipitation reconstruction, utilizing stalagmite luminescence and peat humification records, reveals paleomoisture dynamics over the past 3000 years. With a minimal uncertainty in annual band counting, this method enables the reconstruction of mean annual precipitation and North Atlantic Oscillation patterns from approximately 900 CE to the present day. Comparing decadal patterns with the instrumental records (1879-1990 AD), this reconstruction suggests a positive correlation with temperature and a negative correlation with precipitation.

1-year scale	10-year scale	30-year scale	50-year scale
Mean: 1886.66	Max slope: 24.76	Max slope: 28.06	Max slope: 24.92
St. Dev: 132.77	Min slope: -28.78	Min slope: -23.32	Min slope: -17.08
Min/Max: 1488.9/2170.43	Max diff: 2.74	Max diff: 2.11	Max diff: 2.34
H(ACF-1): 0.99(0.98)	Min diff: -3.3	Min diff: -1.86	Min diff: -1.63

Box 4.4.8. Baker et al. (2010) profile of stalagmite generated precipitation reconstruction.

Tegel et al. (2020)

Region: Upper Rhine Valley
Lon.: 7–8.5°E
Lat.: 47.5–50°N
Proxy: Tree rings
Start: 265 CE
End: 2017 CE
Length: 1753 years
Season: Annual

Basin ID: 23267020
Level: 8
Order: 2
Area: 1757.7 km^2
Mean Elev.: 247 m
Slope: 53%
Mean P: 701 mm

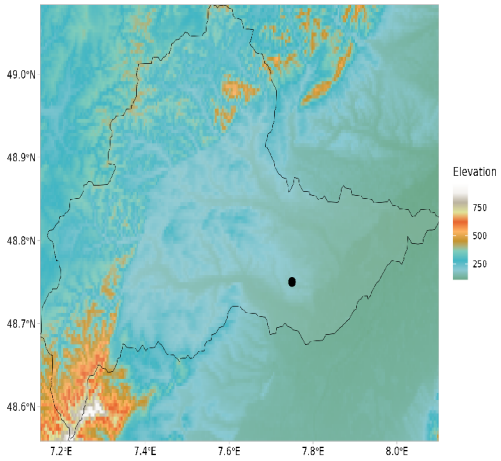

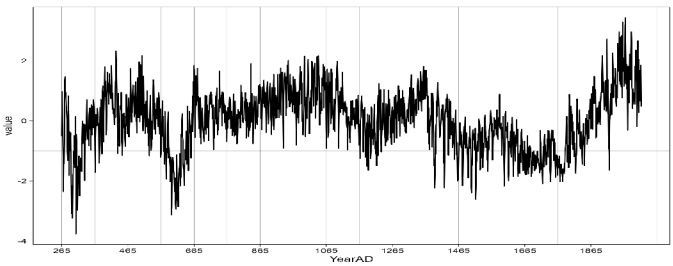

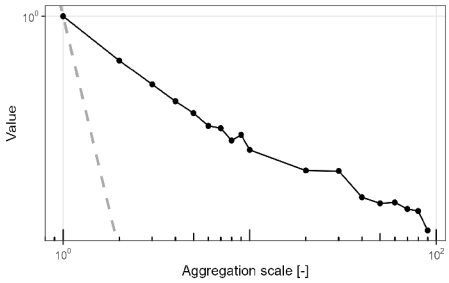

This tree-ring-based reconstruction reveals that warm periods during the late Roman, medieval, and recent times were characterized by higher groundwater levels. Conversely, lower groundwater levels were observed during cold periods, such as the Late Antique Little Ice Age (536 to about 660 CE) and the Little Ice Age, occurring between medieval and recent warming. These fluctuations in groundwater levels align with multidecadal North Atlantic climate variability derived from independent ocean proxies. Furthermore, warm and wet hydroclimate conditions suggest a connection with warm states of the Atlantic Ocean and positive phases of the North Atlantic Oscillation on decadal scales.

1-year scale	10-year scale	30-year scale	50-year scale
Mean: 0.0025	Max slope: 0.13	Max slope: 0.14	Max slope: 0.17
St. Dev: 1	Min slope: -0.15	Min slope: -0.12	Min slope: -0.08
Min/Max: -3.76/3.44	Max diff: 2.77	Max diff: 2.65	Max diff: 3.01
H(ACF-1): 0.91(0.76)	Min diff: -3.31	Min diff: -2.44	Min diff: -1.69

Box 4.4.9. Tegel et al. (2020) profile of Tree rings precipitation reconstruction.

Büntgen et al. (2016)

Region: Alps
Lon.: 10–15°E
Lat.: 45–50°N
Proxy: Tree rings
Start: 1 CE
End: 2003 CE
Length: 2003 years
Season: JJA

Basin ID: 22798
Level: 5
Order: 2
Area: 25920 km^2
Mean Elev.: 1251 m
Slope: 162%
Mean P: 1145 mm

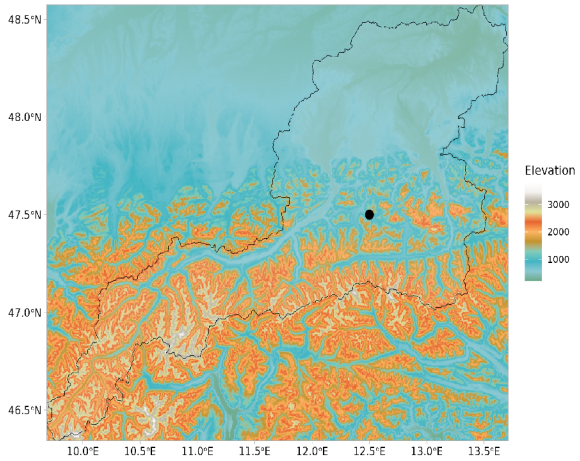

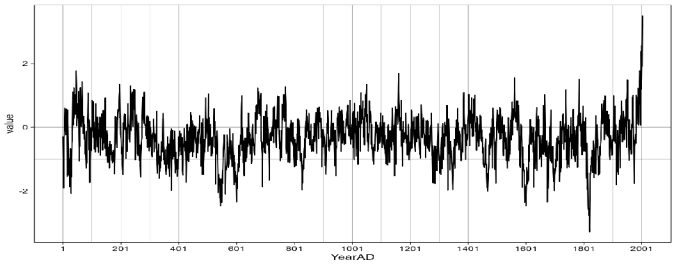

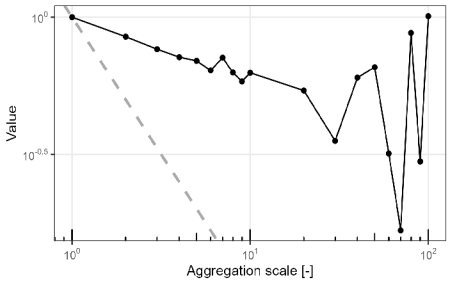

This summer temperature reconstruction, derived from tree-ring chronologies from the Russian Altai and European Alps, reveals spatially synchronized cooling events in 536, 540, and 547 CE. These unprecedented and prolonged conditions were likely the result of ocean and sea-ice feedback, along with a solar minimum. Furthermore, this record identifies the interval from 536 to about 660 CE as the Late Antique Little Ice Age.

1-year scale	10-year scale	30-year scale	50-year scale
Mean: -0.33	Max slope: 0.14	Max slope: 0.11	Max slope: 0.22
St. Dev: 0.69	Min slope: -0.15	Min slope: -0.12	Min slope: -0.09
Min/Max: -3.28/3.50	Max diff: 2.58	Max diff: 2.55	Max diff: 4.13
H(ACF-1): 0.90(0.65)	Min diff: -2.87	Min diff: -2.55	Min diff: -1.83

Box 4.4.10. Büntgen et al. (2016) profile of tree rings temperature reconstruction.

Helama et al. (2014)

Region: Finnish Lakeland
Lon.: 25.48–31.17°E
Lat.: 61.8–62.85°N
Proxy: Tree rings
Start: 760 CE
End: 2000 CE
Length: 1241 years
Season: MJJAS

Basin ID: 24322
Level: 5
Order: 2
Area: 94629.6 km^2
Mean Elev.: 104 m
Slope: 28%
Mean P: 628 mm

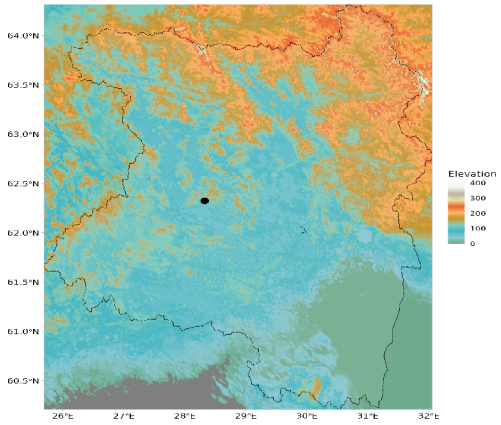

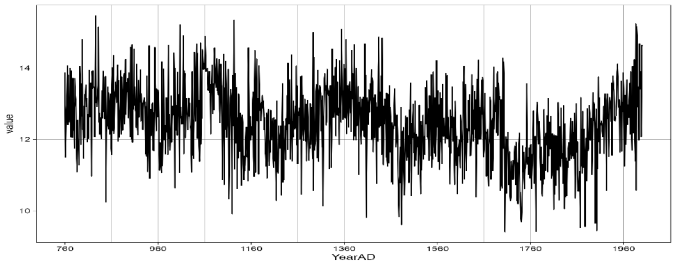

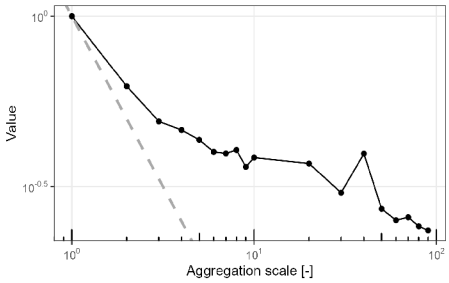

This X-ray-based tree-ring reconstruction provides insights into temperature variability during the warm season across Northern Europe. A pronounced signal of the Little Ice Age is evident between 1407 and 1902 CE, with these periods representing the coolest events. This cooling phenomenon is further corroborated by agro-historical chronicles documenting instances of famine during this time. Additionally, cooling during the early 18th century aligns with the Maunder Minimum, a period characterized by significantly reduced solar radiation.

1-year scale	10-year scale	30-year scale	50-year scale
Mean: 12.46	Max slope: 0.12	Max slope: 0.09	Max slope: 0.16
St. Dev: 1.04	Min slope: -0.11	Min slope: -0.13	Min slope: -0.11
Min/Max: 9.41/15.46	Max diff: 2.69	Max diff: 1.81	Max diff: 2.62
H(ACF-1): 0.66(0.23)	Min diff: -2.65	Min diff: -2.71	Min diff: -2.0

Box 4.4.11. Helama et al. (2014) profile of tree rings temperature reconstruction.

Zhang et al. (2016)

Region: Jämtland
Lon.: 13.2–14.9°E
Lat.: 62.8–63.2°N
Proxy: Tree rings
Start: 850 CE
End: 2011 CE
Length: 1161 years
Season: AMJJAS

Basin ID: 2445025
Level: 7
Order: 1
Area: 3913.4 km^2
Mean Elev.: 388 m
Slope: 36%
Mean P: 606 mm

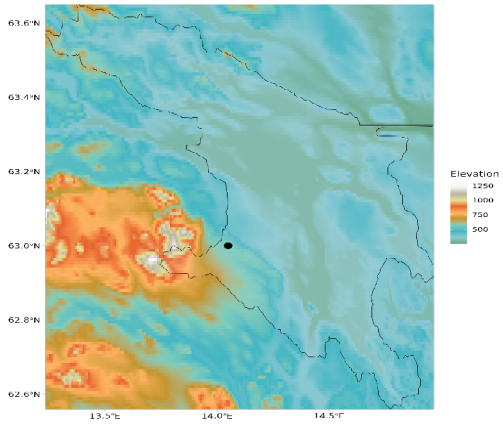

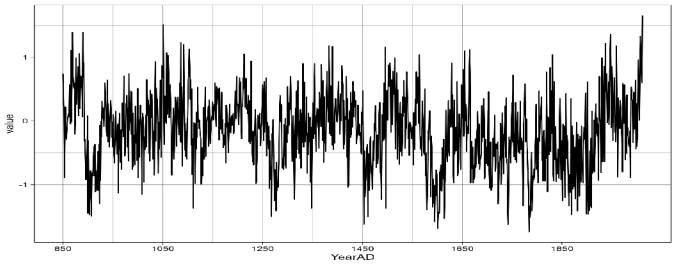

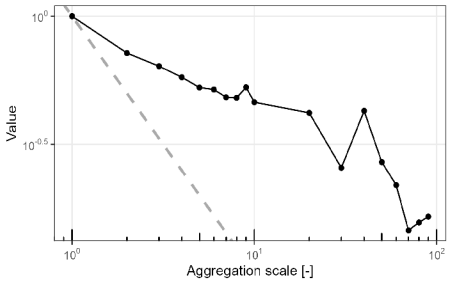

This reconstruction utilizes pine tree-ring density to depict warm-season temperatures during the Medieval Climate Anomaly (MCA) over Scandinavia, spanning primarily from 850 to 2011 CE. The analysis reveals a peak in warmth during the MCA between 1000 and 1100 CE, followed by a colder climate period between 1550 and 1900 CE, commonly referred to as the Little Ice Age. Additionally, the coldest decades occurred around 1600 CE during the last millennium, while the warmest 10 and 30 years are observed in the recent century.

1-year scale	10-year scale	30-year scale	50-year scale
Mean: -0.16	Max slope: 0.06	Max slope: 0.09	Max slope: 0.06
St. Dev: 0.57	Min slope: -0.10	Min slope: -0.10	Min slope: -0.07
Min/Max: -1.74/1.65	Max diff: 1.73	Max diff: 2.25	Max diff: 1.62
H(ACF-1): 0.75(0.42)	Min diff: -3.02	Min diff: -2.65	Min diff: -2.02

Box 4.4.12. Zhang et al. (2016) profile of tree rings temperature reconstruction.

Helama et al. (2012)

Region: N. Fennoscandia
Lon.: 14.05–35.32°E
Lat.: 66.42–70.83°N
Proxy: Tree rings
Start: -5500 CE
End: 2005 CE
Length: 7506 years
Season: July

Basin ID: 2438028
Level: 7
Order: 3
Area: 1282.8 km^2
Mean Elev.: 359 m
Slope: 29%
Mean P: 487 mm

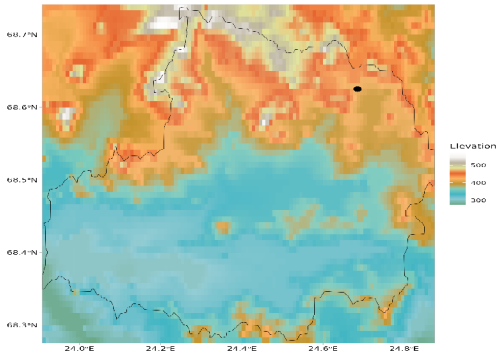

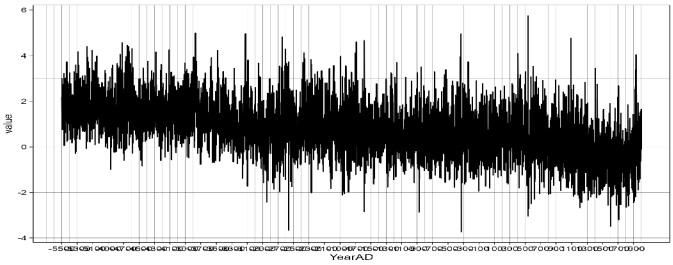

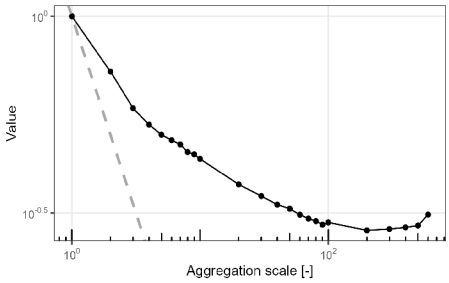

This reconstruction of mid-summer temperatures is based on the fusion of spectra of pollen and tree rings. The analysis suggests a decline in temperatures by 2.0°C over the past 7.5 ka. Furthermore, it indicates that the mid-Holocene warmth terminated between 5 and 4 ka, followed by a cooling phase, the Little Ice Age, evident between 0.7 and 0.1 ka. Additionally, the reconstruction reveals subsequent warming during the past century. On average, the reconstructed Holocene climate was approximately 0.85°C warmer than the twentieth century. Notably, within the modern period, the years 1934 and 1937 are among the warmest, while the years 1903 and 1910 are among the coldest summers in the context of the past 7.5 ka.

1-year scale	10-year scale	30-year scale	50-year scale
Mean: 0.84	Max slope: 0.18	Max slope: 0.15	Max slope: 0.18
St. Dev: 1.14	Min slope: -0.21	Min slope: -0.15	Min slope: -0.1
Min/Max: -3.73/5.75	Max diff: 3.28	Max diff: 3.40	Max diff: 4.27
H(ACF-1): 0.71(0.44)	Min diff: -3.87	Min diff: -2.78	Min diff: -2.27

Box 4.4.13. Helama et al. (2012) profile of tree rings temperature reconstruction.

Matskovsky and Helama (2014)

Region: N. Fennoscandia
Lon.: 19.75–29°E
Lat.: 66.8–69.5°N
Proxy: Tree rings
Start: -7 CE
End: 2010 CE
Length: 2018 years
Season: JJ

Basin ID: 2438
Level: 4
Order: 1
Area: 53537.6 km^2
Mean Elev.: 228m
Slope: 31%
Mean P: 511 mm

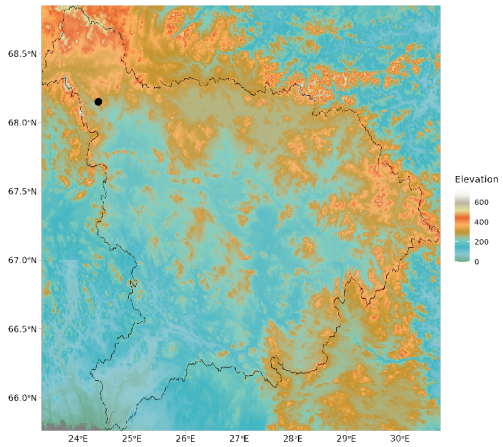

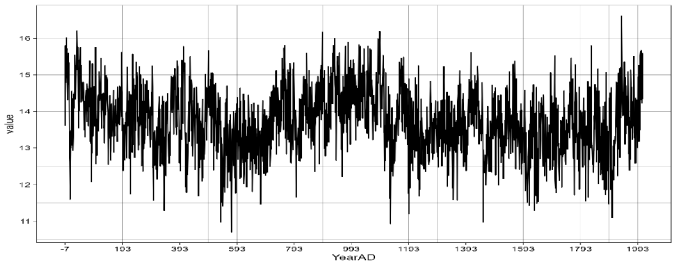

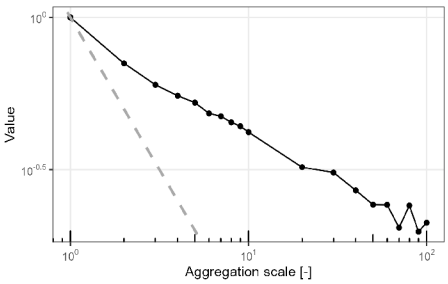

This record presents an analysis of tree-ring density chronologies previously used by Melvin et al., 2013, and Esper et al., 2012, to reconstruct variations in summer temperature from 8 BC to 2010 CE. The reconstruction indicates multi-decadal to multi-centennial variability, with variations in the amplitude of summer temperature averaging 2.2°C during the Common Era. The study highlights that combined data offers a robust proxy for summer temperature in paleoclimate research. However, the presence of bifurcating dendroclimatic signals underscores the need for further investigation into issues such as population density effects, calibration biases, and biological age impact influences on mixed production in tree-ring analysis.

1-year scale	10-year scale	30-year scale	50-year scale
Mean: 13.74	Max slope: 0.12	Max slope: 0.14	Max slope: 0.09
St. Dev: 0.9	Min slope: -0.15	Min slope: -0.13	Min slope: -0.11
Min/Max: 10.70/16.61	Max diff: 2.34	Max diff: 2.55	Max diff: 2.09
H(ACF-1): 0.73(0.42)	Min diff: -2.93	Min diff: -2.45	Min diff: -2.39

Box 4.4.14. Matskovsky and Helama (2014) profile of tree rings temperature reconstruction.

Matskovsky and Helama (2014)

Region: Seebergsee	**Basin ID**: 2160267
Lon.: 7.47°E	**Level**: 7
Lat.: 46.12°N	**Order**: 2
Proxy: Chironomid	**Area**: 6207.5 km^2
Start: 1083 CE	**Mean Elev.**: 1421 m
End: 2001 CE	**Slope**: 178%
Length: 919 years	**Mean P**: 1380 mm
Season: July	

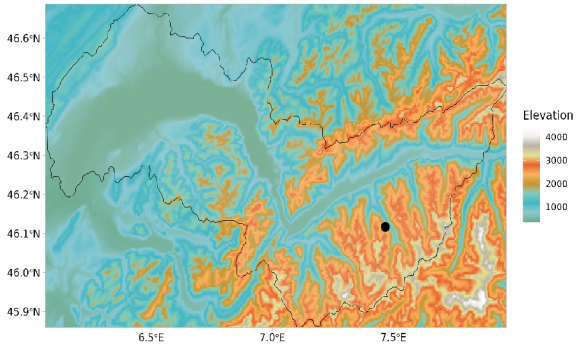

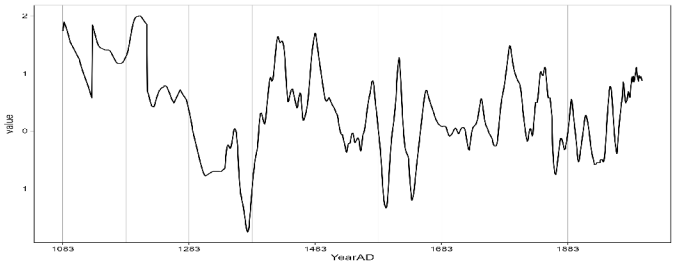

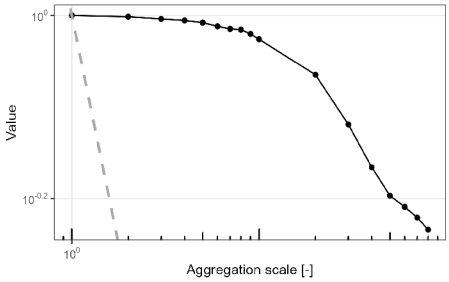

This decadal mean summer temperature reconstruction spanning the past millennium aligns closely with instrumental data, accurately reflecting temperature variations over approximately 250 years. The record highlights a warmer climate during the latter part of the Medieval Climate Anomaly, with temperatures averaging approximately 1.2°C higher compared to the last century, followed by a colder period during the Little Ice Age, with temperatures averaging around -0.5°C lower compared to the last century.

1-year scale	10-year scale	30-year scale	50-year scale
Mean: 0.36	Max slope: 0.10	Max slope: 0.14	Max slope: 0.16
St. Dev: 0.76	Min slope: -0.1	Min slope: -0.11	Min slope: -0.1
Min/Max: -1.75/1.99	Max diff: 2.22	Max diff: 2.39	Max diff: 2.78
H(ACF-1): 0.99(0.99)	Min diff: -2.11	Min diff: -1.74	Min diff: -1.6

Box 4.4.15. Matskovsky and Helama (2014) profile of chironomid temperature reconstruction.

Büntgen et al. (2013)

Region: Tatra region
Lon.: 19–21°E
Lat.: 49–50°N
Proxy: Tree rings
Start: 1040 CE
End: 2011 CE
Length: 972 years
Season: MJ

Basin ID: 2424468
Level: 7
Order: 4
Area: 2220.7 km^2
Mean Elev.: 806 m
Slope: 107%
Mean P: 936 mm

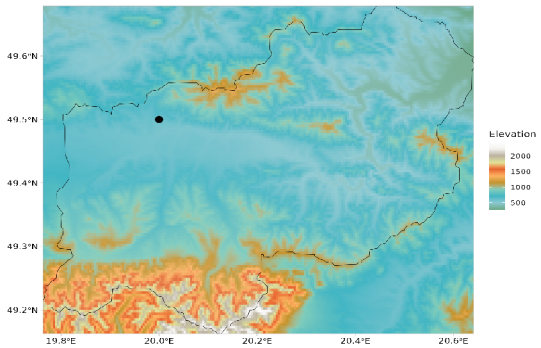

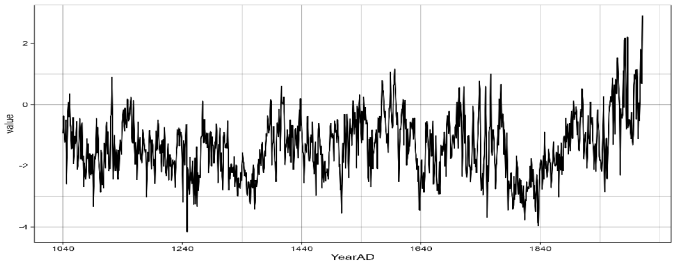

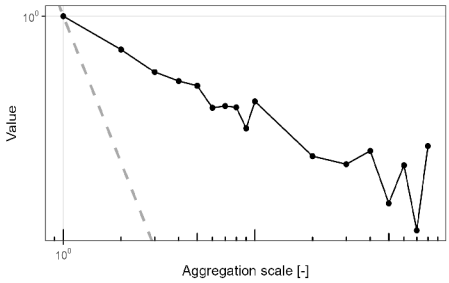

Utilizing 545 tree ring samples from both living trees and historical timbers, this temperature reconstruction endeavors to depict interannual to centennial variations in May-June temperatures across Eastern Europe since 1040 CE. The findings indicate that the mid-14th, early 17th, and early 19th centuries emerged as the coldest periods within the last millennium.

1-year scale	10-year scale	30-year scale	50-year scale
Mean: -1.36	Max slope: 0.15	Max slope: 0.17	Max slope: 0.11
St. Dev: 0.98	Min slope: -0.15	Min slope: -0.11	Min slope: -0.09
Min/Max: -4.16/2.91	Max diff: 2.23	Max diff: 2.45	Max diff: 1.87
H(ACF-1): 0.91(0.68)	Min diff: -2.42	Min diff: -1.91	Min diff: -1.72

Box 4.4.16. Büntgen et al. (2013) profile of tree rings temperature reconstruction.

Loader et al. (2013)

Region: Torneträsk
Lon.: 19.40–20.20°E
Lat.: 68.10–68.30°N
Proxy: δ^{13}C (Cellulose)
Start: 441 CE
End: 2010 CE
Length: 1570 years
Season: Annual

Basin ID: 24420709
Level: 8
Order: 1
Area: 386.2 km^2
Mean Elev.: 632 m
Slope: 62%
Mean P: 496 mm

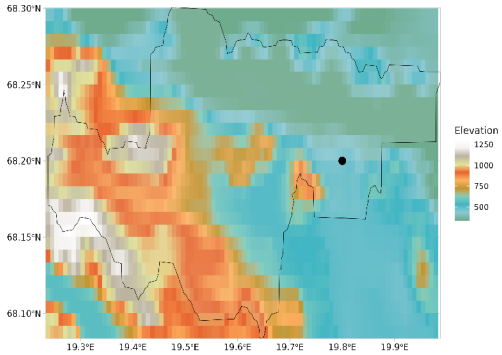

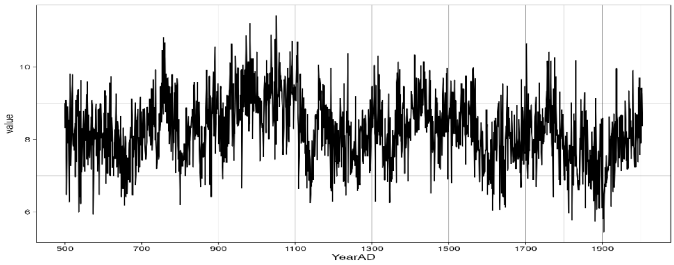

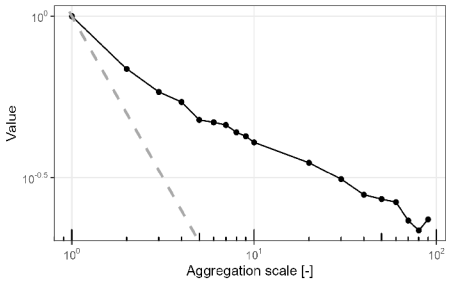

This reconstruction, based on 74 trees, provides a proxy for June-August temperature and sunshine in northern Fennoscandia by calibrating against Abisko's instrumental data. Notable divergences between temperature and sunshine records, especially during the Little Ice Age, highlight shifts in large-scale circulation, offering insights into historical climate variations. The observed temperature changes indicate a correlated response attributed to a shift in large-scale circulation associated with the southward migration of the Polar Front.

1-year scale	10-year scale	30-year scale	50-year scale
Mean: 9.93	Max slope: 0.13	Max slope: 0.12	Max slope: 0.08
St. Dev: 0.69	Min slope: -0.13	Min slope: -0.11	Min slope: -0.09
Min/Max: 8.07/12.85	Max diff: 2.40	Max diff: 2.49	Max diff: 1.73
H(ACF-1): 0.94()	Min diff: -2.49	Min diff: -2.36	Min diff: -2.01

Box 4.4.17. Loader et al. (2013) profile of δ^{13}C-based temperature reconstruction.

Melvin et al. (2013)

Region: Torneträsk
Lon.: 19.45–19.80°E
Lat.: 68.21–68.31°N
Proxy: Tree rings
Start: -39 CE
End: 2010 CE
Length: 2050 years
Season: MJJA

Basin ID: 24420709
Level: 8
Order: 1
Area: 386.2 km^2
Mean Elev.: 632 m
Slope: 69%
Mean P: 496 mm

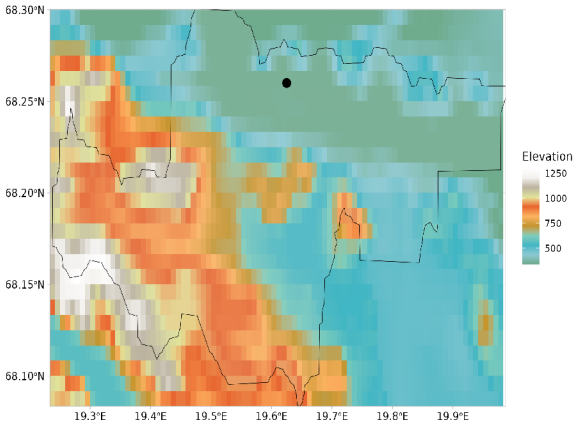

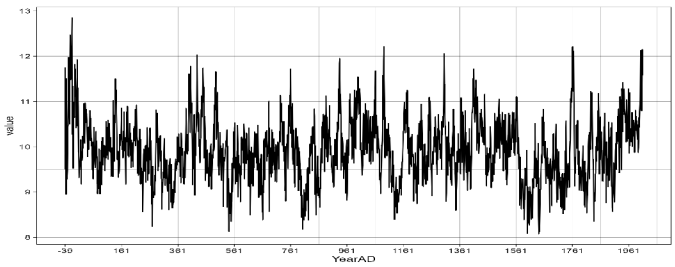

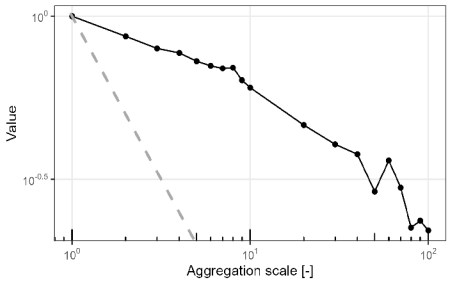

This record is the analysis of latewood density (MXD) and tree-ring width data from the Torneträsk region to reconstruct 1500-year chronologies of summer temperature. A study related to this reconstruction revealed that discrepancies due to systematic bias in MXD data measurements and sample selection from living trees (modern sample bias) can be addressed and refined using the Regional Curve Standardization method. As a result, the new MXD and tree-ring chronologies may offer a more consistent portrayal of long-term changes in past summer temperatures. This reconstruction indicates comparable levels of summer warmth between the medieval period (i.e., 900-1100 CE) and the latter half of the 20th century.

1-year scale	10-year scale	30-year scale	50-year scale
Mean: 8.25	Max slope: 0.14	Max slope: 0.09	Max slope: 0.06
St. Dev: 0.93	Min slope: -0.09	Min slope: -0.13	Min slope: -0.11
Min/Max: 5.45/11.42	Max diff: 3.19	Max diff: 1.2	Max diff: 1.21
H(ACF-1): 0.72(0.37)	Min diff: -2.32	Min diff: -2.78	Min diff: -2.33

Box 4.4.18. Melvin et al. (2013) profile of tree rings temperature reconstruction.

4.5 Spatio-temporal data information across the North America

Grissino and Henri (1995)

Region: El Malpais
Lon.: -108.1°E
Lat.: 34.97°N
Proxy: Tree rings
Start: -136 CE
End: 1992 CE
Length: 2129 years
Season: Annual

Basin ID: 7521946
Level: 7
Order: 3
Area: 7636.1 km^2
Mean Elev.: 2154 m
Slope: 42%
Mean P: 317 mm

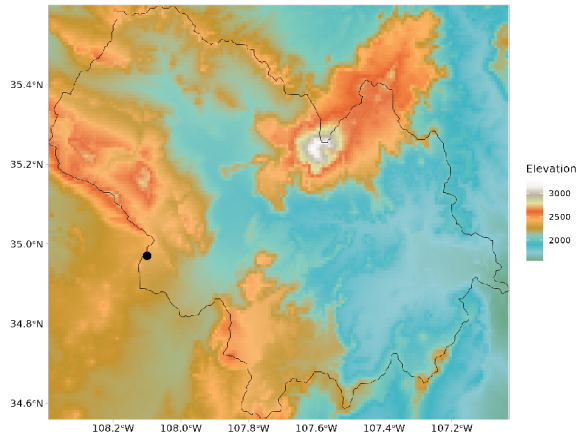

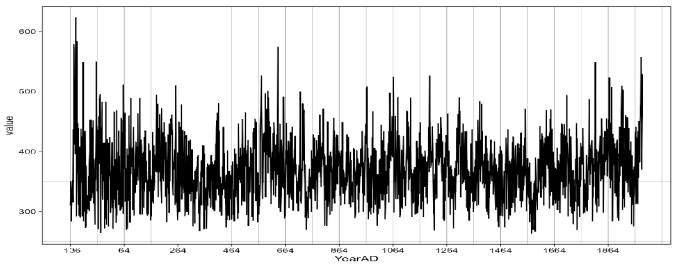

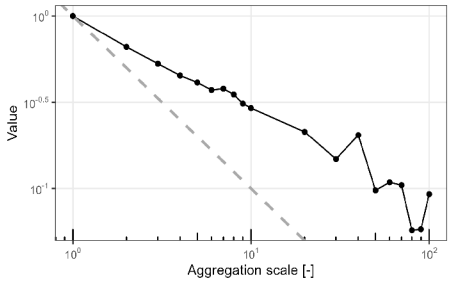

This is the tree-ring chronology-based reconstruction of annual precipitation patterns over the El Malpais region in the Southwestern United States. Spanning 2129 years from 136 BC to 1992 CE, the reconstruction is based on 248 measurement series derived from living trees and sub-fossil wood found on the lava surface. The calibrated annual rainfall data for New Mexico from 1896 to 1992 CE exhibits a remarkable correlation with the chronology, explaining 70 percent of the climatic variance. Notably, the reconstruction captures both high and low-frequency trends in precipitation, revealing seven major long-term trends over the last 1900 years.

1-year scale	10-year scale	30-year scale	50-year scale
Mean: 118.89	Max slope: 10.63	Max slope: 10.54	Max slope: 4.08
St. Dev: 38.87	Min slope: -7.75	Min slope: -4.77	Min slope: -3.59
Min/Max: 263.39/623.32	Max diff: 3.43	Max diff: 4.08	Max diff: 2.20
H(ACF-1): 0.69(0.29)	Min diff: -2.54	Min diff: -1.91	Min diff: -1.93

Box 4.5.1.Grissino and Henri (1995) profile of tree ring precipitation reconstruction.

Stahle et al. (2009)

Region: El Malpais
Lon.: -108.2°E
Lat.: 34.97°N
Proxy: Tree-ring
Start: -136 CE
End: 2002 CE
Length: 2139 years
Season: MJJA

Basin ID: 77240909
Level: 8
Order: 2
Area: 920.6 km^2
Mean Elev.: 2265 m
Slope: 25%
Mean P: 364 mm

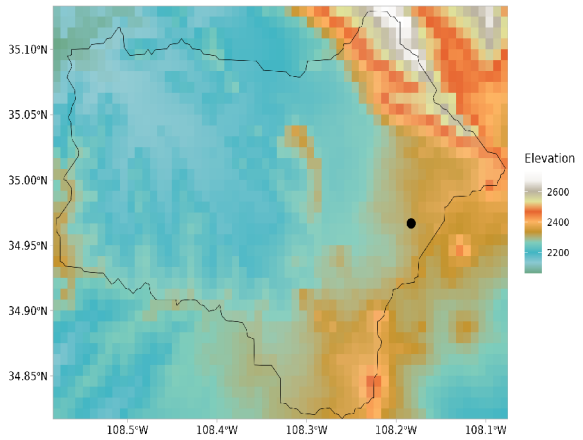

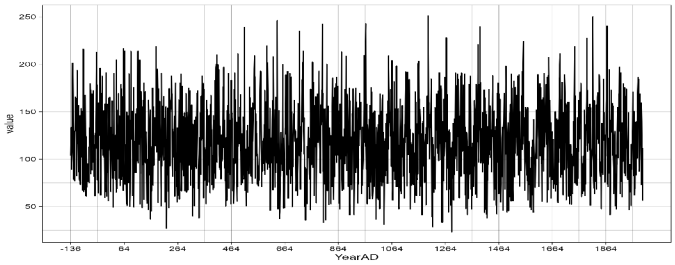

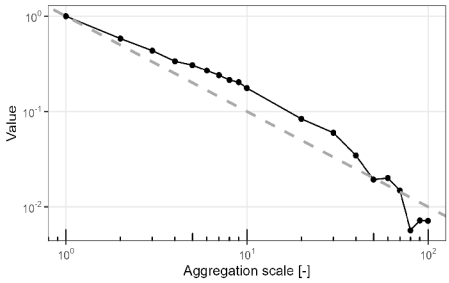

This reconstruction covers cool and warm-season precipitation for the past 2,139 years. These reconstructions align with instrumental precipitation and ocean-atmospheric dynamics, including El Niño and the Pacific decadal oscillation. Interestingly, interannual variations in this precipitation record exhibit correlation, with wet winter-spring periods often followed by dry summers, possibly due to shifts in large-scale forcing or regional feedback mechanisms. This record reveals episodes of prolonged simultaneous inter-seasonal drought that persisted during the 1950s, 8th, and 16th centuries drought.

1-year scale	10-year scale	30-year scale	50-year scale
Mean: 118.98	Max slope: 5.77	Max slope: 2.96	Max slope: 2.34
St. Dev: 38.87	Min slope: -5.99	Min slope: -4.18	Min slope: -3.02
Min/Max: 23.32/251.1	Max diff: 2.35	Max diff: 1.98	Max diff: 2.25
H(ACF-1): 0.60(0.15)	Min diff: -2.44	Min diff: -2.84	Min diff: -2.69

Box 4.5.2. Stahle et al. (2009) profile of tree ring precipitation reconstruction.

Spruce et al. (2020)

Region: Foy lake
Lon.: -114.35°E
Lat.: 48.17°N
Proxy: δ^{18}O
Start: -201 CE
End: 2006 CE
Length: 2208 years
Season: Annual

Basin ID: 78266450
Level: 8
Order: 4
Area: 1183 km^2
Mean Elev.: 1191 m
Slope: 88%
Mean P: 592 mm

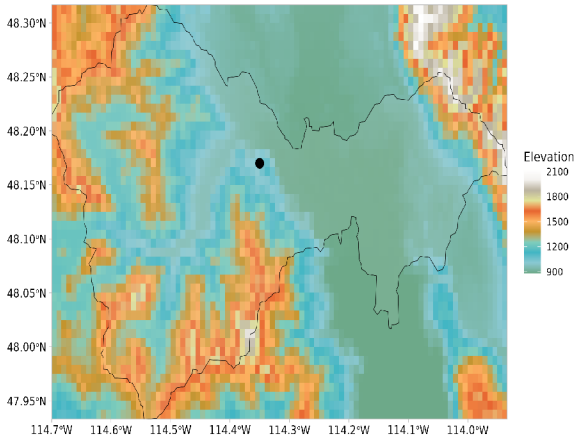

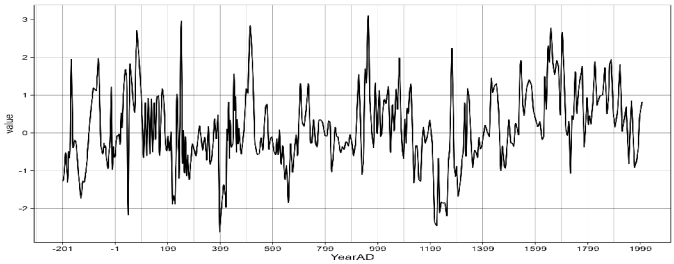

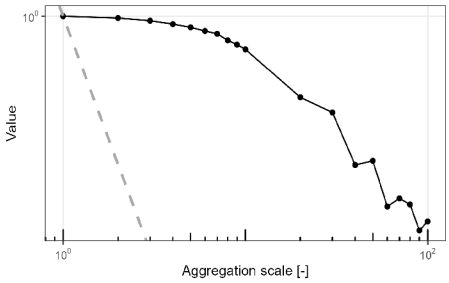

This 2200-year reconstruction based on δ^{18}O measurements of sediment carbonates from Foy Lake provides valuable insights into millennial-scale variability in snowpack dynamics. The significant low-frequency variability observed over millennia, along with the scarcity of historic droughts, underscores the importance of such sediment records. By leveraging these records, our understanding of past snowpack dynamics is greatly enhanced, aiding in the anticipation of future conditions, particularly in light of climatic events such as the mid-Holocene climate optimum.

1-year scale	10-year scale	30-year scale	50-year scale
Mean: 0.13	Max slope: 0.19	Max slope: 0.18	Max slope: 0.19
St. Dev: 0.95	Min slope: -0.21	Min slope: -0.17	Min slope: -0.13
Min/Max: -2.62/3.1	Max diff: 2.64	Max diff: 2.21	Max diff: 2.34
H(ACF-1): 0.99(0.98)	Min diff: -2.97	Min diff: -2.15	Min diff: -1.72

Box 4.5.3. Spruce et al. (2020) profile of cellulose (δ^{18}O) precipitation reconstruction.

Touchan et al. (2021)

Region: S. Sierra Nevada
Lon.: -120.25– -118.6°E
Lat.: 35.8–38.25°N
Proxy: Tree rings
Start: 90 CE
End: 2012 CE
Length: 1923 years
Season: May

Basin ID: 7744280
Level: 7
Order: 3
Area: 5265.3 km^2
Mean Elev.: 1760 m
Slope: 117%
Mean P: 651 mm

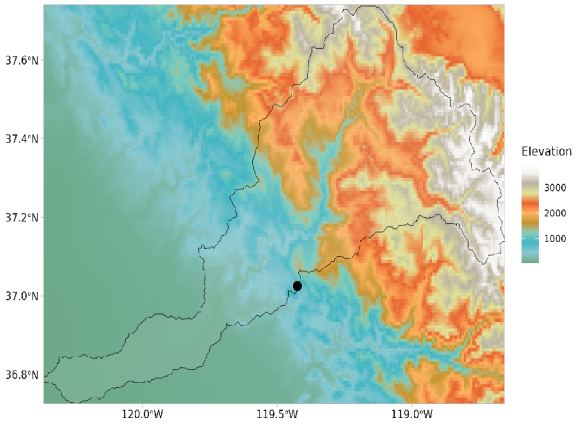

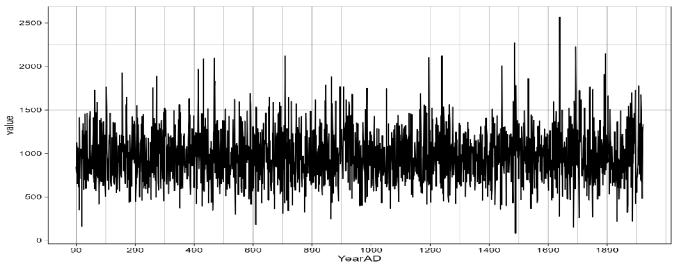

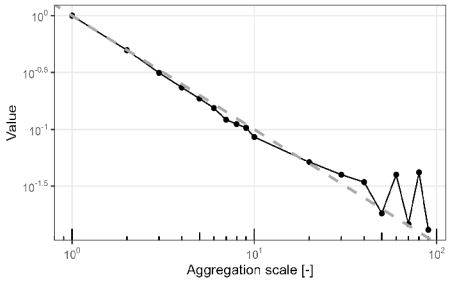

This reconstruction reveals climate variability across interannual to intercentennial time scales. The reconstruction exhibits a strong relationship between the May snow water equivalent (SWE) and tree-ring growth, indicating the changes in the water cycle. Notably, the reconstruction highlights periods of consecutive low and high SWE years, with the highest frequency of lowest SWE years during 710-809 CE, and possible low precipitation. Moreover, SWE positively correlates with northeastern Pacific SST, offering potential predictive insights. Overall, while 20th-century SWE variability in Sequoia groves has largely remained within historical bounds, future changes may pose challenges for water availability and tree health in the region.

1-year scale	**10-year scale**	**30-year scale**	**50-year scale**
Mean: 971.01	Max slope: 36.14	Max slope: 20.12	Max slope: 14.30
St. Dev: 301.40	Min slope: -27.84	Min slope: -18.37	Min slope: -15.99
Min/Max: 81.43/2565.98	Max diff: 2.96	Max diff: 2.74	Max diff: 2.16
H(ACF-1): 0.46(-0.04)	Min diff: -2.30	Min diff: -2.62	Min diff: -2.57

Box 4.5.4. Touchan et al. (2021) profile of tree ring precipitation reconstruction.

Bale et al. (2011)

Region: White Mountains	**Basin ID**: 77320803
Lon.: -118.17°E	**Level**: 8
Lat.: 37.45°N	**Order**: 1
Proxy: Tree rings	**Area**: 519.3 km^2
Start: 90 CE	**Mean Elev.**: 2226 m
End: 2012 CE	**Slope**: 117%
Length: 1923 years	**Mean P**: 250 mm
Season: JJA	

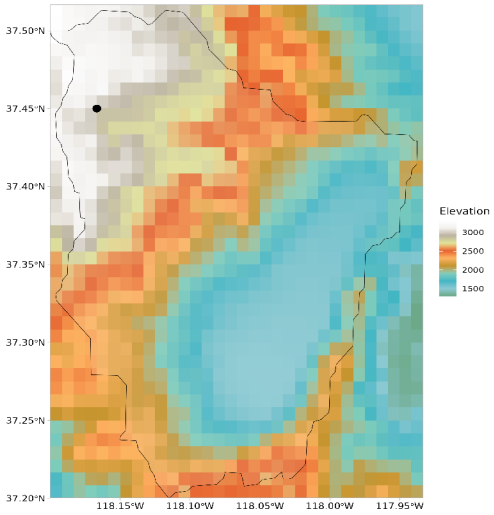

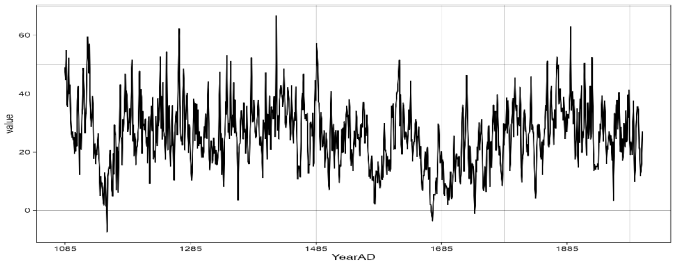

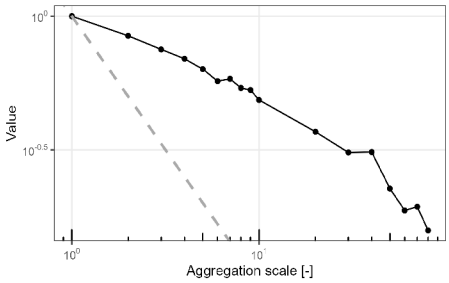

This reconstruction offers a millennium-long stable isotope record derived from bristlecone pines, providing insights into growing season precipitation since 1085 CE. The carbon isotope ratios from seven trees reveal a strong correlation between extremely negative isotope results and severe El Niño events over the past 500 years. Moreover, similar values in the first half of the millennium contributed to the reconstruction of 13 strong El Niño events, primarily noticed in the 12th Century and the mid-13th to 14th Centuries. Additionally, ring-width chronologies from neighboring sites exhibit significant decadal covariance with the δ^{13}C series, although periods of notable divergence are also observed.

1-year scale	**10-year scale**	**30-year scale**	**50-year scale**
Mean: 25.88	Max slope: 1.37	Max slope: 1.77	Max slope: 0.94
St. Dev: 11.06	Min slope: -2.21	Min slope: -2.12	Min slope: -1.70
Min/Max: -7.4/66.7	Max diff: 1.77	Max diff: 2.38	Max diff: 1.45
H(ACF-1): 0.94(0.68)	Min diff: -2.75	Min diff: -2.78	Min diff: -2.25

Box 4.5.5. Bale et al. (2011) profile of tree ring precipitation reconstruction

Hughes et al. (2005)

Region: Baker Lake
Lon.: -114.27°E
Lat.: 45.88°N
Proxy: Tree rings
Start: 12 CE
End: 1997 CE
Length: 1986 years
Season: Seasonality

Basin ID: 7826660
Level: 7
Order: 4
Area: 7395.1 km^2
Mean Elev.: 1747 m
Slope: 157%
Mean P: 452 mm

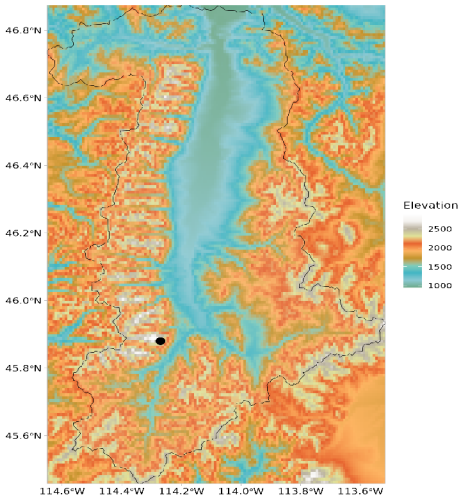

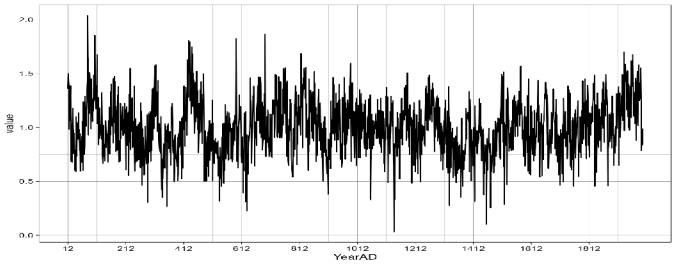

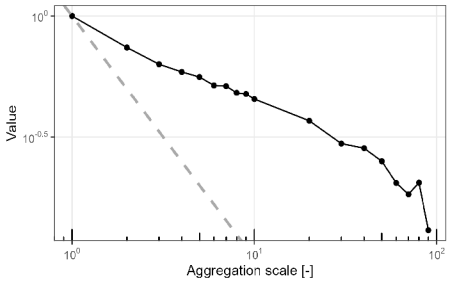

The ring width estimated reconstruction provides insight into temperature variations across the western United States. It notably captures distinct signals of variability during the Medieval Climate Anomaly, characterized by a transition from warm to cold climates between the 12th and 15th centuries.

1-year scale	10-year scale	30-year scale	50-year scale
Mean: 0.99	Max slope: 0.03	Max slope: 0.05	Max slope: 0.04
St. Dev: 0.25	Min slope: -0.04	Min slope: -0.03	Min slope: -0.03
Min/Max: 0.03/2.04	Max diff: 2.09	Max diff: 2.86	Max diff: 2.64
H(ACF-1): 0.78(0.48)	Min diff: -2.78	Min diff: -2.09	Min diff: -1.91

Box 4.5.6. Hughes et al. (2005) profile of tree rings temperature reconstruction.

Graumlich et al. (2005)

Region: Boreal Plateau
Lon.: -118.55°E
Lat.: 36.45°N
Proxy: Tree rings
Start: 831 CE
End: 1992 CE
Length: 1162 years
Season: Seasonality

Basin ID: 7744019
Level: 7
Order: 2
Area: 2772.7 km^2
Mean Elev.: 2435 m
Slope: 167%
Mean P: 631 mm

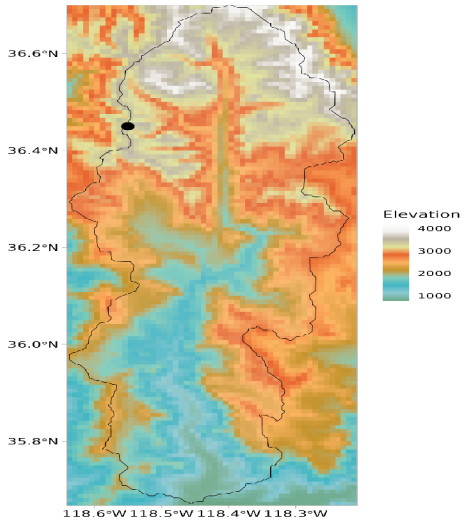

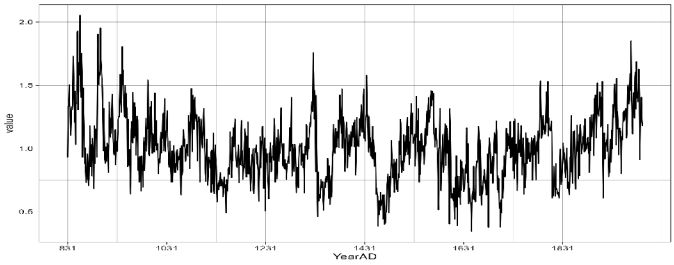

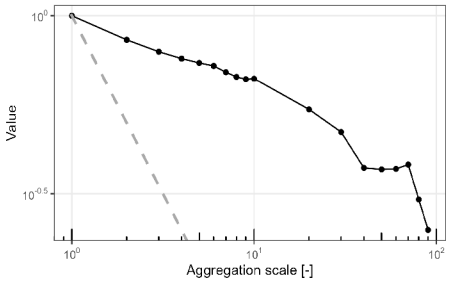

This multispecies tree-ring reconstruction, spanning a millennium, aimed to examine chronologies from high-elevation conifers across western North America. By analyzing approximately 1000-year chronologies encompassing five high-elevation conifer species across 13 sites, this study utilized ordination and cluster analysis to link variability to temperature and precipitation changes.

1-year scale	10-year scale	30-year scale	50-year scale
Mean: 1	Max slope: 0.06	Max slope: 0.03	Max slope: 0.04
St. Dev: 0.26	Min slope: -0.06	Min slope: -0.04	Min slope: -0.04
Min/Max: 0.3/2.05	Max diff: 3.17	Max diff: 2.04	Max diff: 1.97
H(ACF-1): 0.90(0.71)	Min diff: -3.15	Min diff: -2.49	Min diff: -2.42

Box 4.5.7. Graumlich et al. (2005) profile of tree ring temperature reconstruction.

Graybill (1995)

Region: Cirque Peak
Lon.: -118.22°E
Lat.: 36.45°N
Proxy: Tree rings
Start: 917 CE
End: 1987 CE
Length: 1071 years
Season: Seasonality

Basin ID: 7744019
Level: 7
Order: 2
Area: 2772.7 km^2
Mean Elev.: 2435 m
Slope: 167%
Mean P: 631 mm

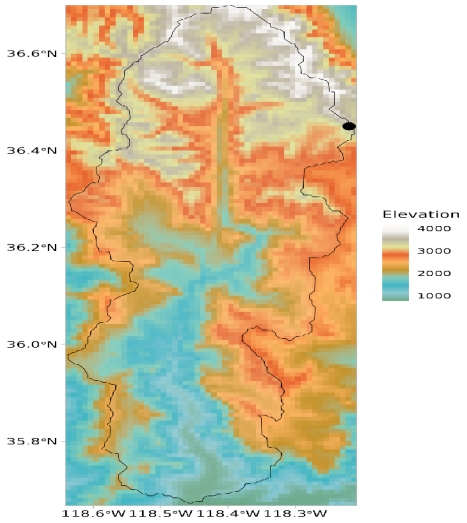

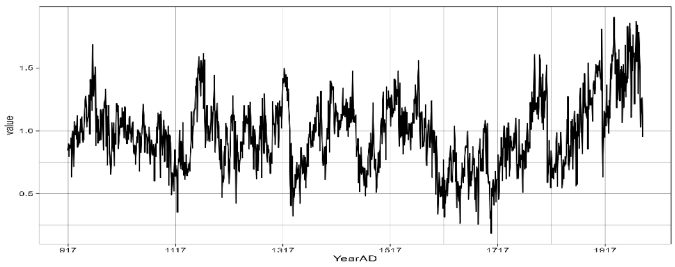

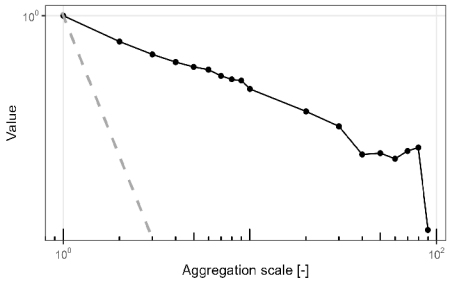

This reconstruction employs tree total ring width, comprising annual rings with earlywood/latewood width and wood density, to depict seasonality changes across the western United States. Notably, it captures distinct signals of climate variation during the warm Medieval Climate Anomaly and the cold Little Ice Age periods.

1-year scale	10-year scale	30-year scale	50-year scale
Mean: 0.98	Max slope: 0.04	Max slope: 0.05	Max slope: 0.04
St. Dev: 0.28	Min slope: -0.07	Min slope: -0.05	Min slope: -0.04
Min/Max: 0.18/1.9	Max diff: 2.12	Max diff: 2.39	Max diff: 1.68
H(ACF-1): 0.90(0.75)	Min diff: -3.81	Min diff: -2.08	Min diff: -1.9

Box 4.5.8. Graybill (1995) profile of tree ring temperature reconstruction.

Hughes et al. (2005)

Region: Flint Creek range
Lon.: -113.15°E
Lat.: 46.28°N
Proxy: Tree rings
Start: 999 CE
End: 1998 CE
Length: 1000 years
Season: Seasonality

Basin ID: 78266980
Level: 8
Order: 4
Area: 573.6 km^2
Mean Elev.: 2078 m
Slope: 124%
Mean P: 426 mm

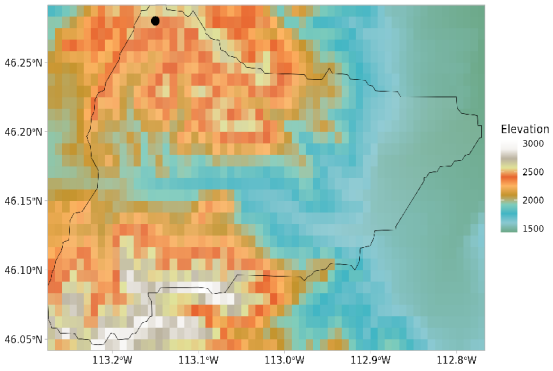

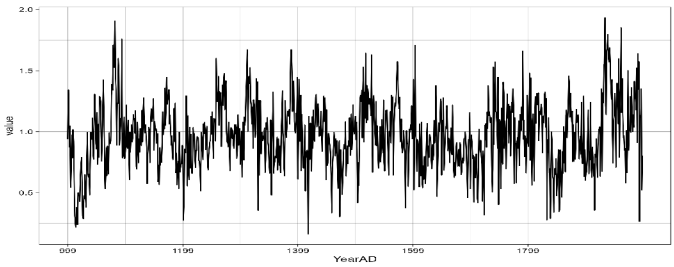

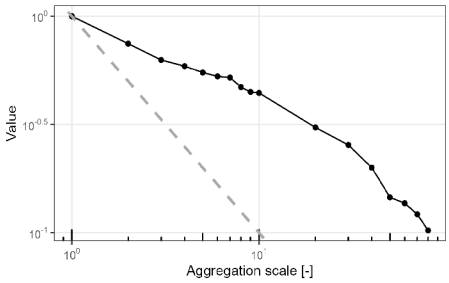

This reconstruction shows seasonal variations across the western United States using tree total ring width. Like the previous record, its capacity to record distinct signals of climatic fluctuation during the cold Little Ice Age and the warm Medieval climatic Anomaly periods is especially remarkable.

1-year scale	10-year scale	30-year scale	50-year scale
Mean: 0.98	Max slope: 0.058	Max slope: 0.04	Max slope: 0.04
St. Dev: 0.27	Min slope: -0.055	Min slope: -0.04	Min slope: -0.02
Min/Max: 0.16/1.93	Max diff: 3.29	Max diff: 2.38	Max diff: 2.55
H(ACF-1): 0.79(0.48)	Min diff: -3.14	Min diff: -2.35	Min diff: -1.6

Box 4.5.9. Hughes et al. (2005) profile of tree ring temperature reconstruction.

Graybill (1995)

Region: Flower lake
Lon.: -118.37°E
Lat.: 36.77°N
Proxy: Tree rings
Start: 898 CE
End: 1987 CE
Length: 1090 years
Season: Seasonality

Basin ID: 7732093
Level: 7
Order: 1
Area: 3271.5 km^2
Mean Elev.: 19.7 m
Slope: 124%
Mean P: 299 mm

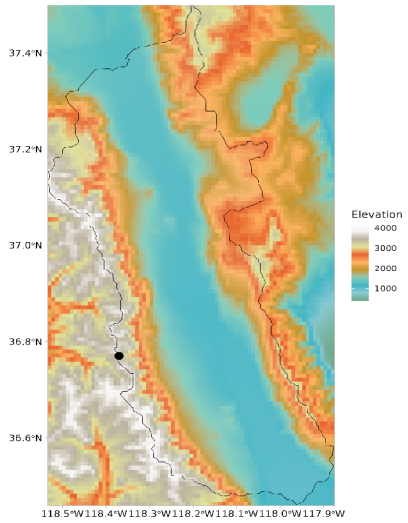

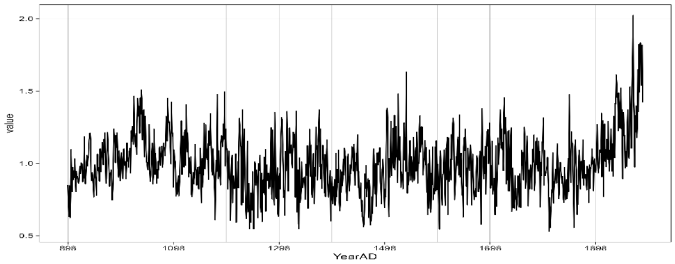

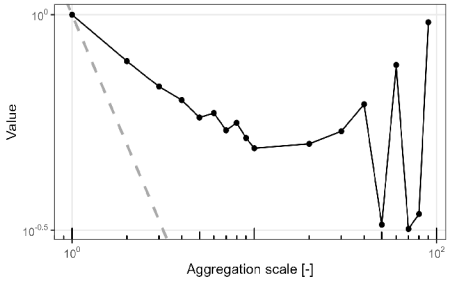

The reconstruction based on tree ring width illustrates seasonal variations across the eastern United States. Remarkably, this record maintains evidence of climatic fluctuations and changes in ocean states over the past millennium.

1-year scale	10-year scale	30-year scale	50-year scale
Mean: 0.99	Max slope: 0.04	Max slope: 0.04	Max slope: 0.022
St. Dev: 0.2	Min slope: -0.03	Min slope: -0.02	Min slope: 0.015
Min/Max: 0.53/2.02	Max diff: 2.93	Max diff: 3.13	Max diff: 1.78
H(ACF-1): 0.81(0.54)	Min diff: -2.46	Min diff: -2.08	Min diff: -1.66

Box 4.5.10. Graybill (1995) profile of tree ring temperature reconstruction.

Colenutt et al. (1995)

Region: French Glacier
Lon.: -115.32°E
Lat.: 50.75°N
Proxy: Tree rings
Start: 1069 CE
End: 1993 CE
Length: 925 years
Season: Seasonality

Basin ID: 7129009
Level: 7
Order: 1
Area: 7906.1 km^2
Mean Elev.: 1876 m
Slope: 164%
Mean P: 599 mm

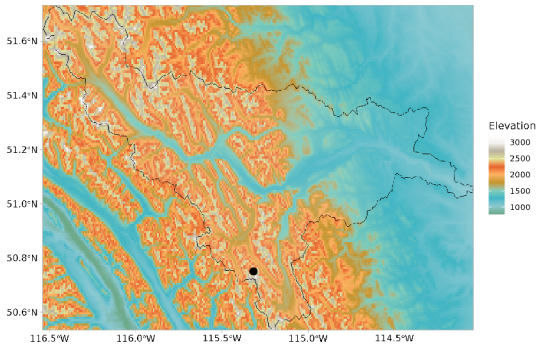

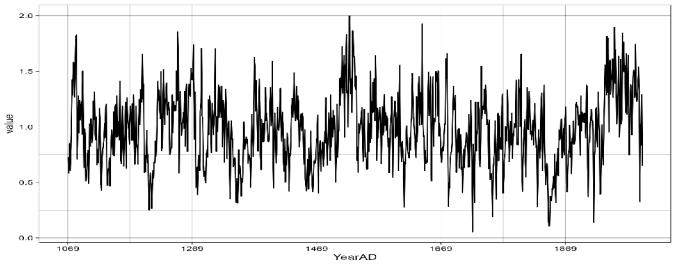

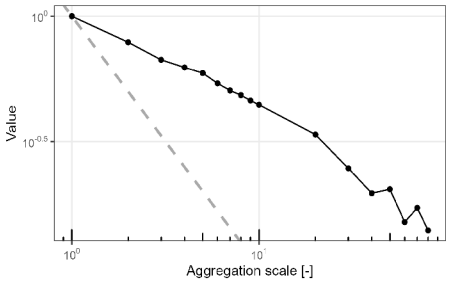

The tree ring-width chronologies reveal distinctive patterns over time, indicating periods of both decreased and increased growth, potentially linked to climate fluctuations. These variations in climate may include increased temperatures with reduced precipitation or lower temperatures with higher precipitation levels. These observations are reflected in the time-series plots, highlighting the dynamic nature of climate variation across different periods.

1-year scale	10-year scale	30-year scale	50-year scale
Mean: 0.98	Max slope: 0.06	Max slope: 0.05	Max slope: 0.04
St. Dev: 0.33	Min slope: -0.06	Min slope: -0.03	Min slope: -0.02
Min/Max: 0.06/2	Max diff: 2.79	Max diff: 2.4	Max diff: 2.54
H(ACF-1): 0.85(0.56)	Min diff: -2.52	Min diff: -1.85	Min diff: -1.34

Box 4.5.11. Colenutt et al. (1995) profile of tree ring temperature reconstruction.

Bellen et al. (2019)

Region: L1-CANA458
Lon.: -71.39°E
Lat.: 54.23°N
Proxy: Tree rings
Start: 910 CE
End: 2011 CE
Length: 1102 years
Season: JJA

Basin ID: 7218089
Level: 7
Order: 2
Area: 2284.1 km^2
Mean Elev.: 476 m
Slope: 20%
Mean P: 758 mm

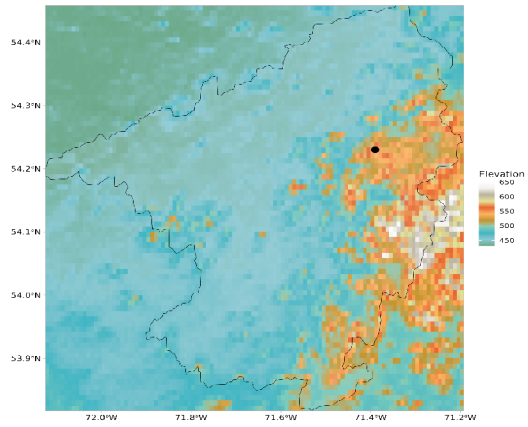

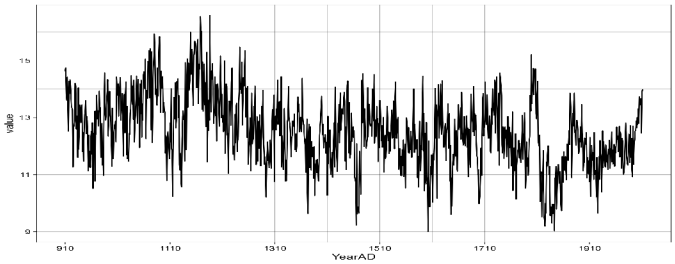

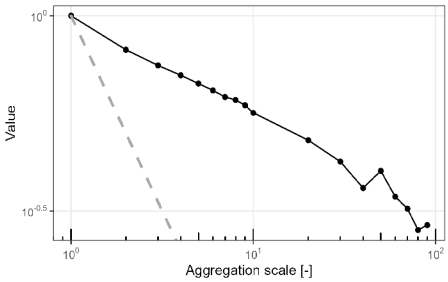

This millennial tree-ring chronology provides a reconstruction of Eastern Canada summer temperatures. It fills a significant temperature data gap across the Northern Hemisphere and supports the notion that both the onset and the coldest phase of the Little Ice Age were due to volcanic activity. Specifically, this data reveals an abrupt shift towards lower average summer temperatures, coinciding precisely with a series of 13th-century eruptions centered around the 1257 Samalas events. This shift closely precedes ice-cap expansion in Arctic Canada, following the well-defined Medieval Climate Anomaly, which encompassed the warmest decades of the last millennium.

1-year scale	10-year scale	30-year scale	50-year scale
Mean: 12.52	Max slope: 0.16	Max slope: 0.2	Max slope: 0.14
St. Dev: 1.24	Min slope: -0.22	Min slope: -0.15	Min slope: -0.12
Min/Max: 9/16.58	Max diff: 2.15	Max diff: 2.66	Max diff: 1.99
H(ACF-1): 0.83(0.62)	Min diff: -2.99	Min diff: -2.06	Min diff: -1.7

Box 4.5.12. Bellen et al. (2019) profile of tree ring temperature reconstruction.

Graybill (1994)

Region: Mt. Washington
Lon.: -114.32°E
Lat.: 38.9°N
Proxy: Tree rings
Start: 825 CE
End: 1983 CE
Length: 1159 years
Season: Seasonality

Basin ID: 773702
Level: 6
Order: 1
Area: 13747.9 km^2
Mean Elev.: 2032 m
Slope: 64%
Mean P: 306 mm

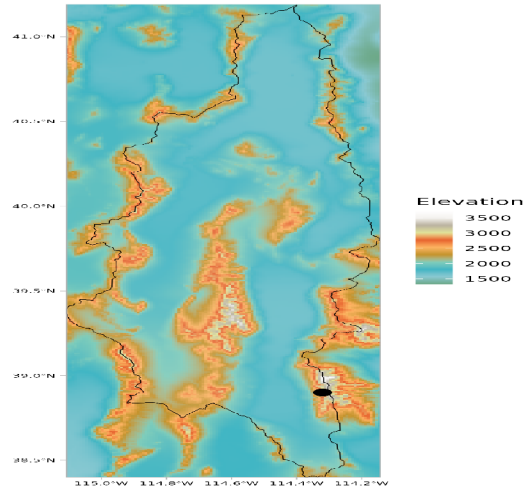

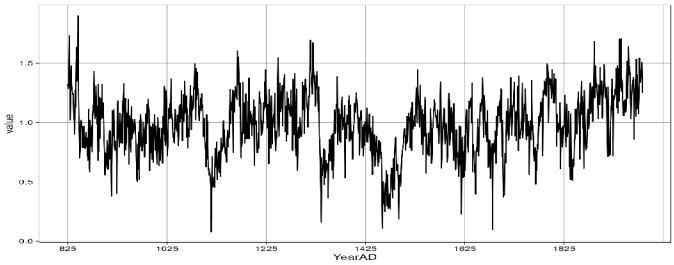

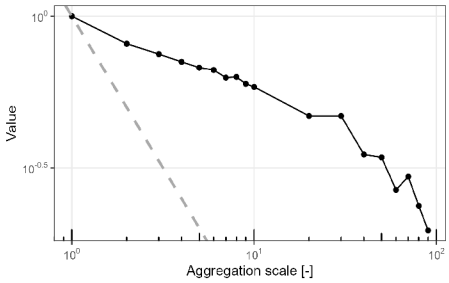

This tree-ring record serves as a reconstruction of seasonality, focusing on recent Holocene climate variability in the easternmost region of the United States. Given the proximity of the eastern United States to the North Atlantic Ocean, fluctuations in climate over this region could be a reflection of variations in Atlantic Ocean state during this data length.

1-year scale	10-year scale	30-year scale	50-year scale
Mean: 0.98	Max slope: 0.04	Max slope: 0.04	Max slope: 0.05
St. Dev: 0.26	Min slope: -0.06	Min slope: -0.04	Min slope: -0.04
Min/Max: 0.08/1.9	Max diff: 2.01	Max diff: 2.42	Max diff: 2.20
H(ACF-1): 0.85(0.63)	Min diff: -3.48	Min diff: -2.42	Min diff: -2.04

Box 4.5.13. Graybill (1994) profile of tree ring temperature reconstruction.

Graybill (1994)

Region: Pearl Peak
Lon.: -115.53°E
Lat.: 40.23°N
Proxy: Tree rings
Start: 320 CE
End: 1985 CE
Length: 1666 years
Season: Seasonality

Basin ID: 773701
Level: 6
Order: 1
Area: 10680.3 km^2
Mean Elev.: 2006 m
Slope: 51%
Mean P: 335 mm

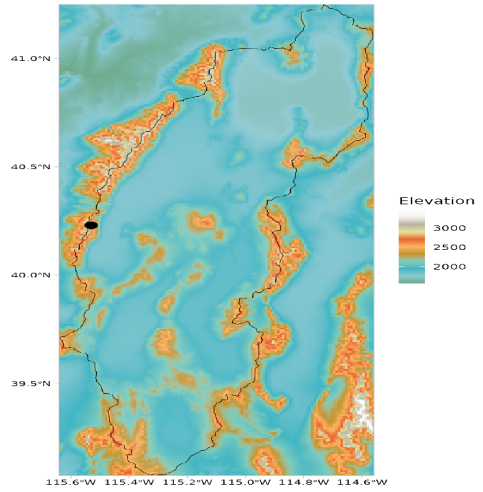

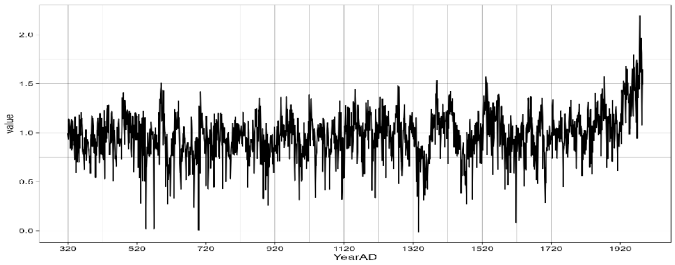

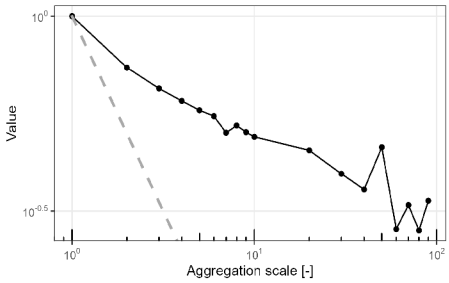

The tree ring-width chronologies unveil pronounced seasonality patterns across the western United States. These variations are clearly depicted in the time-series plots, providing insight into the climate fluctuations across the different periods covered by this extensive dataset.

1-year scale	10-year scale	30-year scale	50-year scale
Mean: 0.98	Max slope: 0.04	Max slope: 0.04	Max slope: 0.03
St. Dev: 0.24	Min slope: -0.44	Min slope: -0.03	Min slope: -0.03
Min/Max: -0.1/2.19	Max diff: 2.44	Max diff: 2.52	Max diff: 2.52
H(ACF-1): 0.77(0.47)	Min diff: -3.06	Min diff: -2.37	Min diff: -2.70

Box 4.5.14. Graybill (1994) profile of tree ring temperature reconstruction.

Gregory et al. (2011)

Region: Pintlers
Lon.: -113.37°E
Lat.: 46.02°N
Proxy: Tree rings
Start: 1026 CE
End: 2005 CE
Length: 980 years
Season: Seasonality

Basin ID: 782669
Level: 6
Order: 3
Area: 9542.3 km^2
Mean Elev.: 1825 m
Slope: 114%
Mean P: 412 mm

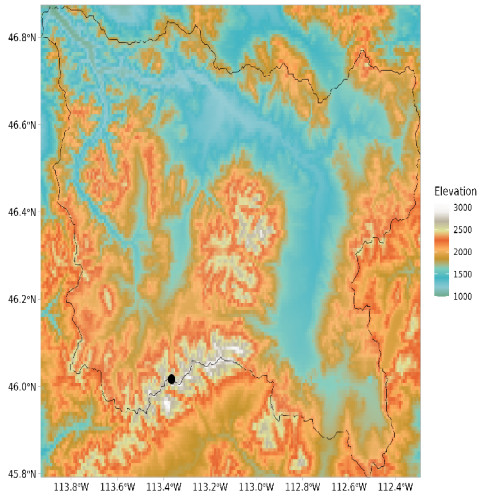

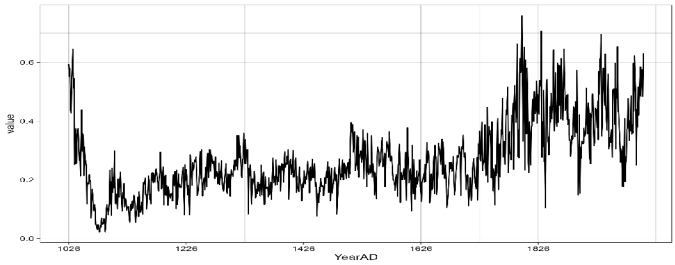

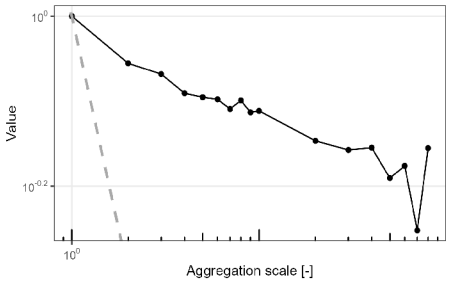

Using snowpack reconstructions from 66 tree-ring chronologies in key runoff-generating regions of the Colorado, Columbia, and Missouri River drainages, this study evaluates the uniqueness of recent declines. The late 20th century snowpack decreases in the northern Rocky Mountains and their synchronized decline across the cordillera are nearly unprecedented in scale over the past millennium. Decadal variability, coupled with anthropogenic warming, contributes to exceptional spring warming, driving both snowpack reductions and synchronization. The increasing influence of global warming on snowpack fluctuations and patterns suggests significant impacts on streamflow and water supply in the western US.

1-year scale	10-year scale	30-year scale	50-year scale
Mean: 0.27	Max slope: 0.01	Max slope: 0.01	Max slope: 0.02
St. Dev: 0.13	Min slope: -0.01	Min slope: -0.03	Min slope: -0.03
Min/Max: 0.02/0.76	Max diff: 2.25	Max diff: 2.1	Max diff: 1.74
H(ACF-1): 0.87(0.76)	Min diff: -2.39	Min diff: -3.92	Min diff: -3.48

Box 4.5.15. Gregory et al. (2011) profile of tree ring temperature reconstruction.

Salzer and Kipfmueller (2005)

Region: S. Fransisco Peak
Lon.: -111.4°E
Lat.: 35.3°N
Proxy: Tree rings
Start: 1 CE
End: 2002 CE
Length: 2003 years
Season: Annual

Basin ID: 772403
Level: 6
Order: 2
Area: 12459.3 km^2
Mean Elev.: 1803 m
Slope: 29%
Mean P: 319 mm

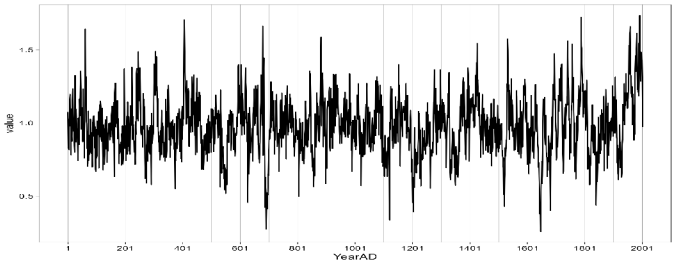

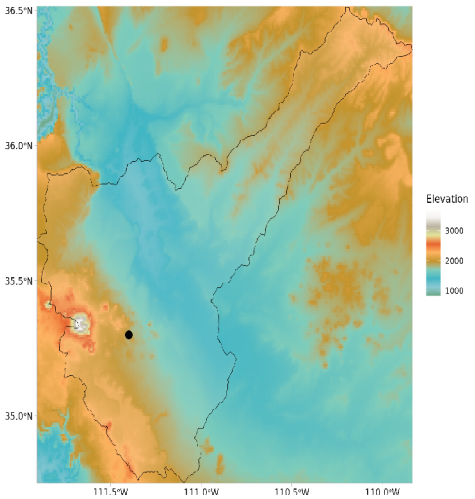

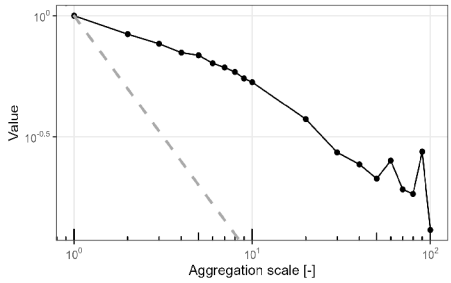

This tree-ring climate reconstruction unveils climatic trends spanning the past two millennia. Combined with precisely dated temperature and precipitation reconstructions, it offers a comprehensive view of climatic variability. The reconstructions identify numerous extreme wet and dry periods in precipitation over 1425 years, as well as cool and warm periods spanning 2262 years. Integration of reconstructions highlights intervals of extreme conditions in both temperature and precipitation. Notably, the post-1976 warm/wet period stands out as unprecedented in magnitude and duration, alongside anomalous late 20th-century warmth. Additionally, substantial decadal-scale variability is observed within the Medieval Warm Period and Little Ice Age intervals.

1-year scale	10-year scale	30-year scale	50-year scale
Mean: 0.98	Max slope: 0.05	Max slope: 0.03	Max slope: 0.03
St. Dev: 0.2	Min slope: -0.04	Min slope: -0.03	Min slope: -0.02
Min/Max: 0.26/1.73	Max diff: 2.92	Max diff: 2.25	Max diff: 2.92
H(ACF-1): 0.94(0.69)	Min diff: -2.72	Min diff: -2.20	Min diff: -1.99

Box 4.5.16. Salzer and Kipfmueller (2005) profile of tree ring temperature reconstruction.

Greybill (1995)

Region: Sheep Mountain
Lon.: -118.1°E
Lat.: 37.2°N
Proxy: Tree rings
Start: 0 CE
End: 1990 CE
Length: 1991 years
Season: Seasonality

Basin ID: 773209
Level: 6
Order: 1
Area: 9096.9 km^2
Mean Elev.: 2065 m
Slope: 113%
Mean P: 322 mm

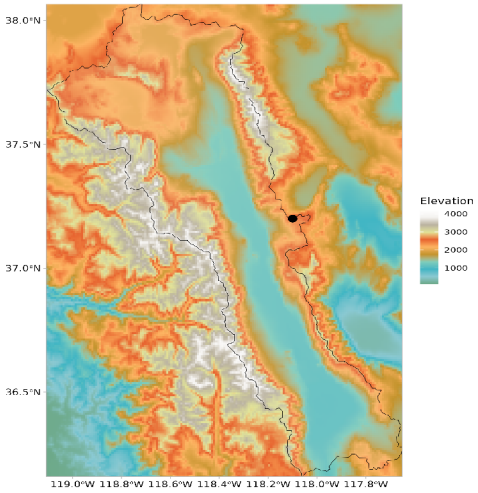

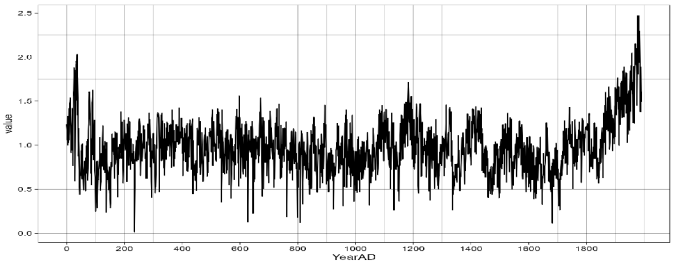

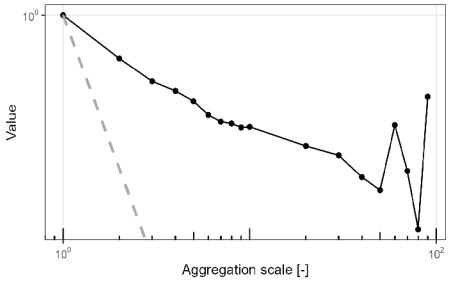

In this reconstruction, significant seasonality trends are revealed by the tree ring-width chronologies in the west central United States. These differences are easily seen in the time-series charts, which offer insight into the fluctuations in the climate throughout the many time periods this large dataset covers.

1-year scale	10-year scale	30-year scale	50-year scale
Mean: 0.98	Max slope: 0.05	Max slope: 0.04	Max slope: 0.03
St. Dev: 0.29	Min slope: -0.09	Min slope: -0.04	Min slope: -0.04
Min/Max: 0.01/2.47	Max diff: 2.57	Max diff: 2.64	Max diff: 1.79
H(ACF-1): 0.84(0.64)	Min diff: -5.03	Min diff: -2.78	Min diff: -2.51

Box 4.5.17. Greybill (1995) profile of tree ring temperature reconstruction.

Kipfmueller et al. (2010)

Region: Siberian Outpost
Lon.: -118.3°E
Lat.: 36.5°N
Proxy: Tree rings
Start: 494 CE
End: 2001 CE
Length: 1508 years
Season: Seasonality

Basin ID: 7744019
Level: 7
Order: 2
Area: 2772.7 km^2
Mean Elev.: 2435 m
Slope: 167%
Mean P: 631 mm

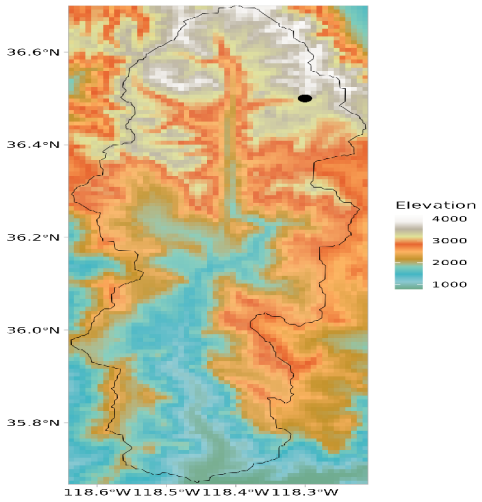

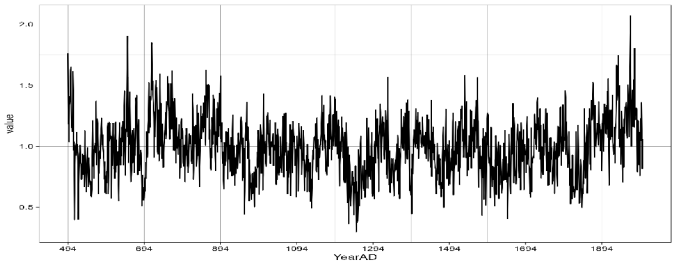

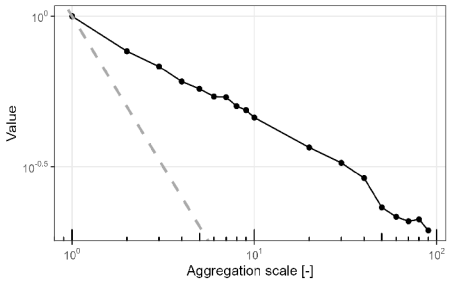

This comprehensive reconstruction combines 66 five-needle pine growth chronologies through a rigorous process involving linear trend analysis, correlation assessments, and cluster analyses. Chronologies were meticulously categorized based on their proximity to the upper treeline, revealing intriguing insights. Cluster analysis unveiled distinct climate response patterns, delineating four groups with varying associations with precipitation and temperature. Particularly, chronologies positively correlated with temperatures, primarily from sites near the upper treeline, also exhibited significant positive linear trends.

1-year scale	10-year scale	30-year scale	50-year scale
Mean: 0.99	Max slope: 0.05	Max slope: 0.04	Max slope: 0.03
St. Dev: 0.24	Min slope: -0.04	Min slope: -0.05	Min slope: -0.04
Min/Max: 0.3/2.07	Max diff: 3.24	Max diff: 2.36	Max diff: 1.95
H(ACF-1): 0.82(0.55)	Min diff: -2.86	Min diff: -3.16	Min diff: -2.22

Box 4.5.18. Kipfmueller et al. (2010) profile of tree ring temperature reconstruction.

King et al. (2000)

Region: Spillway Lake
Lon.: -119.2°E
Lat.: 37.8°N
Proxy: Tree rings
Start: 800 CE
End: 1996 CE
Length: 1197 years
Season: Seasonality

Basin ID: 7744240
Level: 7
Order: 3
Area: 5030 km^2
Mean Elev.: 1437 m
Slope: 110%
Mean P: 789 mm

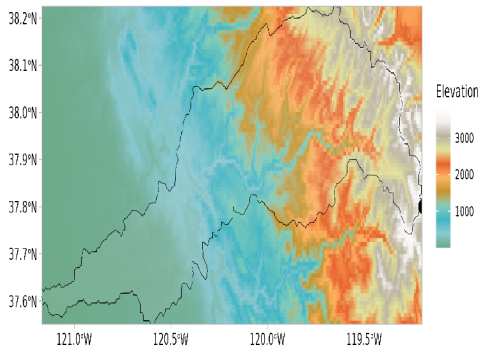

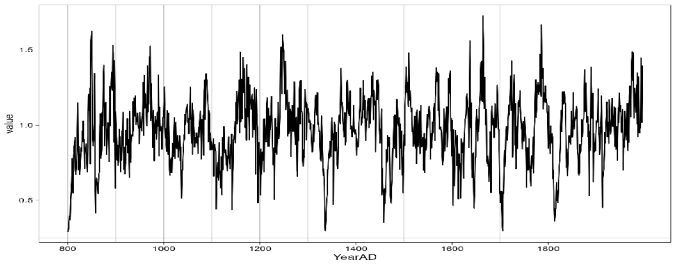

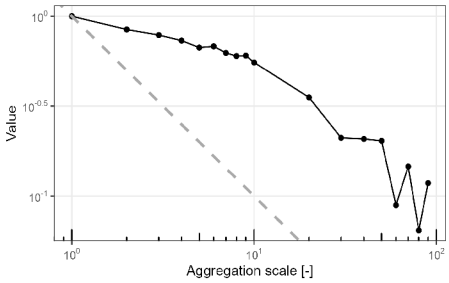

This reconstruction, utilizing tree ring width, elucidates the variability in seasonality throughout the Common Era for the western United States.

1-year scale	10-year scale	30-year scale	50-year scale
Mean: 0.97	Max slope: 0.04	Max slope: 0.04	Max slope: 0.032
St. Dev: 0.22	Min slope: -0.04	Min slope: -0.05	Min slope: -0.029
Min/Max: 0.29/1.73	Max diff: 2.17	Max diff: 1.88	Max diff: 1.83
H(ACF-1): 0.93(0.68)	Min diff: -2.6	Min diff: -2.48	Min diff: -1.78

Box 4.5.19. King et al. (2000) profile of tree ring temperature reconstruction.

Greybill (1995)

Region: Timber Gap Upper
Lon.: -118.4°E
Lat.: 36.3°N
Proxy: Tree rings
Start: 699 CE
End: 1987 CE
Length: 1289 years
Season: Seasonality

Basin ID: 7744019
Level: 7
Order: 2
Area: 2772.7 km^2
Mean Elev.: 2435 m
Slope: 167%
Mean P: 631 mm

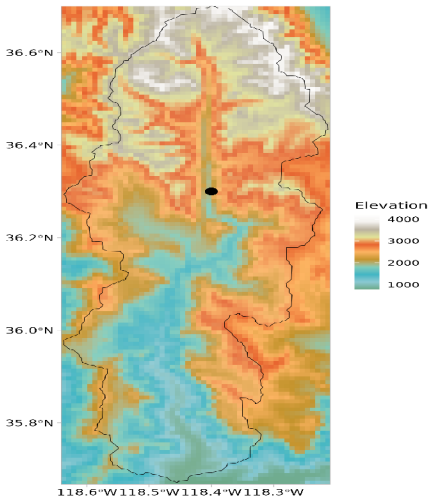

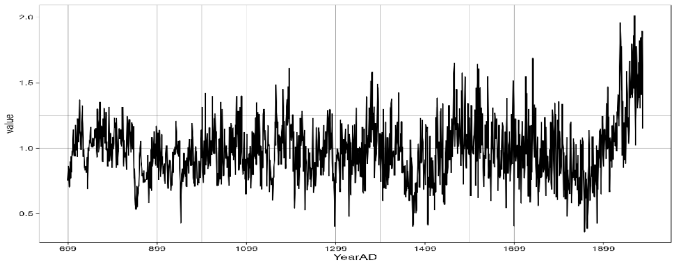

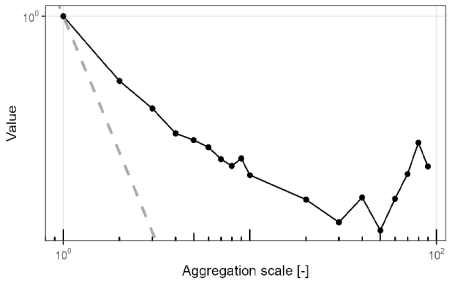

Like the previous record, this reconstruction also, utilizing tree ring width, delineates the variability in seasonality throughout the Common Era for the western United States. mainly, seasonality in time-series refers to recurring patterns or fluctuations that occur within specific periods of time, reflecting changes associated with different seasons across the dataset. In this dataset, notable variability in seasonality becomes evident, particularly following the 12th century.

1-year scale	10-year scale	30-year scale	50-year scale
Mean: 0.98	Max slope: 0.04	Max slope: 0.02	Max slope: 0.03
St. Dev: 0.23	Min slope: -0.03	Min slope: -0.02	Min slope: -0.02
Min/Max: 0.36/2.01	Max diff: 2.77	Max diff: 2.2	Max diff: 2.18
H(ACF-1): 0.76(0.45)	Min diff: -2.45	Min diff: -2.19	Min diff: -1.81

Box 4.5.20. Greybill (1995) profile of tree ring temperature reconstruction.

Bunn et al. (2005)

Region: Upper Wright Lakes
Lon.: -118.2°E
Lat.: 36.4°N
Proxy: Tree rings
Start: -215 CE
End: 1992 CE
Length: 2208 years
Season: Seasonality

Basin ID: 7744018
Level: 7
Order: 3
Area: 2500.8 km^2
Mean Elev.: 1957 m
Slope: 129%
Mean P: 463 mm

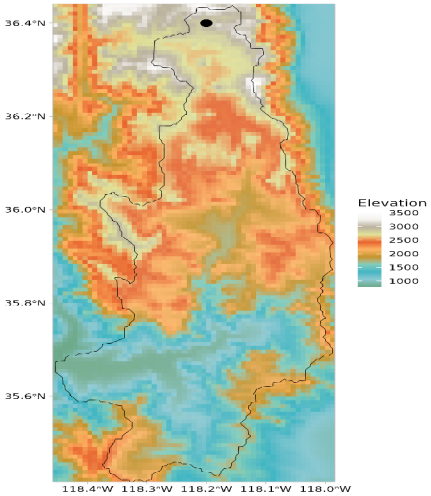

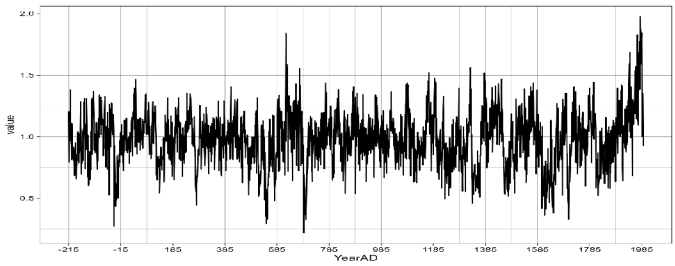

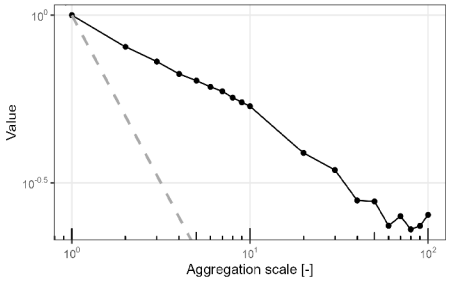

This multispecies tree-ring based reconstruction analyze approximately 1000-year chronologies for five high-elevation conifer species at 13 sites in western North America. Through non-parametric ordination and cluster analysis, the dataset variability at annual to decadal scales was decomposed into two dimensions, both significantly correlated with temperature and precipitation variation. Importantly, this record demonstrates that high-elevation conifer growth rates during the latter half of the 20th century diverge from any period in the past millennium, indicating a distinct biological response to global climate change.

1-year scale	10-year scale	30-year scale	50-year scale
Mean: 0.98	Max slope: 0.045	Max slope: 0.03	Max slope: 0.03
St. Dev: 0.22	Min slope: 0.049	Min slope: -0.04	Min slope: -0.04
Min/Max: 0.22/1.98	Max diff: 2.86	Max diff: 1.97	Max diff: 2.03
H(ACF-1): 0.85(0.60)	Min diff: -3.09	Min diff: -2.68	Min diff: -2.59

Box 4.5.21. Bunn et al. (2005) profile of tree ring temperature reconstruction.

king et al. (2000)

Region: Yellow Mt. Ridge
Lon.: -111.3°E
Lat.: 45.3°N
Proxy: Tree rings
Start: 470 CE
End: 1998 CE
Length: 1529 years
Season: Seasonality

Basin ID: 74299958
Level: 8
Order: 2
Area: 4797.6 km^2
Mean Elev.: 1999 m
Slope: 109%
Mean P: 591 mm

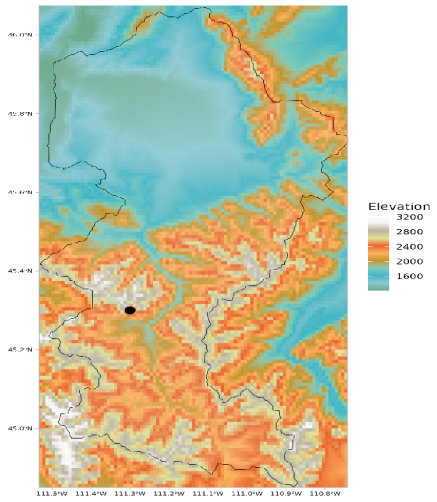

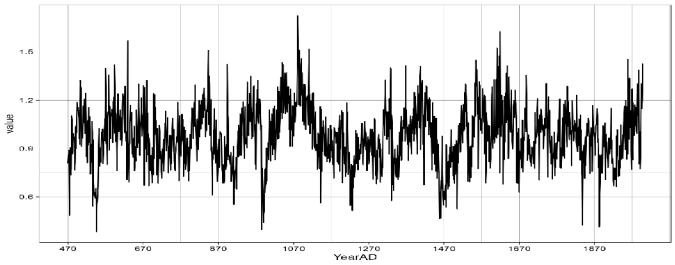

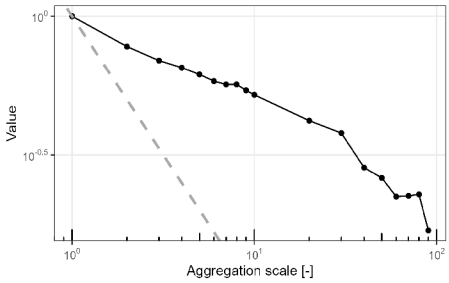

This reconstruction, utilizing tree ring width, depicts variability in seasonality throughout the Common Era for the eastern-southern part of the United States.

1-year scale	10-year scale	30-year scale	50-year scale
Mean: 0.98	Max slope: 0.028	Max slope: 0.03	Max slope: 0.02
St. Dev: 0.18	Min slope: -0.03	Min slope: -0.03	Min slope: -0.03
Min/Max: 0.38/1.73	Max diff: 2.40	Max diff: 2.37	Max diff: 1.74
H(ACF-1): 0.81(0.54)	Min diff: -2.6	Min diff: -2.52	Min diff: -2.74

Box 4.5.22. king et al. (2000) temperature reconstruction using Tree rings.

Chapter 5

The response of the hydrological cycle to temperature changes in recent and distant climatic history

5.1 Summary

The relationship between the hydrological cycle and temperature is rather complex and of great importance to human socioeconomic activities. The prevailing theory suggests that as temperature increases, the hydrological cycle is intensified. Practically, this means more and increased precipitation. However, the exact magnitude of the hydrological cycle response and its spatio-temporal characteristics are still under investigation. To gain a better understanding, this chapter delves into Earth's hydroclimatic history, exploring periods when global temperatures significantly deviated from the present. The chapter provides a comprehensive investigation of some of these periods to present the current knowledge regarding past variations in the hydrological cycle, particularly in terms of precipitation, and its relationship with temperature. The periods examined include the Mid-Miocene Climate Optimum, the Eemian Interglacial Stage, the Last Glacial Maximum, the Heinrich and Dansgaard–Oeschger Events, the Bølling-Allerød, the Younger Dryas, the 8.2 ka event, the Medieval Climate Anomaly, and the Little Ice Age. Through this investigation, it becomes apparent that the hypothesis that a warmer climate equates to a wetter climate might be an oversimplification, as the response of the water cycle exhibits spatiotemporal heterogeneity.

Keywords: Global water cycle, paleoclimate, hydrological cycle, water cycle intensification, hydroclimatic variability

5.2 Introduction

Looking back in Earth's hydroclimatic history, there have been substantial shifts in the hydrological cycle [319]. In the past few million years, many rapid climate transitions have occurred, with time scales ranging from decades to centuries [131]. For example, during the Holocene, i.e., the last 18 – 20 thousand years (ka) Before Present (BP), the paleoclimatic records show considerable fluctuations in both the seasonal and spatial distribution of precipitation [30]. During the late glacial (18-16.5 ka), sea surface temperature (SST) was about 5-10°C colder than the recent Holocene (11.5-9 ka) over both the North Pacific and the North Atlantic [429]. For the same period, the globally averaged precipitation was about 10-14% lower than today, with the maximum reduction over the Northern Hemisphere (NH) due to reduced convective activity [186, 285, 520]. As the Last Glacial ended and the climate became warmer, there was a shift to wetter conditions as well. From 13 to 12 ka BP, the monsoon circulation was intensified, resulting in an increase in precipitation by about 200 – 300 mm at lower latitudes [271, 336, 415]. Stronger monsoons were also observed between 8 to 3 ka BP, coupling the widespread warming [108]. The most affected region was East Asia [440], where precipitation was over 30% higher than today from 7.8 to 5.3 ka BP [596]. All these changes occurred in various spatiotemporal scales and therefore it is still challenging to estimate the hydrological cycle variability and quantify it on global, continental, and regional scales.

Besides natural variability, anthropogenic forcing (GHG emissions and land-use changes) is also regarded as one of the possible drivers of abrupt changes in the hydrological cycle [9]. Global warming is expected to intensify the global hydrologic cycle, and increase the frequencies of extremes like heavy rainfall, flood, and drought conditions [241]. The term intensification of the hydrological cycle is used to describe an acceleration in the rates of atmospheric water vapor content, precipitation, evaporation, and evapotranspiration (ET) [538]. There is a solid theoretical basis that relates atmospheric warming and the intensification of the hydrological cycle. The basis for this relationship is the Clausius–Clapeyron relation, which suggests the exponential response of specific humidity to temperature increase [242]. The Clausius–Clapeyron formulation implies the slope of this relationship has to remain below 6.5% per Kelvin as the evaporation is energy limited [396]. However,

precipitation is also energy-limited, because the atmosphere should be able to radiate away the latent heat produced during precipitation events [407]. This makes the estimation of the precipitation response under energy constraint conditions a complex task.

Due to this complexity, General Circulation Models (GCMs) are being extensively used in the estimation of the intensification hydrological cycle [578]. The GCMs still show strong variance in their results, although there is general agreement that there is a detectable increase of global mean precipitation, also evident in observational records [348]. For example, Allen and Ingram [13] reported that the precipitation will increase by approximately 3.4% per Kelvin degree, while Wentz et al. [585] report a slower rate, between 1 to 3 % per Kelvin. Another study using 20 coupled ocean-land-atmosphere models shows that precipitation, runoff, and evaporation will globally increase by 5.2%, 7.3%, and 5.2% respectively, responding to a mean surface air temperature increase of 2.3°C by 2050 [586]. Durack, Wijffels, and Matear [159] present a 4% increase of precipitation in response to 0.5°C warming. As we see, the precise quantification of the relationship between temperature and the hydrological cycle remains unresolved. A plausible alternative and complementary approach to the GCMs is the study of the past states of the hydrological cycle through paleoclimatic reconstructions. By investigating the past hydroclimatic variability range we can shed more light on the underlying physical mechanisms and/or constrain the climate model simulations [476].

This study aims to map the current knowledge about hydrological cycle variability, and its relationship to temperature. Since it is extremely difficult to assess all the processes related to the global hydrological cycle we focus our review on precipitation and temperature (as approx for evaporation), which can be used indirectly to describe the global water balance [553]. We have selected past periods with significant hydroclimatic fluctuations, that span from centuries to million years. The lengthiest of them is the Mid-Miocene Climate Optimum (MMCO; 17-14.5 million years BP), when global temperature was 3 to 8°C higher than pre-industrial levels. Such a warmer climate can help us determine future changes in the water cycle to extremely high-temperature conditions. Alternatively, warmer periods such as the Eemian Interglacial Stage (temperature 1.3°C higher than today), can provide insight into the near future changes due to global warming. On the other hand, the

study of ice age climates can help us determine the hydrological cycle response to colder regimes (e.g., Last Glacial Maximum when global temperature was 4.3°C lower than today). The rapid transitions between cold and warm conditions are also of interest, and here we will explore the hydrological cycle shifts during the Heinrich and Dansgaard–Oeschger Events. Finally, the study of the Holocene allows us to examine time scales closer to one of the recent temperature increases. We investigate the hydroclimatic conditions for Bølling-Allerød, Younger Dryas, the 8.2 ka event, the Medieval Climate Anomaly, and the Little Ice Age. Assessing the state of the hydrological cycle during all these periods can offer an alternative pathway for anticipating the hydroclimatic changes that are yet to come both in the near and distant future [370].

Please note that the pre-industrial values of temperature or precipitation correspond to the period 1850–1900. On the other hand, there are studies that compare the climatic conditions with today. In this case, we assume today as the reference time when the corresponding study was published (industrial era). We use the same assumption for the studies without any explicit reference to a comparison period.

5.3 Climatic regimes of the distant past

5.3.1 Mid-Miocene Climate Optimum

The Mid-Miocene Climate Optimum (MMCO; 14 million years BP) is a rather long period of significantly warmer conditions compared to present [61]. What makes it particularly interesting is the evidence of enhanced fluctuations in the carbon cycle [229]. Proxy records of alkenones [613], paleosols [81], stomata [199], and marine boron isotopes [198] show that during the MMCO event, atmospheric CO_2 was less than 450 ppm, which is not far from the current CO_2 levels and within the range of near-future CO_2 projections [510]. However, there are also studies that report lower CO_2 concentrations, equal to or less than today [613], implying that CO_2 might not be the main climatic driver [417]. Nevertheless, MMCO presents an excellent opportunity to investigate the functioning of the hydrological cycle in a warmer climate.

Air temperature reconstructions and model simulations suggest that during the MMCO,

the annual mean global temperature was between 3 to 8°C more than the pre-industrial levels [601, 428, 510]. This is in good agreement with temperature proxies of deep-ocean water, which reveal a 5 to 6°C warmer temperature as of today [207, 380, 605]. The regions with higher temperatures are located mostly at mid to high latitudes [61, 93, 600]. Alongside the warmer conditions, the MMCO also exhibited a rather humid climate [604]. This is also supported by model simulations, which show widespread increases in mean annual precipitation across northern and central Africa, North America, northern Eurasia, and Greenland [265, 177, 448, 221, 224].

The prevailing wet conditions are also confirmed by regional studies. Wet conditions of the MMCO have also been reported for Europe, where there was an increase in average annual precipitation of about 830 – 1350 mm [61, 375, 281, 467]. In addition, the isotope estimations at the Pannonian basin (Central Europe) suggest higher summer precipitation during the Late Miocene (about 10 million years BP) [209]. Pollen and leaf proxies from the Nenanacoal field (Alaska Range, Alaska) imply a particular warmer period from about 18 to 14 million years BP [303]. Pollen investigation at the Tian Shan (China) and sediment analysis at northeastward of the Tibetan Plateau (China) show a wet and warm stage [519, 499]. Stable isotope sclerochronology over northern South America (Guajira Peninsula, Colombia), indicates wet conditions with enhanced seasonality in regions that today have semiarid conditions due to a northerly shift of the Inter Tropical Convergence Zone (ITCZ) [472]. Finally, warm and wet climates dominated at Antarctica and some regions of the Southern Hemisphere (SH) high latitudes [600, 166].

We have to note, though, that there is also evidence for increased aridity over Africa [449, 305, 161, 386], Australia [508, 99, 594], South America [411], and some regions of North America [588, 105] and Asia [250, 315]. In the latter, there was an expansion of the arid region from the western to the eastern coast of China, whereas the humid areas were limited to the northern and southern parts [509, 565, 120]. The physical mechanism that regulated the aridification over Asia, and the widespread mid-latitude arid region of the NH remains enigmatic [232]. Analysis of bulk $\delta^{13}C$, over the central-eastern Idaho (Railroad Canyon section, USA) suggests an average mean annual precipitation of about 190 mm (ranges from 10 to 510 mm/year) during the MMCO that is almost equivalent to today's

values (about 236 mm/year) [208]. In addition, a paleosols analysis over northern Pakistan [606] suggests middle Miocene monsoon was similar to today [12].

In Table 4.2, all the analysed studies are presented by region, hemisphere, latitudinal zone, and time period. In order to highlight the spatiotemporal variability of the hydroclimatic conditions some studies appear to have more than one row, e.g., You (2010). In this manner, we can see that even in a much warmer world, there is no uniform shift in the hydrological cycle; some regions became wetter, some became drier and some appear to be similar to today. Still, the comparative examination of temperature and precipitation reveals that warmer conditions favor more an increase in precipitation than drier climate conditions in an approximately 2:1 ratio (Figure 5.1).

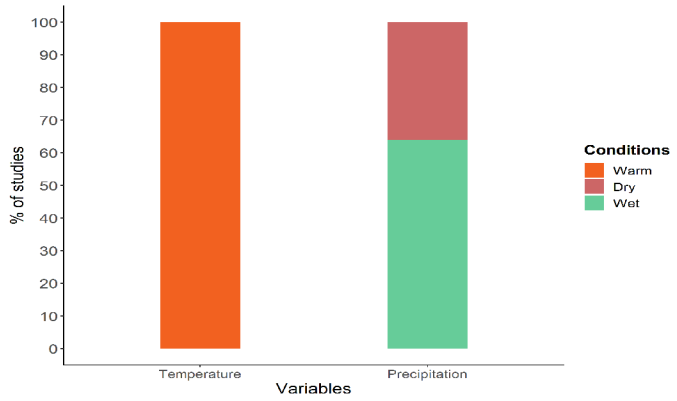

Figure 5.1: Relationship of temperature and precipitation during the MMCO. The number of studies used for the warm/cold or wet/dry conditions can be found in the Table 4.2.

5.3.2 Eemian Interglacial Stage

The Eemian Interglacial Stage, also known as the Marine Isotope Stage (MIS) 5e, is a period that lasted 15 to 17 thousand years at approximately 130 ka BP [1]. Commonly referred to as the Last Interglacial, it is the period that preceded the last glacial stage, with stable climatic conditions similar to the Holocene. Initially, the Eemian was thought to be quite warmer than the interglacial. Andersen et al. [20] reported that the temperature was 5°C higher as to today, according to an oxygen isotope reconstruction. However, more recent studies suggested that global average surface temperature was up to 1.3°C warmer than the pre-industrial levels [170], reaching a 2°C maximum in the middle of the period [496].

The global average temperature over land was 1.7°C warmer than the pre-industrial levels, while the oceans were 0.8°C warmer [405]. The temperature differences were quite heterogeneous over land. The mid and high northern latitudes experienced considerably warmer temperatures, ranging between 2° to 5°C [546], which are comparable to some global warming projections [106]. Similarly to the MMCO, the Eemian is also an excellent analogue for analysing the state of the hydrological cycle in warmer conditions [4].

Most of the available paleoclimatic records show that the Last Interglacial was wetter than Holocene. This is also supported by model simulations, demonstrating an intensified hydrological cycle [579, 418, 254, 610]. Enhanced precipitation is observed mainly at the NH in paleoclimatic records over the low latitudes [587], boreal mid-latitude regions [372], and the Arctic [268]. In addition, the ice melt pulses from Greenland have been suggested to influence the enhanced climate variability across the Mediterranean [547]. During that time, when insolation was at its peak over the NH [391], wet intervals were observed over Southern Europe [78], and specifically, over the Eastern Mediterranean [35, 36]. Continental North America was also wetter and warmer compared to today [22]. However, there were, also, some fluctuations to dry intervals [140], which are further observed in the high values of carbon isotope ($\delta^{13}C_{29}$ and $\delta^{13}C_{31}$) [518].

Furthermore, there is an increase in NH summer monsoons [572]. Both the proxy and model approaches explicitly suggest higher monsoon activity over North Africa and Asia [431, 473]. Terrestrial proxy records suggest a wetter and warmer climate over the Sahara Arabian desert area compared to the present [460, 423]. This is further confirmed by both the oxygen isotopes on speleothems at Soreq Cave (Israel) and climate models, showing increased regional rainfall during the Last Interglacial, attributed to wetter winters and increased summer monsoons [402]. In addition, speleothems and fossil coral reconstructions in the reef terraces, also indicate a wetter Eemian interglacial alongside the Gulf of Aqaba at Arabian Peninsula[597]. Similar speleothem findings, as well confirm a wetter climate over Southern Arabia [548].

On the other hand, there are also regions that experienced enhanced aridity. The evaluation of the Eemian climate across Europe using pollen reconstructions presents a different picture from the one described above. Colder and dryer conditions prevailed in the south-

ern regions and conditions that are similar to today in the higher latitudes [82]. Sediment records from Maar Lake (Germany) show a late Eemian cold and arid event that lasted 468 years [492]. Weakening of the southern summer monsoon has been reported in the modeling and some proxy records [385]. Supporting evidence can be found in the speleothems of Western Australia, which indicate arid conditions [615]. Drier conditions also appeared in Argentina as detected in loess (paleosols) records [535], and Bolivia, where sediment records from Lake Titicaca suggest warmer and more arid conditions during the Eemian period [180]. This seems to be a recurring pattern during warm interstadials and interglacials when the southeastern regions of Australia show comparatively arid conditions [29]. In general, both proxy records and model simulations suggest weakened monsoonal precipitation over the SH compared to the pre-industrial times [395].

Similar to the MMCO, during the MIS-5e, there was a substantial warm-and-wet pattern that was far from homogeneous. The majority of the studies on temperature show warmer climates, i.e., about 85%, while the rest reveal cold conditions (Figure 5.2 and Table 4.3). In precipitation records, the difference is slightly milder with about 75% of the studies suggesting wet conditions and about 25% a drier climate.

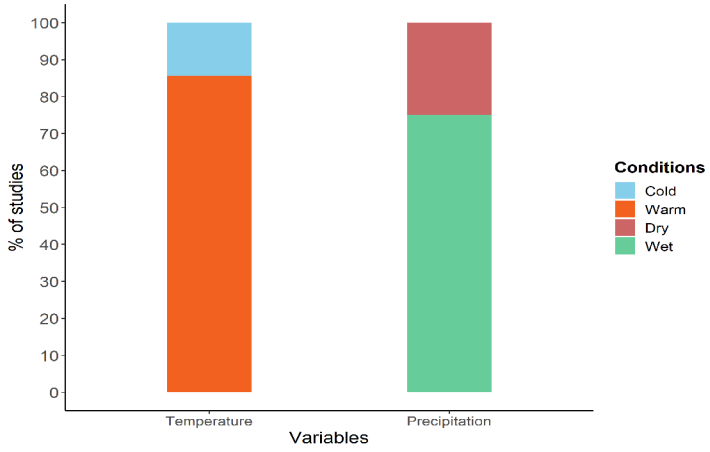

Figure 5.2: Relationship of temperature and precipitation during the Eemian Interglacial Stage. The number of studies used for the warm/cold or wet/dry conditions can be found in the Table 4.3.

5.3.3 Last Glacial Maximum

The Last Glacial Maximum (LGM) corresponds to the period during the last Glacial Stage when the ice sheets extended to their maximum length reaching their highest mass. It occurred between 30 ka to 15 ka [432], although more recent estimates place it between 26.5 to 19 ka BP [117]. During the LGM, the climate conditions at NH high latitudes were much colder and drier than today [53, 406, 598]. The global average temperature is estimated at 3-6°C lower than the modern values [96, 468], while locally, e.g., at Greenland Summit, reached approximately 15-20°C colder than the present levels [251, 139, 378]. Even the tropics were substantially colder, ranging between 2 to 3.5°C below present temperatures [41, 24]. This has also been confirmed by model results, which also estimate the difference around 2.5°C across the equatorial regions [137, 34]. Similarly to the Eemian, the main driver for the temperature decline is the incoming insolation [96, 117].

The decline in temperature is also confirmed by the decrease in the SST over multiple oceans. The Multiproxy Approach for the Reconstruction of the Glacial Ocean surface (MARGO) project suggests that there was an annual tropical SST cooling of 1.7($\pm$1)°C during the LGM. Similarly, the eastern and western equatorial Pacific, northwestern Pacific subarctic gyre, and northwestern tropical Pacific regions also show that the SST was lower (0.9–3.6°C) than the present [279]. The lower SST resulted in increased upwelling of colder water across the continental margin and, finally, a cooler climate, especially over the NH [459]. There is also limited evidence about the SST decline in finer scales. For example, the Mediterranean Sea shows that the SST was about a 1°C lower than the present, particularly in the eastern part [211]. On the other hand, not all the studies agree on a lower SST during the LGM. The SST derived from the central tropical Pacific and northern subtropics were similar to the modern levels of the SST [299], while a few regions have experienced a higher SST, such as the Northwest Pacific margin, southern parts of Iceland–Faroe Ridge, Iberian margin, north-south-west African boundary currents, and Japan Sea [562]. Still, the majority of the SST records advocate for cold conditions, which are expected to affect the hydroclimate of the nearby landmasses [475].

Most of the proxy records suggest that during the LGM the global hydrological cycle

was weaker compared to today [134, 603, 506, 310]. Dry conditions were typical over both hemispheres and model simulations show that the decline in global temperature is linked to a decline in atmospheric water vapor concentration. Otto-Bliesner et al. [406] estimated that precipitable water was 18% less than today resulting to an annual average precipitation of about 2.49 mm per day. The weakening of the global hydrological cycle is due to a reduction of about 10% in both evaporation and precipitation [97, 185]. The simulations, also suggested a surplus of precipitation over evaporation that has lowered the net amount of water vapor in the atmosphere [96, 458].

Proxy records and model simulations (CCSM3) report a weakened summer monsoon for both tropical as well as northern Africa [433]. Moreover, analysis of lake sediments from the Pretoria Saltpan (South Africa) suggests a negative shift in the monsoonal precipitation with total precipitation approximately 15 to 20% less than today [413, 490]. The drier conditions were also confirmed by diatom estimates from the same site [374, 184]. The lake records from the east and southwest Amazonia also suggest lower precipitation levels than the present [3, 489]. Similar changes are reported for high latitudes. Lake sediment records over southern east Siberia (Lake Baikal) show a drop of about 11% in annual precipitation and about 80% drop in summer precipitation, compared to the present climate [403]. Similarly, the yearly precipitation over the Greenland Summit has been found up to three times less than the present values [138, 252].

In Europe, where regional climate modeling suggests that the annual average air temperature was about 6-9°C lower than the present, while the precipitation was quite lower, especially over the northern regions [514]. Interestingly, the decline was linked to a change in the atmospheric circulation pattern that determines the precipitation regime and strength. Currently, the precipitation pattern over central Europe is controlled by a westerly to northwesterly circulation system. During the LGM the atmospheric moisture reached central Europe through south-westerly advection [44]. This was also supported by the oxygen isotope analysis on speleothems of the Sieben Hengste cave (Bernese Alps), which report southwesterly moisture advection (during 26.5–23.5 ka) [322]. The change in atmospheric circulation resulted to an increase in precipitation over southern Europe [282]. In the eastern and central Mediterranean, there has been evidence for an increase in mountain glaciers

at several locations, as well as an increased rate of winter precipitation [514]. The Mediterranean is not the only region where wetter conditions appeared, as there is evidence of similar fluctuations over the extra-tropics [114]. Similar findings were found in the assessment on lake levels over East Africa, even though palaeovegetation analysis points to a dry climate [40]. However, these changes are spatially limited and do not significantly alter the global signal of decline in precipitation.

Contrary to the warm conditions of the MMCO and the Eemian Interglacial Stage, the cold conditions that prevailed in the LGM are mostly associated with a drier climate. However, again, the climatic conditions may differ spatially. For instance, in Figure 5.3 and Table 4.4, we can see that about 20% of precipitation records correspond to regions with wet climates during this doubtlessly cold period. Another plausible explanation, besides spatial heterogeneity, could lie in the climatic proxy nature and the processes involved, which might falsely interpret solid precipitation or glacial extension as a wet regime. In any case, the global signal advocates for a weakening in water cycle strength [310].

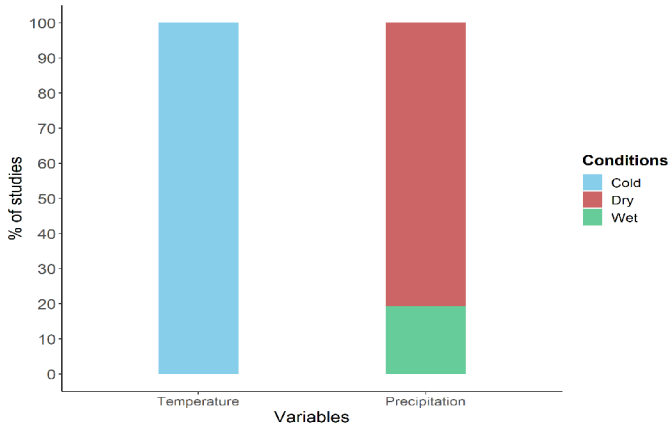

Figure 5.3: Relationship of temperature and precipitation during the LGM. The number of studies used for the warm/cold or wet/dry conditions can be found in the Table 4.4.

5.4 Abrupt climatic events of the Last Glacial

5.4.1 Dansgaard–Oeschger and Heinrich events

During the last glacial period, Earth's climate has gone through some abrupt changes over the North Atlantic region [149]. Proxy records suggest more than 24 cooling and warming

events, termed as the Dansgaard-Oeschger (D-O) events [442]. During the D-O events, most of the NH is influenced by abrupt warming, which is then succeeded by a more gradual cooling [353]. Ice core records collected from Greenland suggest a rapid increase in atmospheric temperature ranging between 10°C to 16°C that occurred within a few decades [253, 293, 94]. In addition, there is evidence that warmer climate conditions were coupled with higher precipitation [187]. The factors driving the D-O events are under vigorous debate, ranging from ocean-atmosphere or sea ice-atmosphere interactions [86, 308] to cyclic Greenland ice sheet calving [551] and Earth's orbital forcing [550]. Widespread signs of D-O events in the Nordic seas and North Atlantic have been found to be associated with the Atlantic Meridional Overturning Circulation (AMOC) instability, influenced by the variability in convection rate [442]. However, there are also D-O events that did not only influence the North Atlantic, but had a large-scale, or even global, impact to the climatic system. The fingerprint of D-O events can be found in deep-sea records, where it can be seen on planktonic and benthic records across the globe [483], or the Vostok ice core record at Antarctica [257]. This is probably due to the relationship between the D-O events and the intensity of the AMOC [465].

The D-O events are also evident over the Mediterranean region, where there was an increase in precipitation over the Iberian Peninsula [390, 94] and Italy [15]. In addition, the D-O events are observed in the oxygen isotope record of the Soreq cave (Israel), where low $\delta^{18}O$ and high $\delta^{13}C$ values suggest wet conditions [37]. An increase in precipitation is also reported for the Great Basin (Nevada; United States), where there is an increase in the lake levels, derived by the analysis of δ^{18}O proxy records [50]. Some D-O events can also be linked with climatic fluctuations across the Indian Ocean [19], such as events D-O events 7 and 8, which occurred at approximately 34 – 41 ka BP [43]. The δ^{18}O estimates in the stalagmites collected from northern Vietnam, Indian, and Chinese caves show strengthening in the Indian and Asian summer monsoons [158, 112, 264]. Additionally, the D-O event 12 (45 ka BP[187]) was linked to the increased intensity of the Asian southwest monsoon during about 50-40 ka [21]. Similar findings have been reported for other regions over Asia [571], while there is evidence that the D-O events can also be detected at South America [421].

Between the D-O events, there are also some abrupt transitions to rather cold periods. They were named after Hartmut Heinrich, who investigated the characteristics of six intervals from 70 to 14 ka BP that occurred between the D-O events and appear to be the coldest events of the glacial [215]. The Heinrich events affected most of Eurasia and North America, resulting to drier and colder conditions [187, 49, 26]. Although the drivers of the Heinrich events are still not fully understood, there is general agreement that they are related to changes in the oceanic circulation over the North Atlantic [528] and in the ice sheets over NH [89]. They are mainly linked with the release of large volumes of freshwater through iceberg melting [59]. These large-scale cold freshwater pulses caused further changes all over the global climatic system.

A 5 to 8°C cooling has been observed over the Mediterranean surface water [457], and significant aridity has been observed over the southwestern United States [563]. The influence of some Heinrich events extends to the tropics, where enhanced aridity has been reported [304]. Other Heinrich events are correlated to arid and cold climates at central China and even to Antarctica [529]. Finally, they can also been detected over the Indian Ocean (Bay of Bengal), linked to increased variability in the summer monsoon and drier conditions all over India [121, 571]. Similarly to the LGM or other glacial stages, there is strong evidence that the decline in atmospheric/oceanic temperature results to the weakening or deceleration of the hydrological cycle and consequently to drier conditions [340, 202].

However, fluctuations to warm and wet conditions have also been reported. Warmer SST has prevailed over Southern California [219], while low isotopic values suggest an extremely wet climate across the western United States between 40 ka – 30 ka, 28.5 ka – 26.5 ka, and around 13 ka [49]. In addition, the δ^{18}O records from the Owens Lake, Great Basin (western United States) present overflow conditions, which were caused by either high precipitation or enhanced ice melting [182, 404]. The substantial growth in central Andean glaciers is an indication of increased precipitation across tropical South America during the Heinrich events 1 and 2 [570] and across northeast Brazil for Heinrich events 1 to 5 [494].

The studies on the Last Glacial abrupt climatic transitions are divided into warm (D-

O) and cold (Heinrich) events. All D-O events are associated with wet conditions, while the hydroclimatic shift for Heinrich events is not so clear (Figure 5.4 and Table 4.5). The cold transitions appear to result to both dry and wet conditions, with the dry conditions appearing more often (about a third of the studies). Thus, the hydrological cycle response to Heinrich events appears more heterogeneous compared to the D-O events. Still, the relatively low number of studies may affect these findings.

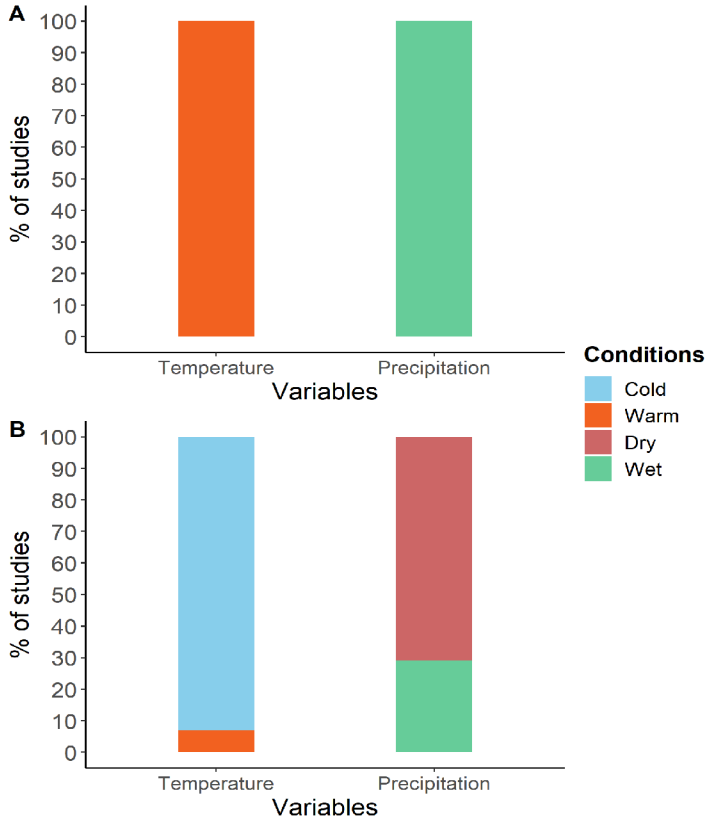

Figure 5.4: Relationship of temperature and precipitation during the Last Glacial. A: D-O events, B: Heinrich events. The number of studies used for the warm/cold or wet/dry conditions can be found in the Table 4.5.

5.4.2 Bølling-Allerød interstadial

During the final stages of the last glacial period an abrupt warm and moist period that occurred between 14.8 and 12.85 ka BP [400]. In some regions, the period is divided into the Bølling oscillation, with a peak closer to 14.5 ka BP and duration around 1400 years, and the Allerød oscillation, with a peak around 13 ka BP and a duration of 700 years [477]. According to the δ^{18}O proxies of the GRIP ice core the Bølling climate was 1°C colder than

today, while Allerød was 5 – 12°C colder [251]. The lake sediments from the Lago di Origlio at Southern Swiss Alps, suggest that during the Bølling-Allerød interstadial the temperature increased about 2.5 to 3.2 °C [463]. Sediment analyses over the Aegean Sea and Lake Maliq show an increased average annual temperature of about 10 °C in the onset of the Bølling-Allerød interstadial, which remained rather stable consequently [67, 276]. Still, its onset is considered amongst the most dramatic deglaciation events over the NH, possibly linked with the revival of the AMOC [526].

The changes in Atlantic oceanic circulation intensified the hydrological cycle over various regions across the globe. One of the regions that were significantly affected is the Mediterranean. Sediment analysis from Lake Prespa (Greece) revealed enhanced humid conditions [27]. Additionally, these increased humid conditions were observed at Lake Maliq [67], Eastern Mediterranean [38], and also Lago Grande di Monticchio (Italy) [11]. At the same time, there was a widespread increase in both tropical and monsoon precipitation. Significant increases are reported for equatorial Africa [435, 533], western Himalayas, Nepal and India [491, 608], and Northwest China [618]. Similar fluctuations in precipitation were observed over Southern and Central America. Wet and warm conditions have been identified in lake sediments of Laguna de Los Anteojos (Venezuela) [502], Petén Itzá (Guatemala) [227], La Yeguada and El Valle (Panama) [98] and Caribbean [237].

All the evidence suggests that the multi-centennial increase in temperature was accompanied by an increase in precipitation too. In Figure 5.5 and Table 4.6, we can see that more than 90% of temperature records are confirming warm conditions and about 85% of precipitation records for wet conditions. Again, this abrupt transition, suffers from a low number of studies, especially at larger spatial scales (global, hemispheric, and continental).

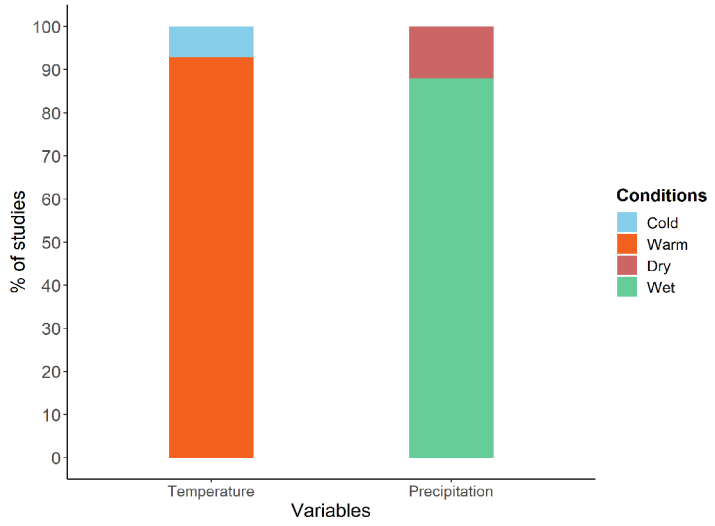

Figure 5.5: Relationship of temperature and precipitation during the Bølling-Allerød interstadial. The number of studies used for the warm/cold or wet/dry conditions can be found in the Table 4.6.

5.4.3 Younger Dryas

The Bølling-Allerød interstadial was followed by another cool phase, the Younger Dryas event (from 13 ka BP to 11.7 ka BP). An abrupt decline in temperature disrupted the general warming trend that was driven by the increasing solar insolation [147]. Similarly to LGM and Heinrich events, the drop in temperature was accompanied by generally dry conditions [227, 361, 359]. The Younger Dryas was mainly observed over the North Atlantic region [164], but is also evident in paleoclimatic records from all over the globe. However, the shift in the global climate was not homogeneous; contrary to the colder conditions of the high latitudes, the tropics were characterized by comparatively warmer conditions [181]. The temperature reconstructions of the Younger Dryas, show a decline in temperature around 15°C over central Greenland [251], and a drop between 6 to 9°C in the Norwegian Sea [263]. There is no doubt that Europe was substantially influenced by the Younger Dryas event [77, 438]. A 4 to 6°C decrease over western Europe has been reported, reaching 6 to 7°C over Poland [193]. There is also evidence of re-extension of the North European ice sheet [27]. Consequently, this process led to the southerly flow of dry and cold northern air masses toward the Mediterranean area [67], which led to colder temperatures in the Aegean Sea [276]. On the other hand, a pollen record from east Beringia revealed a more constrained

drop in temperature, estimated at 1.5°C [179], which is in agreement with evidence that several coastal areas near western Novaya Zemlya (Russia) were ice-free [482].

In terms of hydroclimate, various regions of the NH have experienced drier conditions during the Younger Dryas [143, 165, 238, 504, 554]. However, there are many regions that did not maintain a stable cold and dry regime, but instead the cold climate was coupled by centennial oscillations between dry and wet phases [567]. For instance, the increase in the hydrogen isotope values at about 12 ka BP and 12.2 ka BP suggests wetter and warmer phases over western Europe [438]. This is also evident in Central Europe, where paleoclimatic records [333] and certain periglacial characteristics [259] suggest wet conditions during the Younger Dryas [581], especially during winter [247]. Other evidence of precipitation comparative to the present has been recorded in Poland (Prosna River, about 30% higher) [461], Netherlands [69], and Scotland highlands [323]. A multi-proxy reconstruction from central Poland for the Younger Dryas reports two phases [416]. The first (12.5 -– 12 ka BP) was marked by a decrease in precipitation and temperatures during winter, but a rise in summer precipitation. The second (12 -– 11.5 ka BP) shows increased winter and summer temperature with increased annual precipitation. In the southern Europe, pollen records from the Mediterranean show increased precipitation during the whole deglaciation phase (18 to 10 ka), without any influence by Younger Dryas [412].

A zonal gradient in precipitation response appears in North America. Drier conditions dominate the northern parts of the continent [101, 155], transitioning to considerably wetter conditions as we move southwards [202, 560]. There, the precipitation levels have been estimated at about 15% higher values than today, probably due to increased southern atmospheric moisture flow [447]. Wetter phases over central and southern North America, are further supported by various proxy evidence in plant-macrofossil and palynology studies over Florida, and speleothems from New Mexico [426] and Arizona [563]. Climate model simulations also present a warmer climate with increased precipitation in the central regions of North America during the Younger Dryas when compared to the Bølling-Allerød period [445].

In the SH, there are conflicting results. Some studies provide evidence for enhanced precipitation and conditions similar to the Heinrich Events [25]. For instance, the analysis

of lake sediments from Lake Titicaca (Bolivia, Peru) demonstrates the overflowing of the lake and thus higher precipitation between 13 ka BP and 11.5 ka BP [31]. On the other hand, the lake sediment records at lake Laguna de Los Anteojos (Venezuela) present a transition to an intense cold and dry regime during the Younger Dryas [502]. This is further supported by a significant drop in the Amazon River discharge that is probably a result of reduced monsoon precipitation over the lowland tropical South America [355]. Moreover, arid conditions are reported across the northern tropical Andes and wetter conditions over the southern tropical Andes [502].

With 80% of the studies revealing a transition to cold conditions, there is little doubt about the temperature conditions of the Younger Dryas (Figure 5.6). The same cannot be said about the hydroclimatic regime, where studies remain split almost in the half. About 60% of the records suggest wet conditions, while the remaining 40% present a drier climate. The majority of the studies at larger spatial scales (global and N. Hemisphere) point to dry conditions, while wet conditions are more frequent in the finer scales.

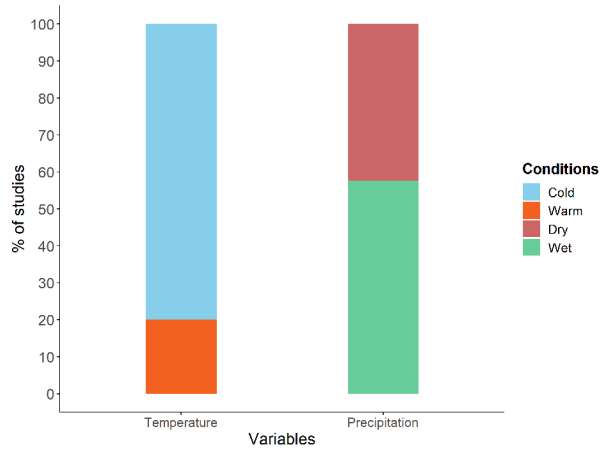

Figure 5.6: Relationship of temperature and precipitation during the Younger Dryas. The number of studies used for the warm/cold or wet/dry conditions can be found in the Table 4.7.

5.5 Climatic fluctuations in the Holocene

5.5.1 The 8.2 ka event

The '8.2 ka cold event' is another abrupt climatic event that was experienced across the entire globe originating from the North Atlantic region [14]. As the name implies it occurred around 8.2 ka BP and lasted for 160.5 ± 5.5 years, with the coldest period spanning 69 ± 2 years [527]. Other estimates suggest a duration between 150 and 200 years [561, 495]. The available proxy records show an abrupt cooling up to 6 ± 2 °C [10, 17, 149], resulting to a global decrease by 0.9 – 1.8°C [214]. Greenland is one of the regions with the most intense drops, about 3 to 8°C [17, 561], as well as, enhanced windy and dry conditions over most parts of the NH [536] at a time when the climatic conditions were similar as of today [17].

The areas with the most rapid transition were widespread across the entire Baltic Sea basin [68], the western Europe [150], and the regions affected by the NAO, in particular [481]. The latter experienced a decline between 1.5 to 3°C, as both land and marine records suggest [270, 62, 561]. The above results are in good agreement with model simulations. The models present cooling around 2 to 5°C over Greenland [185], 2.5°C at the lake Annecy (France) [335], 1 to 2°C over northwestern Europe [446], as well as approximately 2°C over Germany and the North Sea [270].

Some model simulations also suggest a 30% drop in precipitation [185]. This is in good terms with the dry conditions which have been generally observed over the NH [118, 17], particularly in the wintertime [14]. In Europe, the transition to dryer conditions was observed to latitudes over 50°N, as well as a significant part of the Mediterranean, including Spain, Northern Africa, and Italy [334]. On the other hand, during the 8.2 event, a worldwide snowfall increase was observed [68]. This could explain the lake-level rises in many European palaeoclimate records, related to higher runoff [332]. The lake-level rise becomes more evident over the central Alps (Switzerland, France, and northern Italy) [334].

All the evidence suggests that the 8.2 event was characterized by colder and drier climate conditions (Figure 5.7), with only two studies presenting wet conditions over the Alps (Table 4.8). Even though there is good agreement between the records at both coarse and

fine spatial scales, we cannot rule out though a small-sample bias in this conclusion due to the limited number of studies describing the precipitation of this cold period.

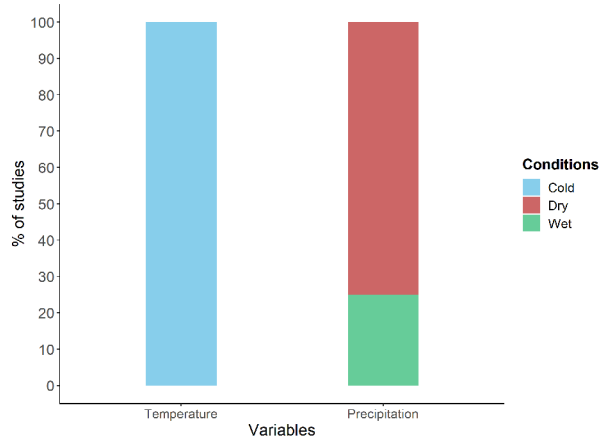

Figure 5.7: Relationship of temperature and precipitation during the 8.2 ka cold event. The number of studies used for the warm/cold or wet/dry conditions can be found in the Table 4.8.

5.5.2 Medieval Climate Anomaly

The Medieval Climate Anomaly (MCA), also known as the Medieval Warm Period, is the most recent period of abrupt warming, with onset around 800 – 1000 CE and termination at 1300 – 1400 CE [239]. It affected mostly Europe and parts of North America, which mainly experienced warmer than average conditions [290]. The centennial-scale patterns of spatio-temporal temperature reconstructions suggest widespread warm and arid conditions over the NH with a similar geographic extent and magnitude as in the 20^{th}-century mean [319]. Between 1200 and 1300 CE, the temperature was similar to the present over northwestern Europe [203]. In addition, a temperature reconstruction across the Alps suggests that in the 12^{th} century the temperature was 0.3°C higher than today [537]. In North America, there is conflicting evidence about the increased magnitude. Viau, Ladd, and Gajewski [557] demonstrated that there was a 0.5-degree increase, which resulted to cooler than the present conditions, whereas Woodhouse et al. [589] report temperatures of about 1°C higher than today. There is also evidence of high temperatures over China [595], South Atlantic [256], and Northern Pacific [342]. Even though the extent of temperature increase during MCA remains under investigation, there is general agreement that there has been a

clear signal of the increase at least in the NH.

The hydroclimatic response, though, was not so homogeneous. Substantial precipitation deficiencies were observed in northern Europe [130] and East Africa [556]. In addition, model and paleoclimatic records show that western North America experienced persistent and extensive aridity from 900 to 1300 CE [589]. On the other hand, anomalously lower δ^{18}C values in bristlecone pine from the White Mountains, California highlight a wet period from 1080 to 1129 CE [239]. Similarly, Mauquoy et al. [358] also suggested the times from 1030 to 1100 CE was a wet period for western North America, while there is also evidence of higher lake levels, or freshwater availability, over the Arizona monsoon-influenced area from 700 to 1350 CE [239]. However, the occurrence of increased aridity over most of the areas of western North America was also evident in tree-ring records between 650 and 1050 CE [410] and from 900 to 1300 CE [129].

In Asia, dry climatic conditions prevailed, mainly linked with atmospheric circulation [111]. This in good terms with the proxy analysis over southern China indicates comparatively weak monsoonal precipitation over most of the regions [111] and the periods of extensive aridity from 1140 to 1220 and 1420 to 1490 [311]. On the contrary, pollen estimates from Maili pond at northeast China reveal wet conditions (from 950 to 1290 CE), suggesting an increase of the East Asian summer monsoon (EASM) during this period [444]. Additionally, the decades between 1230 – 1250 CE, and 1380 – 1410 CE show intensification of the South-Asian monsoon resulting to wet conditions [311]. Most of the proxy records suggest precipitation decreases over the EASM region after the termination of MCA around 1300 CE [292].

South America also experienced a highly variable climate during MCA. Perhaps this is due to a humidity dipole between the southern and northern Amazon Basin [346]. This humidity dipole could suggest an enhanced land-ocean temperature gradient or north-south migration of the ITCZ, driven by seasonal variation in the distribution of insolation [591]. Consequently, the wetter phase over the northeast area was synchronous with the drier phase over Southern Amazonia [530]. For instance, a marine sediment core at Peru (12°S) shows intense aridity between 800 to 1250 CE [443], while a titanium (Ti) record from the Cariaco Basin (Venezuela) indicates wetter conditions between 950 to 1450 CE [210]. Ad-

ditionally, the assessment of lake sediment oxygen isotopes ($\delta^{18}O$) at the Central Peruvian Andes present higher values from 900 to 1100 CE, implying a weakened South American Summer Monsoon and a prolonged period of aridity [55]. On the other hand, wet conditions prevailed in Central America, as indicated by the lower values of oxygen isotope in sediments from Nicaragua from 950 to 1250 CE [503].

Another feature of MCA is the emergence of simultaneous mega-droughts in various regions of the globe [501]. The main region affected of these multi-decadal droughts can be found at North America [125]. There, two prolonged drought events with an approximately 90-year time span have been recorded over North America. The first event occurred between 1197 and 1289 CE, while the second event occurred between 1486 and 1581 CE [410]. Other shorter events have been also detected, presenting higher severity, though, such as the mega-drought from 1140 to 1162 CE or the one between 1150 to 1159 CE [129]. In Europe, the multi-decadal reconstruction over the Sierra Nevada (Spain) highlights four multi-decadal droughts that prevailed during the MCA (800 – 859 CE, 1020 – 1070 CE, 1197 – 1217 CE, and 1249 – 1365 CE) [197].

The main hypothesis about the driver of the enhanced hydroclimatic variability of MCA is the positive state of NAO, which persisted at the centennial time scale [545]. The result was a northeastward shift of the cyclonic storm tracks, and consequently the transport of atmospheric moisture to higher latitudes [498]. The spatial hydroclimatic variability is also evident in finer scales. A typical case is highlighted over the Iberian Peninsula. There, a climate reconstruction shows warmer and humid conditions across the northwest regions, while the rest of the peninsula shows warm and arid conditions [387]. Similar patterns can be seen in tree-ring records over Morocco, where some unusually frequent wet years occurred from 1250 to 1300 CE [534].

During the MCA, all the studies analyzed clearly suggest a warmer climate (Figure 5.8 and Table 4.9). However, contrary to the other warm periods presented in this study, the multi-centennial warming was coupled with dry conditions. About two-thirds of the records indicate a transition to a dry climate, which might be seen as a contradiction to the prevailing theory of water cycle intensification and will be discussed in detail below.

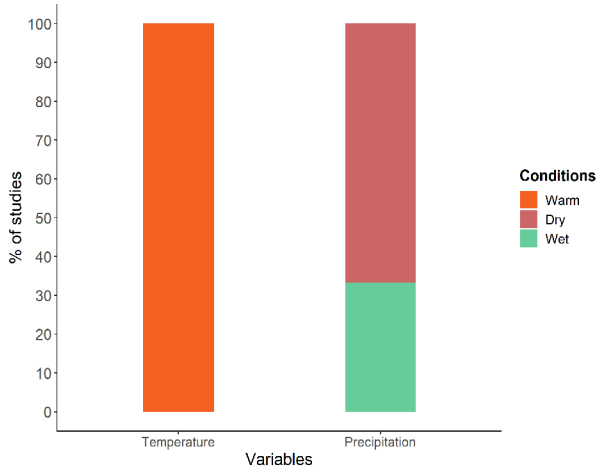

Figure 5.8: Relationship of temperature and precipitation during the MCA. The number of studies used for the warm/cold or wet/dry conditions can be found in the Table 4.9.

5.5.3 Little Ice Age

The Little Ice Age (LIA) is the most recent shift to colder conditions. It lasted from 1350 – 1450 CE to 1900 CE [359], and the global temperature was 0.5 to 1.5°C lower than the 20^{th} century average [136, 197, 341, 113, 470]. Trachsel et al. [537] have reported that during 14th, late 16th, and 17^{th} century, the global temperature was a 1°C lower than the 20^{th} century average. The NH experienced the most substantial decrease (about 0.9°C lower) from 1570 to 1730 CE [74], whereas in Europe LIA peaked in 1650 – 1750 CE [64]. In SH, paleoclimatic oceanic records show an average cooling of 1.6°C ($\pm$1.4) compared to the last 150 years [451]. Ice core analysis near the Ross Sea (Antarctica) shows colder conditions of 2°C in surface temperature, as well as lower SST over the Southern Ocean coupled by enhanced sea ice extent during the LIA [52]. In general, the lowest temperatures were observed in the period of 1680 to 1730 CE, for both Hemispheres [516].

The LIA has been compared to the abrupt changes that occurred in the last glacial stage [65], such as the D-O events [89]. However, even though LIA affected the whole globe, this did not happen simultaneously. Most local or regional paleoclimatic reconstructions show unusually cold phases from 1580 to 1880 CE, interrupted by decades of warmer conditions [7]. Similarly to MCA, the main hypothesis for the spatio-temporal variability lies in the changes of atmospheric circulation [609]. Compared to the current patterns of atmospheric

circulation, LIA experienced stronger meridional transport [291]. This was observed over the North Atlantic and polar South Pacific at the beginning of the LIA, evident in ice cores from central Greenland, Siple Dome, and West Antarctica [277]. The colder and drier conditions that prevailed were a result of the enhanced atmospheric circulation, as reported in numerous paleoclimatic records in the NH and the Equator [531, 397]. Additionally, numerical model experiments have identified sea ice-ocean-atmosphere [617] and volcanic feedbacks [377] as a factor that triggered the LIA cooling over the North Atlantic and Europe.

The drop in temperature was coupled to wet conditions over most of the European territory [327, 90]. Both the speleothem record from Scotland [434] and reconstruction from England-Wales [290] are notably similar, showing a 10% decrease in the precipitation (for September to June) from the late 13th to the mid 14^{th} century, and a constant drop from the mid of 16th to late 18^{th} century. Precipitation reconstructions from southern Moravia (Czech Republic) show that the highest precipitation occurred between 1670 and 1710 CE, succeeding a period with low precipitation [79]. Proxy estimates of seasonal precipitation over Europe exhibit increased winter (DJF) precipitation during the beginning of the 18^{th} century [414], which is attributed to a significant increase in winter temperatures [392]. This is in good agreement with the abrupt increase of floods reported from 1760 to 1800 CE over various locations [57]. Other similar periods are 1560–1580 and 1840–1870, when the climate conditions were abruptly shifted to a warmer phase [189] and consequently increasing precipitation and/or snowmelt [80]. This is particularly true for the end of the LIA, when there has been a monotonic increase towards more humid conditions [130, 351].

Over the North American continent, there is evidence of strong spatiotemporal heterogeneity in the observed changes. In general, wetter conditions were observed in the central regions compared to the present, while drier conditions prevailed over both the West and East Coast [286]. In most of the wet periods, precipitation increased during the winter [410], lasted for a couple of decades and were succeeded by long dry intervals [371]. For instance, a precipitation reconstruction at Banff, Alberta (Canada) shows higher precipitation from 1515 to 1550 CE, 1585 to 1610 CE, 1660 to 1680 CE, and during the 1880s, while 1950 to 1970s exhibit both enhanced precipitation and decreased summer temperatures [321]. On

the other hand, the spatio-temporal drought and precipitation records over North America suggest a widespread limitation in moisture availability during the late 16^{th} century while relative abundance during the early 17^{th} century [126, 75, 357].

Various changes are reported in the rest of the world, related to the fluctuations of atmospheric circulation. Sediment records from the northeastern Arabian Sea show a weakening of the Indian summer monsoon from 1450 to 1750 CE and consequently a shift to drier conditions [5]. Northern China also faced a moderately weak monsoon [111]. The lake-levels and diatom estimates over Africa [515], and dust records in an equatorial ice core [531] also display increased aridity. The paleoclimate records from Argentina show that about 1800 and 1930 as the wet period [358]. However, the isotope (increased values) evidence from Central America suggests the persistence of drier conditions during most of the LIA [503]. Additionally, the tree-ring analysis from southern South America indicates the cold-dry/drought phase between 1280 and 1450, 1550 and 1670, and 1780 to 1830 CE; while the warm-wet/high-rainfall phases from 1220 to 1280, 1450 to 1550, 1720 to 1780, and 1830 to 1905 CE [558].

Increased precipitation was also observed in various regions across the world. A low concentration of microparticles in ice core records from the Antarctic Peninsula indicates likely higher precipitation and intense cyclonic activity [456]. The enhanced meridional circulation has been expected to influence the mid and low-latitude circulation, resulting to a shift of the westerlies belt and increased precipitation over the Patagonia and California around 1400 CE [512]. Additionally, the arid central Asia region is showing relatively wet conditions, and pluvial conditions prevailed over southern China [111]. The wet conditions were often succeeded by arid conditions, resulting to 18 extreme floods and 16 drought events during the LIA in China [616]. Similarly, sediment geochemistry from a subalpine lake at northern Taiwan indicated four pluvials (1660 CE, 1730, 1820, and about 1920) [568, 614]. In South America, the oxygen isotope (δ^{18}O) estimates of a speleothem record at northeastern Peru report enhanced variability in precipitation, with annual precipitation being 10% higher than today from 15^{th} to 18^{th} century [450]. This is in good agreement with the results of an oxygen isotopes (δ^{18}O) analysis at the Central Peruvian Andes lake, showing a prolonged regionally synchronous intensification in the South American Sum-

mer Monsoon [55]. Similar conclusions were drawn in the study of Polissar et al. [424] about the growth of glaciers at high elevations over the Venezuelan Andes, which can be interpreted as evidence of higher precipitation.

The analysis of the corresponding literature advocates that LIA is not the homogeneous event in space and time. There are approximately 25% of studies that reveal some region and/or period of warm conditions (Figure 5.9). This is due to the availability of higher resolution reconstructions, which can detect shorter warmer periods within the prevailing cold conditions, such as for example the 1560 – 1580 and 1840 – 1870 warm intervals over Europe [80, 189]. In addition, there are numerous locations with cold and wet conditions, resulting to a sum of 60% of studies presenting a wet LIA, and 40% of records suggesting otherwise. Similarly to MCA, this is a reversed relationship between temperature and precipitation compared to the other periods studied. A possible explanation for this outcome could lie to the fact that the majority of the studies come from Europe, amplifying the wet signal (Table 4.10).

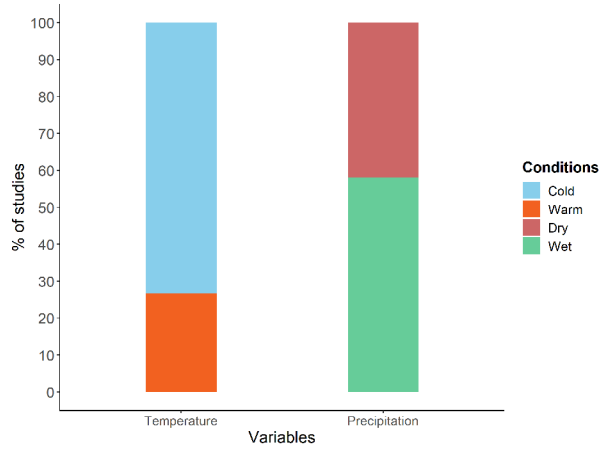

Figure 5.9: Relationship of temperature and precipitation during the LIA. The number of studies used for the warm/cold or wet/dry conditions can be found in the Table 4.10.

5.6 Insights from the past

Although our literature review study focuses in providing the empirical evidence of past hydroclimatic changes, in this last Section we will briefly discuss some plausible explanations for our findings. Perhaps the most striking result is that even during the highest temperature deviations amongst the ones we examined, the hydrological cycle fluctuated

within a reasonable range. No extreme cases of global long-term aridity or humidity have been imprinted in the paleoclimatic records. On the contrary, most climatic shifts present substantial spatial heterogeneity regardless of their time scale. Of course, different physical mechanisms will drive hydroclimatic variability in different spatio-temporal scales. Due to the large uncertainties involved and the scarcity of the data records, it is rather questionable if the exact processes could be described, though. What could be more pragmatic is to distinguish the impact of the thermodynamic and dynamic components.

Higher temperatures appear more strongly related to wet conditions than lower temperatures to dry (Table 4.1). Out of the five warm periods studied, four present a distinct warm-and-wet signal and only during the MCA the dry conditions prevailed. On the other hand, only two out of five cold periods show a cold-and-dry regime, one exhibits cold-and-wet conditions (Little Ice Age) and two remain inconclusive (Younger Dryas and 8.2k event). It is easy to note that the periods that diverge from the Clausius-Clapeyron thermodynamic response are the shorter ones (Figure 5.10). Longer periods with duration comparable to the Holocene, such as the Eemian Interglacial Stage and the Last Glacial Maximum follow the warm-and-wet and cold-and-dry paradigms. A similar pattern manifests in the spatial domain. Global or hemispheric studies are more tightly linked to the thermodynamic response, while as spatial scale becomes finer the heterogeneity increases highlighting the impact of the changes in atmospheric and oceanic circulation [185, 309].

Thus, it is reasonable to claim that the atmospheric/oceanic circulation (dynamic component) appears to have a more dominant role in the regional fluctuations of the hydrological cycle, than the total atmospheric moisture content (thermodynamic component). This is particularly true for the abrupt climatic events. Even though the exact physical mechanisms of their genesis remain under investigation, there is a general agreement that most of the past abrupt climatic transitions are related to changes in the oceanic circulation. Still, it is a concern whether these abrupt climate changes arisen from internal climate system processes or be the consequence of a stimulated response to a progressive external forcing [119]. In the case of longer climatic regimes, warmer/colder oceans develop different circulation patterns, which in turn affect the atmosphere system resulting to different modes of atmospheric circulation [590].

The majority of the abrupt events studied here were mainly associated with the Atlantic long-term variability and AMOC in specific. The AMOC is not a circulation pattern appearing only in the Holocene. Its existence has been confirmed both for the Eemian Interglacial Stage and the D-O intervals [131]. The decline of AMOC strength has also been linked to Heinrich events, Younger Dryas, the 8.2 ka event, and phases of cold conditions in general [160, 447]. It's weakening is related to freshwater pulses caused by the melting of Arctic ice and high latitude glaciers [309]. The AMOC variability can affect the Westerlies, and, thus the atmospheric moisture amount that is transferred over land. When weak, it has been linked to a decline in precipitation from western Europe to continental Asia [331], as well as monsoon activity [204]. The latter is likely due to the links between the weakening of AMOC and the southward shift of the Inter Tropical Convergence Zone (ITCZ). As the AMOC weakens, the temperature gradient between the tropical and North Atlantic becomes more intense and drives ITCZ to the south [384].

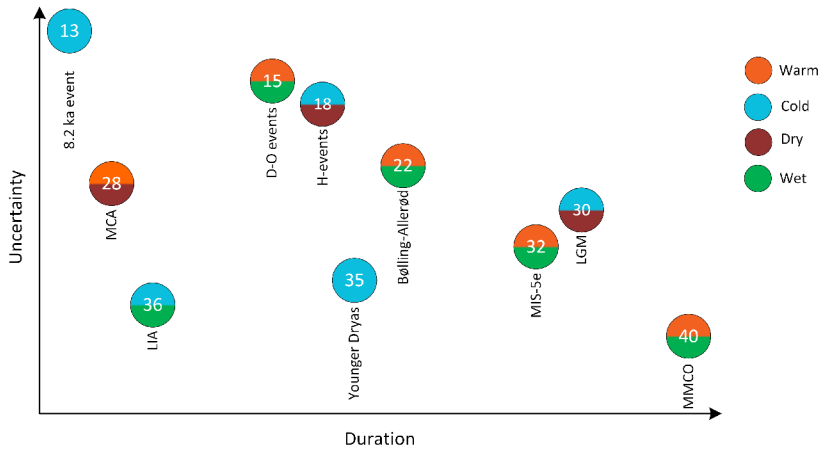

Figure 5.10: Schematic representation of hydroclimatic conditions in terms of the period length and the uncertainty involved. Uncertainty is qualitatively derived from the number of studies.

Overall, the southward shift of the ITCZ has been related to the colder conditions across the northern tropics such as Heinrich events [297], Younger Dryas [420], and the weak monsoon during MIS-5e [367]. In addition, the latitudinal variations of the ITCZ have been identified to affect summer-monsoon variations in tropical and Asian regions during the D-O and Heinrich events [248]. On the contrary, the northward shift of the ITCZ has been reported to intensify the Asian summer monsoon [421, 571], which is also related to warmer

conditions [502, 469]. There is some evidence of this behavior also during the mid-Miocene; the enhanced precipitation observed across northern Colombia was likely due to the northward shift of ITCZ [472]. Most importantly, as ITCZ shifts the regions that are no longer under its effect will become drier, with an opposite outcome to the ones that are no longer affected. This is a straightforward example of why wetter and drier conditions can co-exist when there is some atmospheric reorganization. As ITCZ and the monsoon systems involve a large fraction of global precipitation, further research is increasingly important to further understand the relationship between oceanic circulation and ITCZ/monsoon in past climates.

It is interesting that even though there is substantial evidence of the connection between ITCZ and temperature in the paleoclimatic reconstructions, this was not the case for atmospheric moisture divergence zones as well. Nowadays, the dominant hypothesis suggests that global warming makes the regions with atmospheric divergence to become drier and the regions with atmospheric convergence to become wetter, termed as 'dry gets drier, wet gets wetter' [218]. However, our results are not in favor of this hypothesis, which has also been recently debated by some empirical studies of observational [200] and paleoclimatic records [95]. On the other hand, we notice that in many periods, the prevailing hydroclimatic regime, e.g., warm and wet, appears in 65% to 80% of the studies. This could imply that the convergence/divergence did become stronger in the past warmer periods, but at the same time, a substantial reorganization of the atmospheric circulation patterns occurred. Plainly speaking the intensification did occur, but it might have affected different regions.

To further investigate the spatial heterogeneity of the temperature or precipitation relationship we also examined the hemispheric and latitudinal distribution of the records during cold and warm periods. No significant changes are observed between the hemispheric distribution of studies during cold periods (Figure 5.11 A). In the zonal domain, there is a divergence between mid and high latitudes, with the former exhibiting a tendency to cold-and-wet conditions and the latter cold-and-dry (Figure 5.11 B). In addition, approximately one-third of the studies document warm climates over mid-latitudes, with a higher occurrence in SH. Even though the uneven number of studies per hemisphere and latitudinal zone

makes the interpretation of the results ambiguous, it provides some insight of the enhanced heterogeneity, especially when compared with the warm periods. The warm periods appear quite more homogeneous in terms of temperature for both hemispheres (Figure 5.12 A). The NH appears to favor warm-and-wet conditions in a 2:1 ratio, which drops to approximately 1:1 for SH. The distribution appears quite similar for all three latitudinal zones, also close to 2:1 (Figure 5.12 B). Again, the bias of the low number of studies in SH should be taken into account. Nevertheless, the hemispheric and latitudinal distribution of the records advocates for an asymmetric response of precipitation to temperature increase and decrease. It should be noted though that due to the limited number of records (especially precipitation), it is difficult to adequately describe the spatial features of the water cycle's response.

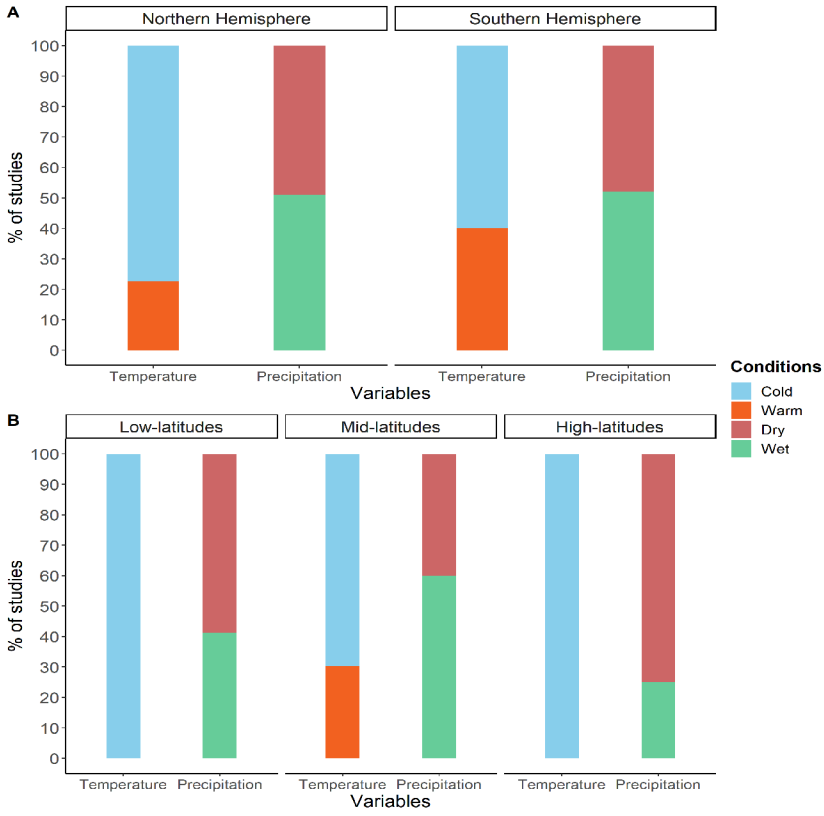

Figure 5.11: Relationship of temperature and precipitation during the cold periods (LGM, Heinrich Events, Younger Dryas, 8.2 ka Event, and LIA). A: studies over different regions, B: studies over the different zones

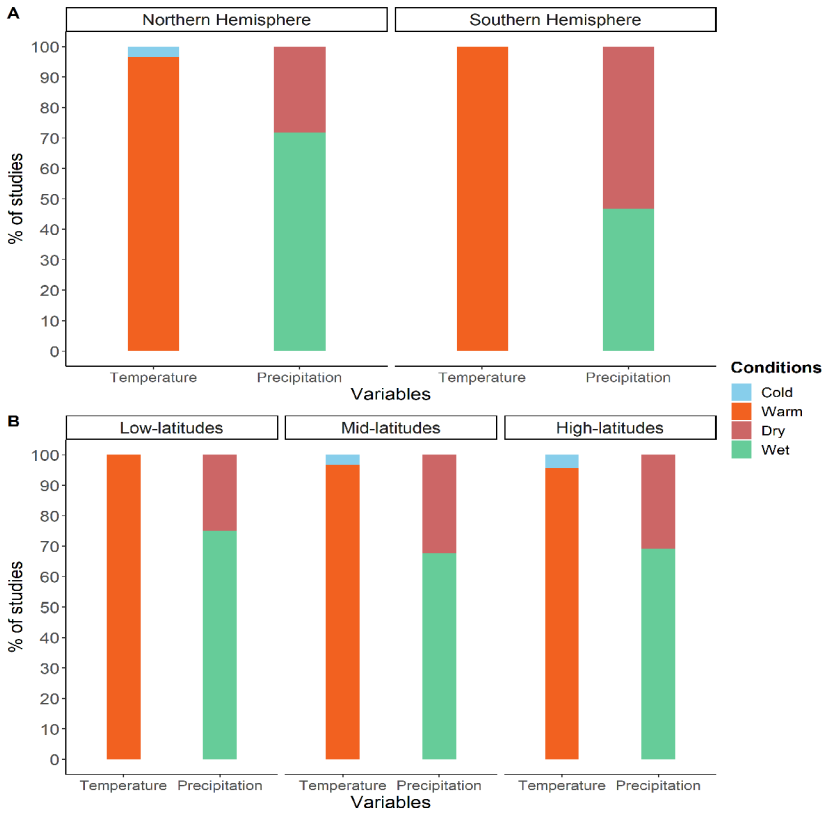

Figure 5.12: Relationship of temperature and precipitation during the warm periods (MMCO, MIS-5e, DO events, Bølling-Allerød interstadial, and MCA). A: studies over different regions, B: studies over the different zones

A plausible approach to overcome the reconstruction scarcity barrier can be found in earth system modelling. Indeed, evidence of abrupt or mild atmospheric reorganization has been presented for some of the climatic periods discussed in our review. For instance, model simulations show that during the MCA was associated to a substantial expansion of the NH Hadley circulation [195]. This change in the atmospheric circulation patterns could explain the drying over the mid-latitudes and the shifts in the monsoon patterns across Africa and South Asia. Other reorganization patterns have been suggested for the termination of the last deglaciation [575] or the LGM [258]. Even though this evidence is far from conclusive, the hypothesis of a circulation-modulated water cycle intensification is a promising direction to reconcile the 'dry gets drier, wet gets wetter' paradigm with the observed changes.

Unfortunately, earth system modelling comes with certain limitations as well. The consistency between model output and proxy data shows agreement over larger scales, but

there are crucial discrepancies in the regional scales [216]. This is a known issue in model performance related to the challenges in reproducing precipitation properties at finer/regional scales [172]. However, some uncertainties still remain in larger scales, due to inconsistencies in the simulation of atmospheric circulation [8] and its modes such as ENSO [46] or NAO [607, 153]. Inevitably, the AMOC is also poorly represented [611], which might be related by a common bias in the model's parameterization regarding AMOC stability [317]. On the other hand, the past millennium scale records reveal no evidence of internally originated multidecadal oscillation. These multidecadal Atlantic Multi-decadal Oscillation-like oscillations have contradicted as the manifestation of high-amplitude explosive volcanism episodes [343]. With all these open challenges in earth system modelling, the need for more high-resolution paleoclimatic reconstructions is increasing.

More paleoclimatic reconstructions would further improve our understanding the interaction between temperature and water cycle. The evidence presented here suggests that the hypothesis that a warmer climate is a wetter climate could be an oversimplification even for centennial scales. On the contrary, precipitation response appear to be spatio-temporally heterogeneous, with certain differences among periods. This should be taken into account when assessing the future intensification of the global water cycle. Even if not regionally precise, the precipitation response heterogeneity should be evident in model simulations or our theoretical constructs of the global water cycle functioning. This qualitative metric could help improve the model performance, and in turn shed more light on the influence of atmospheric and oceanic circulation. The remaining challenge, though, is to quantify the spatial variability of precipitation response in a robust manner. As the number of paleoclimatic reconstructions increases, we will soon be able to have a more coherent picture of specific warm or cold periods, and increase the likelihood to address it.

5.7 Conclusions

Most climate projections report that the hydrological cycle will intensify when the climate will get warmer. As a result, the hydrological cycle sensitivity is a major concern for the coming decades. In this study, we reviewed the relationship between the hydroclimate and temperature in the recent and distant past. We confirmed that, in general, most paleoclimate

records suggest that the hydrological cycle intensified in a warmer climate. Correspondingly, the hydrological cycle weakened during the colder periods. However, the spatial distribution of hydroclimatic changes were not homogeneous around the world.

This lack of homogeneity makes paradigms such as "a warmer climate is a wetter climate" or "dry gets drier, wet gets wetter" appearing as oversimplifications. The evidence presented in this study agrees to the hypothesis that climate changes at the global scale are thermodynamic-driven, while regional climate changes are more related to variations in ocean-atmospheric circulation. However, due to its enhanced spatiotemporal distribution, hydroclimate variability is difficult to be quantified on a regional, continental, and global scale. In this context, large-scale paleo-hydroclimatic shifts, especially during the warm periods, need further investigation as they could provide new insights into the present and future hydroclimatic changes.

Chapter 6

Investigation of Changes in precipitation and temperature patterns related to the state of the North Atlantic Ocean during the Medieval Climate Anomaly

6.1 Summary

While a warmer climate is likely to increase global precipitation, the precise impacts on regional-scale responses under such conditions remain uncertain. Furthermore, it is unclear whether the Atlantic Meridional Overturning Circulation (AMOC), a vital component for maintaining the equilibrium of the global climate, is presently in a weakened state or will weaken by the end of the 21^{st} century due to rising global temperatures. Therefore, this study investigates an interval of the past warm period when substantial changes in both hydroclimate and AMOC are suspected to have occurred, specifically during the Medieval Climate Anomaly (MCA; 800–1400 CE). Utilizing regional-scale multi-proxy data sensitive to AMOC and hydroclimate, we endeavor to investigate the hydroclimate patterns at regional and continental scales across Europe and North America on a centennial timescale. Additionally, our objective is to unveil potential connections between hydroclimate patterns and the variability in the North Atlantic Ocean state, i.e., AMOC, Sea Surface Temperature (SST), and the Inter-Tropical Convergence Zone (ITCZ) in a warm climate context.

We observed a declining trend in SST that began in the 10^{th} century and extended until the end of the 14^{th} century in the North Atlantic region. Simultaneously, our findings indicate a southward shift of the ITCZ, particularly from 9^{th} to 12^{th} century, which may have played a significant role in reducing the northward flow of atmospheric heat and moisture from the tropics. Consequently, this low SST and southward shift of the ITCZ contributed to the cold and arid conditions across the North Atlantic region. We assume that low SST and southward shift of ITCZ could potentially be linked to the onset of AMOC weakening or perturbations in the associated ocean circulation. In the 11^{th} century, the climate became warmer than in previous centuries. This warming likely triggered a perturbation in the AMOC due to increased freshwater inflow into the North Atlantic. Consequently, this perturbation resulted in a weakened AMOC state that persisted from the late 10^{th} to the 13^{th} century. However, the state of AMOC remains elusive; observations from AMOC-sensitive tracers, such as δ^{13}C and cd/ca, reveal notably subtle patterns, whereas sortable silt data presents conflicting indications. Therefore, this hypothesis requires substantiation through further comprehensive investigations using precise AMOC tracers. Although our

investigation unveiled a noteworthy association between SST variation, shifts in the ITCZ, changes in the AMOC (in δ^{13}C and cd/ca), and subsequent hydroclimate changes across both continents. The over three-century-long period of low SST, southward shift in the ITCZ, and weak AMOC may have provoked a transition from warmer to colder climatic conditions, as evidenced during the 12^{th} to 14^{th} centuries. During this time, the western and northern parts of Europe, alongside the eastern and southern parts of North America, emerged as the most sensitive areas, marked by a shift toward colder and drier climates. This transition could be attributed to the prolonged low SST, weakened AMOC, and southward ITCZ, which limited atmospheric moisture flows toward Europe and North America, resulting in lowered temperature and altered precipitation distribution.

Furthermore, at the regional scale, we observed that climates significantly warmer or slightly above than their centennial average were predominantly associated with humid conditions. In mid-latitude regions, warmer climates may lead to arid conditions. In contrast, when climates were slightly colder or below the centennial-scale average, they tended to result in arid climate conditions. At a continental scale, warm climates equivalent to the centennial scale average were associated with humid conditions, e.g., during the 9^{th} to 10^{th} centuries. However, later warm/cold climates appeared to correlate with decreased precipitation/arid conditions over Europe. On the other hand, warm/cold climates in North America seemed to influence wet/dry climate tendencies.

Keywords: Global warming, Sea Surface Temperature, Inter-Tropical Convergence Zone, hydroclimatic variability, Atlantic Meridional Overturning Circulation, Medieval Climate Anomaly

6.2 Introduction

A warmer climate will have far-reaching impacts on socioeconomic life by altering the hydrological cycle and affecting water resources. In recent decades, significant changes have occurred in the global hydrological cycle [225], and it is expected that future global warming will cause even more alterations in precipitation patterns [525]. Most studies project an intensification of the hydrological cycle in warmer climates [542, 157]. This is because warm conditions increase the atmospheric moisture holding limit, which will lead to more intense precipitation [218]. However, some studies have also documented drier conditions in a warmer climate [145, 235]. Owing to these conflicting findings, the behavior of the hydrological cycle in a warm climate remains enigmatic, although there is substantial evidence of its intensification as temperature increases in the paleoclimatic records [430, 274].

In addition to directly modulating the hydrological cycle, warmer conditions also exert strong indirect controls, e.g., via the melting of ice sheets that affect the global ocean circulation. Additionally, a warmer climate also influences SST, resulting in the melting of sea ice and subsequent changes in oceanic circulation, thereby impacting global hydroclimate patterns [621]. The discharge of freshwater into the North Atlantic Ocean from melting ice masses is known to disturb ocean circulation patterns [280], leading to cascading impacts on both regional and global hydroclimate systems (i.e., temperature and precipitation). In a warmer climate, the changes observed in SST and the AMOC compared to the preceding decades have drawn significant global attention. The thermohaline circulation, i.e., the AMOC is a vast ocean currents system that carries warm and salty surface waters northwards (from Equatorial regions towards the Arctic), which sinks down and loses buoyancy over the Arctic region and move southwards (from the Arctic towards Equatorial regions) as cold deep-waters. During this process the AMOC distributes atmospheric heat and moisture, which exerts a strong control on the global water cycle [352, 295]. Recently, the state of the AMOC has drawn wide attention because research indicates that it is slowing down, and numerical models project a further weakening by 2100 [60, 356].

There is an ongoing debate on the prevailing hypothesis that increasing global warming

will weaken the AMOC [583, 60]. Due to the increasing rate of greenhouse gases and the accompanying warm climate [295], freshwater discharge into the ocean alters the density of the surface water, making it more buoyant and less likely to sink. Consequently, a decrease in the North Atlantic surface water density will likely inhibit the ocean deep-water convection and will cause a weakening of the AMOC [66]. Rahmstorf [439] and Caesar et al. [100] suggested that the AMOC is presently in its weakest condition during the past millennium, due to increasing anthropogenic global warming [33]. A shutdown of AMOC has been projected before the end of the present century [60], but the possibility is very uncertain and still largely debated [278]. It is important to note that the variability of the AMOC has a significant impact on hydroclimates in North American and European regions [249]. Anticipated weakening of the AMOC is likely to result in reduced atmospheric moisture transport towards Europe and North America, leading to limited precipitation and cold conditions in these regions [316, 555]. Moreover, a slowdown of the AMOC could impact the monsoon system over Asia and Africa [204], as well as the moisture flows and air temperatures across the globe by pushing away ITCZ southward [132, 92]. A significant weakening of the AMOC and the consequent southward displacement of ITCZ would lead to global hydroclimatic alterations, such as shifts in hydrological cycle patterns across the terrestrial regions [316].

The evidence from the distant past reveals that most of the abrupt events were in response to the Atlantic long-term variability, the AMOC in specific [584]. For instance, the Dansgaard-Oeschger events [465], the last ice age, and the deglaciation period were responses to alterations in the AMOC [329]. A weakened AMOC has been hypothesized in the Heinrich events [11], Younger Dryas [115], the 8.2 ka events [160], and particularly cold climatic phases [6]. The majority of studies conducted thus far have focused on cooler time intervals. Interestingly, AMOC shifts often occurred during the transition time between glacial-interglacial [47] or interglacial-glacial periods. It is still being investigated whether the current warmer climate will lead to colder climates in the future, and what relationship exists between warmer climates and AMOC variability. Therefore, understanding the relationship between AMOC variability and hydrological cycle variability including SST and ITCZ response in warm climates could help predict future hydroclimate shifts. Since SST exerts a substantial influence on the distribution of hydroclimate patterns across the

North Atlantic regions, a comprehensive examination of SST patterns in conjunction with hydroclimate patterns may yield valuable insights into its significance [521].

Only a few observational studies have focused on the behavior of AMOC, SST, and ITCZ, including their relationships with hydroclimate patterns during past warm climates, mainly the MCA period. The lack of data on past AMOC variability poses a challenge for examining AMOC variations and their possible influences on hydroclimate conditions. Additionally, climate models do not fully capture past climatic conditions and ocean circulation, which hinders their ability to provide reliable projections [500]. Consequently, AMOC variability during the MCA is still not well understood. Nevertheless, investigating the relationship between past warm climates, AMOC, and SST could be a foundation for understanding how these parameters will influence the global hydroclimate in a warm climate. Therefore, our study stands as unique due to our focus on investigating North Atlantic variability (SST and AMOC) and its correlation with terrestrial hydroclimate patterns during the MCA period, which was more or less warm like the ongoing interglacial time.

Since the core period of the MCA falls within 1000 and 1300 CE, we selected a time scale from 800 to 1399 CE. This broader temporal scope enables us to examine variations occurring not only during the MCA but also in the periods preceding and succeeding this distinct climatic phase. The climate during the MCA is often suggested to have predominantly warm and arid conditions, specifically during the core period, and cold and humid conditions after that [287, 195]. Despite the widespread acceptance of these hydroclimatic changes, the factor responsible for the abrupt decline in average temperature during the MCA-LIA transition remains elusive. However, it has been suggested that shifting global atmospheric circulation patterns between the MCA and LIA were the main drivers of hydroclimatic changes [288, 192], which still needs to be tested. Our study aims to investigate the changes in precipitation patterns, mainly precipitation minus evaporation (P-E), in response to centennial-scale changes in temperature and AMOC using regional multi-proxies. To do so, we investigate the validity of the following research hypothesis: "*The variability in the North Atlantic region, particularly in SST, AMOC, and ITCZ due to warm climate, results in drying and shifts in temperature and precipitation patterns across most parts of North America and Europe.*"

6.3 Results

6.3.1 Variability in the AMOC, SST, and ITCZ

Our analysis of AMOC-sensitive tracers, at the centennial scale, indicates notably weak and/or non-significant changes in AMOC strength [383]. We employed multiple records to track AMOC variations, each presenting distinct signals of AMOC changes over time. The potential weakening of AMOC due to warmer climates remains uncertain [266], given the divergence in responses observed across various records. It's possible that either the changes are very low or very short, or the proxies are not sensitive enough to capture AMOC weakening responses. In our dataset, specifically, both δ^{13}C and cd/ca exhibit weak signals of AMOC after the mid-10^{th} century. Among the sortable silt records, three (NEAP-4k, Orphan Knoll, GS06-14408GC) indicate weak signals of AMOC from the 10^{th} to 11^{th} century, while two (MD99-2251 and ODP983) present a contrasting response during this period. We observed that sortable silt records from MD99-2251 and ODP983 revealed an early indication of a weak AMOC signal compared to δ^{13}C and cd/ca. Specifically, this signal emerges from the 9^{th} century and extends from the mid-9^{th} century to approximately the mid-10^{th} century, respectively. This earlier response could potentially indicate an earlier sensitivity to AMOC weakening in these specific locations. However, definitive conclusions on the sensitivity of AMOC tracers over both space and time require further investigations.

Despite the challenge of interpreting these faint signals, our overall analysis suggests strengthened AMOC conditions from the 9^{th} to the 10^{th} centuries while gradual weakening from the 10^{th} century and continued until the 14^{th} century. This trend is notably reflected in δ^{13}C, cd/ca, and several sortable silt records. Furthermore, our centennial-scale observations highlight the 11^{th} century as a period marked by weaker signals of AMOC, notably seen in δ^{13}C, cd/ca, and sortable silt records from NEAP-4k, Orphan Knoll, GS06-14408GC. Following this, there was a recovery in AMOC strength during the 12^{th} century, succeeded by a subsequent weakening persisting until the 13^{th} century. Following the 13^{th} century, most AMOC tracers consistently indicated a decline in its strength, followed by an upward trend peaking in the 14^{th} century, while the average trend consistently remained

below the centennial mean. We assume that the decline in the AMOC continued beyond the 14^{th} century and potentially contributed to the onset of the Little Ice Age (LIA). Prior to the AMOC shift, our records indicate that high-latitudes experienced relatively warm conditions, particularly from the 9^{th} to the 11^{th} centuries, with the 11^{th} century exhibiting a warmer climate compared to the preceding centuries. This indicates the potential existence of early warming signs preceding abrupt AMOC shifts [318, 302].

Furthermore, we conducted an examination to investigate variations in SST and ITCZ in the MCA warm climates, in order to track any relationship with AMOC (Figure 6.2). Changes in AMOC influence ocean dynamics, creating an inter-hemispheric radiative gradient that regulates the north and south migrations of the ITCZ [384]. During our examination of the ITCZ, our results support the idea that a weakening of the AMOC is associated with the southward displacement of the ITCZ [71, 366]. Specifically, our investigation reveals a southward shift in the ITCZ during the 10^{th} to late 11^{th} centuries, coinciding with AMOC weakening. A similar southward shift in the ITCZ has also been observed by Tan et al. [524] and Chawchai et al. [108] in their studies. However, in most records, from the 12^{th} to the 13^{th} century, the ITCZ gradually shifted northward and maintained stability until the 14^{th} century. The PHYDA ITCZ assimilation, despite indicating a comparable trend to the proxy, demonstrated more substantial variability than the proxy observations.

Furthermore, AMOC variations significantly influence SST changes [295]. During the investigation of SST, we found that SST over the North Atlantic region was high during the 9^{th} to the 10^{th} centuries, consistent with a warm climate [488]. However, during the 10^{th} century, high SST began to shift, and between the 11^{th} and 14^{th} centuries, the average SST conditions were low. It's been observed that low SST has a correlation with a weak AMOC [262]. This is because the AMOC plays a crucial role in transporting heat, and a weak AMOC leads to a reduction in North Atlantic SST [307]. In our study, we observed that the low SST conditions and the southward shift of the ITCZ during the 11^{th} century correlate with AMOC conditions, suggesting a weakened state of the AMOC. However, additional investigation is required to confirm this relationship conclusively.

Considering all this evidence, we anticipate that ongoing climate warming may lead to a weakening of the AMOC and low SST in the North Atlantic, although these changes may

take place over a very long period of time, maybe spanning centuries or even millennia. Since a weakened AMOC influences the SST and southward displacement of the ITCZ [71, 326], such variability could have adverse effects on the global moisture flow [132] and the monsoon system [204]. Therefore, long-term analysis becomes crucial for a comprehensive understanding of AMOC and SST changes in a warmer climate and their relationship with hydroclimate variations, which might not be apparent in short-term records.

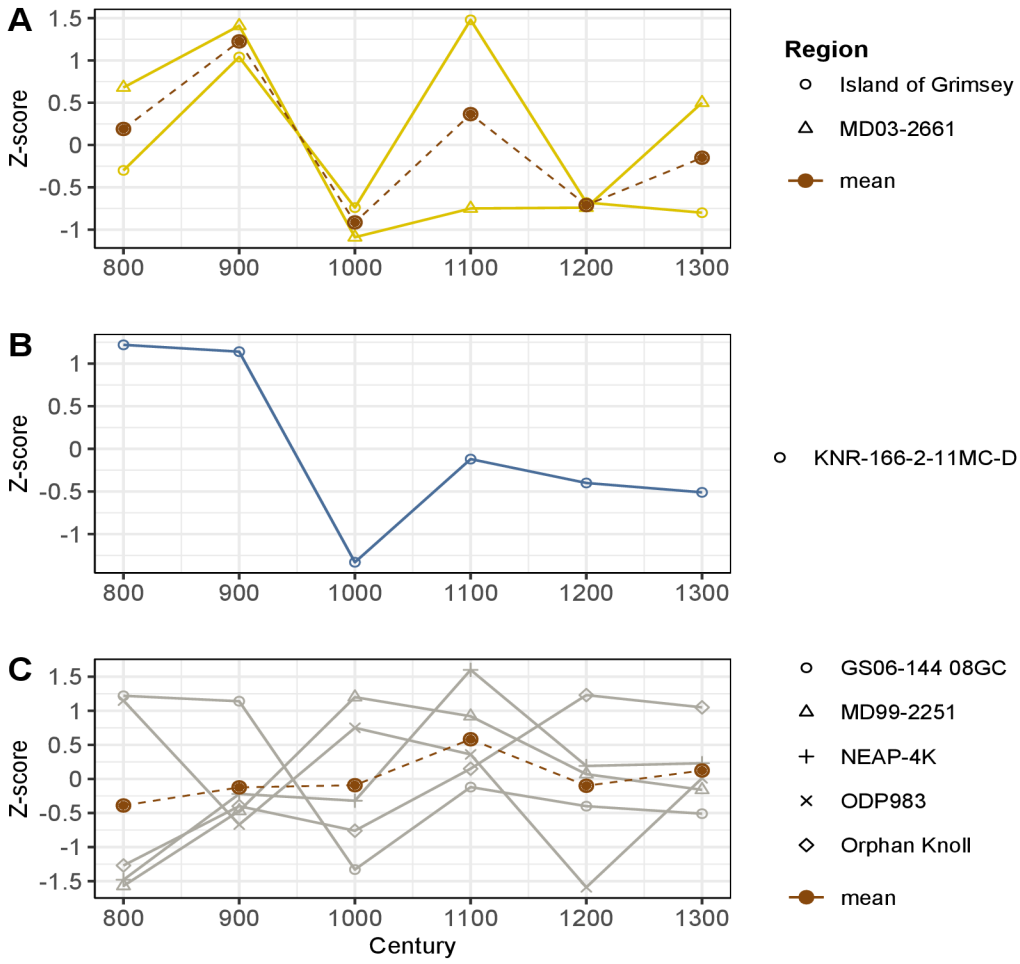

Figure 6.1: State of AMOC in the North Atlantic regions. Variations in δ^{13}C (A), cd/ca ratio (B), and sortable silt (C). The mean reflects the comprehensive average of all records.

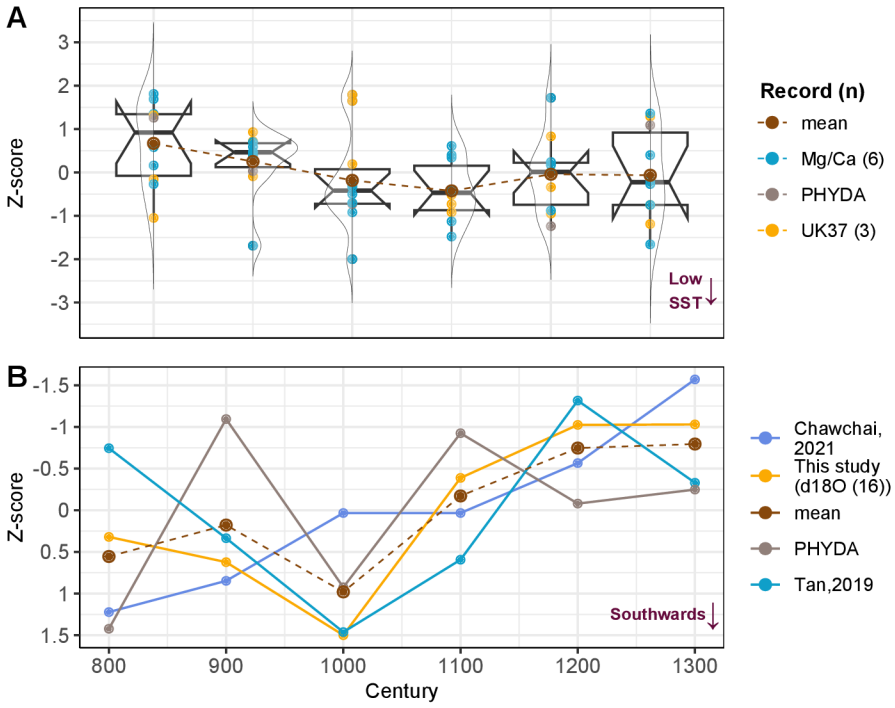

Figure 6.2: SST (A) and ITCZ (B) conditions over North Atlantic. Positive values for ITCZ indicate a southward shift and negative values suggest a northward shift. The 'Record (n)' denotes the proxy and the number of proxies employed for the analysis.

6.3.2 Hydroclimate conditions over Europe

Temperature and precipitation are integral components of the hydroclimate system. Many studies have emphasized the high sensitivity of hydroclimate patterns in Europe to fluctuations in North Atlantic oceanic circulation, with documented occurrences of recurrent drought-like conditions during the MCA [217, 223]. However, the validation and reliability of hydroclimatic records from the MCA in Europe, particularly concerning the origins of drought-like conditions, are uncertain and sometimes contradictory, necessitating further verification [475, 103]. Therefore, this study investigates the hydroclimate changes in Europe and explores their potential connection with alterations in the state of the North Atlantic during the MCA (Figure 6.3 A and B). Our result indicates warm conditions prevailing during the 10^{th} and 11^{th} centuries, followed by colder climates from the 12^{th} to the 14^{th} century, and wet conditions during the 9^{th} century. However, we observed heterogeneous signals of aridity across subsequent centuries at the centennial scale, potentially attributable to spatial heterogeneity (Figure 6.3). Notably, our results highlight the 11^{th} cen-

tury as a period characterized by relatively higher temperatures of MCA. A shift towards colder conditions commenced in the 12^{th} century, prevailing across Europe throughout the 12^{th} to 14^{th} centuries.

Moreover, our findings unveil a notable latitudinal shift in temperature patterns, particularly from the 12^{th} to the 14^{th} centuries (Figure 6.3-A). This shift is characterized by the migration of cold climates from high-latitudes to mid-latitudes. As a result of this latitudinal temperature shift, during the 14^{th} century, most central European regions became even colder than in previous centuries. Precise conclusions on factors influencing hydroclimate variation during the MCA-LIA transition period are not available yet. It is probable that this transition in climate patterns aligns with shifts in oceanic and atmospheric circulation, which are likely influenced by the previously discussed long-term variations in the AMOC, SST, and ITCZ. Consequently, during the transition from the MCA to the LIA, specifically between the 13^{th} and 14^{th} centuries, the majority of northern and western regions, on average, experienced cold conditions. However, our examination of hydrological conditions reveals a complex hydroclimatic scenario during this transitional period. Notably, central (Slowinskie Blota, Stazki Bog) and a few southern areas (Lake Allos, North Aegean) shifted toward humid conditions (Figure 6.3-B). During the central period of the MCA (i.e., 10^{th} and 11^{th} centuries), our analysis demonstrates a warm climate. Nevertheless, the hydrological condition exhibits spatial variability, with certain regions experiencing wet conditions while others depict arid conditions. The arid conditions are likely linked to episodes of drought, which have also been observed and documented by Cook et al. [125] and Chen et al. [109].

Our findings uncover a complex hydroclimatic scenario during this transition period. While some records suggest a cold and arid climate in northern areas, contradictory evidence points to a cold and humid climate regime in southern and western regions. In summary, our observations suggest that during the MCA, coastal regions of Europe mostly experienced humid conditions, except for the 10^{th} and 11^{th} centuries, while inland areas were predominantly arid. The occurrence of arid or humid climates in these land areas could be attributed to localized responses to amplified regional atmospheric warming [523]. The presence of a temperature gradient between the ocean and coastal regions likely con-

strained atmospheric moisture to coastal areas, contributing to the humid coastal climate [479].

The continental-scale temperature overview across Europe reveals warm conditions until the 11^{th} century, followed by cold conditions until the 14^{th} century (Figure 6.4). Regarding precipitation, hydrological conditions at the continental scale appear predominantly wet until the 10^{th} century. However, after this period, while variations in precipitation persist, they tend to remain around their centennial mean values, consistently staying below that average. We show that evidence at the continental scale (Figure 6.4) suggests a correlation between warm climates and wet conditions, while cold climates correspond to dry conditions. However, at the regional level (Figure 6.3, hydrological conditions appear more closely linked to local thermodynamic changes and the availability of water sources [110, 430].

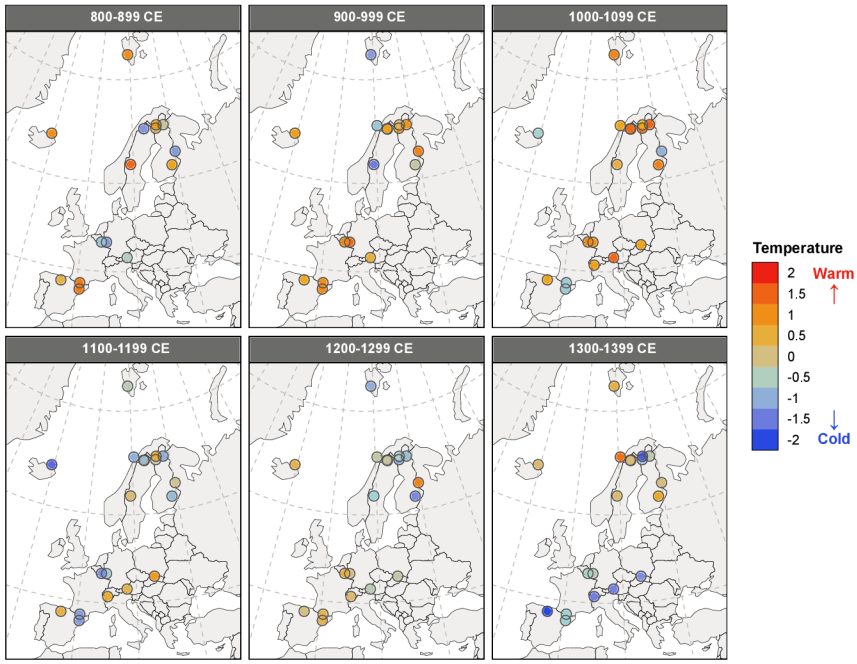

A.

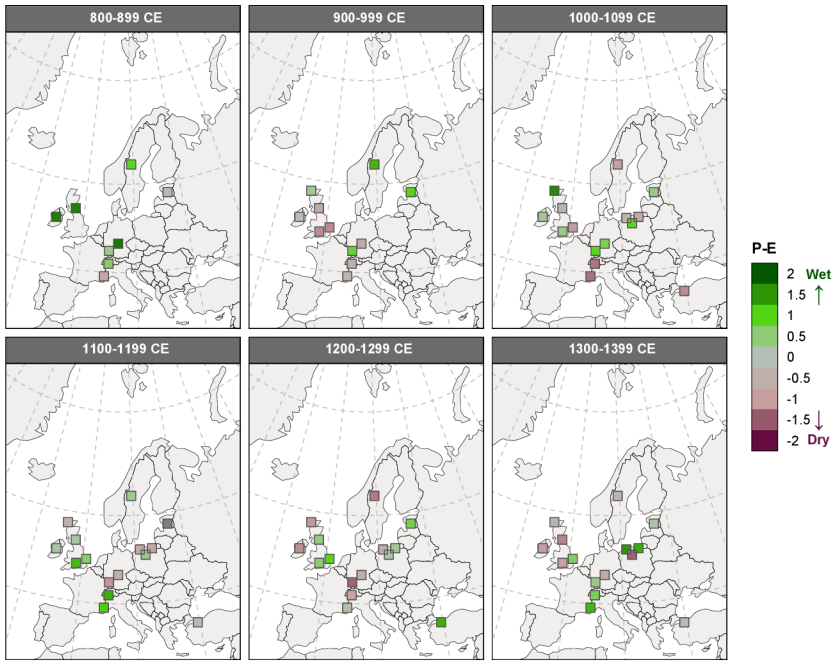

B.

Figure 6.3: Proxy-estimated temperature (A) and aridity (P-E; B) conditions across Europe (z-scores).

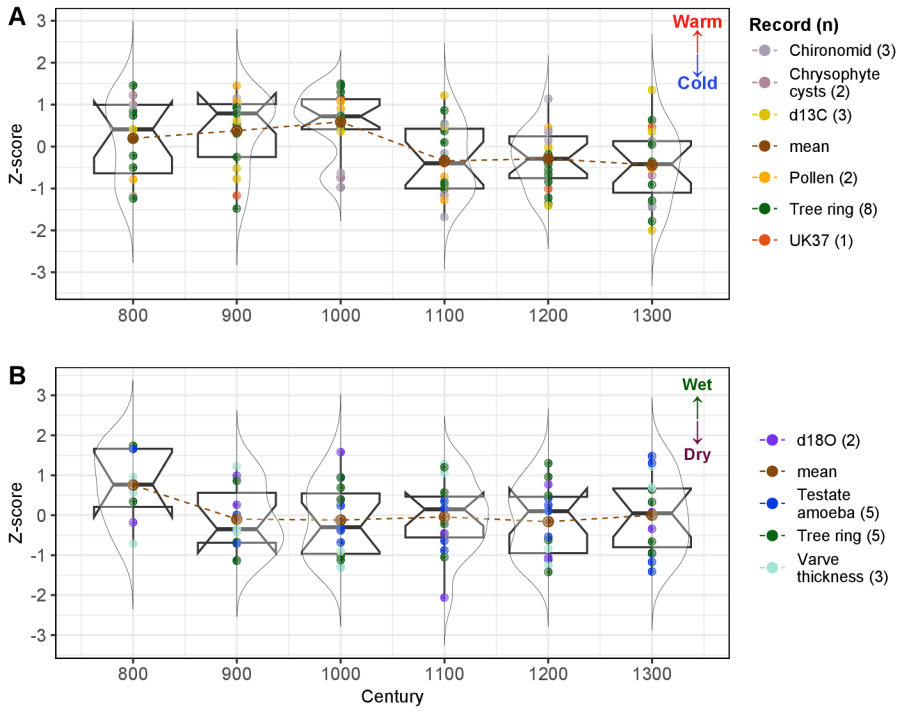

Figure 6.4: Overview of temperature (A) and P-E (B) conditions over Europe. The 'Record (n)' denotes the proxy and the number of proxies employed for the analysis.

6.3.2.1 Comparative assessment of outcomes from proxy and model assimilation

We compared proxy results to model assimilation, specifically PHYDA and Paleoview, as shown in Figure 6.6 and 6.5(A, B). The models assimilation we categorised into two types of outputs: point and grid. The point output represents values at the precise locations of the proxy data, while the grid output presents average conditions across the continent. Upon comparing the proxy and model results, we observed that both sources, i.e., PHYDA and Paleoview, assimilate warmer climatic conditions from 9^{th} to mid-11^{th} century, while it seems the PHYDA grid is overestimating the temperature conditions over a continental scale (Figure 6.6). Specifically, our analysis reveals that Paleoview assimilation for temperature, both at grid and point levels across high and mid-latitudes, aligns closely with the trends observed in proxy records. Contrarily, while PHYDA grid-scale assimilation on temperature aligns with the proxy trends, PHYDA point data portrays an opposing trend beginning from the 9^{th} century in high-latitudes. Additionally, in mid-latitudes, both the PHYDA grid and point data show an underestimation of temperature compared to the proxy records.

In terms of hydrological conditions at high-latitudes, both the proxy data and model assimilation (particularly the PHYDA grid and Paleoview point) indicated predominantly arid conditions. This aridity is particularly notable from the mid-10^{th} to the late-11^{th} century for the PHYDA grid and extends until the mid-13^{th} century for the Paleoview point. Discrepancies arise with the PHYDA point and Paleoview grid showing signals for humid conditions over the high-latitudes and mid-latitudes from mid-10^{th} to the mid-11^{th}. However, at mid-latitudes, differences between the proxy and PHYDA assimilation become evident. PHYDA simulations suggest humid conditions from the 10^{th} to mid-12^{th} century, while the proxy data suggests arid conditions. Simultaneously, Paleoview is showing an underestimation for arid conditions.

In summary, our comparison reveals divergent trends in model assimilation under similar climate conditions. Paleoview indicates that warm climates tend to promote humid conditions at high and mid-latitudes. PHYDA, on the other hand, suggests that warm climates result in arid conditions at high-latitudes and humid conditions at mid-latitudes. At the grid scale, the model simulations (PHYDA and Paleoview) generally demonstrate satisfactory performance in reproducing climatic conditions at mid and high-latitudes. However, at the regional scale, some discrepancies arise, possibly due to high uncertainty and/or limited availability of data for model simulations in those specific regions.

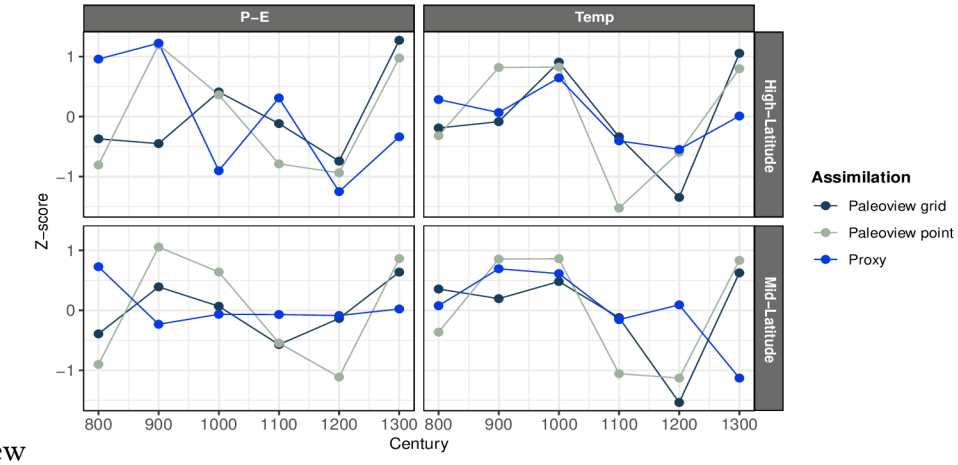

A. Paleoview

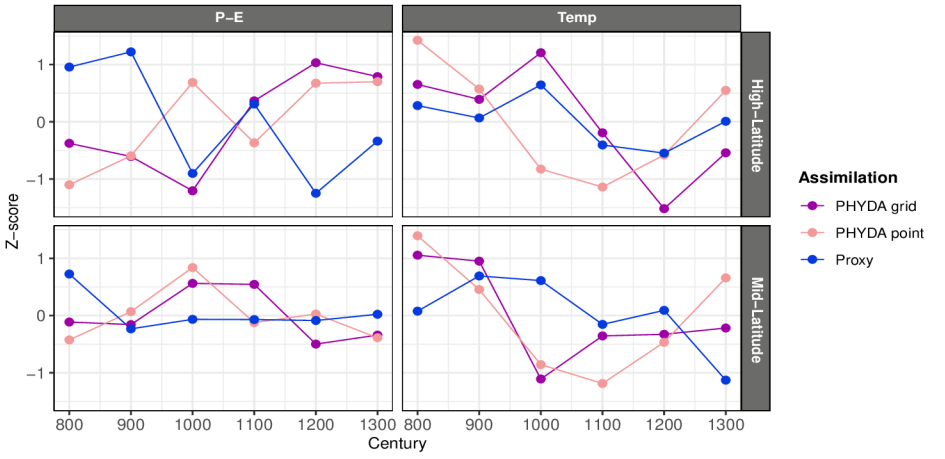

B. PHYDA

Figure 6.5: Evaluation of model (Paleoview (A), PHYDA (B)) and proxy estimated precipitation (Precip) and temperature (Temp) over Europe. The model point represents the exact location of proxy data.

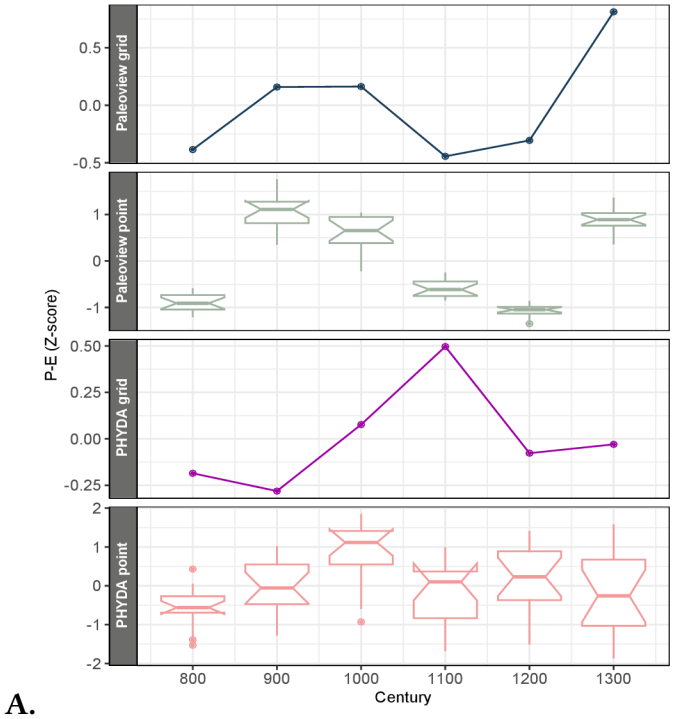

A.

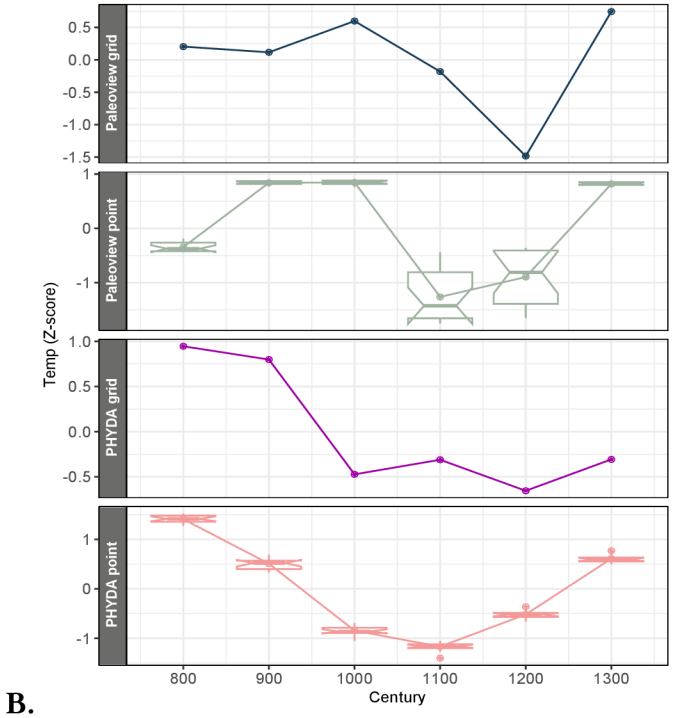

B.

Figure 6.6: Evaluation of model (Paleoview (A), PHYDA (B)) and proxy-estimated precipitation (Precip; P-E) and temperature (Temp) over Europe. Model points represent the exact locations of proxy data.

6.3.3 Hydroclimate conditions over North America

During the MCA, western and central regions of North America experienced warm and arid climatic conditions, characterized by decadal or centennial-scale megadrought events [398]. These megadroughts have been identified in various proxies, including tree rings [127], lake sediments [226], and eolian deposits [376]. While the underlying factors behind these megadrought events are still under investigation, certain findings suggest a connection of North American megadroughts with strong La-Niña-like conditions in the tropical Pacific region [196, 129]. Additionally, other records indicate that drought conditions were associated with warm conditions in the North Atlantic Ocean [362] and the Atlantic Multidecadal Oscillation [398]. Conversely, model-based findings link the occurrence of MCA megadroughts to increased warming resulting due to increased insolation activities [128]. The precise factors influencing hydroclimatic patterns and megadroughts during the MCA in North America remain subject to ongoing debate. Notably, the climatic conditions in North America appear significantly influenced by North Atlantic Ocean circulation fluctuations [244]. Therefore, this study suggests the hypothesis that low SST, a weakened AMOC, and a southward shift of the ITCZ could have been potential drivers of hydroclimate stress in North American regions. To assess the plausibility of this hypothesis, we investigated the variability of temperature and precipitation (P-E) over North America in response to centennial-scale changes in AMOC, SST, and ITCZ. Mainly, our study focused on analyzing the spatio-temporal hydroclimate changes using regional-scale multi-proxy records (Figure 6.7).

At the regional scale, the analysis of temperature distributions in high and mid-latitude regions revealed a predominantly warm climate during the 9^{th} and 11^{th} centuries, albeit with some regions displaying cold conditions as well. Commencing from the 12^{th} century, a transition towards cooler climate began prevailing in high and mid-latitude regions. Initially, this change was most pronounced in coastal areas and gradually extended further inland. More specifically, the onset of cold climates was observed in eastern North America and gradually extended to central and western regions between the 12^{th} to the 14^{th} centuries. In our examination of regional-scale hydroclimate variability, we noted a recurring cyclical pattern of dry and wet conditions at a centennial scale in the northern part of

British Columbia. Dry conditions were evident in the 9^{th}, 11^{th}, and 13^{th} centuries, while wet conditions prevailed during the 10^{th}, 12^{th}, and 14^{th} centuries. In certain regions like the north of Alberta, our observations indicated a dry climate when the temperature was warm but close to its centennial mean. However, as the climate became even warmer, these areas exhibited a wetter climate.

Temperature observations at the continental scale present a different climate trend: from the 9^{th} to the late 11^{th} centuries, the average conditions were warm, followed by the onset of cold climate from the 12^{th} (Figure 6.8-A). Concerning precipitation, from the 9^{th} to the late 11^{th} century, the climate appeared dry, with values slightly below the centennial scale mean (Figure 6.8-B). The 12^{th} century seems to be normal, while the 13^{th} century shows signals of wet conditions.

Hydrological conditions in high and mid-latitude regions exhibited spatial and temporal heterogeneity, with some areas showing humid responses to warm conditions while others experienced arid conditions. This complex spatial pattern of hydrological response persisted during the cold climate phases, with most regions being arid and some remaining humid. Overall, hydroclimate patterns during the MCA in North America included all the possible hydroclimatic combinations, i.e., as warm-humid, warm-arid, cold-humid, and cold-arid regimes. Our findings imply that arid hydrological conditions in North American regions coincided with periods when temperatures exceeded their centennial-scale averages, whereas humid conditions were more prevalent when temperatures were close to or aligned with their centennial-scale averages.

6.3.3.1 Comparative assessment of outcomes from proxy and model assimilation

Figure 6.9 presents the results of our temporal variability assessment using both proxy data and model assimilation. In our investigation, we observed that at the point scale, both models, namely Paleoview and PHYDA, exhibited a pattern similar to proxy records. However, both model assimilations demonstrated an over/underestimation of results for temperature and precipitation. When comparing the proxy and model results, discrepancies become apparent, particularly when considering grid averages in the model simulations. Our findings of the Paleoview and PHYDA assimilation at grid scale highlight the correspondence be-

tween lower temperatures and increased precipitation in eastern North America from the 9^{th} to the 12^{th} century. In contrast, western regions exhibit a correlation between lower temperatures and decreased precipitation during this period. However, after 12^{th} century, lower/higher temperatures are associated with decreased precipitation over both East and West parts of North America. In contrast, a closer examination of the model results at the exact proxy data locations shows a modest agreement with the proxy estimations. Regarding temperature in eastern and western North America, both PHYDA and Paleoview simulations align with the proxy data, indicating elevated temperatures during the 10^{th} to late 11^{th} century.

Our observations highlight agreement between the proxy data and model assimilations, depicting a shift within the climate system from a warm to a cold state. In terms of precipitation, both PHYDA and Paleoview diverge from the proxy data. While the proxy data suggests below-average (centennial-scale) precipitation between the 10^{th} to late 11^{th} centuries, both model simulations indicate an increase during this period. We observe that, in certain cases, the proxy and model point data align to represent the same variability patterns, whereas the model results at the grid scale deviate. This discrepancy underscores the presence of substantial uncertainties in the proxy and model point data, potentially arising from limited data availability or measurement errors. The notable uncertainty in the model simulations highlights the importance of refining the models and reducing measurement errors to enhance our understanding and prediction of hydroclimate variability.

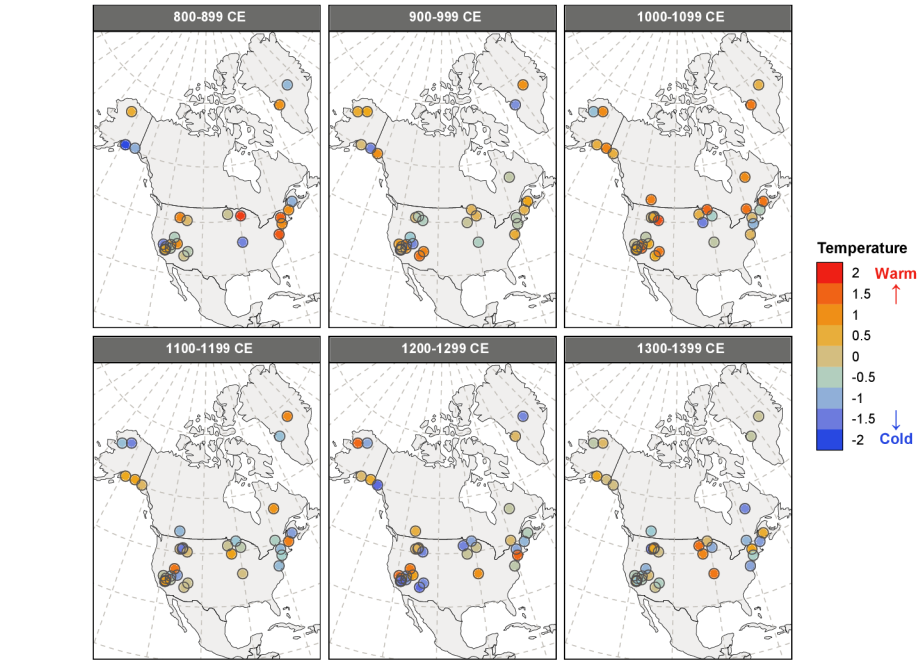

A.

B.

Figure 6.7: Overview of temperature (A) and aridity (P-E; B) conditions over North America. The 'Record (n)' denotes the proxy and the number of proxies employed for the analysis.

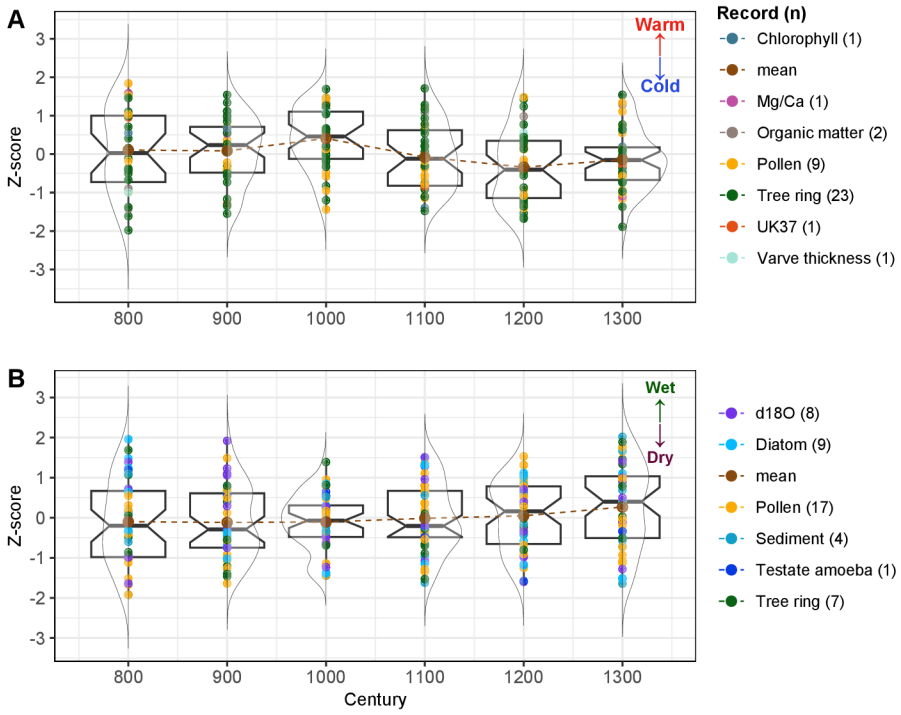

Figure 6.8: Overall view temperature and aridity (P-E) conditions over North America. The 'Record (n)' denotes the proxy and the number of proxies employed for the analysis.

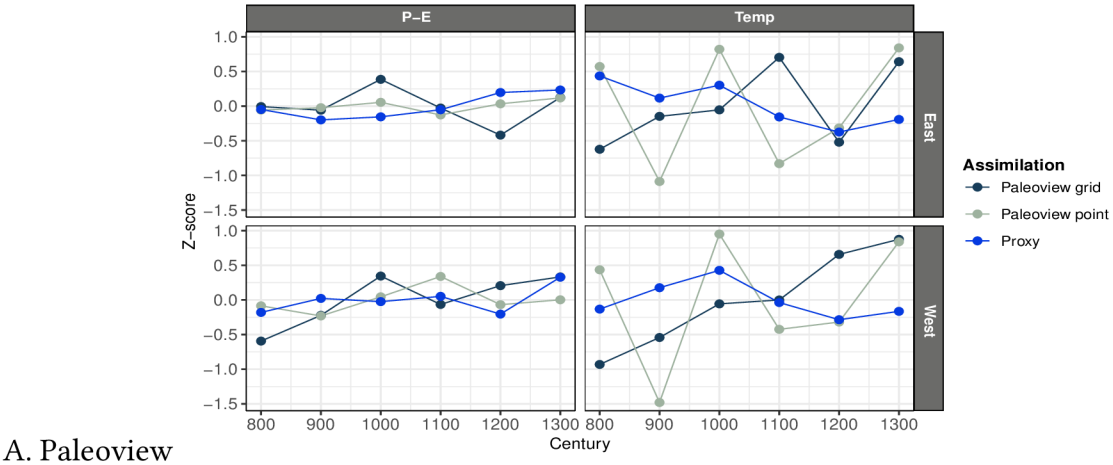

A. Paleoview

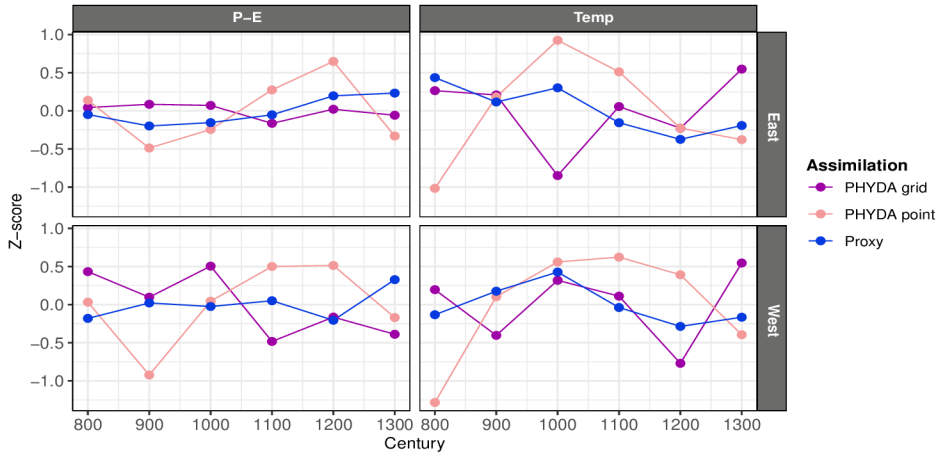

B. PHYDA

Figure 6.9: Evaluation of model (Paleoview (A), PHYDA (B)) and proxy estimated precipitation (Precip) and temperature (Temp) over North America. The model point represents the exact location of proxy data.

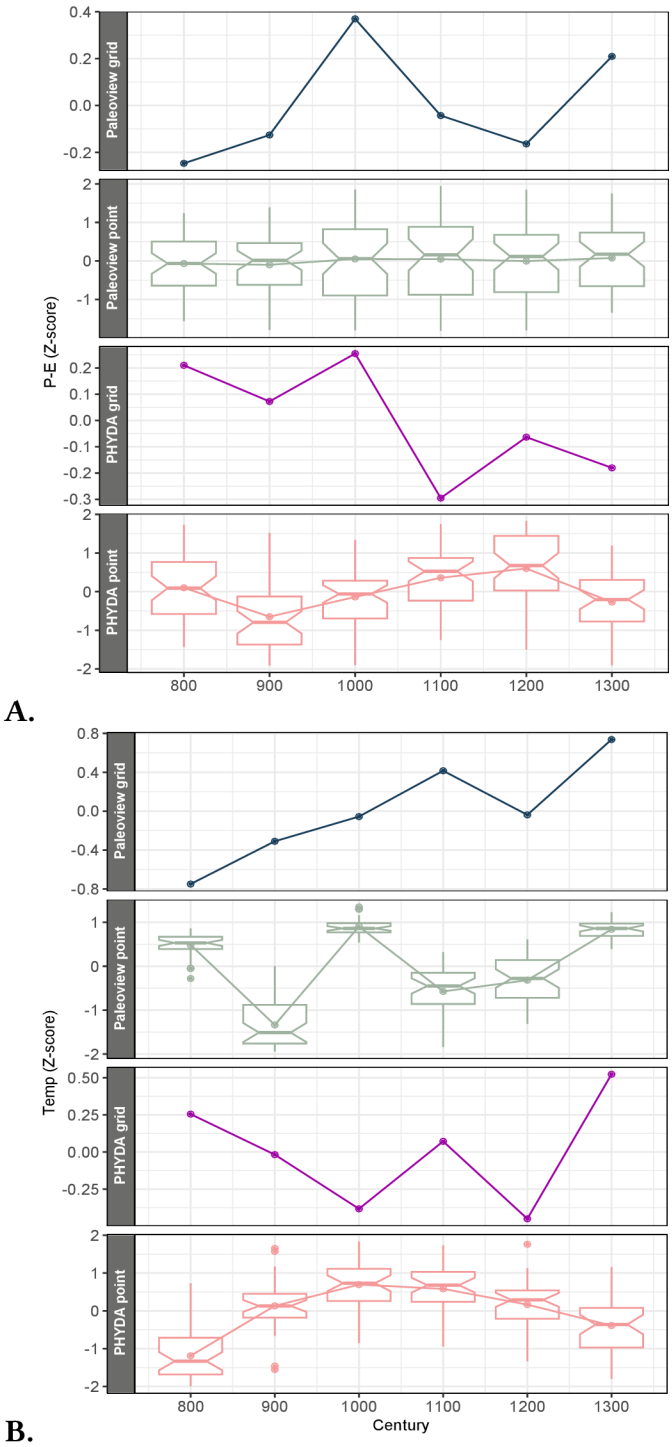

Figure 6.10: Evaluation of model (Paleoview (A), PHYDA (B)) and proxy estimated precipitation (Precip) and temperature (Temp) over North America. The model point represents the exact location of proxy data.

6.3.4 Potential factors contributing hydroclimate variability over North America and Europe

The potential factors contributing to the transition from the MCA to the LIA and subsequent hydroclimate variability remain subjects of ongoing debate. An overview of our investigation indicates that this transition and related hydroclimate changes were likely triggered by centennial-scale variations in the state of the North Atlantic, particularly in relation to alterations in SST, AMOC, and ITCZ dynamics. While the assessment of AMOC variability remains enigmatic, certain records (e.g., δ^{13}C, cd/ca ratio) suggest a link between the warm climate and AMOC state, conflicting with insights from sortable silts data. Notably, during the warm phases of the MCA, we observed warm conditions coinciding with high SST, a strengthened AMOC (considering few records), and a northward shift in the ITCZ. Throughout this period, continental-scale hydroclimate displayed warm and wet conditions across both continents. However, after the peak warmth of the MCA (i.e., after 11^{th} century), the state of SST, AMOC, and ITCZ underwent divergent shifts–transitioning from high to low, strong to weak, and northward to southward, respectively. Concurrently, continental-scale hydroclimate patterns over North America and Europe also shifted. Notably, after 11^{th} century, temperatures shifted from warm to cold, and hydrological conditions transitioned from wet to dry. In the meantime, at a regional scale across both continents, temperature changes appeared associated with shifts in the North Atlantic state, while precipitation patterns remain uncertain. Regional precipitation distribution seems more linked to specific changes in the local climate system, particularly in response to thermodynamic shifts. However, further investigations are needed to confirm the precise response of hydrological conditions in a warm climate. In summary, our observations indicate that variations in SST, AMOC, and ITCZ exert a significant influence on hydroclimate distributions, as the variability in both appears to shift in parallel. These variations in the North Atlantic state impact ocean-atmospheric-land circulation patterns, thereby constraining the distribution of terrestrial moisture and heat, which contribute to shaping the hydroclimate.

6.4 Limitations and validity

As previously emphasized, the uncertainty in estimating the AMOC state might arise from the reactive response of proxies under varying local environments. Moreover, it's plausible that the signals might be too nuanced to be captured by the proxies used for AMOC tracking or that these proxies may lack the sensitivity required to record AMOC signals adequately. Consequently, further investigations are warranted to identify a more suitable proxy that exhibits greater sensitivity to changes in AMOC. Regarding hydroclimate estimation, our data sources comprised well-established records submitted by respective authors to PAGES, PANGEA, and the paleoclimate data portal of NOAA-National Centers for Environmental Information. However, it's important to note that these proxy climate signals may be subject to local physio-chemical uncertainties.

6.5 Discussion

This study investigates centennial-scale hydroclimate patterns across Europe and North America during the MCA, aiming to uncover potential connections between these patterns and the North Atlantic variability (in SST, AMOC, and the ITCZ) within a warm climate context. Through regional-scale multi-proxy investigations, we found that centennial-scale variability in AMOC, SST, and ITCZ dynamics played a pivotal role in shaping hydroclimate patterns across both continents and in the transitional shift from the MCA to the LIA. This transitional period witnessed a shift in hydroclimate across North America and Europe, transitioning from warm to cold and wet to dry climates, with persistent uncertainties in hydrological conditions. During the warm climate, hydroclimate changes and their link with the North Atlantic variability demonstrate a lead-lag relationship, notably prominent in temperature variations. Our interpretation of a lead-lag relationship is rooted in the alignment between a warm climate and a strengthened North Atlantic condition, which later transitioned to weaker states, potentially due to increased input of freshwater from Arctic melting and sea ice.

The persistent warm climate for over three centuries (from 9^{th} to 11^{th} centuries) likely played a significant role in shaping the climate dynamics of the Arctic regions [54]. Con-

sequently, the melting of ice sheets, glaciers, and sea ice resulted in a substantial influx of freshwater into the North Atlantic Ocean. Therefore, we hypothesize a potential linkage between MCA-LIA transition and hydroclimate fluctuations across North America and Europe, stemming from subsequent effects of Arctic freshwater transport to the North Atlantic Ocean [230]. The influx of low-density freshwater during warm climates impacted deep ocean convection by reducing density in the Labrador Sea, resulting in the cooling and freshening of the North Atlantic Current [454]. This process notably regulated the intensity of the AMOC, SST gradient, and ITCZ position in the North Atlantic. Resultant, cooling and freshening led to low SST and a weakened AMOC (not all AMOC tracers agree) during the MCA-LIA transition [544], likely limiting the transport of atmospheric heat and moisture from the tropics [500] by shifting ITCZ southwards. Specifically, the weakened AMOC in the North Atlantic region constrained the northward movement of warm tropical water, influencing the SST gradient [64]. Consequently, the increased SST gradient over the North Atlantic might have contributed to the southward shift of the ITCZ [188].

The southward displacement of the ITCZ, which is influenced by SST and AMOC-controlled variations, is strongly linked to asymmetrical hemispheric atmospheric heat differences [471]. As a result, the southward movement of the ITCZ leads to cold and arid conditions in the Northern Hemisphere, while the Southern Hemisphere experiences warming [92, 367]. This is because the ITCZ significantly influences the Hadley cell, and alterations in the ITCZ position have a direct impact on the Hadley cell, thereby affecting the distribution of precipitation across the mid-latitudes [260, 576]. These oceanic influences likely reshaped atmospheric circulation and dynamics over the North Atlantic region, expanding cold climate regions and constraining moisture flux across North America and Europe [178].

The variations in the AMOC and SST intensity within the North Atlantic are recognized to exert an influence on the European climate system [142, 255]. Previous studies have suggested that a weakened AMOC may result in a surface air temperature decline of 1 to $3°C$ over the North Atlantic region [555]. Most likely, the cooling of the North Atlantic Ocean led to decreased moisture flux towards western Europe, resulting in low precipitation or drought-like conditions. Particularly, decreased temperatures and reduced

availability of atmospheric water from the ocean source contributed to a cold climate and a spatially diverse pattern of precipitation (P-E) across Europe, characterized by both wet and arid conditions [316]. Consequently, these atmospheric changes are likely to have impacted the hydroclimate system across western and northwestern Europe and eastern North America during the MCA (sections 6.3.1 and 6.3.2). On the other hand, the abrupt cold climate that occurred after the 13^{th} century, known as the LIA, may have been a response to the prolonged weakening of the AMOC, low SST, and southward ITCZ on a centennial to multi-centennial scale. Supporting this hypothesis, evidence from deep-ocean sediments also suggests that abrupt climate changes during the last ice age and the deglaciation period were linked to alterations in the AMOC [329].

The increased temperatures in Arctic regions [342] may have contributed to the supply of atmospheric moisture, fostering a wet climate in northwest Europe, particularly during the 11^{th} and 13^{th} centuries. However, in certain locations, humid conditions could be a regional hydrological response to a warm local climate. Our observations suggest that the spatial distribution of temperature and precipitation was significantly influenced by the strength of the AMOC, low SST, and a southward shift of the ITCZ. Nonetheless, in certain instances, regional-scale precipitation variability appeared more sensitive and interconnected with regional atmospheric perturbations, such as local warming. Not only over Europe, hydroclimate variability in the North American region also responded to centennial-scale fluctuations in low SST Cook et al. [124] and weakened AMOC [324]. Most likely, this southward shift in the ITCZ potentially caused drought conditions in North America, especially in the tropical regions.

In periods characterized by warmer climates, we observed notable strength in both the AMOC and SST. As discussed earlier, the AMOC (considering δ^{13}C and cd/ca ratio) and SST were in a strengthening phase from the 9^{th} century until the mid to mid-10^{th} century (Figure 6.1 and 6.2). These strong AMOC and high SST conditions are observed to be linked with a positive phase of the North Atlantic Oscillation (NAO) and intensified westerlies [152, 244, 267]. This condition potentially led to the redistribution of atmospheric heat across both continents, resulting in warm conditions. In contrast, the weakened AMOC and low SST, which inhibited northward meridional heat flow, further contributed to a weakened

NAO and westerlies [301]. Furthermore, the westerlies would have played a significant role in European hydroclimate variability. The weak (strong) strength of the AMOC and low (high) SST influenced the transport of cold (warm) air by weaker (stronger) westerlies to western and southern European regions, thereby causing cold (warm) and arid (humid) climates [545], respectively.

Consequently, the warm conditions observed over North America during the MCA may be linked to intensified heat transport facilitated by the strengthened westerlies. Furthermore, during the 9^{th} to 10^{th} centuries, the high SST and strong AMOC may have contributed to a positive feedback mechanism. This condition likely led to arid or drought-like conditions in western and southern North America [475], while the northwestern regions experienced increased humidity. However, by the late 10^{th} century, the SST and AMOC began shifting towards weaker phases, resulting in North Atlantic cooling and reduced atmospheric moisture supply to eastern and other parts of North America. This, in turn, led to reduced precipitation and drought-like conditions in these regions. Interestingly, our MCA observations revealed spatially distinct precipitation patterns. Coastal areas experienced increased precipitation when temperatures aligned with their centennial-scale averages, while temperatures exceeding this average were associated with arid climates. In contrast, inland regions, further away from the ocean, experienced higher precipitation when temperatures exceeded their centennial-scale average. This heterogeneous distribution suggests that precipitation is primarily influenced by atmospheric water availability. Therefore, temperatures at or near the centennial-scale average are sufficient to generate humid climates over oceanic territories, while higher regional temperatures are required to supply atmospheric water over land-enclosed regions. Our findings in eastern North America demonstrated that temperatures below the centennial average were associated with arid conditions, while increased temperatures were correlated with higher humidity. In western North America, we observed a proportional relationship between temperature and precipitation, with lower temperatures associated with limited precipitation and higher temperatures inducing humidity. These results emphasize the significant influence of temperature variations on precipitation responses across diverse geographical locations.

6.6 Conclusions

We anticipate that given North Atlantic variations, weak AMOC, low SST, and southwards ITCZ shift may have acted as the possible factors in changing the hydroclimate both at a continental and regional scale across both continents. In this study, we have elucidated the impact of a warm climate on the dynamics of hydroclimate patterns, specifically temperature and precipitation, and the variability in the state of the North Atlantic. Our primary focus has been to understand how these hydroclimate patterns in Europe and North America are related to the variability in AMOC, SST, and ITCZ. We employed well-established proxies to assess the state of AMOC, SST, and ITCZ. While we did observe subtle AMOC responses in a few AMOC tracers, these signals were not sufficiently robust to draw conclusive inferences, and overall, an investigation of AMOC remained uncertain. This uncertainty may arise from limitations in the selected proxies ability to capture AMOC signals or the possibility that AMOC signals during that era were too feeble to register with these proxies. However, based on these subtle AMOC signals in few records, our analysis suggests a weakening trend in AMOC after the 10^{th} century, which persisted for approximately three centuries from the 10^{th} to the 14^{th} centuries. Concurrently, our examination of proxies sensitive to SST indicates lower SST conditions during the same period. Given the uncertainty associated with AMOC tracers, this decrease in SST might be indicative of a weakened AMOC or could have contributed to the AMOC weakening [28]. Moreover, we also investigated the ITCZ and observed a southward shift. This southward ITCZ shift was likely influenced by the weakened AMOC. In combination, the simultaneous occurrence of low SST and a southward shift in the ITCZ strongly suggests that the AMOC was likely in a weakened phase during the MCA. The regions most significantly affected by the weakened AMOC were western and southern Europe, as well as eastern North America.

Regarding the hydroclimate response, our observations indicate that at the onset of the MCA period, the climate was warmer [325]. It is plausible that the warm climate during the MCA played a pivotal role in inducing North Atlantic variations. Consequently, due to the weakened AMOC, lower SST, and a southward shift in the ITCZ, the redistribution of atmospheric heat and moisture toward the continents became constrained. This led to cold and arid hydroclimate conditions in Europe and North America, particularly after the

11^{th} century. This transition may have played a significant role in initiating the LIA [545, 566]. When considering the interplay between temperature and precipitation, it is crucial to acknowledge the complexity and spatial variability of their relationship. Our study provides a comprehensive overview, revealing that during the MCA, elevated temperatures exceeding the centennial scale average were generally associated with arid climates. Conversely, slightly warmer conditions than the centennial average tended to coincide with more frequent occurrences of humid conditions. Additionally, our investigation observed that increased precipitation under low temperatures was sporadic, possibly indicating regional climate heterogeneity.

Overall, our findings underscore the significant modulation of hydroclimate variability during the MCA by North Atlantic variability in the AMOC, SST, and shifts in the ITCZ. This North Atlantic modulation influenced the redistribution of atmospheric heat and water vapor, thereby shaping the hydroclimate across the Northern Hemisphere. Based on the evidence from the MCA, it is plausible to consider that ongoing climate warming may contribute to the future weakening of the AMOC and, subsequently, to low SSTs and a southward shift in ITCZ. Indeed, current instrumental data indicate a reduced overturning state in the AMOC [493, 620], and a weakened phase of the AMOC has been observed prior to cold events [330]. However, the intricate relationship between hydroclimate variability, its latitudinal heterogeneity, and oceanic circulation, particularly under warmer climate conditions, remains enigmatic and warrants further in-depth investigation.

Chapter 7

Conclusions

7.1 Summary of thesis

The thesis primarily focuses on examining how changes in temperature and the state of the Ocean impact precipitation distribution at regional and continental scales. To achieve this, the first objective, which is the literature review (Chapter 3), identified research gaps by extensively examining literature covering both distant and recent past hydroclimate investigations. This step revealed that existing literature does not provide a clear consensus on (1) whether a warmer climate will result in dry or wet conditions [246]. Furthermore, the role of ocean circulation in warmer climates and its influence on hydroclimate patterns globally are subjects under investigation. (2) While some perspectives suggest that a warmer climate would cause weakening in the AMOC and limit hydroclimate patterns [28, 307], others oppose this view [191, 154].

Addressing (1) research gap reveals that the hypothesis that a warmer climate implies a wetter climate might be an oversimplification, as the response of the water cycle exhibits spatiotemporal heterogeneity (Chapter 5). Further detailed investigation (Chapter 6) underscores the substantial impact of temperature and the ocean's state on modifying the spatial extent, duration, and timing of hydrological conditions [168, 478]. At the continental scale, the findings indicate that temperature levels equivalent to or near centennial means are predominantly associated with humid climates. Conversely, deviations beyond this threshold often align with drier conditions. Furthermore, this thesis observed that hydroclimate changes at the regional scale seem to be heavily influenced by the availability of water resources and local climate dynamics.

Moreover, the analysis of the other (2) research gap highlights the North Atlantic Ocean's pivotal role in hydroclimate dynamics, notably in shaping terrestrial hydroclimate variability across continents (Chapter 6). Certainly, as a consequence of warmer climates, lower SST and a weakened AMOC coincide with a southward shift in the ITCZ. These conditions collectively restrict the distribution of atmospheric heat and moisture toward continents, resulting in decreased precipitation or drought-like conditions. Based on the evidence examined from the warmer climate, it is anticipated that ongoing climate warming may contribute to the future weakening of the AMOC. However, further research is essential to

deepen our understanding of the underlying mechanisms linking changes in the North Atlantic state to hydroclimate variability worldwide.

7.2 Key research findings

Due to its uncertain behavior, understanding the relationship between hydrological variability and temperature change across different temporal and spatial scales is crucial for developing effective long-term socio-economic management strategies. Therefore, the thesis addresses specific research questions and major key outcomes concerning the relationship between temperature, precipitation, and ocean state as follows:

1. Does a warmer climate contribute to intensifying the global hydrologic cycle?

While exploring this question, this study found that an increase in temperature does not consistently correlate with intensified precipitation patterns. Spatiotemporal analysis revealed that certain regions may experience drier climates despite similar temperature increases. However, in the examination of the hydrological cycle under both warm and cold climates, this study observed a general intensification of the hydrological cycle in warmer climates, with a corresponding weakening during colder climates, on a global scale.

In another objective specifically focused on regional hydroclimate in warm climates (i.e., MCA), it was found that at a larger spatial scale (e.g., continental), the hydrological conditions appear to be more correlated with the thermodynamic response. However, at the regional scale, hydrological variations and its spatial heterogeneity seem to be more closely associated with changes in regional climate dynamics and water resources.

2. Is the state of ocean circulation affected by a warmer climate?

Exploring this question (Chapter 6) suggests that during warmer climatic conditions, there was an adverse impact on the state of ocean circulation. The warming climate led to the melting of Arctic glaciers and sea ice, resulting in noticeable changes in the North Atlantic SST (low) and the ITCZ (southward shift). However, the subtle response of the AMOC leaves uncertainty regarding whether a warm climate can weaken its state.

3. Can a warm climate cause the weakening of the Atlantic Meridional Over-

turning Circulation (AMOC)?

It remains uncertain, as this study discovered very subtle signals of AMOC weakening, and not all paleo-oceanic records concurred on this matter. Various samples indicated differing responses over time; some records (e.g., cd/ca ratios) suggested a weak AMOC in warm climates, while others (e.g., δ^{13}C and sortable silt) depicted the opposite trend. It is possible that either the AMOC did not respond or responded very slowly to a warm climate, which might not be strong enough to be recorded in ocean proxies. Alternatively, the proxies used to trace AMOC signals may not be sensitive enough to capture the variations in AMOC strength.

4. How is the change in hydroclimate (mainly precipitation and temperature) linked with the change in the ocean's state?

This study reveals that variability in the North Atlantic Ocean, particularly in SST, AMOC, and ITCZ, leads to shifts in temperature and precipitation patterns across much of North America and Europe. When SST is low and AMOC is weak (as indicated by cd/ca ratios), resulting in a southward shift of the ITCZ, regions in Western and Northwestern Europe experience reduced precipitation or drought-like conditions. Similarly, Eastern regions of North America also experience decreased precipitation under these conditions. The low SST, weak AMOC, and southward-shifting ITCZ collectively restrict the distribution of atmospheric moisture from the ocean toward terrestrial regions, leading to decreased precipitation. Additionally, these conditions contribute to a transition from warmer to colder climatic conditions over the continents by impeding atmospheric heat flow.

5. Does changes in ocean circulation state affect shifts in hydroclimatic regimes?

This thesis's findings provide new insights into the relationship between ocean circulation state change and shifts in the hydroclimatic regimes. During the MCA-LIA transition, clear signals of changes in ocean circulation patterns can be observed, impacting temperature distribution across Europe and North America. As the climate shifted from warmer to colder conditions, temperatures decreased across most regions, with colder climates prevailing from High-latitudes towards Mid and Low-latitude regions.

In terms of hydrological conditions, the responses were complex and heterogeneous.

Many regions in Europe and North America experienced and shifted to arid or low precipitation conditions during this transition period. However, there were some regions with a humid climate, which could be attributed to the availability of regional water resources and the influence of warm regional climates.

7.3 Limitations

Limited proxies are available to track the signals of the AMOC. It is possible that the proxies selected in this study, although well-established, exhibit uncertainty in estimating the state of AMOC, possibly due to their reactive response to varying local environments. Therefore, further studies are needed to confirm the reliability of existing proxies in capturing AMOC variability. Additionally, identifying more suitable proxies with greater sensitivity to changes in AMOC is necessary to improve our understanding of its dynamics.

For the estimation of the hydroclimate, this study relied on the hydroclimate information provided by the original investigators. Specifically, if the investigators identified a proxy for representing temperature or precipitation, this study utilized the same information without altering or modifying it. However, it is plausible that variations in methodologies and proxies employed by different researchers may limit the suitability of regional proxies for capturing changes at broader scales, such as continental or global scales. For broader insights into climate dynamics, it is essential to utilize hydroclimate signals derived from consistent types of proxies and employ uniform methodologies across all proxies for signal interpretation.

Undoubtedly, proxy data play a crucial role in interpreting past climates, yet they also possess inherent biases and limitations. These limitations can impact the accuracy of the relationship between the proxy response and the climate variable being studied. For example, proxies like tree rings and lake records may be influenced by factors such as temperature, precipitation, or human interference, making it challenging to discern the true climate signature. Additionally, proxy data may suffer from limitations in spatiotemporal resolution. Regional proxies like tree rings may only provide climate information for specific locations and might not capture climate variations occurring over short timescales. Therefore, care-

ful selection of proxies based on research objectives is essential for obtaining accurate and reliable climate information.

7.4 Future research

The above-mentioned limitations pave the way for future research. This study has demonstrated that the temporal occurrence of hydroclimate events varies depending on the types of proxies used, as different proxies exhibit limited sensitivity and temporal expressions. Consequently, estimating terrestrial hydroclimate variability at regional and local scales remains uncertain. The uncertainties present at the regional level play a crucial role in comprehending not only the typical climate conditions but also the frequency and intensity of extreme events. Accordingly, obtaining insights into these regional-scale processes and their interaction with global climate forcings is essential for improving our predictive abilities concerning future climate alterations and their impacts on society and ecosystems.

The new research focusing on investigating interannual variability of hydroclimate in regions exhibiting spatially coherent responses will help in understanding the local hydroclimate and processes that introduce feedback mechanisms that can either amplify or inhibit global responses. Given the limited availability of instrumental data and the ongoing global debate regarding the accuracy of climate models, observation-based analyses using proxy records continue to be the primary method for investigating long-term climate variability. However, a significant challenge with proxy records is the potential presence of physio-chemical responses that may be misinterpreted as climate signals, leading to inaccurate assessments of climate variability.

Therefore, there is a pressing need for improved methodologies and measurement techniques to produce more precise proxy responses, particularly from those offering high-resolution data across various temporal and geographical scales. This may involve creating new proxy records and enhancing the quality and reliability of existing ones to advance our understanding of past climate dynamics and their implications for the future. Specifically, future directions in paleoclimate research could involve the integration of proxy records with climate models. By combining information from proxy records with climate models,

researchers can enhance the accuracy of climate model simulations. This integration will facilitate the validation and refinement of these simulations, enabling more precise interpretation and reconstruction of past, present, and projected climate conditions.

The behavior of the hydrological cycle in warmer climates remains uncertain. Therefore, focusing on past warmer climates, investigating the regional/ local mechanisms driving hydroclimate variability, including natural climate forcings such as volcanic eruptions, solar variability, and orbital variations, oceanic forcings, as well as anthropogenic forcings such as greenhouse gas emissions and land use changes, could be instrumental in identifying and understanding hydroclimate change more precisely. Examining climate sensitivity to various forcings (land-ocean-atmosphere) and feedback mechanisms through integrating proxy data and climate models may offer a promising avenue for quantifying the magnitude and timing of hydroclimate changes in warmer climates. Furthermore, utilizing this information can enhance climate projections for future change, providing valuable insights for developing mitigation and adaptation strategies.

Overall, future research in paleoclimate should prioritize improving proxy response interpretation, enhancing our understanding of past climate dynamics by integrating land-ocean-atmosphere forcings and assessing their relevance to current and future hydroclimate change. By addressing these research priorities, paleo-climatologists can provide valuable insights to the broader scientific community and contribute to efforts aimed at mitigating and adapting to climate change.

7.5 Concluding remarks

The findings of this study offer valuable insights into how hydrological cycles respond to temperature changes, particularly in warmer climates. Long-term paleohydroclimate analyses, spanning centuries to millennia, provide a unique opportunity for the scientific community to assess the pace and nature of hydroclimatic changes resulting from moderate to rapid warming. Importantly, these long-scale data timescales are often overlooked in modern climate model simulations. Consequently, our study outcomes serve as a representation of the spatiotemporal response of regional hydroclimate to warming conditions. Moreover,

our findings contribute to a deeper understanding of hydroclimate variability, serving as a benchmark for future climate change studies and providing essential insights into how hydroclimate reacts to warmer climates.

The MCA-LIA transition remains relatively unexplored by researchers. Our study's findings regarding this transition provide valuable insights into how a warmer climate may precipitate climate shifts and elucidate the potential hydroclimatic consequences. Furthermore, our insights into the state of ocean circulation and its correlation with hydroclimate offer a foundational framework for further investigations, enabling researchers to delve into the influence of oceanic variability on regional hydroclimate change. Given the ongoing inquiry into AMOC weakening in response to warming, our findings provide valuable guidance for the scientific community in identifying suitable proxies to accurately estimate AMOC responses. Additionally, as climate model outputs on precipitation analysis continue to provoke debate due to occasional over- or underestimations, the outcomes of this thesis serve as a crucial validation tool for refining climate models and enhancing the accuracy of climate predictions.

The implications of our thesis and proposed future research outcomes extend beyond the scientific community to benefit society and humanity in various ways. Our findings underscore the significant impacts of warmer climates on altering ocean states, leading to shifts in climate from warm to cold and changes in regional hydroclimate regimes, including reduced terrestrial precipitation. By considering these outcomes in the context of future warmer climate scenarios and identifying regions vulnerable to hydroclimate change, policymakers and government entities can formulate strategies for improved water resource management, agriculture planning, infrastructure development, and disaster preparedness. Additionally, these efforts can contribute to the preservation of ecosystems, biodiversity, and natural resources.

Disseminating our research findings through outreach programs and educational initiatives will enhance public awareness of past climate dynamics and the importance of understanding climate change for effective adaptation. By fostering a more informed and engaged society, we can collectively address key challenges related to hydroclimate variability and climate change adaptation. Overall, both our current and proposed research outcomes have

the potential to make significant contributions to both the scientific community and societal well-being by addressing key challenges related to hydroclimate variability and climate change adaptation.

Appendix A

Publication on Chapter 2

Article related with the literature research has been published as Shailendra Pratap & Yannis Markonis 2022, with the title '***The response of the hydrological cycle to temperature changes in recent and distant climatic history***'. *Progress in Earth and Planetary Science*, volume 9, Article number: 30 (2022), https://rdcu.be/dj1bE.

Pratap and Markonis
Progress in Earth and Planetary Science (2022) 9:30
https://doi.org/10.1186/s40645-022-00489-0

Progress in Earth and Planetary Science

REVIEW Open Access

The response of the hydrological cycle to temperature changes in recent and distant climatic history

Shailendra Pratap* and Yannis Markonis

Abstract

The relationship between the hydrological cycle and the temperature is rather complex and of great importance to human socioeconomic activities. The prevailing theory suggests that as temperature increases the hydrological cycle is intensified. Practically, this means more and heavier precipitation. However, the exact magnitude of hydrological cycle response and its spatio-temporal characteristics is still under investigation. Looking back in Earth's hydroclimatic history, it is easy to find some periods where global temperature was substantially different than present. Here, we examine some of these periods to present the current knowledge about past hydrological cycle variability (specifically precipitation), and its relationship to temperature. The periods under investigation are the Mid-Miocene Climate Optimum, the Eemian Interglacial Stage, the Last Glacial Maximum, the Heinrich and Dansgaard–Oeschger Events, the Bølling–Allerød, the Younger Dryas, the 8.2 ka event, the Medieval Climate Anomaly, and the Little Ice Age. We report that the hypothesis that a warmer climate is a wetter climate could be an oversimplification, because the response of water cycle appears to be spatio-temporally heterogeneous.

Keywords: Global water cycle, Paleoclimate, Hydrological cycle, Water cycle intensification, Hydroclimatic variability

1 Introduction

Looking back in Earth's hydroclimatic history, there have been substantial shifts in the hydrological cycle (Ljungqvist et al. 2016). In the past few million years, many rapid climate transitions have occurred, with time scales ranging from decades to centuries (Corrick et al. 2020). For example, during Holocene, i.e. the last 18–20 thousand years (ka) before present (BP), the paleoclimatic records show considerable fluctuations in both the seasonal and spatial distribution of precipitation (Badgeley et al. 2020). During the late glacial (18–16.5 ka), sea surface temperature (SST) was about 5–10 °C colder than the recent Holocene (11.5–9 ka) over both the North Pacific and the North Atlantic (Praetorius et al. 2020). For the same period, the global averaged precipitation was about 10–14% lower than today, with the maximum reduction over the Northern Hemisphere (NH) due to reduced convective activity (Gates 1976; Kwiecien et al. 2009; Sun et al. 2019). As the Last Glacial ended and the climate became warmer, there was a shift to wetter conditions as well. From 13 to 12 ka BP, the monsoon circulation was intensified, resulting to an increase in precipitation by about 200–300 mm at lower latitudes (Knox and Wright 1983; Maher 2008; Pausata et al. 2020). Stronger monsoons were also observed between 8 to 3 ka BP, coupling the widespread warming (Chawchai et al. 2021). The most affected region was East Asia (Rao et al. 2016), where precipitation was over 30% higher than today from 7.8 to 5.3 ka BP (Yang et al. 2016). All these changes occurred in various spatiotemporal scales, and therefore, it is still challenging to estimate the hydrological cycle variability and quantify it on global, continental, and regional scales.

*Correspondence: pratap@fzp.czu.cz

Faculty of Environmental Sciences, Czech University of Life Sciences Prague, Kamýcká 129, Praha – Suchdol 165 00, Czech Republic

Bibliography

[1] Henry DI Abarbanel and Upmanu Lall. "Nonlinear dynamics of the Great Salt Lake: system identification and prediction". In: *Climate Dynamics* 12.4 (1996), pp. 287–297.

[2] Mark B Abbott et al. "Holocene paleohydrology of the tropical Andes from lake records". In: *Quaternary research* 47.1 (1997), pp. 70–80.

[3] ML Absy et al. "Mise en évidence de quatre phases d'ouverture de la forêt dense dans le Sud-Est de l'Amazonie au cours des 60 000 dernières années: première comparaison avec d'autres régions tropicales". In: *Comptes Rendus de l'Académie des Sciences. Série 2: Mécanique...* 312.6 (1991), pp. 673–678.

[4] Jonathan Adams, Mark Maslin, and Ellen Thomas. "Sudden climate transitions during the Quaternary". In: *Progress in Physical Geography* 23.1 (1999), pp. 1–36.

[5] Rajesh Agnihotri et al. "Evidence for solar forcing on the Indian monsoon during the last millennium". In: *Earth and Planetary Science Letters* 198.3-4 (2002), pp. 521–527.

[6] Wilton Aguiar et al. "Magnitude of the 8.2 ka event freshwater forcing based on stable isotope modelling and comparison to future Greenland melting". In: *Scientific reports* 11.1 (2021), pp. 1–10.

[7] Moinuddin Ahmed et al. "Continental-scale temperature variability during the past two millennia". In: *Nature geoscience* 6.5 (2013), pp. 339–346.

[8] Richard Allan et al. "Advances in understanding large-scale responses of the water cycle to climate change". In: *Annals of the New York Academy of Sciences* (2020).

[9] Richard P Allan et al. "Physically consistent responses of the global atmospheric hydrological cycle in models and observations". In: *Surveys in Geophysics* 35.3 (2014), pp. 533–552.

[10] Judy RM Allen et al. "Holocene climate variability in northernmost Europe". In: *Quaternary Science Reviews* 26.9-10 (2007), pp. 1432–1453.

[11] Judy RM Allen et al. "Rapid environmental changes in southern Europe during the last glacial period". In: *Nature* 400.6746 (1999), pp. 740–743.

[12] Mark B Allen and Howard A Armstrong. "Reconciling the Intertropical Convergence Zone, Himalayan/Tibetan tectonics, and the onset of the Asian monsoon system". In: *Journal of Asian Earth Sciences* 44 (2012), pp. 36–47.

[13] Myles R Allen and William J Ingram. "Constraints on future changes in climate and the hydrologic cycle". In: *Nature* 419.6903 (2002), pp. 228–232.

[14] Richard B Alley and Anna Maria Ágústsdóttir. "The 8k event: cause and consequences of a major Holocene abrupt climate change". In: *Quaternary Science Reviews* 24.10-11 (2005), pp. 1123–1149.

[15] Richard B Alley and Peter U Clark. "The deglaciation of the northern hemisphere: a global perspective". In: *Annual Review of Earth and Planetary Sciences* 27.1 (1999), pp. 149–182.

[16] Richard B Alley et al. "Abrupt climate change". In: *science* 299.5615 (2003), pp. 2005–2010.

[17] Richard B Alley et al. "Holocene climatic instability: A prominent, widespread event 8200 yr ago". In: *Geology* 25.6 (1997), pp. 483–486.

[18] Richard B Alley et al. "Ice-sheet and sea-level changes". In: *science* 310.5747 (2005), pp. 456–460.

[19] Mark A Altabet, Matthew J Higginson, and David W Murray. "The effect of millennial-scale changes in Arabian Sea denitrification on atmospheric CO 2". In: *Nature* 415.6868 (2002), pp. 159–162.

[20] Katrine K Andersen et al. "High-resolution record of the Northern Hemisphere climate extending into the last interglacial period". In: *Nature* 431 (2004), pp. 147–151.

[21] David M Anderson and Warren L Prell. "A 300 kyr record of upwelling off Oman during the late Quaternary: evidence of the Asian southwest monsoon". In: *Paleoceanography* 8.2 (1993), pp. 193–208.

[22] R Scott Anderson et al. "High-elevation paleoenvironmental change during MIS 6–4 in the central Rockies of Colorado as determined from pollen analysis". In: *Quaternary Research* 82.3 (2014), pp. 542–552.

[23] Timothy Andrews, Piers M Forster, and Jonathan M Gregory. "A surface energy perspective on climate change". In: *Journal of Climate* 22.10 (2009), pp. 2557–2570.

[24] JD Annan and Julia Catherine Hargreaves. "A new global reconstruction of temperature changes at the Last Glacial Maximum". In: *Climate of the Past* 9.1 (2013), pp. 367–376.

[25] Helge W Arz, Jürgen Pätzold, and Gerold Wefer. "Correlated millennial-scale changes in surface hydrography and terrigenous sediment yield inferred from last-glacial marine deposits off northeastern Brazil". In: *Quaternary Research* 50.2 (1998), pp. 157–166.

[26] Yemane Asmerom, Victor J Polyak, and Stephen J Burns. "Variable winter moisture in the southwestern United States linked to rapid glacial climate shifts". In: *Nature Geoscience* 3.2 (2010), pp. 114–117.

[27] Anne Aufgebauer et al. "Climate and environmental change in the Balkans over the last 17 ka recorded in sediments from Lake Prespa (Albania/FYR of Macedonia/-Greece)". In: *Quaternary International* 274 (2012), pp. 122–135.

[28] Mohamed Ayache et al. "Multi-centennial variability of the AMOC over the Holocene: A new reconstruction based on multiple proxy-derived SST records". In: *Global and Planetary Change* 170 (2018), pp. 172–189.

[29] Linda K Ayliffe et al. "500 ka precipitation record from southeastern Australia: evidence for interglacial relative aridity". In: *Geology* 26.2 (1998), pp. 147–150.

[30] Jessica A Badgeley et al. "Greenland temperature and precipitation over the last 20 000 years using data assimilation". In: *Climate of the Past* 16.4 (2020), pp. 1325–1346.

[31] Paul A Baker et al. "The history of South American tropical precipitation for the past 25,000 years". In: *science* 291.5504 (2001), pp. 640–643.

[32] Jostein Bakke et al. "Rapid oceanic and atmospheric changes during the Younger Dryas cold period". In: *Nature Geoscience* 2.3 (2009), pp. 202–205.

[33] Pepijn Bakker et al. "Fate of the Atlantic Meridional Overturning Circulation: Strong decline under continued warming and Greenland melting". In: *Geophysical Research Letters* 43.23 (2016), pp. 12–252.

[34] AP Ballantyne et al. "Meta-analysis of tropical surface temperatures during the Last Glacial Maximum". In: *Geophysical Research Letters* 32.5 (2005).

[35] M Bar-Matthews. "History of water in the Middle East and North Africa". In: *Reference Module in Earth Systems and Environmental Sciences, Treatise on Geochemistry (Second Edition)* (2014), pp. 109–128.

[36] M Bar-Matthews, J Keinan, and A Ayalon. "Hydro-climate research of the late Quaternary of the Eastern Mediterranean-Levant region based on speleothems research–A review". In: *Quaternary Science Reviews* 221 (2019), p. 105872.

[37] Miryam Bar-Matthews, Avner Ayalon, and Aaron Kaufman. "Timing and hydrological conditions of Sapropel events in the Eastern Mediterranean, as evident from speleothems, Soreq cave, Israel". In: *Chemical Geology* 169.1-2 (2000), pp. 145–156.

[38] Miryam Bar-Matthews et al. “The Eastern Mediterranean paleoclimate as a reflection of regional events: Soreq cave, Israel”. In: *Earth and Planetary Science Letters* 166.1-2 (1999), pp. 85–95.

[39] Donald C Barber et al. “Forcing of the cold event of 8,200 years ago by catastrophic drainage of Laurentide lakes”. In: *Nature* 400.6742 (1999), pp. 344–348.

[40] Philip Barker and Françoise Gasse. “New evidence for a reduced water balance in East Africa during the Last Glacial Maximum: implication for model-data comparison”. In: *Quaternary Science Reviews* 22.8-9 (2003), pp. 823–837.

[41] Stephen Barker et al. “Planktonic foraminiferal Mg/Ca as a proxy for past oceanic temperatures: a methodological overview and data compilation for the Last Glacial Maximum”. In: *Quaternary Science Reviews* 24.7-9 (2005), pp. 821–834.

[42] J Warren Beck et al. “Abrupt changes in early Holocene tropical sea surface temperature derived from coral records”. In: *Nature* 385.6618 (1997), pp. 705–707.

[43] J Warren Beck et al. “Extremely large variations of atmospheric 14C concentration during the last glacial period”. In: *Science* 292.5526 (2001), pp. 2453–2458.

[44] Patrick Becker et al. “Last Glacial Maximum precipitation pattern in the Alps inferred from glacier modelling”. In: *Geographica Helvetica* 71.3 (2016), pp. 173–187.

[45] David B Bell et al. “Local and regional trends in Plio-Pleistocene δ18O records from benthic foraminifera”. In: *Geochemistry, Geophysics, Geosystems* 15.8 (2014), pp. 3304–3321.

[46] Hugo Bellenger et al. “ENSO representation in climate models: From CMIP3 to CMIP5”. In: *Climate Dynamics* 42.7-8 (2014), pp. 1999–2018.

[47] Katinka Bellomo et al. “Future climate change shaped by inter-model differences in Atlantic meridional overturning circulation response”. In: *Nature Communications* 12.1 (2021), pp. 1–10.

[48] James Bendle and Antoni Rosell-Melé. “Distributions of UK37 and UK37 in the surface waters and sediments of the Nordic Seas: Implications for paleoceanography”. In: *Geochemistry, Geophysics, Geosystems* 5.11 (2004).

[49] Larry V Benson et al. “Climatic and hydrologic oscillations in the Owens Lake Basin and adjacent Sierra Nevada, California”. In: *Science* 274.5288 (1996), pp. 746–749.

[50] Larry V Benson et al. “Correlation of late-Pleistocene lake-level oscillations in Mono Lake, California, with North Atlantic climate events”. In: *Quaternary Research* 49.1 (1998), pp. 1–10.

[51] AndréL Berger. “Long-term variations of daily insolation and Quaternary climatic changes”. In: *Journal of the atmospheric sciences* 35.12 (1978), pp. 2362–2367.

[52] NAN Bertler, PA Mayewski, and L Carter. “Cold conditions in Antarctica during the Little Ice Age—Implications for abrupt climate change mechanisms”. In: *Earth and Planetary Science Letters* 308.1-2 (2011), pp. 41–51.

[53] Nancy H Bigelow et al. “Climate change and Arctic ecosystems: 1. Vegetation changes north of 55° N between the last glacial maximum, mid-Holocene, and present”. In: *Journal of Geophysical Research: Atmospheres* 108.D19 (2003).

[54] Nathaniel L Bindoff et al. “Detection and attribution of climate change: from global to regional”. In: (2013).

[55] Broxton W Bird et al. “A 2,300-year-long annually resolved record of the South American summer monsoon from the Peruvian Andes”. In: *Proceedings of the National Academy of Sciences* 108.21 (2011), pp. 8583–8588.

[56] Paul Blanchon et al. “Rapid sea-level rise and reef back-stepping at the close of the last interglacial highstand”. In: *Nature* 458.7240 (2009), pp. 881–884.

[57] Günter Blöschl et al. “Current European flood-rich period exceptional compared with past 500 years”. In: *Nature* 583.7817 (2020), pp. 560–566.

[58] Ocean Studies Board, National Research Council, et al. *Abrupt Climate Change: Inevitable Surprises*. National Academies Press, 2002.

[59] Niklas Boers. “Early-warning signals for Dansgaard-Oeschger events in a high-resolution ice core record”. In: *Nature communications* 9.1 (2018), pp. 1–8.

[60] Niklas Boers. “Observation-based early-warning signals for a collapse of the Atlantic Meridional Overturning Circulation”. In: *Nature Climate Change* 11.8 (2021), pp. 680–688.

[61] Madelaine Böhme, Angela A Bruch, and Alfred Selmeier. “The reconstruction of Early and Middle Miocene climate and vegetation in Southern Germany as determined from the fossil wood flora”. In: *Palaeogeography, Palaeoclimatology, Palaeoecology* 253.1-2 (2007), pp. 91–114.

[62] Gerard Bond et al. “A pervasive millennial-scale cycle in North Atlantic Holocene and glacial climates”. In: *science* 278.5341 (1997), pp. 1257–1266.

[63] Gerard Bond et al. “Evidence for massive discharges of icebergs into the North Atlantic ocean during the last glacial period”. In: *Nature* 360.6401 (1992), pp. 245–249.

[64] Gerard Bond et al. “Persistent solar influence on North Atlantic climate during the Holocene”. In: *science* 294.5549 (2001), pp. 2130–2136.

[65] Gerard C Bond et al. “The North Atlantic’s 1-2 kyr climate rhythm: relation to Heinrich events, Dansgaard/Oeschger cycles and the Little Ice Age”. In: *Geophysical Monograph-American Geophysical Union* 112 (1999), pp. 35–58.

[66] Claus W Böning et al. “Emerging impact of Greenland meltwater on deepwater formation in the North Atlantic Ocean”. In: *Nature Geoscience* 9.7 (2016), pp. 523–527.

[67] Amandine Bordon et al. “Pollen-inferred late-glacial and Holocene climate in southern Balkans (Lake Maliq)”. In: *Quaternary International* 200.1-2 (2009), pp. 19–30.

[68] Irena Borzenkova et al. “Climate change during the Holocene (past 12,000 years)”. In: *Second assessment of climate change for the Baltic Sea basin*. Springer, 2015, pp. 25–49.

[69] Johanna AA Bos, Sjoerd JP Bohncke, and C Roel Janssen. “Lake-level fluctuations and small-scale vegetation patterns during the late glacial in The Netherlands”. In: *Journal of Paleolimnology* 35.2 (2006), pp. 211–238.

[70] Michael G Bosilovich, Siegfried D Schubert, and Gregory K Walker. “Global changes of the water cycle intensity”. In: *Journal of Climate* 18.10 (2005), pp. 1591–1608.

[71] Chris A Boulton, Lesley C Allison, and Timothy M Lenton. “Early warning signals of Atlantic Meridional Overturning Circulation collapse in a fully coupled climate model”. In: *Nature communications* 5.1 (2014), pp. 1–9.

[72] Claude F Boutron. “Historical reconstruction of the earth’s past atmospheric environment from Greenland and Antarctic snow and ice cores”. In: *Environmental Reviews* 3.1 (1995), pp. 1–28.

[73] Pascale Braconnot et al. “Evaluation of climate models using palaeoclimatic data”. In: *Nature Climate Change* 2.6 (2012), pp. 417–424.

[74] Raymond S Bradley and Philip D Jonest. “’Little Ice Age’summer temperature variations: their nature and relevance to recent global warming trends”. In: *The Holocene* 3.4 (1993), pp. 367–376.

[75] Raymond S Bradley et al. “The climate of the last millennium”. In: *Paleoclimate, global change and the future*. Springer, 2003, pp. 105–141.

[76] RS Bradley and PD Jones. "Climate since AD 1500: introduction". In: *Climate since AD 1500*. Routledge London, 1992, pp. 1–16.

[77] Achim Brauer et al. "An abrupt wind shift in western Europe at the onset of the Younger Dryas cold period". In: *Nature Geoscience* 1.8 (2008), pp. 520–523.

[78] Achim Brauer et al. "Evidence for last interglacial chronology and environmental change from Southern Europe". In: *Proceedings of the National Academy of Sciences* 104.2 (2007), pp. 450–455.

[79] Rudolf Brázdil et al. "Fir tree-ring reconstruction of March-July precipitation in southern Moravia (Czech Republic), 1376-1996". In: *Climate Research* 20.3 (2002), pp. 223–239.

[80] Rudolf Brázdil et al. "Flood events of selected European rivers in the sixteenth century". In: *Climatic change* 43.1 (1999), pp. 239–285.

[81] DO Breecker and GJ Retallack. "Refining the pedogenic carbonate atmospheric CO2 proxy and application to Miocene CO2". In: *Palaeogeography, Palaeoclimatology, Palaeoecology* 406 (2014), pp. 1–8.

[82] S Brewer et al. "The climate in Europe during the Eemian: a multi-method approach using pollen data". In: *Quaternary Science Reviews* 27.25-26 (2008), pp. 2303–2315.

[83] AJ Broccoli and Syukuro Manabe. "The influence of continental ice, atmospheric CO 2, and land albedo on the climate of the last glacial maximum". In: *Climate dynamics* 1.2 (1987), pp. 87–99.

[84] Wallace S Broecker. "Was a change in thermohaline circulation responsible for the Little Ice Age?" In: *Proceedings of the National Academy of Sciences* 97.4 (2000), pp. 1339–1342.

[85] Wallace S Broecker, Dorothy M Peteet, and David Rind. "Does the ocean–atmosphere system have more than one stable mode of operation?" In: *Nature* 315.6014 (1985), pp. 21–26.

[86] Wallace S Broecker et al. "A salt oscillator in the glacial Atlantic? 1. The concept". In: *Paleoceanography* 5.4 (1990), pp. 469–477.

[87] Wallace S Broecker et al. "Routing of meltwater from the Laurentide Ice Sheet during the Younger Dryas cold episode". In: *Nature* 341.6240 (1989), pp. 318–321.

[88] Wallace S Broecker et al. "The chronology of the last deglaciation: Implications to the cause of the Younger Dryas event". In: *Paleoceanography* 3.1 (1988), pp. 1–19.

[89] Wallace Smith Broecker. "Abrupt climate change: causal constraints provided by the paleoclimate record". In: *Earth-Science Reviews* 51.1-4 (2000), pp. 137–154.

[90] Stefan Brönnimann et al. "Last phase of the Little Ice Age forced by volcanic eruptions". In: *Nature geoscience* 12.8 (2019), pp. 650–656.

[91] Edward J Brook, Todd Sowers, and Joe Orchardo. "Rapid variations in atmospheric methane concentration during the past 110,000 years". In: *Science* 273.5278 (1996), pp. 1087–1091.

[92] Victor Brovkin et al. "Past abrupt changes, tipping points and cascading impacts in the Earth system". In: *Nature Geoscience* (2021), pp. 1–9.

[93] Angela A Bruch, Dieter Uhl, and Volker Mosbrugger. *Miocene climate in Europe—patterns and evolution: a first synthesis of NECLIME*. 2007.

[94] Alexander Budsky et al. "Western Mediterranean Climate Response to Dansgaard/Oeschger Events: New Insights From Speleothem Records". In: *Geophysical Research Letters* 46.15 (2019), pp. 9042–9053.

[95] Natalie J Burls and Alexey V Fedorov. "Wetter subtropics in a warmer world: Contrasting past and future hydrological cycles". In: *Proceedings of the National Academy of Sciences* 114.49 (2017), pp. 12888–12893.

[96] Andrew BG Bush and S George H Philander. "The climate of the Last Glacial Maximum: Results from a coupled atmosphere-ocean general circulation model". In: *Journal of Geophysical Research: Atmospheres* 104.D20 (1999), pp. 24509–24525.

[97] Andrew BG Bush and S George H Philander. "The role of ocean-atmosphere interactions in tropical cooling during the last glacial maximum". In: *Science* 279.5355 (1998), pp. 1341–1344.

[98] Mark B Bush et al. "A 14 300-yr paleoecological profile of a lowland tropical lake in Panama". In: *Ecological Monographs* 62.2 (1992), pp. 251–275.

[99] M Byrne et al. "Birth of a biome: insights into the assembly and maintenance of the Australian arid zone biota". In: *Molecular Ecology* 17.20 (2008), p. 4398.

[100] Levke Caesar et al. "Observed fingerprint of a weakening Atlantic Ocean overturning circulation". In: *Nature* 556.7700 (2018), pp. 191–196.

[101] Anders E Carlson. "Paleoclimate| The younger Dryas climate event". In: *Reference Module in Earth Systems and Environmental Sciences, Encyclopedia of Quaternary Science (Second Edition)* (2013), pp. 126–134.

[102] Anders E Carlson et al. "Routing of western Canadian Plains runoff during the 8.2 ka cold event". In: *Geophysical Research Letters* 36.14 (2009).

[103] Carlos M Carrillo et al. "Megadrought: a series of unfortunate La Niña events?" In: *Journal of Geophysical Research: Atmospheres* 127.21 (2022), e2021JD036376.

[104] Moustafa T Chahine. "The hydrological cycle and its influence on climate". In: *Nature* 359.6394 (1992), pp. 373–380.

[105] Charles P Chamberlain et al. "The impact of Neogene grassland expansion and aridification on the isotopic composition of continental precipitation". In: *Global Biogeochemical Cycles* 28.9 (2014), pp. 992–1004.

[106] Intergovernmental Panel On Climate Change. *Climate change 2013: the physical science basis: Working Group I contribution to the Fifth assessment report of the Intergovernmental Panel on Climate Change*. Cambridge University Press, 2014.

[107] J Chappellaz et al. "Synchronous changes in atmospheric CH4 and Greenland climate between 40 and 8 kyr BP". In: *Nature* 366.6454 (1993), pp. 443–445.

[108] Sakonvan Chawchai et al. "Hydroclimate variability of central Indo-Pacific region during the Holocene". In: *Quaternary Science Reviews* 253 (2021), p. 106779.

[109] Deliang Chen et al. "Hydroclimate changes over Sweden in the twentieth and twenty-first centuries: a millennium perspective". In: *Geografiska Annaler: Series A, Physical Geography* 103.2 (2021), pp. 103–131.

[110] Gang Chen et al. "Thermodynamic and dynamic mechanisms for hydrological cycle intensification over the full probability distribution of precipitation events". In: *Journal of the Atmospheric Sciences* 76.2 (2019), pp. 497–516.

[111] Jianhui Chen et al. "Hydroclimatic changes in China and surroundings during the Medieval Climate Anomaly and Little Ice Age: spatial patterns and possible mechanisms". In: *Quaternary Science Reviews* 107 (2015), pp. 98–111.

[112] Hai Cheng et al. "The Asian monsoon over the past 640,000 years and ice age terminations". In: *nature* 534.7609 (2016), pp. 640–646.

[113] Bo Christiansen and Fredrik Charpentier Ljungqvist. "The extra-tropical Northern Hemisphere temperature in the last two millennia: reconstructions of low-frequency variability". In: *Climate of the Past* 8.2 (2012), pp. 765–786.

[114] Peter U Clark and Alan C Mix. "Ice sheets and sea level of the Last Glacial Maximum". In: *Quaternary Science Reviews* 21.1-3 (2002), pp. 1–7.

[115] Peter U Clark et al. "Global climate evolution during the last deglaciation". In: *Proceedings of the National Academy of Sciences* 109.19 (2012), E1134–E1142.

[116] Peter U Clark et al. "Rapid rise of sea level 19,000 years ago and its global implications". In: *Science* 304.5674 (2004), pp. 1141–1144.

[117] Peter U Clark et al. "The last glacial maximum". In: *science* 325.5941 (2009), pp. 710–714.

[118] Garry KC Clarke et al. "Paleohydraulics of the last outburst flood from glacial Lake Agassiz and the 8200BP cold event". In: *Quaternary Science Reviews* 23.3-4 (2004), pp. 389–407.

[119] Amy C Clement, Mark A Cane, and Richard Seager. "An orbitally driven tropical source for abrupt climate change". In: *Journal of Climate* 14.11 (2001), pp. 2369–2375.

[120] Peter D Clift, Shiming Wan, and Jerzy Blusztajn. "Reconstructing chemical weathering, physical erosion and monsoon intensity since 25 Ma in the northern South China Sea: a review of competing proxies". In: *Earth-Science Reviews* 130 (2014), pp. 86–102.

[121] C Colin et al. "Magnetic properties of sediments in the Bay of Bengal and the Andaman Sea: impact of rapid North Atlantic Ocean climatic events on the strength of the Indian monsoon". In: *Earth and Planetary Science Letters* 160.3-4 (1998), pp. 623–635.

[122] Matthew Collins et al. "El Niño-or La Niña-like climate change?" In: *Climate Dynamics* 24.1 (2005), pp. 89–104.

[123] William D Collins et al. "The community climate system model version 3 (CCSM3)". In: *Journal of Climate* 19.11 (2006), pp. 2122–2143.

[124] Benjamin I Cook et al. "Megadroughts in the Common Era and the Anthropocene". In: *Nature Reviews Earth & Environment* 3.11 (2022), pp. 741–757.

[125] Benjamin I Cook et al. "Pan-continental droughts in North America over the last millennium". In: *Journal of Climate* 27.1 (2014), pp. 383–397.

[126] Edward R Cook, David M Meko, and Charles W Stockton. "A new assessment of possible solar and lunar forcing of the bidecadal drought rhythm in the western United States". In: *Journal of Climate* 10.6 (1997), pp. 1343–1356.

[127] Edward R Cook et al. "Long-term aridity changes in the western United States". In: *Science* 306.5698 (2004), pp. 1015–1018.

[128] Edward R Cook et al. "Megadroughts in North America: Placing IPCC projections of hydroclimatic change in a long-term palaeoclimate context". In: *Journal of Quaternary Science* 25.1 (2010), pp. 48–61.

[129] Edward R Cook et al. "North American drought: Reconstructions, causes, and consequences". In: *Earth-Science Reviews* 81.1-2 (2007), pp. 93–134.

[130] Edward R Cook et al. "Old World megadroughts and pluvials during the Common Era". In: *Science advances* 1.10 (2015), e1500561.

[131] Ellen C Corrick et al. "Synchronous timing of abrupt climate changes during the last glacial period". In: *Science* 369.6506 (2020), pp. 963–969.

[132] Isabelle Couchoud et al. "Millennial-scale climate variability during the Last Interglacial recorded in a speleothem from south-western France". In: *Quaternary Science Reviews* 28.27-28 (2009), pp. 3263–3274.

[133] National Research Council et al. *Surface temperature reconstructions for the last 2,000 years*. National Academies Press, 2007.

[134] JH Cragin et al. "Interhemispheric comparison of changes in the composition of atmospheric precipitation during the late Cenozoic era". In: *Polar Oceans* (1977), pp. 617–631.

[135] Thomas J Crowley. "Causes of climate change over the past 1000 years". In: *Science* 289.5477 (2000), pp. 270–277.

[136] Thomas J Crowley and Gerald R North. *Paleoclimatology*. New York, NY (United States); Oxford University Press, 1991, 339 p. :

[137] TJ Crowley. "CLIMAP SSTs re-revisited". In: *Climate Dynamics* 16.4 (2000), pp. 241–255.

[138] Kurt M Cuffey and Gary D Clow. "Temperature, accumulation, and ice sheet elevation in central Greenland through the last deglacial transition". In: *Journal of Geophysical Research: Oceans* 102.C12 (1997), pp. 26383–26396.

[139] Kurt M Cuffey et al. "Large arctic temperature change at the Wisconsin-Holocene glacial transition". In: *Science* 270.5235 (1995), pp. 455–458.

[140] B Brandon Curry and Richard G Baker. "Palaeohydrology, vegetation, and climate since the late Illinois Episode (130 ka) in south-central Illinois". In: *Palaeogeography, Palaeoclimatology, Palaeoecology* 155.1-2 (2000), pp. 59–81.

[141] William B Curry and Delia W Oppo. "Synchronous, high-frequency oscillations in tropical sea surface temperatures and North Atlantic Deep Water production during the last glacial cycle". In: *Paleoceanography* 12.1 (1997), pp. 1–14.

[142] Arnaud Czaja and Claude Frankignoul. "Observed impact of Atlantic SST anomalies on the North Atlantic Oscillation". In: *Journal of Climate* 15.6 (2002), pp. 606–623.

[143] Svein Olaf Dahl and Atle Nesje. "Paleoclimatic implications based on equilibrium-line altitude depressions of reconstructed Younger Dryas and Holocene cirque glaciers in inner Nordfjord, western Norway". In: *Palaeogeography, Palaeoclimatology, Palaeoecology* 94.1-4 (1992), pp. 87–97.

[144] Dorthe Dahl-Jensen et al. "Eemian interglacial reconstructed from a Greenland folded ice core". In: *Nature* 493.7433 (2013), pp. 489–494.

[145] Aiguo Dai. "Increasing drought under global warming in observations and models". In: *Nature climate change* 3.1 (2013), pp. 52–58.

[146] Aiguo Dai, Inez Y Fung, and Anthony D Del Genio. "Surface observed global land precipitation variations during 1900–88". In: *Journal of climate* 10.11 (1997), pp. 2943–2962.

[147] WHITE Dansgaard, JWC White, and SJ Johnsen. "The abrupt termination of the Younger Dryas climate event". In: *Nature* 339.6225 (1989), pp. 532–534.

[148] Willi Dansgaard. "Stable isotopes in precipitation". In: *Tellus* 16.4 (1964), pp. 436–468.

[149] Willi Dansgaard et al. "Evidence for general instability of past climate from a 250-kyr ice-core record". In: *Nature* 364.6434 (1993), pp. 218–220.

[150] Basil AS Davis et al. "The temperature of Europe during the Holocene reconstructed from pollen data". In: *Quaternary science reviews* 22.15-17 (2003), pp. 1701–1716.

[151] Anthony D Del Genfo, Andrew A Lacis, and Reto A Ruedy. "Simulations of the effect of a warmer climate on atmospheric humidity". In: *Nature* 351.6325 (1991), pp. 382–385.

[152] Thomas L Delworth and Richard J Greatbatch. "Multidecadal thermohaline circulation variability driven by atmospheric surface flux forcing". In: *Journal of Climate* 13.9 (2000), pp. 1481–1495.

[153] Clara Deser, James W Hurrell, and Adam S Phillips. "The role of the North Atlantic Oscillation in European climate projections". In: *Climate dynamics* 49.9-10 (2017), pp. 3141–3157.

[154] Peter Ditlevsen and Susanne Ditlevsen. "Warning of a forthcoming collapse of the Atlantic meridional overturning circulation". In: *Nature Communications* 14.1 (2023), pp. 1–12.

[155] JA Dorale et al. "Isotopic evidence for Younger Dryas aridity in the North American midcontinent". In: *Geology* 38.6 (2010), pp. 519–522.

[156] Hervé Douville et al. "Anthropogenic influence on multidecadal changes in reconstructed global evapotranspiration". In: *Nature Climate Change* 3.1 (2013), pp. 59–62.

[157] Hervé Douville et al. "Water cycle changes". In: (2021).

[158] Nguyen Chi Dung et al. "A decadal-resolution stalagmite record of strong Asian summer monsoon from Northwestern Vietnam over the Dansgaard–Oeschger events 2–4". In: *Journal of Asian Earth Sciences: X* (2020), p. 100027.

[159] Paul J Durack, Susan E Wijffels, and Richard J Matear. "Ocean salinities reveal strong global water cycle intensification during 1950 to 2000". In: *science* 336.6080 (2012), pp. 455–458.

[160] Christopher RW Ellison, Mark R Chapman, and Ian R Hall. "Surface and deep ocean interactions during the cold climate event 8200 years ago". In: *Science* 312.5782 (2006), pp. 1929–1932.

[161] Jussi T Eronen et al. "Neogene aridification of the Northern Hemisphere". In: *Geology* 40.9 (2012), pp. 823–826.

[162] Jan Esper and David Frank. "Divergence pitfalls in tree-ring research". In: *Climatic Change* 94.3 (2009), pp. 261–266.

[163] David M Etheridge et al. "Natural and anthropogenic changes in atmospheric CO2 over the last 1000 years from air in Antarctic ice and firn". In: *Journal of Geophysical Research: Atmospheres* 101.D2 (1996), pp. 4115–4128.

[164] Richard G Fairbanks. "The age and origin of the "Younger Dryas climate event" in Greenland ice cores". In: *Paleoceanography* 5.6 (1990), pp. 937–948.

[165] Peter J Fawcett et al. "The Younger Dryas termination and North Atlantic Deep Water formation: Insights from climate model simulations and Greenland ice cores". In: *Paleoceanography* 12.1 (1997), pp. 23–38.

[166] Sarah J Feakins, Sophie Warny, and Jung-Eun Lee. "Hydrologic cycling over Antarctica during the middle Miocene warming". In: *Nature Geoscience* 5.8 (2012), pp. 557–560.

[167] Shannon Ferguson et al. "Breaching of Mustang Island in response to the 8.2 ka sea-level event and impact on Corpus Christi Bay, Gulf of Mexico: Implications for future coastal change". In: *The Holocene* 28.1 (2018), pp. 166–172.

[168] Christopher B Field et al. "IPCC, 2012: Managing the risks of extreme events and disasters to advance climate change adaptation. A special report of Working Groups I and II of the Intergovernmental Panel on Climate Change". In: *Cambridge University Press, Cambridge, UK, and New York, NY, USA* 30.11 (2012), pp. 7575–7613.

[169] Matthew S Finkenbinder et al. "A 31,000 year record of paleoenvironmental and lake-level change from Harding Lake, Alaska, USA". In: *Quaternary Science Reviews* 87 (2014), pp. 98–113.

[170] H Fischer et al. "Palaeoclimate constraints on a world with post-industrial warming of 2 degrees and beyond". In: (2018).

[171] Hubertus Fischer et al. "Palaeoclimate constraints on the impact of 2 C anthropogenic warming and beyond". In: *Nature geoscience* 11.7 (2018), pp. 474–485.

[172] Gregory Flato et al. "Evaluation of climate models". In: *Climate change 2013: the physical science basis. Contribution of Working Group I to the Fifth Assessment Report of the Intergovernmental Panel on Climate Change*. Cambridge University Press, 2014, pp. 741–866.

[173] Dominik Fleitmann et al. "Timing and climatic impact of Greenland interstadials recorded in stalagmites from northern Turkey". In: *Geophysical Research Letters* 36.19 (2009).

[174] Benjamin P Flower and James P Kennett. "The middle Miocene climatic transition: East Antarctic ice sheet development, deep ocean circulation and global carbon cycling". In: *Palaeogeography, palaeoclimatology, palaeoecology* 108.3-4 (1994), pp. 537–555.

[175] Damien A Fordham et al. "PaleoView: a tool for generating continuous climate projections spanning the last 21 000 years at regional and global scales". In: *Ecography* 40.11 (2017), pp. 1348–1358.

[176] Gavin L Foster, Caroline H Lear, and James WB Rae. "The evolution of pCO2, ice volume and climate during the middle Miocene". In: *Earth and Planetary Science Letters* 341 (2012), pp. 243–254.

[177] David L Fox and Paul L Koch. "Carbon and oxygen isotopic variability in Neogene paleosol carbonates: constraints on the evolution of the C4-grasslands of the Great Plains, USA". In: *Palaeogeography, Palaeoclimatology, Palaeoecology* 207.3-4 (2004), pp. 305–329.

[178] Claude Frankignoul and Elodie Kestenare. "Observed Atlantic SST anomaly impact on the NAO: An update". In: *Journal of climate* 18.19 (2005), pp. 4089–4094.

[179] Michael Fritz et al. "Late glacial and Holocene sedimentation, vegetation, and climate history from easternmost Beringia (northern Yukon Territory, Canada)". In: *Quaternary Research* 78.3 (2012), pp. 549–560.

[180] Sherilyn C Fritz et al. "Quaternary glaciation and hydrologic variation in the South American tropics as reconstructed from the Lake Titicaca drilling project". In: *Quaternary Research* 68.3 (2007), pp. 410–420.

[181] MK Gagan et al. "New views of tropical paleoclimates from corals". In: *Quaternary Science Reviews* 19.1-5 (2000), pp. 45–64.

[182] H S Gale. "Overflow of Owens Lake occurs when wetness exceeds 2.4 times the historical mean". In: *U.S. Geol. Sum. Bull* 580-L (1914), p. 251.

[183] Chaochao Gao, Alan Robock, and Caspar Ammann. "Volcanic forcing of climate over the past 1500 years: An improved ice core-based index for climate models". In: *Journal of Geophysical Research: Atmospheres* 113.D23 (2008).

[184] F Gasse and E Van Campo. "Late Quaternary environmental changes from a pollen and diatom record in the southern tropics (Lake Tritrivakely, Madagascar)". In: *Palaeogeography, Palaeoclimatology, Palaeoecology* 167.3-4 (2001), pp. 287–308.

[185] Françoise Gasse. "Hydrological changes in the African tropics since the Last Glacial Maximum". In: *Quaternary Science Reviews* 19.1-5 (2000), pp. 189–211.

[186] W Lawrence Gates. "The numerical simulation of ice-age climate with a global general circulation model". In: *Journal of the Atmospheric Sciences* 33.10 (1976), pp. 1844–1873.

[187] Dominique Genty et al. “Precise dating of Dansgaard–Oeschger climate oscillations in western Europe from stalagmite data”. In: *Nature* 421.6925 (2003), pp. 833–837.

[188] Alessandra Giannini, Yochanan Kushnir, and Mark A Cane. “Interannual variability of Caribbean rainfall, ENSO, and the Atlantic Ocean”. In: *Journal of Climate* 13.2 (2000), pp. 297–311.

[189] Rüdiger Glaser et al. “The variability of European floods since AD 1500”. In: *Climatic change* 101.1-2 (2010), pp. 235–256.

[190] A Goldner, N Herold, and Matthew Huber. “The Challenge of Simulating the Warmth of the Mid-Miocene Climatic Optimun in CESM1”. In: *Climate of the Past* (2014).

[191] Xun Gong et al. “Of Atlantic Meridional Overturning Circulation in the CMIP6 Project”. In: *Deep Sea Research Part II: Topical Studies in Oceanography* 206 (2022), p. 105193.

[192] JF Gonzalez-Rouco et al. “Medieval Climate Anomaly to Little Ice Age transition as simulated by current climate models”. In: *PAGES news* 19.1 (2011), pp. 7–8.

[193] Tomasz Goślar, Maurice Arnold, and Mieczysław F Pazdur. “The Younger Dryas cold event—was it synchronous over the North Atlantic region?” In: *Radiocarbon* 37.1 (1995), pp. 63–70.

[194] Ulrich von Grafenstein et al. “A mid-European decadal isotope-climate record from 15,500 to 5000 years BP”. In: *Science* 284.5420 (1999), pp. 1654–1657.

[195] Nicholas E Graham et al. “Support for global climate reorganization during the “Medieval Climate Anomaly””. In: *Climate Dynamics* 37.5 (2011), pp. 1217–1245.

[196] Nicholas E Graham et al. “Tropical Pacific–mid-latitude teleconnections in medieval times”. In: *Climatic Change* 83.1 (2007), pp. 241–285.

[197] Lisa J Graumlich. “A 1000-year record of temperature and precipitation in the Sierra Nevada”. In: *Quaternary Research* 39.2 (1993), pp. 249–255.

[198] Rosanna Greenop et al. “Middle Miocene climate instability associated with high-amplitude CO2 variability”. In: *Paleoceanography* 29.9 (2014), pp. 845–853.

[199] Michaela Grein et al. “Atmospheric CO2 from the late Oligocene to early Miocene based on photosynthesis data and fossil leaf characteristics”. In: *Palaeogeography, Palaeoclimatology, Palaeoecology* 374 (2013), pp. 41–51.

[200] Peter Greve et al. “Global assessment of trends in wetting and drying over land”. In: *Nature geoscience* 7.10 (2014), pp. 716–721.

[201] Laurie D Grigg, Cathy Whitlock, and Walter E Dean. “Evidence for millennial-scale climate change during marine isotope stages 2 and 3 at Little Lake, western Oregon, USA”. In: *Quaternary Research* 56.1 (2001), pp. 10–22.

[202] Eric C Grimm et al. “Evidence for warm wet Heinrich events in Florida”. In: *Quaternary Science Reviews* 25.17-18 (2006), pp. 2197–2211.

[203] Joel Guiot. “The combination of historical documents and biological data in the reconstruction of climate variations in space and time”. In: *European Climate Reconstructed from Documentary Data: Methods and Results* (1992), pp. 93–104.

[204] Anil K Gupta, David M Anderson, and Jonathan T Overpeck. “Abrupt changes in the Asian southwest monsoon during the Holocene and their links to the North Atlantic Ocean”. In: *Nature* 421.6921 (2003), pp. 354–357.

[205] James Hansen et al. “Global surface temperature change”. In: *Reviews of Geophysics* 48.4 (2010).

[206] James Hansen et al. "Ice melt, sea level rise and superstorms: evidence from paleoclimate data, climate modeling, and modern observations that 2° C global warming is highly dangerous." In: *Atmospheric Chemistry & Physics Discussions* 15.14 (2015).

[207] Bilal Ul Haq. "Transgressions, climatic change and the diversity of calcareous nannoplankton". In: *Marine Geology* 15.2 (1973), pp. M25–M30.

[208] Elisha B Harris, Matthew J Kohn, and Caroline AE Strömberg. "Stable isotope compositions of herbivore teeth indicate climatic stability leading into the mid-Miocene Climatic Optimum, in Idaho, USA". In: *Palaeogeography, Palaeoclimatology, Palaeoecology* 546 (2020), p. 109610.

[209] Mathias Harzhauser, Christine Latal, and Werner E Piller. "The stable isotope archive of Lake Pannon as a mirror of Late Miocene climate change". In: *Palaeogeography, Palaeoclimatology, Palaeoecology* 249.3-4 (2007), pp. 335–350.

[210] Gerald H Haug et al. "Southward migration of the intertropical convergence zone through the Holocene". In: *Science* 293.5533 (2001), pp. 1304–1308.

[211] Angela Hayes et al. "Glacial Mediterranean sea surface temperatures based on planktonic foraminiferal assemblages". In: *Quaternary Science Reviews* 24.7-9 (2005), pp. 999–1016.

[212] Gabriele C Hegerl et al. "Causes of climate change over the historical record". In: *Environmental Research Letters* 14.12 (2019), p. 123006.

[213] Gabriele C Hegerl et al. "Challenges in quantifying changes in the global water cycle". In: *Bulletin of the American Meteorological Society* 96.7 (2015), pp. 1097–1115.

[214] MAIJA HEIKKILÄ and Heikki Seppä. "Holocene climate dynamics in Latvia, eastern Baltic region: a pollen-based summer temperature reconstruction and regional comparison". In: *Boreas* 39.4 (2010), pp. 705–719.

[215] Hartmut Heinrich. "Origin and consequences of cyclic ice rafting in the northeast Atlantic Ocean during the past 130,000 years". In: *Quaternary research* 29.2 (1988), pp. 142–152.

[216] Oliver Heiri et al. "Validation of climate model-inferred regional temperature change for late-glacial Europe". In: *Nature communications* 5.1 (2014), pp. 1–7.

[217] Samuli Helama, Jouko Meriläinen, and Heikki Tuomenvirta. "Multicentennial megadrought in northern Europe coincided with a global El Niño–Southern Oscillation drought pattern during the Medieval Climate Anomaly". In: *Geology* 37.2 (2009), pp. 175–178.

[218] Isaac M Held and Brian J Soden. "Robust responses of the hydrological cycle to global warming". In: *Journal of climate* 19.21 (2006), pp. 5686–5699.

[219] Ingrid L Hendy and James P Kennett. "Dansgaard-Oeschger cycles and the California Current System: Planktonic foraminiferal response to rapid climate change in Santa Barbara Basin, Ocean Drilling Program hole 893A". In: *Paleoceanography* 15.1 (2000), pp. 30–42.

[220] KJ Hennessy, Jonathan M Gregory, and JFB Mitchell. "Changes in daily precipitation under enhanced greenhouse conditions". In: *Climate Dynamics* 13.9 (1997), pp. 667–680.

[221] A-J Henrot et al. "Effects of CO 2, continental distribution, topography and vegetation changes on the climate at the Middle Miocene: a model study." In: *Climate of the Past* 6.5 (2010).

[222] LG Henry et al. "North Atlantic ocean circulation and abrupt climate change during the last glaciation". In: *Science* 353.6298 (2016), pp. 470–474.

[223] Armand Hernández et al. "A 2,000-year Bayesian NAO reconstruction from the Iberian Peninsula". In: *Scientific reports* 10.1 (2020), pp. 1–15.

[224] N Herold, Matthew Huber, and RD Müller. "Modeling the Miocene climatic optimum. Part I: Land and atmosphere". In: *Journal of Climate* 24.24 (2011), pp. 6353–6372.

[225] Sanaa Hobeichi et al. "Reconciling historical changes in the hydrological cycle over land". In: *npj Climate and Atmospheric Science* 5.1 (2022), pp. 1–9.

[226] David A Hodell, Mark Brenner, and Jason H Curtis. "Terminal Classic drought in the northern Maya lowlands inferred from multiple sediment cores in Lake Chichancanab (Mexico)". In: *Quaternary Science Reviews* 24.12-13 (2005), pp. 1413–1427.

[227] David A Hodell et al. "An 85-ka record of climate change in lowland Central America". In: *Quaternary Science Reviews* 27.11-12 (2008), pp. 1152–1165.

[228] Jeremy S Hoffman et al. "Regional and global sea-surface temperatures during the last interglaciation". In: *Science* 355.6322 (2017), pp. 276–279.

[229] Ann Holbourn et al. "Middle Miocene climate cooling linked to intensification of eastern equatorial Pacific upwelling". In: *Geology* 42.1 (2014), pp. 19–22.

[230] N Penny Holliday et al. "Ocean circulation causes the largest freshening event for 120 years in eastern subpolar North Atlantic". In: *Nature communications* 11.1 (2020), pp. 1–15.

[231] YT Hong et al. "A 6000-year record of changes in drought and precipitation in northeastern China based on a δ13C time series from peat cellulose". In: *Earth and Planetary Science Letters* 185.1-2 (2001), pp. 111–119.

[232] Zhanfang Hou et al. "Understanding Miocene climate evolution in Northeastern Tibet: Stable carbon and oxygen isotope records from the Western Tianshui Basin, China". In: *Journal of Earth Science* 25.2 (2014), pp. 357–365.

[233] John Theodore Houghton et al. *Climate change 2001: the scientific basis*. The Press Syndicate of the University of Cambridge, 2001.

[234] FS Hu et al. "Abrupt changes in North American climate during early Holocene times". In: *Nature* 400.6743 (1999), pp. 437–440.

[235] Jianping Huang et al. "Accelerated dryland expansion under climate change". In: *Nature climate change* 6.2 (2016), pp. 166–171.

[236] Konrad A Hughen et al. "El Nino during the last interglacial period recorded by a fossil coral from Indonesia". In: *Geophysical Research Letters* 26.20 (1999), pp. 3129–3132.

[237] Konrad A Hughen et al. "Rapid climate changes in the tropical Atlantic region during the last deglaciation". In: *Nature* 380.6569 (1996), pp. 51–54.

[238] Konrad A Hughen et al. "Synchronous radiocarbon and climate shifts during the last deglaciation". In: *Science* 290.5498 (2000), pp. 1951–1954.

[239] Malcolm K Hughes and Henry F Diaz. "Was there a 'Medieval Warm Period', and if so, where and when?" In: *Climatic change* 26.2-3 (1994), pp. 109–142.

[240] Mike Hulme, Timothy J Osborn, and Timothy C Johns. "Precipitation sensitivity to global warming: Comparison of observations with HadCM2 simulations". In: *Geophysical research letters* 25.17 (1998), pp. 3379–3382.

[241] Thomas G Huntington. "Climate warming-induced intensification of the hydrologic cycle: an assessment of the published record and potential impacts on agriculture". In: *Advances in agronomy*. Vol. 109. Elsevier, 2010, pp. 1–53.

[242] Thomas G Huntington. "Evidence for intensification of the global water cycle: review and synthesis". In: *Journal of Hydrology* 319.1-4 (2006), pp. 83–95.

[243] James W Hurrell. "Decadal trends in the North Atlantic Oscillation: regional temperatures and precipitation". In: *Science* 269.5224 (1995), pp. 676–679.

[244] James W Hurrell and Clara Deser. "North Atlantic climate variability: the role of the North Atlantic Oscillation". In: *Journal of marine systems* 79.3-4 (2010), pp. 231–244.

[245] Andreas Indermühle et al. "Holocene carbon-cycle dynamics based on CO 2 trapped in ice at Taylor Dome, Antarctica". In: *Nature* 398.6723 (1999), pp. 121–126.

[246] IPCC. "Impacts of 1.5°C Global Warming on Natural and Human Systems". In: *Global Warming of 1.5°C: IPCC Special Report on Impacts of Global Warming of 1.5°C above Pre-industrial Levels in Context of Strengthening Response to Climate Change, Sustainable Development, and Efforts to Eradicate Poverty*. Cambridge University Press, 2022, 175–312. DOI: 10.1017/9781009157940.005.

[247] René FB Isarin and Sjoerd JP Bohncke. "Mean July temperatures during the Younger Dryas in northwestern and central Europe as inferred from climate indicator plant species". In: *Quaternary Research* 51.2 (1999), pp. 158–173.

[248] Tara S Ivanochko et al. "Variations in tropical convection as an amplifier of global climate change at the millennial scale". In: *Earth and Planetary Science Letters* 235.1-2 (2005), pp. 302–314.

[249] LC Jackson et al. "Global and European climate impacts of a slowdown of the AMOC in a high resolution GCM". In: *Climate dynamics* 45.11 (2015), pp. 3299–3316.

[250] Hanchao Jiang and Zhongli Ding. "Eolian grain-size signature of the Sikouzi lacustrine sediments (Chinese Loess Plateau): Implications for Neogene evolution of the East Asian winter monsoon". In: *Bulletin* 122.5-6 (2010), pp. 843–854.

[251] Sigfus J Johnsen et al. "Greenland palaeotemperatures derived from GRIP bore hole temperature and ice core isotope profiles". In: *Tellus B: Chemical and Physical Meteorology* 47.5 (1995), pp. 624–629.

[252] Sigfus J Johnsen et al. "Oxygen isotope and palaeotemperature records from six Greenland ice-core stations: Camp Century, Dye-3, GRIP, GISP2, Renland and NorthGRIP". In: *Journal of Quaternary Science: Published for the Quaternary Research Association* 16.4 (2001), pp. 299–307.

[253] SJ Johnsen, W Dansgaard, and JWC White. "The origin of Arctic precipitation under present and glacial conditions". In: *Tellus B: Chemical and Physical Meteorology* 41.4 (1989), pp. 452–468.

[254] VE Johnston et al. "Evidence of thermophilisation and elevation-dependent warming during the Last Interglacial in the Italian Alps". In: *Scientific reports* 8.1 (2018), pp. 1–11.

[255] E Peter Jones and Leif G Anderson. "Is the global conveyor belt threatened by Arctic Ocean fresh water outflow?" In: *Arctic–Subarctic Ocean Fluxes*. Springer, 2008, pp. 385–404.

[256] Philip D Jones and Michael E Mann. "Climate over past millennia". In: *Reviews of Geophysics* 42.2 (2004).

[257] Jean Jouzel et al. "Vostok ice core: a continuous isotope temperature record over the last climatic cycle (160,000 years)". In: *Nature* 329.6138 (1987), pp. 403–408.

[258] Flávio Justino et al. "Synoptic reorganization of atmospheric flow during the Last Glacial Maximum". In: *Journal of Climate* 18.15 (2005), pp. 2826–2846.

[259] Knut Kaiser and Ingo Clausen. "Palaeopedology and stratigraphy of the late palaeolithic Alt Duvenstedt site, Schleswig-Holstein (Northwest Germany)". In: *Archäologisches Korrespondenzblatt* 35.4 (2005), pp. 447–466.

[260] Sarah M Kang, Yechul Shin, and Shang-Ping Xie. "Extratropical forcing and tropical rainfall distribution: energetics framework and ocean Ekman advection". In: *Npj Climate and Atmospheric Science* 1.1 (2018), pp. 1–10.

[261] Thomas R Karl et al. *Global climate change impacts in the United States*. Cambridge University Press, 2009.

[262] Kristopher B Karnauskas, Lei Zhang, and Dillon J Amaya. "The atmospheric response to North Atlantic SST trends, 1870–2019". In: *Geophysical Research Letters* 48.2 (2021), e2020GL090677.

[263] Nalân Koç Karpuz and Eystein Jansen. "A high-resolution diatom record of the last deglaciation from the SE Norwegian Sea: Documentation of rapid climatic changes". In: *Paleoceanography* 7.4 (1992), pp. 499–520.

[264] Gayatri Kathayat et al. "Indian monsoon variability on millennial-orbital timescales". In: *Scientific reports* 6 (2016), p. 24374.

[265] JP Kennett. "The middle Miocene climatic transition: East Antarctic ice sheet development, deep ocean circulation and global carbon cycling". In: *Palaeogeography, Palaeoclimatololgy, Palaeoecology* 108 (1994), pp. 537–555.

[266] K Halimeda Kilbourne et al. "Atlantic circulation change still uncertain". In: *Nature Geoscience* 15.3 (2022), pp. 165–167.

[267] Hyo-Jeong Kim et al. "North Atlantic Oscillation impact on the Atlantic Meridional Overturning Circulation shaped by the mean state". In: *npj Climate and Atmospheric Science* 6.1 (2023), p. 25.

[268] Seong-Joong Kim et al. "Climate response over Asia/Arctic to change in orbital parameters for the last interglacial maximum". In: *Geosciences Journal* 14.2 (2010), pp. 173–190.

[269] Matthew E Kirby. "Climate science: Water's past revisited to predict its future". In: *Nature* 532.7597 (2016), pp. 44–45.

[270] Dorthe Klitgaard-Kristensen et al. "A regional 8200 cal. yr BP cooling event in northwest Europe, induced by final stages of the Laurentide ice-sheet deglaciation?" In: *Journal of Quaternary Science: Published for the Quaternary Research Association* 13.2 (1998), pp. 165–169.

[271] James C Knox and HE Wright. "Responses of river systems to Holocene climates". In: *Late quaternary environments of the United States* 2 (1983), pp. 26–41.

[272] Reto Knutti and Jan Sedláček. "Robustness and uncertainties in the new CMIP5 climate model projections". In: *Nature Climate Change* 3.4 (2013), p. 369.

[273] Goutam Konapala et al. "Climate change will affect global water availability through compounding changes in seasonal precipitation and evaporation". In: *Nature Communications* 11.1 (2020), pp. 1–10.

[274] Bronwen L Konecky et al. "Globally coherent water cycle response to temperature change during the past two millennia". In: *Nature Geoscience* (2023), pp. 1–8.

[275] Robert E Kopp et al. "Probabilistic assessment of sea level during the last interglacial stage". In: *Nature* 462.7275 (2009), pp. 863–867.

[276] Ulrich Kotthoff et al. "Impact of Lateglacial cold events on the northern Aegean region reconstructed from marine and terrestrial proxy data". In: *Journal of Quaternary Science* 26.1 (2011), pp. 86–96.

[277] Karl J Kreutz et al. "Bipolar changes in atmospheric circulation during the Little Ice Age". In: *Science* 277.5330 (1997), pp. 1294–1296.

[278] Elmar Kriegler et al. “Imprecise probability assessment of tipping points in the climate system”. In: *Proceedings of the national Academy of Sciences* 106.13 (2009), pp. 5041–5046.

[279] Michal Kucera et al. “Reconstruction of sea-surface temperatures from assemblages of planktonic foraminifera: multi-technique approach based on geographically constrained calibration data sets and its application to glacial Atlantic and Pacific Oceans”. In: *Quaternary Science Reviews* 24.7-9 (2005), pp. 951–998.

[280] Till Kuhlbrodt et al. “On the driving processes of the Atlantic meridional overturning circulation”. In: *Reviews of Geophysics* 45.2 (2007).

[281] Joachim Kuhlemann and Oliver Kempf. “Post-Eocene evolution of the North Alpine Foreland Basin and its response to Alpine tectonics”. In: *Sedimentary Geology* 152.1-2 (2002), pp. 45–78.

[282] Joachim Kuhlemann et al. “Regional synthesis of Mediterranean atmospheric circulation during the Last Glacial Maximum”. In: *Science* 321.5894 (2008), pp. 1338–1340.

[283] Arun Kumar et al. “Differing trends in the tropical surface temperatures and precipitation over land and oceans”. In: *Journal of Climate* 17.3 (2004), pp. 653–664.

[284] Wolfram M Kürschner, Zlatko Kvaček, and David L Dilcher. “The impact of Miocene atmospheric carbon dioxide fluctuations on climate and the evolution of terrestrial ecosystems”. In: *Proceedings of the National Academy of Sciences* 105.2 (2008), pp. 449–453.

[285] Olga Kwiecien et al. “North Atlantic control on precipitation pattern in the eastern Mediterranean/Black Sea region during the last glacial”. In: *Quaternary Research* 71.3 (2009), pp. 375–384.

[286] M Ladd et al. “Variations in precipitation in North America during the past 2000 years”. In: *The Holocene* 28.4 (2018), pp. 667–675.

[287] Valmore C LaMarche Jr. “Paleoclimatic Inferences from Long Tree-Ring Records: Intersite comparison shows climatic anomalies that may be linked to features of the general circulation.” In: *Science* 183.4129 (1974), pp. 1043–1048.

[288] Hubert H Lamb. “Climatic fluctuations”. In: *World survey of climatology* 2 (1969), pp. 173–249.

[289] Hubert H Lamb. “Climatic history and the future”. In: *present past and future* 2 (1977), p. 835.

[290] Hubert H Lamb. “The early medieval warm epoch and its sequel”. In: *Palaeogeography, Palaeoclimatology, Palaeoecology* 1 (1965), pp. 13–37.

[291] Hubert Horace Lamb. *Climate: Present, Past and Future (Routledge Revivals): Volume 2: Climatic History and the Future*. Vol. 2. Routledge, 2013.

[292] Jianghu Lan et al. “Dramatic weakening of the East Asian summer monsoon in northern China during the transition from the Medieval Warm Period to the Little Ice Age”. In: *Geology* 48.4 (2020), pp. 307–312.

[293] C Lang et al. “16° C rapid temperature variation in central Greenland 70,000 years ago”. In: *Science* 286.5441 (1999), pp. 934–937.

[294] Narasimhan K Larkin and DE Harrison. “ENSO warm (El Niño) and cold (La Niña) event life cycles: Ocean surface anomaly patterns, their symmetries, asymmetries, and implications”. In: *Journal of climate* 15.10 (2002), pp. 1118–1140.

[295] Mojib Latif et al. “Natural variability has dominated Atlantic Meridional Overturning Circulation since 1900”. In: *Nature Climate Change* 12.5 (2022), pp. 455–460.

[296] David W Lea et al. “Synchroneity of tropical and high-latitude Atlantic temperatures over the last glacial termination”. In: *Science* 301.5638 (2003), pp. 1361–1364.

[297] Guillaume Leduc et al. “Moisture transport across Central America as a positive feedback on abrupt climatic changes”. In: *Nature* 445.7130 (2007), pp. 908–911.

[298] June-Yi Lee and Bin Wang. “Future change of global monsoon in the CMIP5”. In: *Climate Dynamics* 42.1-2 (2014), pp. 101–119.

[299] KE Lee, NC Slowey, and TD Herbert. “Glacial SSTs in the subtropical North Pacific: a comparison of UK0 37 δ18O and foraminiferal assemblage temperature estimates”. In: *Paleoceanography* 16 (2001), pp. 268–279.

[300] Scott J Lehman and Lloyd D Keigwin. “Sudden changes in North Atlantic circulation during the last deglaciation”. In: *Nature* 356.6372 (1992), pp. 757–762.

[301] Flavio Lehner et al. “Amplified inception of European Little Ice Age by sea ice–ocean–atmosphere feedbacks”. In: *Journal of climate* 26.19 (2013), pp. 7586–7602.

[302] Timothy M Lenton et al. “Using GENIE to study a tipping point in the climate system”. In: *Philosophical Transactions of the Royal Society A: Mathematical, Physical and Engineering Sciences* 367.1890 (2009), pp. 871–884.

[303] EB Leopold and MF Denton. “Comparative age of grassland and steppe east and west of the northern rocky mountain”. In: *Annals of the Missouri Botanical Garden* (1987), pp. 841–867.

[304] Dirk C Leuschner and Frank Sirocko. “The low-latitude monsoon climate during Dansgaard–Oeschger cycles and Heinrich events”. In: *Quaternary Science Reviews* 19.1-5 (2000), pp. 243–254.

[305] Naomi E Levin et al. “A stable isotope aridity index for terrestrial environments”. In: *Proceedings of the National Academy of Sciences* 103.30 (2006), pp. 11201–11205.

[306] Richard C Levine and Grant R Bigg. “Sensitivity of the glacial ocean to Heinrich events from different iceberg sources, as modeled by a coupled atmosphere-iceberg-ocean model”. In: *Paleoceanography* 23.4 (2008).

[307] Elan J Levy et al. “Weakened AMOC related to cooling and atmospheric circulation shifts in the last interglacial Eastern Mediterranean”. In: *Nature communications* 14.1 (2023), p. 5180.

[308] Camille Li and Andreas Born. “Coupled atmosphere-ice-ocean dynamics in Dansgaard-Oeschger events”. In: *Quaternary Science Reviews* 203 (2019), pp. 1–20.

[309] Yong-Xiang Li et al. “Synchronizing a sea-level jump, final Lake Agassiz drainage, and abrupt cooling 8200 years ago”. In: *Earth and Planetary Science Letters* 315 (2012), pp. 41–50.

[310] Yu Li and Yuxin Zhang. “Synergy of the westerly winds and monsoons in the lake evolution of global closed basins since the Last Glacial Maximum and implications for hydrological change in central Asia”. In: *Climate of the Past* 16.6 (2020), pp. 2239–2254.

[311] Zhaoyan Li et al. *The climatic changes of drought–wet in ancient Chang-an region of China during the last 1604 years*. 1987.

[312] Joseph M Licciardi et al. “Deglaciation of a soft-bedded Laurentide Ice Sheet”. In: *Quaternary Science Reviews* 17.4-5 (1998), pp. 427–448.

[313] Braddock K Linsley. “Oxygen-isotope record of sea level and climate variations in the Sulu Sea over the past 150,000 years”. In: *Nature* 380.6571 (1996), pp. 234–237.

[314] E Lioubimtseva et al. “Impacts of climate and land-cover changes in arid lands of Central Asia”. In: *Journal of Arid Environments* 62.2 (2005), pp. 285–308.

[315] Liping Liu, Jussi T Eronen, and Mikael Fortelius. "Significant mid-latitude aridity in the middle Miocene of East Asia". In: *Palaeogeography, Palaeoclimatology, Palaeoecology* 279.3-4 (2009), pp. 201–206.

[316] Wei Liu et al. "Climate impacts of a weakened Atlantic Meridional Overturning Circulation in a warming climate". In: *Science advances* 6.26 (2020), eaaz4876.

[317] Wei Liu et al. "Overlooked possibility of a collapsed Atlantic Meridional Overturning Circulation in warming climate". In: *Science Advances* 3.1 (2017), e1601666.

[318] Valerie N Livina and Timothy M Lenton. "A modified method for detecting incipient bifurcations in a dynamical system". In: *Geophysical research letters* 34.3 (2007).

[319] Fredrik Charpentier Ljungqvist et al. "Northern Hemisphere hydroclimate variability over the past twelve centuries". In: *Nature* 532.7597 (2016), pp. 94–98.

[320] Jeremy M Lloyd et al. "Foraminiferal reconstruction of mid-to late-Holocene ocean circulation and climate variability in Disko Bugt, West Greenland". In: *The Holocene* 17.8 (2007), pp. 1079–1091.

[321] Brian H Luckman. "The little ice age in the Canadian Rockies". In: *Geomorphology* 32.3-4 (2000), pp. 357–384.

[322] Marc Luetscher et al. "North Atlantic storm track changes during the Last Glacial Maximum recorded by Alpine speleothems". In: *Nature Communications* 6.1 (2015), pp. 1–6.

[323] Sven Lukas and Tom Bradwell. "Reconstruction of a Lateglacial (Younger Dryas) mountain ice field in Sutherland, northwestern Scotland, and its palaeoclimatic implications". In: *Journal of Quaternary Science: Published for the Quaternary Research Association* 25.4 (2010), pp. 567–580.

[324] David C Lund, Jean Lynch-Stieglitz, and William B Curry. "Gulf Stream density structure and transport during the past millennium". In: *Nature* 444.7119 (2006), pp. 601–604.

[325] S Lüning et al. "The Medieval climate anomaly in the Mediterranean region". In: *Paleoceanography and Paleoclimatology* 34.10 (2019), pp. 1625–1649.

[326] Sebastian Lüning et al. "Hydroclimate in Africa during the medieval climate anomaly". In: *Palaeogeography, Palaeoclimatology, Palaeoecology* 495 (2018), pp. 309–322.

[327] Tomi P Luoto and Liisa Nevalainen. "Temperature-precipitation relationship of the Common Era in northern Europe". In: *Theoretical and Applied Climatology* 132.3-4 (2018), pp. 933–938.

[328] Mitchell Lyle et al. "Out of the tropics: the Pacific, Great Basin Lakes, and Late Pleistocene water cycle in the western United States". In: *Science* 337.6102 (2012), pp. 1629–1633.

[329] Jean Lynch-Stieglitz. "The Atlantic meridional overturning circulation and abrupt climate change". In: *Annual review of marine science* 9 (2017), pp. 83–104.

[330] Jean Lynch-Stieglitz et al. "Muted change in Atlantic overturning circulation over some glacial-aged Heinrich events". In: *Nature Geoscience* 7.2 (2014), pp. 144–150.

[331] Anson W Mackay et al. "Hydrological instability during the Last Interglacial in central Asia: a new diatom oxygen isotope record from Lake Baikal". In: *Quaternary Science Reviews* 66 (2013), pp. 45–54.

[332] Michel Magny. "Holocene lake-level fluctuations in Jura and the northern subalpine ranges, France: regional pattern and climatic implications". In: *Boreas* 21.4 (1992), pp. 319–334.

[333] Michel Magny. "Palaeohydrological changes as reflected by lake-level fluctuations in the Swiss Plateau, the Jura Mountains and the northern French Pre-Alps during the Last Glacial–Holocene transition: a regional synthesis". In: *Global and Planetary Change* 30.1-2 (2001), pp. 85–101.

[334] Michel Magny and Carole Bégeot. "Hydrological changes in the European midlatitudes associated with freshwater outbursts from Lake Agassiz during the Younger Dryas event and the early Holocene". In: *Quaternary Research* 61.2 (2004), pp. 181–192.

[335] Michel Magny et al. "Reconstruction and palaeoclimatic interpretation of mid-Holocene vegetation and lake-level changes at Saint-Jorioz, Lake Annecy, French Pre-Alps". In: *The Holocene* 13.2 (2003), pp. 265–275.

[336] Barbara A Maher. "Holocene variability of the East Asian summer monsoon from Chinese cave records: a re-assessment". In: *The Holocene* 18.6 (2008), pp. 861–866.

[337] Irene Malmierca-Vallet et al. "Simulating the last interglacial Greenland stable water isotope peak: The role of Arctic sea ice changes". In: *Quaternary Science Reviews* 198 (2018), pp. 1–14.

[338] S Manabe and RT Wetherald. "Large-scale changes of soil wetness induced by an increase in atmospheric carbon dioxide". In: *Journal of the Atmospheric Sciences* 44.8 (1987), pp. 1211–1236.

[339] Benoit B Mandelbrot. *The fractal geometry of nature*. Vol. 173. WH freeman New York, 1983.

[340] Jan Mangerud et al. "Paleomagnetic correlations between scandinavian ice-sheet fluctuations and greenland dansgaard–oeschger events, 45,000–25,000 yr BP". In: *Quaternary Research* 59.2 (2003), pp. 213–222.

[341] Michael E Mann, Raymond S Bradley, and Malcolm K Hughes. "Global-scale temperature patterns and climate forcing over the past six centuries". In: *Nature* 392.6678 (1998), pp. 779–787.

[342] Michael E Mann et al. "Global signatures and dynamical origins of the Little Ice Age and Medieval Climate Anomaly". In: *Science* 326.5957 (2009), pp. 1256–1260.

[343] Michael E Mann et al. "Multidecadal climate oscillations during the past millennium driven by volcanic forcing". In: *Science* 371.6533 (2021), pp. 1014–1019.

[344] Thomas M Marchitto Jr, Delia W Oppo, and William B Curry. "Paired benthic foraminiferal Cd/Ca and Zn/Ca evidence for a greatly increased presence of Southern Ocean Water in the glacial North Atlantic". In: *Paleoceanography* 17.3 (2002), pp. 10–1.

[345] Shaun A Marcott et al. "A reconstruction of regional and global temperature for the past 11,300 years". In: *science* 339.6124 (2013), pp. 1198–1201.

[346] José A Marengo. "Interdecadal variability and trends of rainfall across the Amazon basin". In: *Theoretical and applied climatology* 78.1-3 (2004), pp. 79–96.

[347] Y Markonis et al. "A cross-scale framework for integrating multi-source data in Earth system sciences". In: *Environmental Software Modelling* (), in revision.

[348] Y Markonis et al. "Assessment of water cycle intensification over land using a multisource global gridded precipitation dataset". In: *Journal of Geophysical Research: Atmospheres* 124.21 (2019), pp. 11175–11187.

[349] Y Markonis et al. "Global estimation of long-term persistence in annual river runoff". In: *Advances in Water Resources* 113 (2018), pp. 1–12.

[350] Y Markonis et al. "Persistent multi-scale fluctuations shift European hydroclimate to its millennial boundaries". In: *Nature communications* 9.1 (2018), pp. 1–12.

[351] Y Markonis et al. “Persistent multi-scale fluctuations shift European hydroclimate to its millennial boundaries”. In: *Nature communications* 9.1 (2018), p. 1767.

[352] J Marshall et al. “The ocean’s role in setting the mean position of the Inter-Tropical Convergence Zone”. In: *Climate Dynamics* 42.7 (2014), pp. 1967–1979.

[353] Belen Martrat et al. “Abrupt temperature changes in the Western Mediterranean over the past 250,000 years”. In: *Science* 306.5702 (2004), pp. 1762–1765.

[354] M Maslin, M Sarnthein, and J-J Knaack. “Subtropical eastern Atlantic climate during the Eemian”. In: *Naturwissenschaften* 83.3 (1996), pp. 122–126.

[355] Mark A Maslin and Stephen J Burns. “Reconstruction of the Amazon Basin effective moisture availability over the past 14,000 years”. In: *Science* 290.5500 (2000), pp. 2285–2287.

[356] Valérie Masson-Delmotte et al. “Climate change 2021: the physical science basis”. In: *Contribution of working group I to the sixth assessment report of the intergovernmental panel on climate change* 2 (2021).

[357] John A Matthews and Keith R Briffa. “The ‘Little Ice Age’: re-evaluation of an evolving concept”. In: *Geografiska Annaler: Series A, Physical Geography* 87.1 (2005), pp. 17–36.

[358] Dmitri Mauquoy et al. “Late Holocene climatic changes in Tierra del Fuego based on multiproxy analyses of peat deposits”. In: *Quaternary Research* 61.2 (2004), pp. 148–158.

[359] Paul A Mayewski and Michael Bender. “The GISP2 ice core record—Paleoclimate highlights”. In: *Reviews of Geophysics* 33.S2 (1995), pp. 1287–1296.

[360] Paul A Mayewski et al. “Major features and forcing of high-latitude northern hemisphere atmospheric circulation using a 110,000-year-long glaciochemical series”. In: *Journal of Geophysical Research: Oceans* 102.C12 (1997), pp. 26345–26366.

[361] Paul A Mayewski et al. “The atmosphere during the Younger Dryas”. In: *Science* 261.5118 (1993), pp. 195–197.

[362] Gregory J McCabe, Michael A Palecki, and Julio L Betancourt. “Pacific and Atlantic Ocean influences on multidecadal drought frequency in the United States”. In: *Proceedings of the National Academy of Sciences* 101.12 (2004), pp. 4136–4141.

[363] Gregory J McCabe Jr and David M Wolock. “Climate change and the detection of trends in annual runoff”. In: *Climate Research* 8.2 (1997), pp. 129–134.

[364] Gerard D McCarthy et al. “Measuring the Atlantic meridional overturning circulation at 26 N”. In: *Progress in Oceanography* 130 (2015), pp. 91–111.

[365] James J McCarthy et al. *Climate change 2001: impacts, adaptation, and vulnerability: contribution of Working Group II to the third assessment report of the Intergovernmental Panel on Climate Change*. Vol. 2. Cambridge University Press, 2001.

[366] David McGee et al. “Hemispherically asymmetric trade wind changes as signatures of past ITCZ shifts”. In: *Quaternary Science Reviews* 180 (2018), pp. 214–228.

[367] Hamish McGowan et al. “Evidence of wet-dry cycles and mega-droughts in the Eemian climate of southeast Australia”. In: *Scientific reports* 10.1 (2020), pp. 1–10.

[368] Jerry F McManus et al. “Collapse and rapid resumption of Atlantic meridional circulation linked to deglacial climate changes”. In: *Nature* 428.6985 (2004), pp. 834–837.

[369] LO Mearns et al. “Analysis of daily variability of precipitation in a nested regional climate model: comparison with observations and doubled CO2 results”. In: *Global and Planetary Change* 10.1-4 (1995), pp. 55–78.

[370] Gerard A Meehl et al. “Global climate projections”. In: (2007).

[371] DM Meko. *Dendroclimatic evidence from the Great Plains of the United States. In “Climate Since AD 1500”(RS Bradley and PD Jones, Eds.)* 1992.

[372] CAPE-Last Interglacial Project Members. “Last Interglacial Arctic warmth confirms polar amplification of climate change”. In: *Quaternary Science Reviews* 25.13-14 (2006), pp. 1383–1400.

[373] Cohmap Members. “Climatic changes of the last 18,000 years: observations and model simulations”. In: *Science* (1988), pp. 1043–1052.

[374] SE Metcalfe. “Diatoms from the Pretoria Saltpan–a record of lake evolution and environmental change”. In: *Tswaing, investigations into the origin, age and palaeoenvironments of the Pretoria Saltpan. Council of Geoscience (Geological Survey of South Africa)* 172 (1999), p. 192.

[375] Katharina Methner et al. “Middle Miocene long-term continental temperature change in and out of pace with marine climate records”. In: *Scientific reports* 10.1 (2020), pp. 1–10.

[376] Xiaodong Miao et al. “A 10,000 year record of dune activity, dust storms, and severe drought in the central Great Plains”. In: *Geology* 35.2 (2007), pp. 119–122.

[377] Gifford H Miller et al. “Abrupt onset of the Little Ice Age triggered by volcanism and sustained by sea-ice/ocean feedbacks”. In: *Geophysical Research Letters* 39.2 (2012).

[378] Gifford H Miller et al. “Temperature and precipitation history of the Arctic”. In: *Quaternary Science Reviews* 29.15-16 (2010), pp. 1679–1715.

[379] Kenneth G Miller. “Southern Ocean influences on late Eocene to Miocene deepwater circulation”. In: *The Antarctic paleoenvironment: a perspective on global change* 60 (1993), pp. 1–25.

[380] Kenneth G Miller, James D Wright, and Richard G Fairbanks. “Unlocking the ice house: Oligocene-Miocene oxygen isotopes, eustasy, and margin erosion”. In: *Journal of Geophysical Research: Solid Earth* 96.B4 (1991), pp. 6829–6848.

[381] P CD Milly and KA Dunne. “Sensitivity of the global water cycle to the water-holding capacity of land”. In: *Journal of Climate* 7.4 (1994), pp. 506–526.

[382] Diego G Miralles et al. “El Niño–La Niña cycle and recent trends in continental evaporation”. In: *Nature Climate Change* 4.2 (2014), pp. 122–126.

[383] Paola Moffa-Sánchez et al. “Variability in the northern North Atlantic and Arctic oceans across the last two millennia: A review”. In: *Paleoceanography and Paleoclimatology* 34.8 (2019), pp. 1399–1436.

[384] Mahyar Mohtadi et al. “North Atlantic forcing of tropical Indian Ocean climate”. In: *Nature* 509.7498 (2014), pp. 76–80.

[385] Marisa Montoya, Hans von Storch, and Thomas J Crowley. “Climate simulation for 125 kyr BP with a coupled ocean–atmosphere general circulation model”. In: *Journal of Climate* 13.6 (2000), pp. 1057–1072.

[386] Nuria Melisa Morales-García, Laura K Saila, Christine M Janis, et al. “The Neogene savannas of North America: a retrospective analysis on artiodactyl faunas”. In: *Frontiers in Earth Science* (2020).

[387] Ana Moreno et al. “The Medieval Climate Anomaly in the Iberian Peninsula reconstructed from marine and lake records”. In: *Quaternary Science Reviews* 43 (2012), pp. 16–32.

[388] Raimund Muscheler, Jürg Beer, and Maura Vonmoos. “Causes and timing of the 8200 yr BP event inferred from the comparison of the GRIP 10Be and the tree ring Δ14C record”. In: *Quaternary Science Reviews* 23.20-22 (2004), pp. 2101–2111.

[389] Gustavo Naumann et al. “Global changes in drought conditions under different levels of warming”. In: *Geophysical Research Letters* 45.7 (2018), pp. 3285–3296.

[390] N Combourieu Nebout et al. “Enhanced aridity and atmospheric high-pressure stability over the western Mediterranean during the North Atlantic cold events of the past 50 ky”. In: *Geology* 30.10 (2002), pp. 863–866.

[391] C Nehme et al. “Reconstruction of MIS 5 climate in the central Levant using a stalagmite from Kanaan Cave, Lebanon”. In: *Climate of the Past* 11.12 (2015), pp. 1785–1799.

[392] Atle Nesje et al. “The ‘Little Ice Age’glacial expansion in western Scandinavia: summer temperature or winter precipitation?” In: *Climate dynamics* 30.7-8 (2008), pp. 789–801.

[393] Mark New et al. “Precipitation measurements and trends in the twentieth century”. In: *International Journal of Climatology: A Journal of the Royal Meteorological Society* 21.15 (2001), pp. 1889–1922.

[394] Alicia Newton, Robert Thunell, and Lowell Stott. “Climate and hydrographic variability in the Indo-Pacific Warm Pool during the last millennium”. In: *Geophysical Research Letters* 33.19 (2006).

[395] I Nikolova et al. *The last interglacial (Eemian) climate simulated by LOVECLIM and CCSM3, Clim. Past, 9, 1789–1806.* 2013.

[396] Jesse Norris, Gang Chen, and J David Neelin. “Thermodynamic versus dynamic controls on extreme precipitation in a warming climate from the Community Earth System Model Large Ensemble”. In: *Journal of Climate* 32.4 (2019), pp. 1025–1045.

[397] Suzanne R O’Brien et al. “Complexity of Holocene climate as reconstructed from a Greenland ice core”. In: *Science* 270.5244 (1995), pp. 1962–1964.

[398] JR Oglesby et al. “Medieval drought in North America: The role of the Atlantic multidecadal oscillation”. In: *PAGES news* 19.1 (2011), pp. 18–19.

[399] Paul A O’Gorman and Tapio Schneider. “The physical basis for increases in precipitation extremes in simulations of 21st-century climate change”. In: *Proceedings of the National Academy of Sciences* 106.35 (2009), pp. 14773–14777.

[400] Z Bora Ön et al. “Climate proxies for the last 17.3 ka from Lake Hazar (Eastern Anatolia), extracted by independent component analysis of μ-XRF data”. In: *Quaternary International* 486 (2018), pp. 17–28.

[401] Delia W Oppo, Jerry F McManus, and James L Cullen. “Evolution and demise of the Last Interglacial warmth in the subpolar North Atlantic”. In: *Quaternary Science Reviews* 25.23-24 (2006), pp. 3268–3277.

[402] Ian J Orland et al. “Resolving seasonal rainfall changes in the Middle East during the last interglacial period”. In: *Proceedings of the National Academy of Sciences* 116.50 (2019), pp. 24985–24990.

[403] Eduard Y Osipov and Oleg M Khlystov. “Glaciers and meltwater flux to Lake Baikal during the Last Glacial Maximum”. In: *Palaeogeography, Palaeoclimatology, Palaeoecology* 294.1-2 (2010), pp. 4–15.

[404] Jessica L Oster et al. “Millennial-scale variations in western Sierra Nevada precipitation during the last glacial cycle MIS 4/3 transition”. In: *Quaternary Research* 82.1 (2014), pp. 236–248.

[405] Bette L Otto-Bliesner et al. “How warm was the last interglacial? New model–data comparisons”. In: *Philosophical Transactions of the Royal Society A: Mathematical, Physical and Engineering Sciences* 371.2001 (2013), p. 20130097.

[406] Bette L Otto-Bliesner et al. “Last glacial maximum and Holocene climate in CCSM3”. In: *Journal of Climate* 19.11 (2006), pp. 2526–2544.

[407] Paul A O’Gorman. “Sensitivity of tropical precipitation extremes to climate change”. In: *Nature Geoscience* 5.10 (2012), pp. 697–700.

[408] D Paillard and L Labeyriet. “Role of the thermohaline circulation in the abrupt warming after Heinrich events”. In: *Nature* 372.6502 (1994), pp. 162–164.

[409] Gérémy Panthou et al. “Relationship between surface temperature and extreme rainfalls: A multi-time-scale and event-based analysis”. In: *Journal of hydrometeorology* 15.5 (2014), pp. 1999–2011.

[410] Meredith C Parish, W John Calder, and Bryan N Shuman. “Millennial-scale increase in winter precipitation in the southern Rocky Mountains during the Common Era”. In: *Quaternary Research* 94 (2020), pp. 1–13.

[411] Rosendo Pascual and Edgardo Ortiz Jaureguizar. “Evolving climates and mammal faunas in Cenozoic South America”. In: *The Platyrrhine Fossil Record*. Elsevier, 1990, pp. 23–60.

[412] Martine Paterne et al. “Hydrological relationship between the North Atlantic Ocean and the Mediterranean Sea during the past 15-75 kyr”. In: *Paleoceanography* 14.5 (1999), pp. 626–638.

[413] TC Patridge et al. “Orbital forcing of climate over South Africa: a 200,000-year rainfall record from the Pretoria Saltpan”. In: (1997).

[414] Andreas Pauling et al. “Five hundred years of gridded high-resolution precipitation reconstructions over Europe and the connection to large-scale circulation”. In: *Climate dynamics* 26.4 (2006), pp. 387–405.

[415] Francesco SR Pausata et al. “The greening of the Sahara: past changes and future implications”. In: *One Earth* 2.3 (2020), pp. 235–250.

[416] Dominik Pawłowski et al. “A multiproxy study of Younger Dryas and Early Holocene climatic conditions from the Grabia River paleo-oxbow lake (central Poland)”. In: *Palaeogeography, Palaeoclimatology, Palaeoecology* 438 (2015), pp. 34–50.

[417] Paul N Pearson and Martin R Palmer. “Atmospheric carbon dioxide concentrations over the past 60 million years”. In: *Nature* 406.6797 (2000), pp. 695–699.

[418] Rasmus A Pedersen, Peter L Langen, and Bo M Vinther. “The last interglacial climate: comparing direct and indirect impacts of insolation changes”. In: *Climate Dynamics* 48.9 (2017), pp. 3391–3407.

[419] M Cristina Peñalba Garmendia. “Dynamique de végétation tardiglaciaire et holocène du Centre-Nord de l’Espagne d’après l’analyse pollinique”. PhD thesis. Aix-Marseille 3, 1989.

[420] Larry C Peterson and Gerald H Haug. “Variability in the mean latitude of the Atlantic Intertropical Convergence Zone as recorded by riverine input of sediments to the Cariaco Basin (Venezuela)”. In: *Palaeogeography, Palaeoclimatology, Palaeoecology* 234.1 (2006), pp. 97–113.

[421] Larry C Peterson et al. “Rapid changes in the hydrologic cycle of the tropical Atlantic during the last glacial”. In: *Science* 290.5498 (2000), pp. 1947–1951.

[422] Jean-Robert Petit et al. “Climate and atmospheric history of the past 420,000 years from the Vostok ice core, Antarctica”. In: *Nature* 399.6735 (1999), p. 429.

[423] Nicole Petit-Maire et al. “A vast Eemian palaeolake in Southern Jordan (29 N)”. In: *Global and Planetary Change* 72.4 (2010), pp. 368–373.

[424] PJ Polissar et al. "Solar modulation of Little Ice Age climate in the tropical Andes". In: *Proceedings of the National Academy of Sciences* 103.24 (2006), pp. 8937–8942.

[425] D Polson et al. "Have greenhouse gases intensified the contrast between wet and dry regions?" In: *Geophysical Research Letters* 40.17 (2013), pp. 4783–4787.

[426] Victor J Polyak, Jessica BT Rasmussen, and Yemane Asmerom. "Prolonged wet period in the southwestern United States through the Younger Dryas". In: *Geology* 32.1 (2004), pp. 5–8.

[427] Stephen C Porter. "Onset of neoglaciation in the Southern Hemisphere". In: *Journal of Quaternary Science: Published for the Quaternary Research Association* 15.4 (2000), pp. 395–408.

[428] Matthew J Pound et al. "Global vegetation dynamics and latitudinal temperature gradients during the Mid to Late Miocene (15.97–5.33 Ma)". In: *Earth-Science Reviews* 112.1-2 (2012), pp. 1–22.

[429] Summer K Praetorius et al. "The role of Northeast Pacific meltwater events in deglacial climate change". In: *Science advances* 6.9 (2020), eaay2915.

[430] Shailendra Pratap and Yannis Markonis. "The response of the hydrological cycle to temperature changes in recent and distant climatic history". In: *Progress in Earth and Planetary Science* 9.1 (2022), pp. 1–37.

[431] Warren L Prell and John E Kutzbach. "Monsoon variability over the past 150,000 years". In: *Journal of Geophysical Research: Atmospheres* 92.D7 (1987), pp. 8411–8425.

[432] I Colin Prentice, Joël Guiot, and Sandy P Harrison. "Mediterranean vegetation, lake levels and palaeoclimate at the Last Glacial Maximum". In: *Nature* 360.6405 (1992), pp. 658–660.

[433] I Colin Prentice, Dominique Jolly, and Biome 6000 Participants. "Mid-Holocene and glacial-maximum vegetation geography of the northern continents and Africa". In: *Journal of biogeography* 27.3 (2000), pp. 507–519.

[434] CJ Proctor et al. "A thousand year speleothem proxy record of North Atlantic climate from Scotland". In: *Climate Dynamics* 16.10-11 (2000), pp. 815–820.

[435] Aaron E Putnam and Wallace S Broecker. "Human-induced changes in the distribution of rainfall". In: *Science Advances* 3.5 (2017), e1600871.

[436] Jay Quade and WS Broecker. "Dryland hydrology in a warmer world: Lessons from the Last Glacial period". In: *The European Physical Journal Special Topics* 176.1 (2009), pp. 21–36.

[437] A R Core Team, R Core Team, et al. *R: A language and environment for statistical computing. R Foundation for Statistical Computing, Vienna, Austria. 2012.* 2022.

[438] Oliver Rach et al. "Delayed hydrological response to Greenland cooling at the onset of the Younger Dryas in western Europe". In: *Nature Geoscience* 7.2 (2014), pp. 109–112.

[439] Stefan Rahmstorf. "Shifting seas in the greenhouse?" In: *Nature* 399.6736 (1999), pp. 523–524.

[440] Zhiguo Rao et al. "Investigating the long-term palaeoclimatic controls on the δD and δ18O of precipitation during the Holocene in the Indian and East Asian monsoonal regions". In: *Earth-Science Reviews* 159 (2016), pp. 292–305.

[441] Sune Olander Rasmussen et al. "A new Greenland ice core chronology for the last glacial termination". In: *Journal of Geophysical Research: Atmospheres* 111.D6 (2006).

[442] Tine L Rasmussen, Erik Thomsen, and Matthias Moros. "North Atlantic warming during Dansgaard-Oeschger events synchronous with Antarctic warming and out-of-phase with Greenland climate". In: *Scientific reports* 6 (2016), p. 20535.

[443] Bert Rein, Andreas Lückge, and Frank Sirocko. "A major Holocene ENSO anomaly during the Medieval period". In: *Geophysical Research Letters* 31.17 (2004).

[444] Guoyu Ren. "Pollen evidence for increased summer rainfall in the Medieval warm period at Maili, Northeast China". In: *Geophysical Research Letters* 25.11 (1998), pp. 1931–1934.

[445] Hans Renssen. "Comparison of Climate Model Simulations of the Younger Dryas Cold Event". In: *Quaternary* 3.4 (2020), p. 29.

[446] Hans Renssen et al. "The 8.2 kyr BP event simulated by a global atmosphere—sea-ice—ocean model". In: *Geophysical Research Letters* 28.8 (2001), pp. 1567–1570.

[447] Hans Renssen et al. "The global hydroclimate response during the Younger Dryas event". In: *Quaternary Science Reviews* 193 (2018), pp. 84–97.

[448] Gregory J Retallack. "Cenozoic paleoclimate on land in North America". In: *The Journal of Geology* 115.3 (2007), pp. 271–294.

[449] Gregory J Retallack. "Middle Miocene fossil plants from Fort Ternan (Kenya) and evolution of African grasslands". In: *Paleobiology* (1992), pp. 383–400.

[450] Justin Reuter et al. "A new perspective on the hydroclimate variability in northern South America during the Little Ice Age". In: *Geophysical Research Letters* 36.21 (2009).

[451] Rachael Rhodes et al. "Little Ice Age climate and oceanic conditions of the Ross Sea, Antarctica from a coastal ice core record". In: *Climate of the Past* 8.4 (2012), pp. 1223–1238.

[452] JO Roads et al. "Sensitivity of the CCM1 hydrologic cycle to CO2". In: *Journal of Geophysical Research: Atmospheres* 101.D3 (1996), pp. 7321–7339.

[453] Alan Robock. "Volcanic eruptions and climate". In: *Reviews of geophysics* 38.2 (2000), pp. 191–219.

[454] Jon Robson et al. "Atlantic overturning in decline?" In: *Nature Geoscience* 7.1 (2014), pp. 2–3.

[455] Antonio B Rodriguez, Alexander R Simms, and John B Anderson. "Bay-head deltas across the northern Gulf of Mexico back step in response to the 8.2 ka cooling event". In: *Quaternary Science Reviews* 29.27-28 (2010), pp. 3983–3993.

[456] Jeffery C Rogers. "Spatial variability of Antarctic temperature anomalies and their association with the Southern Hemisphere atmospheric circulation". In: *Annals of the Association of American Geographers* 73.4 (1983), pp. 502–518.

[457] EJ Rohling et al. "Abrupt cold spells in the northwest Mediterranean". In: *Paleoceanography* 13.4 (1998), pp. 316–322.

[458] Maisa Rojas et al. "The Southern Westerlies during the last glacial maximum in PMIP2 simulations". In: *Climate Dynamics* 32.4 (2009), pp. 525–548.

[459] Antoni Rosell-Melé et al. "Sea surface temperature anomalies in the oceans at the LGM estimated from the alkenone-U37K index: Comparison with GCMs". In: *Geophysical Research Letters* 31.3 (2004).

[460] Thomas M Rosenberg et al. "Middle and Late Pleistocene humid periods recorded in palaeolake deposits of the Nafud desert, Saudi Arabia". In: *Quaternary Science Reviews* 70 (2013), pp. 109–123.

[461] K Rotnicki. "Retrodiction of palaeodischarges of meandering and sinuous alluvial rivers and its palaeohydroclimatic implications". In: *Temperate palaeohydrology. Fluvial processes in the temperate zone during the last 15 000 years.* 1991, pp. 431–471.

[462] William F Ruddiman and Andrew McIntyre. "Oceanic mechanisms for amplification of the 23,000-year ice-volume cycle". In: *Science* 212.4495 (1981), pp. 617–627.

[463] Stéphanie Samartin et al. "Climate warming and vegetation response after Heinrich event 1 (16 700–16 000 cal yr BP) in Europe south of the Alps". In: *Climate of the Past* 8.6 (2012), pp. 1913–1927.

[464] Benjamin D Santer et al. "A search for human influences on the thermal structure of the atmosphere". In: *Nature* 382.6586 (1996), pp. 39–46.

[465] Thiago P Santos et al. "Asymmetric response of the subtropical western South Atlantic thermocline to the Dansgaard-Oeschger events of Marine Isotope Stages 5 and 3". In: *Quaternary Science Reviews* 237 (2020), p. 106307.

[466] Michael E Schlesinger and John FB Mitchell. "Climate model simulations of the equilibrium climatic response to increased carbon dioxide". In: *Reviews of Geophysics* 25.4 (1987), pp. 760–798.

[467] Fritz Schlunegger et al. "Magnetostratigraphic calibration of the Oligocene to Middle Miocene (30-15 Ma) mammal biozones and depositional sequences of the Swiss Molasse Basin". In: *Eclogae Geologicae Helvetiae* 89.2 (1996), pp. 753–788.

[468] Andreas Schmittner et al. "Climate sensitivity estimated from temperature reconstructions of the Last Glacial Maximum". In: *Science* 334.6061 (2011), pp. 1385–1388.

[469] Larissa Schneider et al. "Effects of climate variability on mercury deposition during the Older Dryas and Younger Dryas in the Venezuelan Andes". In: *Journal of Paleolimnology* 63.3 (2020), pp. 211–224.

[470] Lea Schneider et al. "Revising midlatitude summer temperatures back to AD 600 based on a wood density network". In: *Geophysical Research Letters* 42.11 (2015), pp. 4556–4562.

[471] Tapio Schneider, Tobias Bischoff, and Gerald H Haug. "Migrations and dynamics of the intertropical convergence zone". In: *Nature* 513.7516 (2014), pp. 45–53.

[472] Serena R Scholz et al. "Isotope sclerochronology indicates enhanced seasonal precipitation in northern South America (Colombia) during the Mid-Miocene Climatic Optimum". In: *Geology* (2020).

[473] Paolo Scussolini et al. "Agreement between reconstructed and modeled boreal precipitation of the Last Interglacial". In: *Science advances* 5.11 (2019), eaax7047.

[474] Richard Seager, Naomi Naik, and Gabriel A Vecchi. "Thermodynamic and dynamic mechanisms for large-scale changes in the hydrological cycle in response to global warming". In: *Journal of Climate* 23.17 (2010), pp. 4651–4668.

[475] Richard Seager et al. "Blueprints for Medieval hydroclimate". In: *Quaternary Science Reviews* 26.19-21 (2007), pp. 2322–2336.

[476] Kristina Seftigen et al. "Hydroclimate variability in Scandinavia over the last millennium-insights from a climate model-proxy data comparison". In: *Climate of the Past* 13 (2017), p. 1831.

[477] Inger K Seierstad et al. "The duration of the Bølling-Allerød period (Greenland Interstadial 1) in the GRIP ice core". In: *Annals of Glaciology* 42 (2005), pp. 337–344.

[478] Sonia Seneviratne et al. "Changes in climate extremes and their impacts on the natural physical environment". In: (2012).

[479] Sonia I Seneviratne et al. "Weather and climate extreme events in a changing climate (Chapter 11)". In: (2021).

[480] Heikki Seppä and Harry John Betteley Birks. "July mean temperature and annual precipitation trends during the Holocene in the Fennoscandian tree-line area: pollen-based climate reconstructions". In: *The Holocene* 11.5 (2001), pp. 527–539.

[481] Heikki Seppä et al. "Late-Quaternary summer temperature changes in the northern-European tree-line region". In: *Quaternary Research* 69.3 (2008), pp. 404–412.

[482] Leonid Serebryanny et al. "Lateglacial and early-Holocene environments of Novaya Zemlya and the Kara Sea region of the Russian Arctic". In: *The Holocene* 8.3 (1998), pp. 323–330.

[483] Nicholas J Shackleton, Michael A Hall, and Edith Vincent. "Phase relationships between millennial-scale events 64,000–24,000 years ago". In: *Paleoceanography* 15.6 (2000), pp. 565–569.

[484] Nicholas John Shackleton. "The last interglacial in the marine and terrestrial records". In: *Proceedings of the Royal Society of London. Series B. Biological Sciences* 174.1034 (1969), pp. 135–154.

[485] Justin Sheffield, Eric F Wood, and Michael L Roderick. "Little change in global drought over the past 60 years". In: *Nature* 491.7424 (2012), pp. 435–438.

[486] YF Shi et al. "Basic Characteristics of Warm Period Climate and Environment of the Holocene Warm Period in China". In: *China Ocean Press, Beijing* 35 (1992), pp. 1–15.

[487] Lyudmila S Shumilovskikh et al. "Vegetation and environmental dynamics in the southern Black Sea region since 18 kyr BP derived from the marine core 22-GC3". In: *Palaeogeography, Palaeoclimatology, Palaeoecology* 337 (2012), pp. 177–193.

[488] M-A Sicre et al. "Labrador current variability over the last 2000 years". In: *Earth and Planetary Science Letters* 400 (2014), pp. 26–32.

[489] Abdelfettah Sifeddine et al. "Variations of the Amazonian rainforest environment: a sedimentological record covering 30,000 years". In: *Palaeogeography, palaeoclimatology, palaeoecology* 168.3-4 (2001), pp. 221–235.

[490] Margit H Simon et al. "Eastern South African hydroclimate over the past 270,000 years". In: *Scientific reports* 5.1 (2015), pp. 1–10.

[491] Ashish Sinha et al. "Variability of Southwest Indian summer monsoon precipitation during the Bølling-Allerød". In: *Geology* 33.10 (2005), pp. 813–816.

[492] Frank Sirocko et al. "A late Eemian aridity pulse in central Europe during the last glacial inception". In: *Nature* 436.7052 (2005), pp. 833–836.

[493] David A Smeed et al. "The North Atlantic Ocean is in a state of reduced overturning". In: *Geophysical Research Letters* 45.3 (2018), pp. 1527–1533.

[494] Jacqueline A Smith and Donald T Rodbell. "Cross-cutting moraines reveal evidence for North Atlantic influence on glaciers in the tropical Andes". In: *Journal of Quaternary Science: Published for the Quaternary Research Association* 25.3 (2010), pp. 243–248.

[495] Ian Snowball, Lovisa Zillén, and Marie-José Gaillard. "Rapid early-Holocene environmental changes in northern Sweden based on studies of two varved lake-sediment sequences". In: *The Holocene* 12.1 (2002), pp. 7–16.

[496] Carolyn W Snyder. "Evolution of global temperature over the past two million years". In: *Nature* 538.7624 (2016), pp. 226–228.

[497] S Solomon. "The physical science basis: Contribution of Working Group I to the fourth assessment report of the Intergovernmental Panel on Climate Change". In: *Intergovernmental Panel on Climate Change (IPCC), Climate change 2007* 996 (2007).

[498] Susan Solomon et al. *Climate change 2007-the physical science basis: Working group I contribution to the fourth assessment report of the IPCC*. Vol. 4. Cambridge university press, 2007.

[499] Yougui Song et al. “Mid-Miocene climatic optimum: Clay mineral evidence from the red clay succession, Longzhong Basin, Northern China”. In: *Palaeogeography, Palaeoclimatology, Palaeoecology* 512 (2018), pp. 46–55.

[500] MA Srokosz and HL Bryden. “Observing the Atlantic Meridional Overturning Circulation yields a decade of inevitable surprises”. In: *Science* 348.6241 (2015), p. 1255575.

[501] J Curt Stager et al. “Solar variability and the levels of Lake Victoria, East Africa, during the last millenium”. In: *Journal of Paleolimnology* 33.2 (2005), pp. 243–251.

[502] Nathan D Stansell et al. “Abrupt Younger Dryas cooling in the northern tropics recorded in lake sediments from the Venezuelan Andes”. In: *Earth and Planetary Science Letters* 293.1-2 (2010), pp. 154–163.

[503] Nathan D Stansell et al. “Lacustrine stable isotope record of precipitation changes in Nicaragua during the Little Ice Age and Medieval Climate Anomaly”. In: *Geology* 41.2 (2013), pp. 151–154.

[504] Leszek Starkel. “Environmental changes at the Younger Dryas-Preboreal transition and during the early Holocene: some distinctive aspects in central Europe”. In: *The Holocene* 1.3 (1991), pp. 234–242.

[505] Leszek Starkel. “Global paleohydrology”. In: *Quaternary International* 2 (1989), pp. 25–33.

[506] Jørgen Peder Steffensen. “The size distribution of microparticles from selected segments of the Greenland Ice Core Project ice core representing different climatic periods”. In: *Journal of Geophysical Research: Oceans* 102.C12 (1997), pp. 26755–26763.

[507] Nathan J Steiger et al. “A reconstruction of global hydroclimate and dynamical variables over the Common Era”. In: *Scientific data* 5.1 (2018), pp. 1–15.

[508] Rüdiger Stein and C Robert. “Siliciclastic sediments at sites 588, 590, and 591: Neogene and Paleogene evolution in the southwest Pacific and Australian climate”. In: *Initial Reports DSDP* 90 (1985), pp. 1437–1455.

[509] Fritz F Steininger. “Chronostratigraphy, geochronology and biochronology of the Miocene" European Land Mammal Mega-Zones"(ELMMZ) and the Miocene" Mammal-Zones (MN-Zones)"”. In: *The Miocene: Land Mammals of Europe* (1999), pp. 9–24.

[510] M Steinthorsdottir, PE Jardine, and WC Rember. “Near-Future pCO2 during the hot Mid Miocene Climatic Optimum”. In: *Paleoceanography and Paleoclimatology* (2020), e2020PA003900.

[511] Graeme L Stephens and Todd D Ellis. “Controls of global-mean precipitation increases in global warming GCM experiments”. In: *Journal of Climate* 21.23 (2008), pp. 6141–6155.

[512] Scott Stine. “Extreme and persistent drought in California and Patagonia during mediaeval time”. In: *Nature* 369.6481 (1994), pp. 546–549.

[513] Thomas F Stocker et al. “Technical summary”. In: *Climate change 2013: the physical science basis. Contribution of Working Group I to the Fifth Assessment Report of the Intergovernmental Panel on Climate Change*. Cambridge University Press, 2013, pp. 33–115.

[514] Gustav Strandberg et al. “High-resolution regional simulation of last glacial maximum climate in Europe”. In: *Tellus A: Dynamic Meteorology and Oceanography* 63.1 (2011), pp. 107–125.

[515] F Alayne Street-Perrott and R Alan Perrott. “Abrupt climate fluctuations in the tropics: the influence of Atlantic Ocean circulation”. In: *Nature* 343.6259 (1990), pp. 607–612.

[516] Minze Stuiver, Pieter M Grootes, and Thomas F Braziunas. "The GISP2 δ18O climate record of the past 16,500 years and the role of the sun, ocean, and volcanoes". In: *Quaternary research* 44.3 (1995), pp. 341–354.

[517] Zhan Su, Andrew P Ingersoll, and Feng He. "On the abruptness of Bølling–Allerød warming". In: *Journal of Climate* 29.13 (2016), pp. 4965–4975.

[518] Yeon Jee Suh et al. "Last interglacial (MIS 5e) and Holocene paleohydrology and paleovegetation of midcontinental North America from Gulf of Mexico sediments". In: *Quaternary Science Reviews* 227 (2020), p. 106066.

[519] Jimin Sun and Zhenqing Zhang. "Palynological evidence for the mid-Miocene climatic optimum recorded in Cenozoic sediments of the Tian Shan Range, northwestern China". In: *Global and Planetary Change* 64.1-2 (2008), pp. 53–68.

[520] Jue Sun et al. "Quantitative precipitation reconstruction in the east-central monsoonal China since the late glacial period". In: *Quaternary international* 521 (2019), pp. 175–184.

[521] Rowan T Sutton and Daniel LR Hodson. "Atlantic Ocean forcing of North American and European summer climate". In: *science* 309.5731 (2005), pp. 115–118.

[522] Jozef Syktus, Hal Gordon, and John Chappell. "Sensitivity of a coupled atmosphere-dynamic upper ocean GCM to variations of CO2, solar constant, and orbital forcing". In: *Geophysical research letters* 21.15 (1994), pp. 1599–1602.

[523] Hossein Tabari. "Climate change impact on flood and extreme precipitation increases with water availability". In: *Scientific reports* 10.1 (2020), p. 13768.

[524] Liangcheng Tan et al. "Rainfall variations in central Indo-Pacific over the past 2,700 y". In: *Proceedings of the national academy of sciences* 116.35 (2019), pp. 17201–17206.

[525] Chad W Thackeray et al. "Constraining the increased frequency of global precipitation extremes under warming". In: *Nature Climate Change* 12.5 (2022), pp. 441–448.

[526] Nivedita Thiagarajan et al. "Abrupt pre-Bølling–Allerød warming and circulation changes in the deep ocean". In: *Nature* 511.7507 (2014), pp. 75–78.

[527] Elizabeth R Thomas et al. "The 8.2 ka event from Greenland ice cores". In: *Quaternary Science Reviews* 26.1-2 (2007), pp. 70–81.

[528] Ellen Thomas et al. "Northeastern Atlantic benthic foraminifera during the last 45,000 years: changes in productivity seen from the bottom up". In: *Paleoceanography* 10.3 (1995), pp. 545–562.

[529] Lonnie G Thompson. "Ice-core records with emphasis on the global record of the last 2000 years". In: *Global Changes of the Past* 2 (1991), pp. 201–224.

[530] Lonnie G Thompson et al. "Annually resolved ice core records of tropical climate variability over the past˜ 1800 years". In: *Science* 340.6135 (2013), pp. 945–950.

[531] Lonnie G Thompson et al. "Late glacial stage and Holocene tropical ice core records from Huascaran, Peru". In: *Science* 269.5220 (1995), pp. 46–50.

[532] Philip K Thornton et al. "Climate variability and vulnerability to climate change: a review". In: *Global change biology* 20.11 (2014), pp. 3313–3328.

[533] Jessica E Tierney and Peter B deMenocal. "Abrupt shifts in Horn of Africa hydroclimate since the Last Glacial Maximum". In: *Science* 342.6160 (2013), pp. 843–846.

[534] Claudine Till, Joël Guiot, et al. "Reconstruction of precipitation in Morocco since 1100 AD based on Cedrus atlantica tree-ring widths". In: *Quaternary Research* 33.3 (1990), pp. 337–351.

[535] Ofelia Tofalo et al. "Characterization of a loess–paleosols section including a new record of the last interglacial stage in Pampean plain, Argentina". In: *Journal of South American Earth Sciences* 31.1 (2011), pp. 81–92.

[536] Torbjörn E Törnqvist et al. "Tracking the sea-level signature of the 8.2 ka cooling event: New constraints from the Mississippi Delta". In: *Geophysical Research Letters* 31.23 (2004).

[537] Mathias Trachsel et al. "Multi-archive summer temperature reconstruction for the European Alps, AD 1053–1996". In: *Quaternary Science Reviews* 46 (2012), pp. 66–79.

[538] Kevin E Trenberth. "Atmospheric moisture residence times and cycling: Implications for rainfall rates and climate change". In: *Climatic change* 39.4 (1998), pp. 667–694.

[539] Kevin E Trenberth. "Conceptual framework for changes of extremes of the hydrological cycle with climate change". In: *Weather and Climate Extremes*. Springer, 1999, pp. 327–339.

[540] Kevin E Trenberth, John Fasullo, and Lesley Smith. "Trends and variability in column-integrated atmospheric water vapor". In: *Climate dynamics* 24.7-8 (2005), pp. 741–758.

[541] Kevin E Trenberth, Yongxin Zhang, and Maria Gehne. "Intermittency in precipitation: Duration, frequency, intensity, and amounts using hourly data". In: *Journal of Hydrometeorology* 18.5 (2017), pp. 1393–1412.

[542] Kevin E Trenberth et al. "The changing character of precipitation". In: *Bulletin of the American Meteorological Society* 84.9 (2003), pp. 1205–1218.

[543] Kerstin S Treydte et al. "The twentieth century was the wettest period in northern Pakistan over the past millennium". In: *Nature* 440.7088 (2006), pp. 1179–1182.

[544] Valérie Trouet, JD Scourse, and CC Raible. "North Atlantic storminess and Atlantic Meridional Overturning Circulation during the last Millennium: Reconciling contradictory proxy records of NAO variability". In: *Global and Planetary Change* 84 (2012), pp. 48–55.

[545] Valérie Trouet et al. "Persistent positive North Atlantic Oscillation mode dominated the medieval climate anomaly". In: *science* 324.5923 (2009), pp. 78–80.

[546] Chris SM Turney and Richard T Jones. "Does the Agulhas Current amplify global temperatures during super-interglacials?" In: *Journal of Quaternary Science* 25.6 (2010), pp. 839–843.

[547] PC Tzedakis et al. "Enhanced climate instability in the North Atlantic and southern Europe during the Last Interglacial". In: *Nature communications* 9.1 (2018), pp. 1–14.

[548] A Vaks et al. "Paleoclimate and location of the border between Mediterranean climate region and the Saharo–Arabian Desert as revealed by speleothems from the northern Negev Desert, Israel". In: *Earth and Planetary Science Letters* 249.3-4 (2006), pp. 384–399.

[549] Shannon G Valley et al. "Seawater cadmium in the Florida Straits over the Holocene and implications for upper AMOC variability". In: *Paleoceanography and Paleoclimatology* 37.5 (2022), e2021PA004379.

[550] Bas Van Geel et al. "The role of solar forcing upon climate change". In: *Quaternary Science Reviews* 18.3 (1999), pp. 331–338.

[551] S Van Kreveld et al. "Potential links between surging ice sheets, circulation changes, and the Dansgaard-Oeschger cycles in the Irminger Sea, 60–18 kyr". In: *Paleoceanography* 15.4 (2000), pp. 425–442.

[552] Ulrike J Van Raden et al. "High-resolution late-glacial chronology for the Gerzensee lake record (Switzerland): δ18O correlation between a Gerzensee-stack and NGRIP". In: *Palaeogeography, Palaeoclimatology, Palaeoecology* 391 (2013), pp. 13–24.

[553] Mijael Rodrigo Vargas Godoy et al. "The Global Water Cycle Budget: A Chronological Review". In: *Surveys in Geophysics* 42.5 (2021), pp. 1075–1107.

[554] AA Velichko et al. "Climate changes in East Europe and Siberia at the Late glacial–holocene transition". In: *Quaternary International* 91.1 (2002), pp. 75–99.

[555] Michael Vellinga and Richard A Wood. "Global climatic impacts of a collapse of the Atlantic thermohaline circulation". In: *Climatic change* 54.3 (2002), pp. 251–267.

[556] Dirk Verschuren, Kathleen R Laird, and Brian F Cumming. "Rainfall and drought in equatorial east Africa during the past 1,100 years". In: *Nature* 403.6768 (2000), pp. 410–414.

[557] AE Viau, M Ladd, and K Gajewski. "The climate of North America during the past 2000 years reconstructed from pollen data". In: *Global and Planetary Change* 84 (2012), pp. 75–83.

[558] Ricardo Villalba. "Tree-ring and glacial evidence for the Medieval Warm Epoch and the Little Ice Age in southern South America". In: *The Medieval Warm Period*. Springer, 1994, pp. 183–197.

[559] Edith Vincent and Wolfgang H Berger. "Carbon dioxide and polar cooling in the Miocene: The Monterey hypothesis". In: *The carbon cycle and atmospheric CO2: Natural variations Archean to present* 32 (1985), pp. 455–468.

[560] Steven L Voelker et al. "Deglacial hydroclimate of midcontinental North America". In: *Quaternary Research* 83.2 (2015), pp. 336–344.

[561] U Von Grafenstein et al. "The cold event 8200 years ago documented in oxygen isotope records of precipitation in Europe and Greenland". In: *Climate dynamics* 14.2 (1998), pp. 73–81.

[562] Claire Waelbroeck et al. "Constraints on the magnitude and patterns of ocean cooling at the Last Glacial Maximum". In: *Nature Geoscience* (2009).

[563] Jennifer DM Wagner et al. "Moisture variability in the southwestern United States linked to abrupt glacial climate change". In: *Nature Geoscience* 3.2 (2010), pp. 110–113.

[564] M Wahlen et al. "Initial measurements of CO2 concentrations (1530 to 1940 AD) in air occluded in the GISP 2 ice core from central Greenland". In: *Geophysical Research Letters* 18.8 (1991), pp. 1457–1460.

[565] Shiming Wan et al. "Development of the East Asian monsoon: mineralogical and sedimentologic records in the northern South China Sea since 20 Ma". In: *Palaeogeography, Palaeoclimatology, Palaeoecology* 254.3-4 (2007), pp. 561–582.

[566] Alan D Wanamaker et al. "Surface changes in the North Atlantic meridional overturning circulation during the last millennium". In: *Nature Communications* 3.1 (2012), pp. 1–7.

[567] L Wang et al. "Prolonged heavy snowfall during the Younger Dryas". In: *Journal of Geophysical Research: Atmospheres* 123.24 (2018), pp. 13–748.

[568] Liang-Chi Wang et al. "Increased precipitation during the Little Ice Age in northern Taiwan inferred from diatoms and geochemistry in a sediment core from a subalpine lake". In: *Journal of Paleolimnology* 49.4 (2013), pp. 619–631.

[569] SM Wang and L Ji. "Lake Hulun: study on paleolimnology". In: *University of Science and Technology Press, Hefei, China* (1995), pp. 87–93.

[570] Xianfeng Wang et al. “Wet periods in northeastern Brazil over the past 210 kyr linked to distant climate anomalies”. In: *Nature* 432.7018 (2004), pp. 740–743.

[571] Yong-Jin Wang et al. “A high-resolution absolute-dated late Pleistocene monsoon record from Hulu Cave, China”. In: *Science* 294.5550 (2001), pp. 2345–2348.

[572] Yongjin Wang et al. “Millennial-and orbital-scale changes in the East Asian monsoon over the past 224,000 years”. In: *Nature* 451.7182 (2008), pp. 1090–1093.

[573] Heinz Wanner et al. “Mid-to Late Holocene climate change: an overview”. In: *Quaternary Science Reviews* 27.19-20 (2008), pp. 1791–1828.

[574] Warren M Washington and Gerald A Meehl. “Seasonal cycle experiment on the climate sensitivity due to a doubling of CO2 with an atmospheric general circulation model coupled to a simple mixed-layer ocean model”. In: *Journal of Geophysical Research: Atmospheres* 89.D6 (1984), pp. 9475–9503.

[575] Jasper A Wassenburg et al. “Reorganization of the North Atlantic Oscillation during early Holocene deglaciation”. In: *Nature Geoscience* 9.8 (2016), pp. 602–605.

[576] Oliver Watt-Meyer and Dargan MW Frierson. “ITCZ width controls on Hadley cell extent and eddy-driven jet position and their response to warming”. In: *Journal of Climate* 32.4 (2019), pp. 1151–1166.

[577] IG Watterson. “An analysis of the global water cycle of present and doubled CO2 climates simulated by the CSIRO general circulation model”. In: *Journal of Geophysical Research: Atmospheres* 103.D18 (1998), pp. 23113–23129.

[578] IG Watterson, SP O’Farrell, and MR Dix. “Energy and water transport in climates simulated by a general circulation model that includes dynamic sea ice”. In: *Journal of Geophysical Research: Atmospheres* 102.D10 (1997), pp. 11027–11037.

[579] Andrew J Weaver and Tertia MC Hughes. “Rapid interglacial climate fluctuations driven by North Atlantic ocean circulation”. In: *Nature* 367.6462 (1994), pp. 447–450.

[580] Robert S Webb et al. “Influence of ocean heat transport on the climate of the Last Glacial Maximum”. In: *Nature* 385.6618 (1997), pp. 695–699.

[581] Mara-Julia Weber, Sonja B Grimm, and Michael Baales. “Between warm and cold: Impact of the Younger Dryas on human behavior in Central Europe”. In: *Quaternary International* 242.2 (2011), pp. 277–301.

[582] Gangjian Wei et al. “Mg/Ca, Sr/Ca and U/Ca ratios of a porites coral from Sanya Bay, Hainan Island, South China Sea and their relationships to sea surface temperature”. In: *Palaeogeography, Palaeoclimatology, Palaeoecology* 162.1-2 (2000), pp. 59–74.

[583] Wilbert Weijer et al. “CMIP6 models predict significant 21st century decline of the Atlantic meridional overturning circulation”. In: *Geophysical Research Letters* 47.12 (2020), e2019GL086075.

[584] Wilbert Weijer et al. “Stability of the Atlantic Meridional Overturning Circulation: A review and synthesis”. In: *Journal of Geophysical Research: Oceans* 124.8 (2019), pp. 5336–5375.

[585] Frank J Wentz et al. “How much more rain will global warming bring?” In: *Science* 317.5835 (2007), pp. 233–235.

[586] Richard T Wetherald and Syukuro Manabe. “Simulation of hydrologic changes associated with global warming”. In: *Journal of Geophysical Research: Atmospheres* 107.D19 (2002), ACL–7.

[587] Charles JR Williams et al. “CMIP6/PMIP4 simulations of the mid-Holocene and Last Interglacial using HadGEM3: comparison to the pre-industrial era, previous model versions and proxy data”. In: *Climate of the Past* 16.4 (2020), pp. 1429–1450.

[588] Jack A Wolfe. "Distribution of major vegetational types during the Tertiary". In: *The carbon cycle and atmospheric CO2: natural variations Archean to present* 32 (1985), pp. 357–375.

[589] Connie A Woodhouse et al. "A 1,200-year perspective of 21st century drought in southwestern North America". In: *Proceedings of the National Academy of Sciences* 107.50 (2010), pp. 21283–21288.

[590] James D Wright, Kenneth G Miller, and Richard G Fairbanks. "Early and middle Miocene stable isotopes: implications for deepwater circulation and climate". In: *Paleoceanography* 7.3 (1992), pp. 357–389.

[591] Jonathon S Wright et al. "Rainforest-initiated wet season onset over the southern Amazon". In: *Proceedings of the National Academy of Sciences* 114.32 (2017), pp. 8481–8486.

[592] Peili Wu, Nikolaos Christidis, and Peter Stott. "Anthropogenic impact on Earth's hydrological cycle". In: *Nature Climate Change* 3.9 (2013), pp. 807–810.

[593] Peili Wu et al. "Temporary acceleration of the hydrological cycle in response to a CO2 rampdown". In: *Geophysical Research Letters* 37.12 (2010).

[594] Sheng-Dan Wu et al. "Insights into the historical assembly of global dryland floras: The diversification of zygophyllaceae". In: *BMC evolutionary biology* 18.1 (2018), p. 166.

[595] Bao Yang et al. "General characteristics of temperature variation in China during the last two millennia". In: *Geophysical research letters* 29.9 (2002), pp. 38–1.

[596] Qing Yang et al. "Quantitative reconstruction of summer precipitation using a mid-Holocene δ 13 C common millet record from Guanzhong Basin, northern China". In: *Climate of the Past* 12.12 (2016), pp. 2229–2240.

[597] Maayan Yehudai et al. "U–Th dating of calcite corals from the Gulf of Aqaba". In: *Geochimica et Cosmochimica Acta* 198 (2017), pp. 285–298.

[598] Yusuke Yokoyama et al. "Timing of the Last Glacial Maximum from observed sea-level minima". In: *Nature* 406.6797 (2000), pp. 713–716.

[599] Jin-Ho Yoon et al. "Increasing water cycle extremes in California and in relation to ENSO cycle under global warming". In: *Nature Communications* 6.1 (2015), pp. 1–6.

[600] Y You. "Climate-model evaluation of the contribution of sea-surface temperature and carbon dioxide to the Middle Miocene Climate Optimum as a possible analogue of future climate change". In: *Australian Journal of Earth Sciences* 57.2 (2010), pp. 207–219.

[601] Y You et al. "Simulation of the middle Miocene climate optimum". In: *Geophysical Research Letters* 36.4 (2009).

[602] Zicheng Yu and Ulrich Eicher. "Three amphi-Atlantic century-scale cold events during the Bølling-Allerød warm period". In: *Géographie physique et Quaternaire* 55.2 (2001), pp. 171–179.

[603] Yuk L Yung et al. "Dust: A diagnostic of the hydrologic cycle during the Last Glacial Maximum". In: *Science* 271.5251 (1996), pp. 962–963.

[604] James Zachos et al. "Trends, rhythms, and aberrations in global climate 65 Ma to present". In: *science* 292.5517 (2001), pp. 686–693.

[605] James C Zachos, Gerald R Dickens, and Richard E Zeebe. "An early Cenozoic perspective on greenhouse warming and carbon-cycle dynamics". In: *Nature* 451.7176 (2008), pp. 279–283.

[606] Michael J Zaleha. "Siwalik Paleosols (Miocene, northern Pakistan); genesis and controls on their formation". In: *Journal of Sedimentary Research* 67.5 (1997), pp. 821–839.

[607] Giuseppe Zappa and Theodore G Shepherd. "Storylines of atmospheric circulation change for European regional climate impact assessment". In: *Journal of Climate* 30.16 (2017), pp. 6561–6577.

[608] Michael Zech et al. "A 16-ka δ 18 O record of lacustrine sugar biomarkers from the High Himalaya reflects Indian Summer Monsoon variability". In: *Journal of paleolimnology* 51.2 (2014), pp. 241–251.

[609] Mingming Zhang et al. "Hydrological variation recorded in a subalpine peatland of Northeast Asia since the Little Ice Age and its possible driving mechanisms". In: *Science of The Total Environment* 772 (2021), p. 144923.

[610] Qiong Zhang et al. "Simulating the mid-Holocene, Last Interglacial and mid-Pliocene climate with EC-Earth3-LR". In: *Geoscientific Model Development* 14.2 (2021), pp. 1147–1169.

[611] Rong Zhang et al. "A review of the role of the Atlantic meridional overturning circulation in Atlantic multidecadal variability and associated climate impacts". In: *Reviews of Geophysics* 57.2 (2019), pp. 316–375.

[612] Xuebin Zhang et al. "Detection of human influence on twentieth-century precipitation trends". In: *Nature* 448.7152 (2007), pp. 461–465.

[613] Yi Ge Zhang et al. "A 40-million-year history of atmospheric CO2". In: *Philosophical Transactions of the Royal Society A: Mathematical, Physical and Engineering Sciences* 371.2001 (2013), p. 20130096.

[614] Jiaju Zhao et al. "Major increase in winter and spring precipitation during the Little Ice Age in the westerly dominated northern Qinghai-Tibetan Plateau". In: *Quaternary Science Reviews* 199 (2018), pp. 30–40.

[615] Jian-xin Zhao, Qikai Xia, and Kenneth D Collerson. "Timing and duration of the Last Interglacial inferred from high resolution U-series chronology of stalagmite growth in Southern Hemisphere". In: *Earth and Planetary Science Letters* 184.3-4 (2001), pp. 635–644.

[616] Jingyun Zheng et al. "Precipitation variability and extreme events in eastern China during the past 1500 years". In: *TAO: Terrestrial, Atmospheric and Oceanic Sciences* 17.3 (2006), p. 579.

[617] Y Zhong et al. "Centennial-scale climate change from decadally-paced explosive volcanism: a coupled sea ice-ocean mechanism". In: *Climate Dynamics* 37.11-12 (2011), pp. 2373–2387.

[618] Weijian Zhou, M John Head, and Lin Deng. "Climate changes in northern China since the late Pleistocene and its response to global change". In: *Quaternary International* 83 (2001), pp. 285–292.

[619] Weijian Zhou et al. "High-resolution evidence from southern China of an early Holocene optimum and a mid-Holocene dry event during the past 18,000 years". In: *Quaternary Research* 62.1 (2004), pp. 39–48.

[620] Chenyu Zhu et al. "Likely accelerated weakening of Atlantic overturning circulation emerges in optimal salinity fingerprint". In: *Nature Communications* 14.1 (2023), p. 1245.

[621] Anastasia Zhuravleva et al. "Caribbean salinity anomalies contributed to variable North Atlantic circulation and climate during the Common Era". In: *Science Advances* 9.44 (2023), eadg2639.

[622] Alan D Ziegler et al. “Detection of intensification in global-and continental-scale hydrological cycles: Temporal scale of evaluation”. In: *Journal of Climate* 16.3 (2003), pp. 535–547.